HIDDEN SECRETS AND LESSONS FROM THE CRYSTAL STRUCTURES OF INTEGRAL MEMBRANE PROTEINS CHANNELS, PUMPS AND RECEPTORS

EDITED BY: Mario Díaz and Garth L. Nicolson
PUBLISHED IN: Frontiers in Physiology

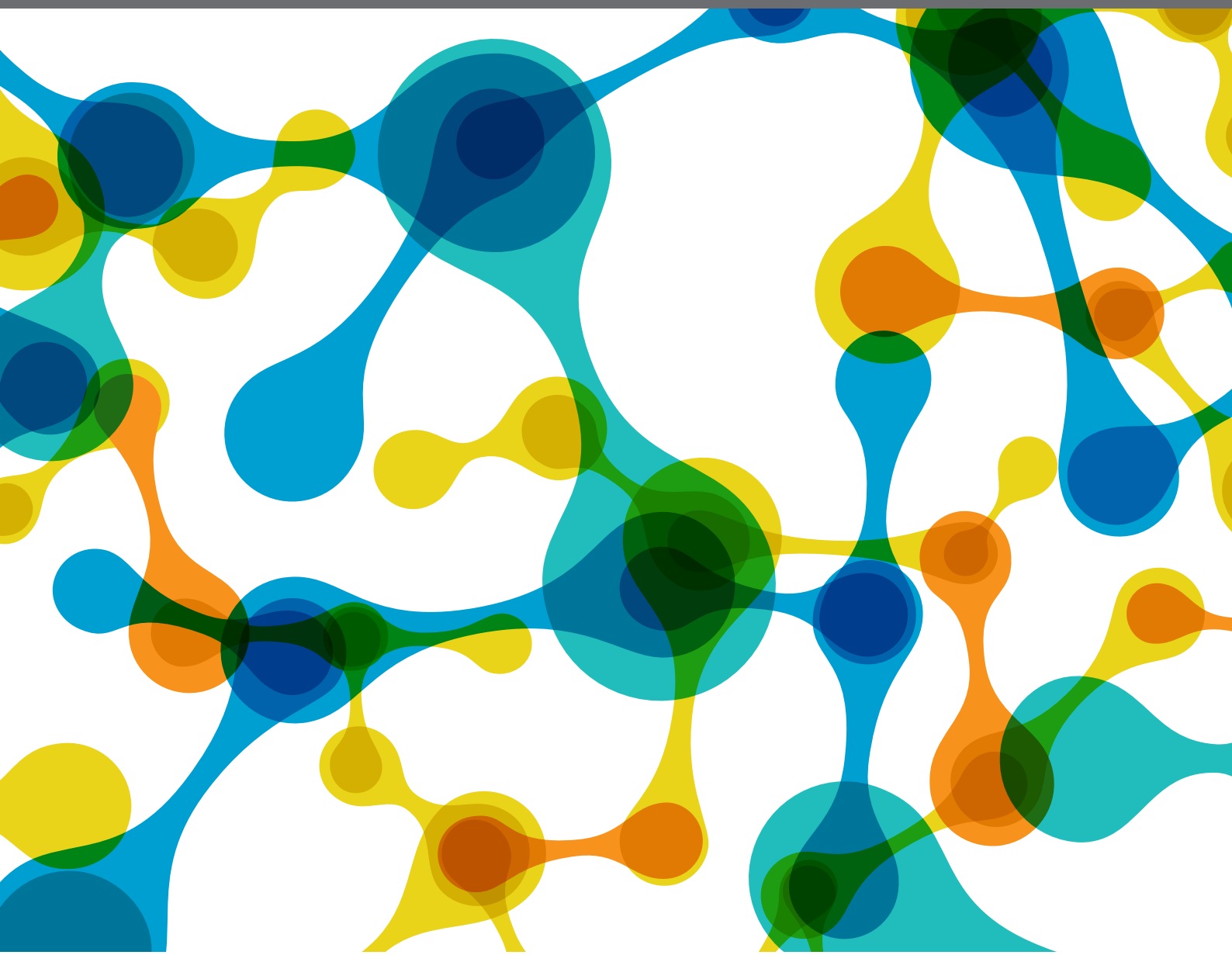

frontiers Research Topics

frontiers

ISSN 1664-8714
ISBN 978-2-88945-719-9
DOI 10.3389/978-2-88945-719-9

About Frontiers

Frontiers is more than just an open-access publisher of scholarly articles: it is a pioneering approach to the world of academia, radically improving the way scholarly research is managed. The grand vision of Frontiers is a world where all people have an equal opportunity to seek, share and generate knowledge. Frontiers provides immediate and permanent online open access to all its publications, but this alone is not enough to realize our grand goals.

Frontiers Journal Series

The Frontiers Journal Series is a multi-tier and interdisciplinary set of open-access, online journals, promising a paradigm shift from the current review, selection and dissemination processes in academic publishing. All Frontiers journals are driven by researchers for researchers; therefore, they constitute a service to the scholarly community. At the same time, the Frontiers Journal Series operates on a revolutionary invention, the tiered publishing system, initially addressing specific communities of scholars, and gradually climbing up to broader public understanding, thus serving the interests of the lay society, too.

Dedication to Quality

Each Frontiers article is a landmark of the highest quality, thanks to genuinely collaborative interactions between authors and review editors, who include some of the world's best academicians. Research must be certified by peers before entering a stream of knowledge that may eventually reach the public - and shape society; therefore, Frontiers only applies the most rigorous and unbiased reviews.
Frontiers revolutionizes research publishing by freely delivering the most outstanding research, evaluated with no bias from both the academic and social point of view. By applying the most advanced information technologies, Frontiers is catapulting scholarly publishing into a new generation.

What are Frontiers Research Topics?

Frontiers Research Topics are very popular trademarks of the Frontiers Journals Series: they are collections of at least ten articles, all centered on a particular subject. With their unique mix of varied contributions from Original Research to Review Articles, Frontiers Research Topics unify the most influential researchers, the latest key findings and historical advances in a hot research area! Find out more on how to host your own Frontiers Research Topic or contribute to one as an author by contacting the Frontiers Editorial Office: researchtopics@frontiersin.org

HIDDEN SECRETS AND LESSONS FROM THE CRYSTAL STRUCTURES OF INTEGRAL MEMBRANE PROTEINS CHANNELS, PUMPS AND RECEPTORS

Topic Editors:
Mario Díaz, Universidad de La Laguna, Spain
Garth L. Nicolson, Institute for Molecular Medicine, United States

Citation: Díaz, M., Nicolson, G. L., eds. (2019). Hidden Secrets and Lessons From the Crystal Structures of Integral Membrane Proteins Channels, Pumps and Receptors. Lausanne: Frontiers Media. doi: 10.3389/978-2-88945-719-9

Table of Contents

frontiers in Physiology

EDITORIAL
published: 31 October 2018
doi: 10.3389/fphys.2018.01466

Editorial: Hidden Secrets and Lessons From the Crystal Structures of Integral Membrane Proteins: Channels, Pumps and Receptors

Mario Díaz[1,2]* *and Garth L. Nicolson*[3]

[1] Departamento de Biología Animal, Edafología y Geología, Facultad de Ciencias, Sección Biología, Universidad de La Laguna, Tenerife, Spain, [2] Unidad Asociada de Investigación CSIC-Universidad de La Laguna "Fisiología y Biofísica de la Membrana Celular en Patologías Neurodegenerativas y Tumorales", Tenerife, Spain, [3] Institute for Molecular Medicine, Huntington Beach, CA, United States

Keywords: integral membrane proteins, crystal structure, structure dynamics, ion channels, active transporters, membrane exchangers, X-ray crystal and molecular structure

Editorial on the Research Topic

Hidden Secrets and Lessons From the Crystal Structures of Integral Membrane Proteins: Channels, Pumps, and Receptors

OPEN ACCESS

Edited by:
Christoph Fahlke, Forschungszentrum Jülich, Helmholtz-Gemeinschaft Deutscher Forschungszentren (HZ), Germany

Reviewed by:
Gabriel Stölting, Charité Universitätsmedizin Berlin, Germany

***Correspondence:**
Mario Díaz
madiaz@ull.es

Specialty section:
This article was submitted to Membrane Physiology and Membrane Biophysics, a section of the journal Frontiers in Physiology

Received: *14 August 2018*
Accepted: *28 September 2018*
Published: *31 October 2018*

Citation:
Díaz M and Nicolson GL (2018) Editorial: Hidden Secrets and Lessons From the Crystal Structures of Integral Membrane Proteins: Channels, Pumps and Receptors. Front. Physiol. 9:1466. doi: 10.3389/fphys.2018.01466

Our current understanding of the integral membrane protein structure and function has changed dramatically in the last two decades, thanks to novel experimental, and methodological approaches that take advantage of the latest technologies. From the earliest high-resolution crystallographic studies on bacteriorhodopsin (Deisenhofer et al., 1985) to newer studies on eukaryotic multi-subunit membrane proteins undergoing structural changes during their catalytic cycles, opening and closing, specificity, binding to modulators, and voltage-induced changes amongst other mechanistic events, membrane proteins have steadily started to reveal their longtime hidden structural secrets. This research topic intends to offer a wider view of our current understanding of the membrane protein structure and function that has emerged from the studies of crystal structures and other breakthrough methodologies, including focused reviews on the latest research in the field of membrane proteins, which includes protein crystallography, mass spectrometry, or cryo-electron microscopy (EM) and their usefulness to unravel important biological details of the structure-function relationships of membrane protein complexes, often leading to a better comprehension of their role in pathological events and human diseases.

METHODS

Membrane proteins represent a challenging family of macromolecules, particularly related to the methodology aimed at characterizing their three-dimensional structure. This is mostly due to their amphipathic nature as well as requirements of ligand bindings to stabilize or control their function. In this perspective article, Montenegro et al. argue on the usefulness of combining mass spectrometry and X-ray crystallography to unravel hidden mysteries of the membrane protein function. This technological implementation has helped to identify the overall stoichiometry of native-like membrane proteins complexed to ligand bindings as well as to provide insights into the transport mechanism across the membrane, as they illustrate several protein-lipid complexes (in particular transporters, ion channels, and molecular machines).

TRANSPORTERS AND EXCHANGERS

Sun and Zheng focus their review on the unique properties of a dual function nitrate transporter NRT1.1, a member of the nitrate transporters superfamily in plants, which may switch between low- and high-affinity states to cope with the large nitrate fluctuation in soil. By means of structural studies on NRT1.1 in *Arabidopsis,* they show that single residue phosphorylation leads to changes in protein oligomerization. Notably, such secondary changes in protein oligomerization are sufficient to increase structural flexibility of NRT1.1 and to modify nitrate affinity. The authors propose a novel paradigm in which protein oligomerization and posttranslational modification can synergistically convey to modulate the functional capacity of dual-affinity transporters.

Recent structural and biophysical studies have shed light on the structural basis of ion transport and the allosteric regulation of sodium-calcium exchanger (NCX) proteins. The NCX proteins include a family of Na^+/Ca^{2+} exchangers, which extrude Ca^{2+} from the cell to maintain cellular homeostasis. Within eukaryotic cells, NCX proteins exist as a complex set of orthologs, isoforms, and splice variants expressed in a tissue-specific manner. In this research topic, Giladi et al. review the structural basis for the diverse regulatory responses to Ca^{2+} binding in different orthologs and splice variants in relation to the dynamic of the two regulatory Ca^{2+}-binding domains, CBD1 and CBD2.

Zhang et al. review the recent structural findings of proton-translocating nicotinamide nucleotide transhydrogenase (TH). Transhydrogenase is an enzyme complex in animal mitochondria and bacteria that utilizes the electrochemical proton gradient across membranes to drive the production of NADPH. The enzyme plays an important role in maintaining the redox balance of cells, and it has been shown to have implications in aging and human diseases. Structural insights into the mechanism of dynamics of TH require structural determinations of the protein complex in many conformational states. Here, Zhang et al. compile the information from recent technological breakthroughs in X-ray crystallography and cryo-EM to outline a comprehensive and detailed structural understanding of this very complex enzyme.

PUMPS

Clausen et al. review the various roles and expression patterns of the Na-K ATPase subunit (namely, the α, β, and FXYD subunits) isoforms. The Na-K ATPase was first described 60 years ago by Skou (1957), and it is perhaps the best primary active transporter studied so far. However, novel discoveries into the pump's atomic structure, cellular regulation, and pathophysiological roles continue to emerge. The distribution pattern of different isoforms is fine-tuned to cope with the different cellular needs, and mutations in the genes encoding for the different subunits/isoforms are associated with a plethora of pathophysiological effects, which are often linked to neurological diseases. Differences in the mutations of Na-K ATPase subunits (particularly in the α-subunit) affect kinetic parameters, pump regulation, and protein-protein/protein-lipid interactions.

ION CHANNELS

The major protein in the outer membrane of mitochondria is the voltage-dependent anion channel (VDAC), which mediates signal transmission across the outer membrane but also the exchange of metabolites, most importantly ADP and ATP. Over the past 10 years, complementary structural and functional information on proteins of the VDAC superfamily have been collected from *in organello*, *in vitro*, and *in silico* studies. Most of these findings have confirmed the validity of the original structures (19-stranded anti-parallel beta-barrel with an N-terminal helix located inside). The article by Zeth and Zachariae reviews the most important advances on the structure and function of VDAC superfamily members, and the review summarizes how they enhanced our understanding of the channel.

The mammalian Sec61 complex existing in the membrane of the endoplasmic reticulum (ER) forms a dynamic gated channel, which provides an aqueous path for nascent polypeptides in the cytosol into the ER lumen and is regulated by various allosteric effectors. Further, when the pore forming subunit of the complex (gated pathway) is open, it also provides a pathway for the efflux of calcium ions from the ER into the cytosol. Lang et al. suggest that this feature is linked to the regulation of ATP import into the ER and the initiation of the intrinsic pathway to apoptosis. Recently, cryoelectron tomography of translocons in native ER membrane vesicles has given unprecedented insights into the architecture and dynamics of the native translocon harboring the Sec61 channel. In this review by Lang et al., this structural information is discussed in light of different Sec61 channel activities including ribosome receptor function, membrane insertion, and translocation of newly synthesized polypeptides as well as the putative physiological roles of the Sec61 channel as a passive ER calcium leak channel.

A total of 27 renowned researchers from seven countries (Denmark, United Kingdom, USA, Chile, Netherlands, Germany, and Israel) have contributed to this research topic. We hope this compilation provides a stimulating knowledge base for upcoming research in this very active and promising investigation field.

AUTHOR CONTRIBUTIONS

MD and GN have edited the research topic and have written and drafted the manuscript.

ACKNOWLEDGMENTS

Supported by Research grant SAF2014-61644-EXP and SAF2014-52582-R from MINECO (Spain).

REFERENCES

Deisenhofer, J., Epp, O., Miki, K., Huber, R., and Michel, H. (1985). Structure of the protein subunits in the photosynthetic reaction centre of *Rhodopseudomonas viridis* at 3Å resolution. *Nature* 318, 618–624. doi: 10.1038/318618a0

Skou, J. C. (1957). The influence of some cations on an adenosine triphosphatase from peripheral nerves. *Biochim. Biophys. Acta* 23, 394–401. doi: 10.1016/0006-3002(57)90343-8

Conflict of Interest Statement: The authors declare that the research was conducted in the absence of any commercial or financial relationships that could be construed as a potential conflict of interest.

frontiers in Physiology

MINI REVIEW
published: 07 March 2018
doi: 10.3389/fphys.2018.00108

Ten Years of High Resolution Structural Research on the Voltage Dependent Anion Channel (VDAC)—Recent Developments and Future Directions

Kornelius Zeth[1]* *and Ulrich Zachariae*[2,3]*

[1] Department for Science and Environment, Roskilde University, Roskilde, Denmark, [2] School of Science and Engineering, University of Dundee, Dundee, United Kingdom, [3] School of Life Sciences, University of Dundee, Dundee, United Kingdom

Mitochondria are evolutionarily related to Gram-negative bacteria and both comprise two membrane systems with strongly differing protein composition. The major protein in the outer membrane of mitochondria is the voltage-dependent anion channel (VDAC), which mediates signal transmission across the outer membrane but also the exchange of metabolites, most importantly ADP and ATP. More than 30 years after its discovery three identical high-resolution structures were determined in 2008. These structures show a 19-stranded anti-parallel beta-barrel with an N-terminal helix located inside. An odd number of beta-strands is also shared by Tom40, another member of the VDAC superfamily. This indicates that this superfamily is evolutionarily relatively young and that it has emerged in the context of mitochondrial evolution. New structural information obtained during the last decade on Tom40 can be used to cross-validate the structure of VDAC and vice versa. Interpretation of biochemical and biophysical studies on both protein channels now rests on a solid basis of structural data. Over the past 10 years, complementary structural and functional information on proteins of the VDAC superfamily has been collected from *in-organello*, *in-vitro,* and *in silico* studies. Most of these findings have confirmed the validity of the original structures. This short article briefly reviews the most important advances on the structure and function of VDAC superfamily members collected during the last decade and summarizes how they enhanced our understanding of the channel.

Keywords: VDAC, structural biology, x-ray, NMR, Tom40

OPEN ACCESS

Edited by:
Mario Diaz,
Universidad de La Laguna, Spain

Reviewed by:
Maria Isabel Bahamonde Santos,
Instituto de Traumatología Barcelona (ITB), Spain
Alexi K. Alekov,
Hannover Medical School, Germany

***Correspondence:**
Kornelius Zeth
kzeth@ruc.dk
Ulrich Zachariae
u.zachariae@dundee.ac.uk

Specialty section:
This article was submitted to Membrane Physiology and Membrane Biophysics, a section of the journal Frontiers in Physiology

Received: *15 November 2017*
Accepted: *02 February 2018*
Published: *07 March 2018*

Citation:
Zeth K and Zachariae U (2018) Ten Years of High Resolution Structural Research on the Voltage Dependent Anion Channel (VDAC)—Recent Developments and Future Directions. Front. Physiol. 9:108. doi: 10.3389/fphys.2018.00108

INTRODUCTION

Gram-negative bacteria, mitochondria, and chloroplasts are enveloped by two lipid bilayers, termed the inner and outer membrane. While all inner membrane proteins are alpha-helical, proteins in the outer membrane display beta-barrel structures with a wide variation in the number and tilt of beta-strands as well as the way the strands are interconnected by loops and turns (Fairman et al., 2011). The mitochondrial porin VDAC (voltage-dependent anion channel) is the major protein in the mitochondrial outer membrane (MOM). It confers a sieve-like structure to the outer membrane due to its high abundance, covering about ∼30%

of the membrane surface (Gonçalves et al., 2007). The high density of VDAC in the outer membrane is surprising, but may be explained by the wide range of functions performed by VDAC isoforms in metabolite exchange and their interactions with proteins of the cytoplasm and the intermembrane space (Lemasters and Holmuhamedov, 2006). In particular, hexokinase-VDAC interactions were shown to dominate on the mitochondrial surface with a high surface density of this complex, including clusters of hVDAC3 isoforms with hexokinase I (Neumann et al., 2010). Further important interactions of VDAC at the mitochondrial surface are those undergone with pro- and anti-apoptotic proteins such as Bax, Bak, or tBid (Rostovtseva and Bezrukov, 2008; Ott et al., 2009).

VDAC can form semi-crystalline arrays in the MOM at high protein concentration (Mannella et al., 1983; Gonçalves et al., 2007) (see **Figures 1**, **3B**). Early studies by electron microscopy (EM), performed in the laboratories of Frank and Mannella in the 1980s, yielded structural information on semi-crystalline arrays of a pore-forming channel isolated from the MOM (Mannella et al., 1983) (see **Figures 1A,B**). These studies showed hexagons of two channel triplets related by two-fold symmetry with a channel diameter of ∼4 nm. Later studies of VDAC using electron microscopy in combination with single particle analysis revealed the 3D shape and dimensions of the channel at medium resolution (Guo et al., 1995). It took until 2008 however to unravel the structure of VDAC at atomic resolution.

THREE HIGH-RESOLUTION STRUCTURES OF VDAC INDEPENDENTLY CONFIRM AN UNEXPECTED FOLD

In 2008, the simultaneous structure determination of VDAC in three independent laboratories, based on NMR spectroscopy and X-ray crystallography, provided a dramatically enhanced view on the architecture of VDAC (see **Figures 2A,B**) (Bayrhuber et al., 2008; Hiller et al., 2008; Ujwal et al., 2008). These studies were the first to reveal the structure of a member of the small class of proteins located within the MOM. They raised particular interest in the community for two further reasons, one of which was the discovery of the precise VDAC fold, while the second was to unravel the structural deviation from porins of Gram-negative bacteria (Bayrhuber et al., 2008; Zeth and Thein, 2010; Bay et al., 2012). The structures confirmed the dimensions of the VDAC pore previously observed by electron microscopy and revealed important further structural features, such as the 19-stranded nature of the channel, the presence of an alpha-helix located inside the pore and the strong internal positive charge (see **Figures 2B,C**) (Bayrhuber et al., 2008; Hiller et al., 2008; Ujwal et al., 2008). Additional structural information included the dimeric assembly of the protein reported by Bayrhuber et al. (2008), which resembled the oligomeric species revealed by the early EM data (see **Figures 1C**, **2D**). Furthermore, the tilt of the beta-sheets, the length and orientation of surface-exposed loops and turns, and the electrostatic properties of VDAC were unraveled. It was also shown that E73, a residue potentially critical for apoptosis, unexpectedly faces toward the membrane environment (Villinger et al., 2010; Shoshan-Barmatz et al., 2017). Although the three structures differed in some details (for instance, the NMR structure did not fully resolve the alpha-helix and rather assigned a random coil structure in this area), the number and tilt of beta-strands and overall dimensions were clearly identical. Even though these structures were initially placed into doubt, due to the generation of the proteins by recombinant techniques followed by refolding, they were considered to be a breakthrough for the understanding of the MOM and their correctness was never challenged in the field of structural biology (Colombini, 2009; Hiller and Wagner, 2009).

STRUCTURAL AND FUNCTIONAL STUDIES ON VDAC AND TOM40 CONFIRM THE VDAC-LIKE FOLD *IN VIVO* AND PROVIDE NEW MECHANISTIC DETAILS

During the last decade, new studies offering refined structural and functional insights on VDAC have been conducted in the fields of biochemistry, structural, and computational biology (see **Table 1**). In a recent study of hVDAC1, high-resolution NMR spectroscopy was applied to determine the structure of the E73V mutant (Jaremko et al., 2016). Notably, and as previously mentioned, residue E73 has the unusual location at the outer face of the beta-barrel, with its side-chain pointing toward the membrane (Bayrhuber et al., 2008; Hiller et al., 2008; Ujwal et al., 2008). The N15 NMR data acquired returned a model that shows a strongly distorted beta-barrel relative to the mVDAC1 and hVDAC1 structures (a substantial r.m.s.d of ∼3 Å for the Cα atoms after structure superposition) with an unusually narrow pore diameter (see **Figure 3A**). While this study primarily aimed at the development of NMR techniques in the context of a large membrane protein, a potentially altered function of the artificially constricted barrels remains conceivable. Another structural study published recently presents structures of hVDAC1 which were solved using protein produced in an *E. coli* cell-free expression system, but lacking the denaturation step previously applied to all VDAC preparations (Hosaka et al., 2017). This protein yielded the archetypical monomeric structure but showed two different crystal packings based on weak protein-protein interactions. The authors speculate that this feature might represent a potential binding interaction which may be important to form mixed oligomers of VDAC isoforms in membranes (Hosaka et al., 2017).

Arguably, a new level of insight into the structures of the VDAC superfamily emerged from recent papers on Tom40. Due to the close evolutionary relationship between VDAC and Tom40, data from both proteins taken together have enhanced the understanding of the VDAC structure. *In-organello,* cysteine and protease-accessibility mapping studies of Tom40 in the MOM clearly supported the 19-stranded VDAC model (Lackey et al., 2014) (see **Figure 3C**). More recently, cryo-electron microscopy (EM) of isolated and dimeric Tom40 complexes from *N. crassa* provided additional evidence for the accuracy of the 19-stranded VDAC structure, since it was used to construct the

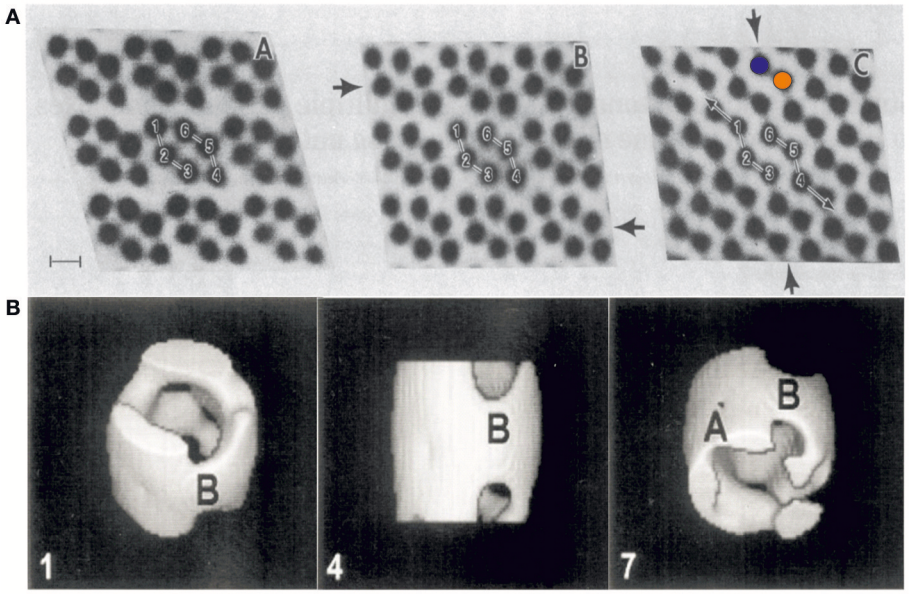

FIGURE 1 | First electron micrographs of VDAC from the early 1980s. **(A)** Electron-microscopic investigations of ncVDAC arranged in isolated native membrane vesicles show three two-dimensional molecular arrays: two slightly different hexameric arrangements of VDAC pores around a two-fold symmetry axis (right and left) and another arrangement where dimeric VDAC pores form chain-like superstructures (colored circles mark two independent monomers) (Mannella et al., 1983). **(B)** A single particle analysis of small membrane arrays yielded the first 3D representation of VDAC at a resolution of ~2 nm (Guo et al., 1995). Figures reproduced with permission.

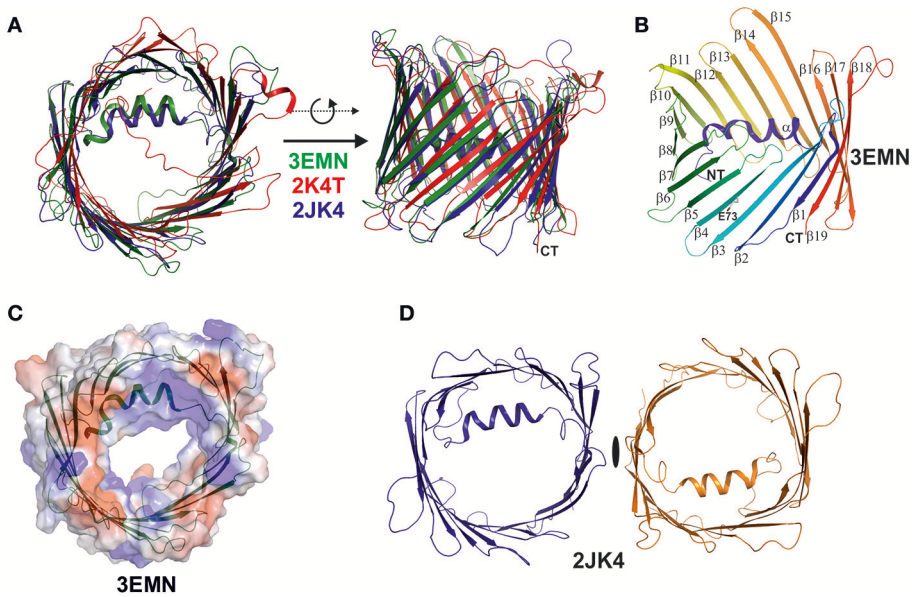

FIGURE 2 | Superposition of the three VDAC structures published simultaneously in 2008. The three structures were determined by X-ray, NMR spectroscopy, and a combination of both methods (Bayrhuber et al., 2008; Hiller et al., 2008; Ujwal et al., 2008). **(A)** Here, we superimposed the three structures and displayed them in ribbon representation to highlight their analogies and differences. The X-ray structure (3EMN) is shown in green, the NMR structure (2K4T) is shown in red, while the hybrid structure (2JK4) is displayed in blue. The structures are viewed from two different perspectives related by a 90° rotation around the x-axis. The major difference between the structures is the location and secondary structure assigned to the N-terminal helix in the NMR structure. **(B)** Structure of mVDAC displaying the fold of the VDAC superfamily proteins. The structure is color coded from the N- (blue) to the C-terminus (red) and secondary structure elements are annotated (alpha, beta1-beta19). **(C)** A primary function of VDAC in the MOM is to translocate nucleotides and the surface representation of VDAC color coded in surface charge potentials is provided. This representation shows the channel pore together with the electrostatic surface potential which is primarily positive around the channel eyelet. **(D)** The crystal structure of 2JK4 showed a potential VDAC dimer in the crystal lattice and although the dimer contacts are rather weak, the interface formed by strands beta1 and beta19 appears to be biologically important. All figures were prepared using PYMOL (www.pymol.org).

TABLE 1 | 3D structures of VDAC published since 2008.

Isoform	Species	Modification	Method	Oligomerization	Resolution (Å)	PDB code	References
zfVDAC2	Zebra fish	Wildtype	X-ray	Dimer	2.8	4BUM	Schredelseker et al., 2014
mVDAC1	Mouse	Wildtype ATP complex	X-ray	Monomer	2.3	4C69	Choudhary et al., 2014
hVDAC1	Human	E73V	NMR	Monomer	–	5JDP	Jaremko et al., 2016
hVDAC1	Human	Wildtype	X-ray	Monomer	3.2	5XDN	Hosaka et al., 2017
hVDAC1	Human	Wildtype	X-ray	Monomer	3.1	5XDO	Hosaka et al., 2017

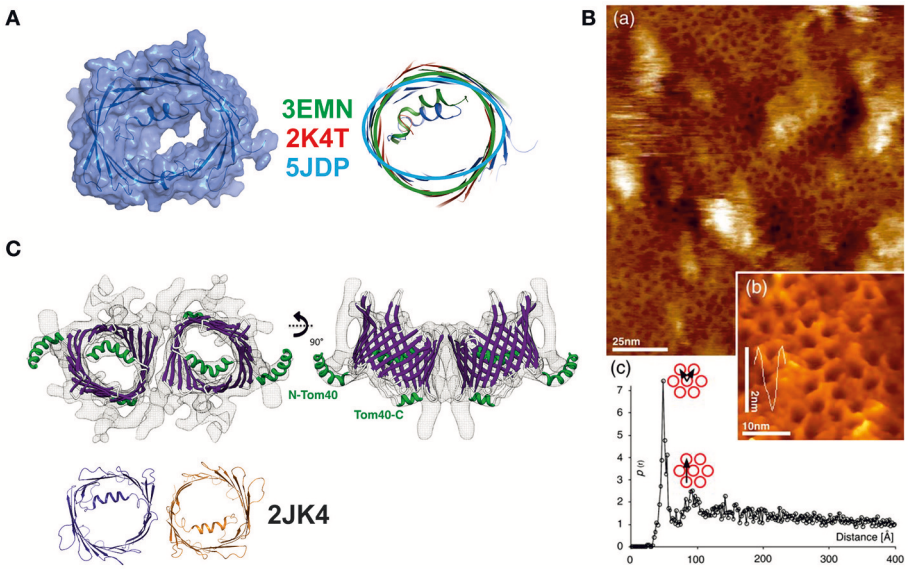

FIGURE 3 | New structural details collected on members of the VDAC-superfamily of 19-stranded β-barrels. **(A)** Structure determination of the E73V mutant of human VDAC. This mutant was previously described to have altered biophysical properties in comparison to the wildtype protein. The NMR determination of the structure yielded a structurally significantly changed beta-barrel with an oval rather than a circular form and a smaller channel diameter. Three structures of the mVDAC1 (in green), hVDAC1 (in red), and the mutant structure (in light blue) were superimposed to show the deviation in the barrel section. A surface representation of the latest NMR structure (5JDP) shows the particular small diameter of the pore eyelet in E73V (Jaremko et al., 2016). **(B)** (a) High resolution AFM topographs of densely packed scVDAC natively embedded in membranes of *S. cerevisiae* (large picture) and (b) high resolution view of VDAC molecules in an arrangement similar to the early electron microscopy images (inset picture). (c) Peak analysis of the separation between two VDAC molecules yields a distance of 53 Å (pore to pore; see graph) (Gonçalves et al., 2007). **(C)** Structural analysis of the Tom40 complex shows a dimeric arrangement of the pore structures with the alpha-helix inside the barrel or exposed to the surface. The structure at 1 nm resolution was modeled by a Tom40-homology model based on the mVDAC structure (PDB-entry 3EMN) and can accommodate the 19 beta-strands unambiguously. The dimeric arrangement is mediated by the same beta1/beta19 strands as previously reported for the hVDAC1 dimer (2JK4—dimer shown in orange and dark blue) (Bayrhuber et al., 2008; Bausewein et al., 2017). Figures reproduced with permission.

Tom40 model (Bausewein et al., 2017). This number of beta-strands also agrees with the pore diameter and the dimensions along the barrel. This EM study also provided insights into the natural dimerization mechanism and the flexibility of the internal N-terminal helix. Interestingly, the N-terminal helix in Tom40 can adopt two conformations, one of which is the bent conformation inside the barrel also observed in the VDAC structures, while the second conformation places the folded helix outside the channel. Dimerization of Tom40 is accomplished via the β1 and β19 strands in the same way as described by Bayrhuber et al. (2008) for VDAC1 and later confirmed for the VDAC2 structure from zebra fish (zVDAC2) (Schredelseker et al., 2014). Interface mutants based on the zVDAC2 structure further confirmed the crystallographic interface previously reported. Sequence comparison of ncTom40 and hVDAC1 shows that identical or highly conserved residues are located on the b1 and b19 strands (Bay et al., 2012 and our unpublished data).

ION PERMEATION AND GATING OF VDAC ELUCIDATED BY MOLECULAR DYNAMICS SIMULATIONS

A wide range of simulation studies have addressed the question of VDAC dynamics and permeation. Molecular dynamics (MD) simulations based on the mVDAC1 (PDB-entry: 4C69) structure combined with a Markov state model showed the capacity to pass millions of ATP molecules per second via hundreds of different permeation pathways along a network of basic residues (Choudhary et al., 2014). Prior to this, MD and Brownian Dynamics studies on the mVDAC1 structure

(PDB-entry: 3EMN) had established ion transfer pathways and the ion conductance and selectivity of VDAC, reporting a high level of agreement with experiment and illuminating the molecular basis of the pronounced anion-selectivity of VDAC (Lee et al., 2011; Rui et al., 2011). Poisson-Nernst-Planck and electrostatics calculations shed further light on the anion-selective permeation across VDAC and highlighted mutations that could reverse this selectivity to transform VDAC into a cation-selective porin (Choudhary et al., 2010). The crystal structure of murine mVDAC1 (PDB-entry: 3EMN) was also used to elucidate the energetic and kinetic basis of ATP and ADP translocation across the pore by umbrella sampling calculation as well as its molecular interaction with the cytoskeletal protein tubulin by ROSETTA-based protein-protein docking (Noskov et al., 2013). These computational findings characterized the binding between mVDAC1 and tubulin, which was previously reported from experimental work. This interaction is considered to be physiologically important for the gating of VDAC and, consequently, for the permeability of the MOM. Finally, two studies using a combination of solution or solid-state NMR and extended molecular dynamics simulations based on the mVDAC1 structure arrived at the conclusion that the beta-barrel structure of VDAC exhibits a particularly high flexibility (Villinger et al., 2010) and that, especially following a voltage-dependent dislodgement of the internal alpha-helix, a significant deformation of the barrel can explain subconductance states at greatly altered ion-selectivity, as previously described experimentally (Zachariae et al., 2012). In the latter study, ion conduction and selectivity was probed in fully open and semi-collapsed barrel states with the Computational Electrophysiology (CompEL) simulation technique (Kutzner et al., 2016). The role of the beta-barrel in VDAC and porin channel gating was confirmed in a range of experimental electrophysiology studies by Essen and colleagues (Grosse et al., 2014), which also characterized its dependence on the dynamics of the N-terminal helix (Mertins et al., 2014), and its flexibility in the membrane corroborated by further NMR studies (Ge et al., 2016). The subconductance states of VDAC were recently also addressed in a combined experimental and computational study using CompEL and single-channel electrophysiology (Briones et al., 2016), which confirmed the existence and further elucidated the conformation of cation-selective subconductance levels in VDAC. Furthermore, a recent review collating a wide array of experimental and computational data came to the conclusion that the beta-barrel collapse model is in agreement with the majority of experimental observations on VDAC including its lipid-sensitivity (Shuvo et al., 2016).

RECENT DEVELOPMENTS AND FUTURE DIRECTIONS

For the last 10 years, research on VDAC has rested on high resolution structures, which clearly described the fold of VDAC-superfamily proteins. Recent investigations have therefore focused on the interpretation of physiological data by molecular dynamics, for example to explain functional changes such as the switch from anion- to cation-selectivity on the basis of structural dynamics as well as the decreasing channel diameter upon voltage application. Despite a wealth of such studies, and a remarkable level of new insight achieved, some basic physiological questions remain open. These include the structural basis for the initiation of the transition between high and low conductance states, clearly defined binding sites for nucleotides, and the molecular interactions formed with apoptosis-related proteins (see also Noskov et al., 2016). However, STED microscopy improved our understanding of VDAC-HK complexes formation under physiological conditions on the molecular level (Neumann et al., 2010). Most recent NMR and X-ray structures were not able to enhance our view on how VDAC is embedded into natural membranes, and the best images of natively enriched VDAC samples still come from early EM data and data from atomic force microscopy. Using Tom40 as a representative of the VDAC superfamily, two recent investigations clearly confirmed its specific fold under biological conditions. Although corroborative in terms of the VDAC-fold, the EM study of Tom40 in particular provided a genuine breakthrough for the field, as for the first time protein complexes in the MOM were structurally unveiled at 1 nm resolution (Bausewein et al., 2017).

FURTHER VDAC STRUCTURES, WHICH WOULD HELP TO UNDERSTAND ITS PHYSIOLOGY AS A CHANNEL CONNECTING MITOCHONDRIA WITH THE CYTOPLASM:

- Structure and putative function of the closed or semi-open state
- Structure of metabolite (e.g., ATP/ADP, citrate) and drug complexes (e.g., erastin)
- Structure of VDAC3
- Structures of VDAC-ANT complexes
- Structures of VDAC in complex with pro-apoptotic proteins such as tBid, Bax, or Bak.

AUTHOR CONTRIBUTIONS

KZ and UZ contributed to conception and design of the manuscript and wrote the manuscript.

ACKNOWLEDGMENTS

This work was supported by Roskilde University (KZ) and the Scottish Universities' Physics Alliance (SUPA, UZ). We thank Giulia Tamburrino for critical reading of the manuscript.

REFERENCES

Bausewein, T., Mills, D. J., Langer, J. D., Nitschke, B., Nussberger, S., and Kühlbrandt, W. (2017). Cryo-EM structure of the TOM core complex from Neurospora crassa. *Cell* 170, 693–700. doi: 10.1016/j.cell.2017.07.012

Bay, D. C., Hafez, M., Young, M. J., and Court, D. A. (2012). Phylogenetic and coevolutionary analysis of the β-barrel protein family comprised of mitochondrial porin (VDAC) and Tom40. *Biochim. Biophys. Acta* 1818, 1502–1519. doi: 10.1016/j.bbamem.2011.11.027

Bayrhuber, M., Meins, T., Habeck, M., Becker, S., Giller, K., Villinger, S., et al. (2008). Structure of the human voltage-dependent anion channel. *Proc. Natl. Acad. Sci. U.S.A.* 105, 15370–15375. doi: 10.1073/pnas.0808115105

Briones, R., Weichbrodt, C., Paltrinieri, L., Mey, I., Villinger, S., Giller, K., et al. (2016). Voltage dependence of conformational dynamics and subconducting states of VDAC-1. *Biophys. J.* 111, 1223–1234. doi: 10.1016/j.bpj.2016.08.007

Choudhary, O. P., Paz, A., Adelman, J. L., Colletier, J. P., Abramson, J., and Grabe, M. (2014). Structure-guided simulations illuminate the mechanism of ATP transport through VDAC1. *Nat. Struct. Mol. Biol.* 21, 626–632. doi: 10.1038/nsmb.2841

Choudhary, O. P., Ujwal, R., Kowallis, W., Coalson, R., Abramson, J., and Grabe, M. (2010). The electrostatics of VDAC: implications for selectivity and gating. *J. Mol. Biol.* 396, 580–592. doi: 10.1016/j.jmb.2009.12.006

Colombini, M. (2009). The published 3D structure of the VDAC channel: native or not? *Trends Biochem. Sci.* 34, 382–389. doi: 10.1016/j.tibs.2009.05.001

Fairman, J. W., Noinaj, N., and Buchanan, S. K. (2011). The structural biology of β-barrel membrane proteins: a summary of recent reports. *Curr. Opin. Struct. Biol.* 21, 523–531. doi: 10.1016/j.sbi.2011.05.005

Ge, L., Villinger, S., Mari, S. A., Giller, K., Griesinger, C., Becker, S., et al. (2016). Molecular plasticity of the human voltage-dependent anion channel embedded into a membrane. *Structure* 24, 585–594. doi: 10.1016/j.str.2016.02.012

Gonçalves, R. P., Buzhynskyy, N., Prima, V., Sturgis, J. N., and Scheuring, S. (2007). Supramolecular assembly of VDAC in native mitochondrial outer membranes. *J. Mol. Biol.* 369, 413–418. doi: 10.1016/j.jmb.2007.03.063

Grosse, W., Psakis, G., Mertins, B., Reiss, P., Windisch, D., Brademann, F., et al. (2014). Structure-based engineering of a minimal porin reveals loop-independent channel closure. *Biochemistry* 53, 4826–4838. doi: 10.1021/bi500660q

Guo, X. W., Smith, P. R., Cognon, B., D'Arcangelis, D., Dolginova, E., and Mannella, C. A. (1995). Molecular design of the voltage-dependent, anion-selective channel in the mitochondrial outer membrane. *J. Struct. Biol.* 114, 41–59. doi: 10.1006/jsbi.1995.1004

Hiller, S., Garces, R. G., Malia, T. J., Orekhov, V. Y., Colombini, M., and Wagner, G. (2008). Solution structure of the integral human membrane protein VDAC-1 in detergent micelles. *Science* 321, 1206–1210. doi: 10.1126/science.1161302

Hiller, S., and Wagner, G. (2009). The role of solution NMR in the structure determinations of VDAC-1 and other membrane proteins. *Curr. Opin. Struct. Biol.* 19, 396–401. doi: 10.1016/j.sbi.2009.07.013

Hosaka, T., Okazaki, M., Kimura-Someya, T., Ishizuka-Katsura, Y., Ito, K., Yokoyama, S., et al. (2017), Crystal structural characterization reveals novel oligomeric interactions of human voltage-dependent anion channel 1. *Protein Sci.* 26, 1749–1758. doi: 10.1002/pro.3211

Jaremko, M., Jaremko, Ł., Villinger, S., Schmidt, C. D., Griesinger, C., Becker, S., et al. (2016). High Resolution NMR Determination of the Dynamic Structure of Membrane Proteins. *Angew. Chem. Int. Ed.* 55, 10518–10521. doi: 10.1002/anie.201602639

Kutzner, C., Köpfer, D. A., Machtens, J. P., de Groot, B. L., Song, C., and Zachariae, U. (2016). Insights into the function of ion channels by computational electrophysiology simulations. *Biochim. Biophys. Acta* 1858, 1741–1752. doi: 10.1016/j.bbamem.2016.02.006

Lackey, S. W., Taylor, R. D., Go, N. E., Wong, A., Sherman, E. L., and Nargang, F. E. (2014). Evidence supporting the 19 β-strand model for Tom40 from cysteine scanning and protease site accessibility studies. *J. Biol. Chem.* 289, 21640–21650. doi: 10.1074/jbc.M114.578765

Lee, K. I., Rui, H., Pastor, R. W., and Im, W. (2011). Brownian dynamics simulations of ion transport through the VDAC. *Biophys. J.* 100, 611–619. doi: 10.1016/j.bpj.2010.12.3708

Lemasters, J. J., and Holmuhamedov, E. (2006). Voltage-dependent anion channel (VDAC) as mitochondrial governator—thinking outside the box. *Biochim. Biophys. Acta* 1762, 181–190. doi: 10.1016/j.bbadis.2005.10.006

Mannella, C. A., Colombini, M., and Frank, J. (1983). Structural and functional evidence for multiple channel complexes in the outer membrane of *Neurospora crassa* mitochondria. *Proc. Natl. Acad. Sci. U.S.A.* 80, 2243–2247. doi: 10.1073/pnas.80.8.2243

Mertins, B., Psakis, G., and Essen, L. O. (2014). Voltage-dependent anion channels: the wizard of the mitochondrial outer membrane. *Biol. Chem.* 395, 1435–1442. doi: 10.1515/hsz-2014-0203

Neumann, D., Bückers, J., Kastrup, L., Hell, S. W., and Jakobs, S. (2010). Two-color STED microscopy reveals different degrees of colocalization between hexokinase-I and the three human VDAC isoforms. *PMC Biophys.* 3:4. doi: 10.1186/1757-5036-3-4

Noskov, S. Y., Rostovtseva, T. K., and Bezrukov, S. M. (2013). ATP transport through VDAC and the VDAC–tubulin complex probed by equilibrium and Nonequilibrium MD simulations. *Biochemistry* 52, 9246–9256. doi: 10.1021/bi4011495

Noskov, S. Y., Rostovtseva, T. K., Chamberlin, A. C., Teijido, O., Jiang, W., and Bezrukov, S. M. (2016). Current state of theoretical and experimental studies of the voltage-dependent anion channel (VDAC). *Biochim. Biophys. Acta* 1858, 1778–1790. doi: 10.1016/j.bbamem.2016.02.026

Ott, M., Norberg, E., Zhivotovsky, B., and Orrenius, S. (2009). Mitochondrial targeting of tBid/Bax: a role for the TOM complex?. *Cell Death Diff.* 16, 1075–1082. doi: 10.1038/cdd.2009.61

Rostovtseva, T. K., and Bezrukov, S. M. (2008). VDAC regulation: role of cytosolic proteins and mitochondrial lipids. *J. Bioenerg. Biomembr.* 40, 163–170. doi: 10.1007/s10863-008-9145-y

Rui, H., Lee, K. I., Pastor, R. W., and Im, W. (2011). Molecular dynamics studies of ion permeation in VDAC. *Biophys. J.* 100, 602–610. doi: 10.1016/j.bpj.2010.12.3711

Schredelseker, J., Paz, A., López, C. J., Altenbach, C., Leung, C. S., Drexler, M. K., et al. (2014). High resolution structure and double electron-electron resonance of the zebrafish voltage-dependent anion channel 2 reveal an oligomeric population. *J. Biol. Chem.* 289, 12566–12577. doi: 10.1074/jbc.M113.497438

Shoshan-Barmatz, V., Krelin, Y., and Chen, Q. (2017). VDAC1 as a player in mitochondria-mediated apoptosis and target for modulating apoptosis. *Curr. Med. Chem.* 24, 4435–4446. doi: 10.2174/0929867324666170616105200

Shuvo, S. R., Ferens, F. G., and Court, D. A. (2016). The N-terminus of VDAC: structure, mutational analysis, and a potential role in regulating barrel shape. *Biochim. Biophys. Acta* 1858, 1350–1361. doi: 10.1016/j.bbamem.2016.03.017

Ujwal, R., Cascio, D., Colletier, J. P., Faham, S., Zhang, J., Toro, L., et al. (2008). The crystal structure of mouse VDAC1 at 2.3 Å resolution reveals mechanistic insights into metabolite gating. *Proc. Natl. Acad. Sci. U.S.A.* 105, 17742–17747. doi: 10.1073/pnas.0809634105

Villinger, S., Briones, R., Giller, K., Zachariae, U., Lange, A., de Groot, B. L., et al. (2010). Functional dynamics in the voltage-dependent anion channel. *Proc. Natl. Acad. Sci. U.S.A.* 107, 22546–22551. doi: 10.1073/pnas.1012310108

Zachariae, U., Schneider, R., Briones, R., Gattin, Z., Demers, J. P., Giller, K., et al. (2012). β-Barrel mobility underlies closure of the voltage-dependent anion channel. *Structure* 20, 1540–1549. doi: 10.1016/j.str.2012.06.015

Zeth, K., and Thein, M. (2010). Porins in prokaryotes and eukaryotes: common themes and variations. *Biochem. J.* 431, 13–22. doi: 10.1042/BJ20100371

Conflict of Interest Statement: The authors declare that the research was conducted in the absence of any commercial or financial relationships that could be construed as a potential conflict of interest.

frontiers in Physiology

MINI REVIEW
published: 19 December 2017
doi: 10.3389/fphys.2017.01089

Proton-Translocating Nicotinamide Nucleotide Transhydrogenase: A Structural Perspective

Qinghai Zhang, Pius S. Padayatti and Josephine H. Leung*

Department of Integrative Structural and Computational Biology, The Scripps Research Institute, La Jolla, CA, United States

Nicotinamide nucleotide transhydrogenase (TH) is an enzyme complex in animal mitochondria and bacteria that utilizes the electrochemical proton gradient across membranes to drive the production of NADPH. The enzyme plays an important role in maintaining the redox balance of cells with implications in aging and a number of human diseases. TH exists as a homodimer with each protomer containing a proton-translocating transmembrane domain and two soluble nucleotide binding domains that mediate hydride transfer between NAD(H) and NADP(H). The three-domain architecture of TH is conserved across species but polypeptide composition differs substantially. The complex domain coupling mechanism of TH is not fully understood despite extensive biochemical and structural characterizations. Herein the progress is reviewed, focusing mainly on structural findings from 3D crystallization of isolated soluble domains and more recently of the transmembrane domain and the holo-enzyme from *Thermus thermophilus*. A structural perspective and impeding challenges in further elucidating the mechanism of TH are discussed.

Keywords: hydride transfer, lipidic cubic phase, membrane protein, nucleotide binding, NADPH, proton channel, transhydrogenase, X-ray crystallography

OPEN ACCESS

Edited by:
Mario Diaz,
Universidad de La Laguna, Spain

Reviewed by:
Luis Gonzalo Cuello,
Texas Tech University Health Sciences Center, United States
Ian Kerr,
University of Nottingham, United Kingdom

****Correspondence:***
Qinghai Zhang
qinghai@scripps.edu

Specialty section:
This article was submitted to Membrane Physiology and Membrane Biophysics, a section of the journal Frontiers in Physiology

Received: *07 July 2017*
Accepted: *11 December 2017*
Published: *19 December 2017*

Citation:
Zhang Q, Padayatti PS and Leung JH (2017) Proton-Translocating Nicotinamide Nucleotide Transhydrogenase: A Structural Perspective. Front. Physiol. 8:1089. doi: 10.3389/fphys.2017.01089

INTRODUCTION

Nicotinamide nucleotide transhydrogenase (TH) is a key enzyme residing in mitochondrial inner membrane and bacterial cytoplasmic membrane that helps to maintain cellular redox balance through the following reaction:

$$H^{+}{}_{out} + NADP^{+} + NADH \leftrightarrow H^{+}{}_{in} + NADPH + NAD^{+}$$

In this reaction, proton motive force across the membrane is utilized to drive hydride transfer from NADH to $NADP^{+}$, resulting in the generation of NADPH under most physiological conditions (Jackson, 2003). TH is estimated to account for the generation of about 40% of NADPH in *E. coli* and an even higher percentage in the mitochondria of vertebrates (Sauer et al., 2004; Rydström, 2006a). Mitochondria utilize NADPH to maintain high levels of glutathione, a key component in cellular defense against the accumulation of reactive oxygen species which are implicated in many pathological conditions, such as cancer, diabetes, hypertension, heart disease, Alzheimer's, and Parkinson's diseases, as well as cell death and aging (Rydström, 2006b; Albracht et al., 2011; Gameiro et al., 2013; Ghosh et al., 2014; Lopert and Patel, 2014; Picard et al., 2015; Ho et al., 2017). Animal model and clinical investigations have indicated that some of these conditions can be attributed to the dysfunction or misexpression of TH (Heiker et al., 2013; Nickel et al., 2015; Roucher-Boulez et al., 2016; Leskov et al., 2017; Santos et al., 2017; Scott et al., 2017).

Mutations in the enzyme have also been shown in patients with glucocorticoid deficiency syndrome (Meimaridou et al., 2012; Fujisawa et al., 2015; Weinberg-Shukron et al., 2015).

TH is a complex multi-domain protein arranged as a dimer, where each protomer has two soluble domains and a transmembrane domain (**Figure 1**) (Leung et al., 2015). Extensive biochemical and structural characterizations have essentially established the domain architecture, the catalytic reaction sites as well as the proton translocating pathway as will be discussed in this review. The soluble domains are located in the mitochondrial matrix or prokaryotic cytosol and include a 40 kDa NAD(H)-binding domain (domain I) and a 20 kDa NADP(H)-binding domain (domain III) which together catalyze the hydride transfer reaction. The 40 kDa transmembrane domain (domain II) forms the proton translocation channel. This three-domain architecture is universally conserved, suggesting a common mechanism for function. However, TH topologies and sequences vary substantially among species. For example, human TH is encoded by a single polypeptide chain, whereas TH from *E. coli* and *T. thermophilus* are encoded by two and three polypeptide chains, respectively. In *E. coli* TH, domain I and the first four transmembrane helices (TM 1–4) of domain II are encoded by one gene α, whereas in *T. thermophilus, two* separate genes (α1 and α2) encode domain I and the first three TM helices (TM 2–4) of domain II; the remaining TM helices (TM 6–14) of domain II together with domain III in both species are encoded by gene β. Of note, domain II differs in the number of TM helices in different species, for example, with 14 for human, 13 for *E. coli* and 12 for *T. thermophilus*. To date, most functional and structural characterizations have been performed on TH from lower organisms (Pedersen et al., 2008; Jackson, 2012), and it will be interesting to learn how function is conducted in TH from higher organisms with evolved sequences, and how mutations in human TH cause disease.

Mechanistic understanding of TH has been advanced significantly by the structure determinations of isolated soluble domains and more recently of the transmembrane domain and the holo-enzyme from *T. thermophilus* (Leung et al., 2015; Padayatti et al., 2017). The architecture of the three domains of TH is explicitly established with the NADP(H)-binding domain III sandwiched between domains I and II and showing significant conformational mobility. A novel mechanism of domain III swiveling has been proposed for its communication with each of the other two domains alternately within the biological dimer (Jackson et al., 2015). This manuscript will review progress in determining TH structure, new mechanistic insights that have resulted, and some questions that remain in order to fully elucidate the conformational dynamics and mechanism by which proton translocation is coupled to hydride transfer events that occur remotely.

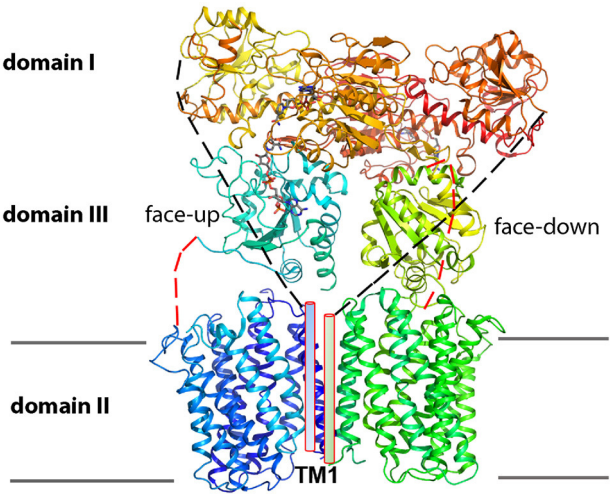

FIGURE 1 | Architecture of holo-TH. TH varies in polypeptide compositions in different species but displays an overall conserved domain architecture. The cartoon is based on a holo-TH crystal structure from *T. thermophilus* (PDB: 4O9U), shown as a dimer with three domains. Domain I and domain III protrude from membrane-intercalated domain II (membrane boundaries in gray line), with domain III placed in the middle. A linker of 14–19 amino acids (red dashed lines), which is not revealed in 4O9U, connects domain II and III in all TH homologs. Domain I is expressed as a single polypeptide in *T. thermophilus*, but in mitochondrial TH it is fused with domain II through a linker (black dashed lines) and an additional TM1 (rod).

STRUCTURES OF NUCLEOTIDE BINDING DOMAINS I AND III

Individual crystal structures of the two soluble domains of TH showed overall similarity across multiple species including human, bovine, *E. coli*, and *R. rubrum* (Prasad et al., 1999, 2002; White et al., 2000; Sundaresan et al., 2003; Johansson et al., 2005). Domain I is present as a dimer in solution and always crystallized as such, with the dimeric interface stabilized by a swapping beta-hairpin structure and two helices. Each monomer of domain I has two subdomains with the characteristic nucleotide binding Rossmann fold (Rossmann et al., 1974); yet only one of the subdomains actually binds NAD(H). Thus, in the domain I dimer that adopts a two-fold axis symmetry, the two NAD(H) binding sites are situated on opposite sides. In comparison, domain III is about half the size of domain I, also adopts the Rossmann fold for NADP(H) binding, but only exists as a monomer in solution. Of note, the orientation of NADP(H) in the binding pocket of domain III is flipped relative to that of NAD(H) in domain I.

Local conformational changes are observed in nucleotide-binding regions in domain I and domain III. Various modes of NAD(H) binding such as open, intermediate, and closed forms have been demonstrated, both in domain I structures and the apo structures (Prasad et al., 2002; Johansson et al., 2005). In *E. coli* TH holoenzyme, the dissociation constant (Kd) for NAD^+ is 100–500 μM and that for NADH is 50 μM, comparable to values for the isolated domain I (Bizouarn et al., 2005). Domain III has hitherto only been crystallized in the presence of NADP(H), with loop D either in open or closed conformation (Prasad et al., 1999; White et al., 2000; Sundaresan et al., 2003). Notably, NADP(H) has extremely high binding affinity with the isolated domain III (apparent Kd value < nM) (Diggle et al., 1995; Fjellstrom et al., 1997; Peake et al.,

1999), which is partly attributed to adjacent loop E folding over NADP(H) like a lid. Interestingly, for domain III in the intact *E. coli* TH, the binding affinity of NADP(H) is orders of magnitude weaker: the Kd values are 16 μM for $NADP^+$ and 0.87 μM for NADPH (Bizouarn et al., 2005). It is not understood why the binding affinity of NADP(H) differs so widely between isolated domain III and the intact TH, but existing data suggest that the NADP(H)-binding site is affected by protein-protein interactions between domain III and other domains. For completion of the TH catalytic cycle, all nucleotide reactants must bind and products must dissociate from the binding sites. The holoenzyme likely uses protein conformational changes to alter nucleotide binding affinities and move the reaction (Jackson, 2012).

STRUCTURES OF DOMAIN I AND DOMAIN III IN COMPLEX

Co-crystallization of isolated domains I and III either from *R. rubrum* or *T. thermophilus* consistently yields a heterotrimeric complex at a 2:1 ratio (**Figure 2A**) (Cotton et al., 2001; Mather et al., 2004; Sundaresan et al., 2005; Bhakta et al., 2007; Leung et al., 2015). This stoichiometry agrees with findings in solution (Venning et al., 1998, 2001). The Kd of domain III binding to the domain I dimer is < 60 nM (Venning et al., 2001), while a second domain III binds with significantly lower affinity (Kd about 10^{-5} M) (Quirk et al., 1999). In the heterotrimeric structures, the two domain I components adopt the same two-fold axis as in the isolated domain I dimer structure, with similar protein fold and contact regions between the polypeptides; in addition a domain III is placed underneath one domain I subunit with the NADP(H) binding site face up. However, using the same two-fold axis to model a second "face-up" domain III into the void space under the other domain I subunit results in a steric clash between the two domain III subunits. This leaves a question of how the second domain III is made to fit in the dimeric structure of the holo-TH.

The heterotrimeric structures of domain I and domain III reveal proximity between the NAD(H) and NADP(H) binding sites (**Figure 2A**). In these structures, the single copy of domain III is inserted into the NAD(H)-binding cleft of one of the domain I subunits, and the flipped orientation of NADP(H) in domain III apparently facilitates a direct hydride transfer between the nicotinamide rings of NAD(H) and NADP(H) when the two ligands get close. Local conformational changes in the NAD(H) binding site as well as relative movement between the two subdomains within domain I appear to cause a "distal-to-proximal" motion of bound NAD(H) (Mather et al., 2004).

STRUCTURES OF TRANSMEMBRANE DOMAIN II

Structural determination of the transmembrane domain of TH has recently been achieved by the use of lipidic cubic phase (LCP) crystallization (Leung et al., 2015; Padayatti et al., 2017). The LCP is a viscous bilayer matrix that is thought to better stabilize membrane proteins than detergents and more frequently results in a tighter and layered crystal packing (Caffrey and Cherezov, 2009). LCP crystallization succeeded for a truncated *T. thermophilus* TH domain II construct (containing two hydrophobic polypeptide chains: subunit α_2 and a truncated version of subunit β from which the soluble domain III was removed from the C-terminus), using 1-(8*Z*-pentadecenoyl)-*rac*-glycerol (MAG 8.7) as the host lipid. Compared to the commonly used monoolein (MAG 9.9), MAG 8.7 has a shorter alkyl chain and tends to form a more fluidic cubic phase.

Domain II was crystallized at pH 8.5 and 6.5, respectively, and the solved crystal structures both appear as a dimer with TM2-TM2 association at the interface (**Figure 2B**). The two structures

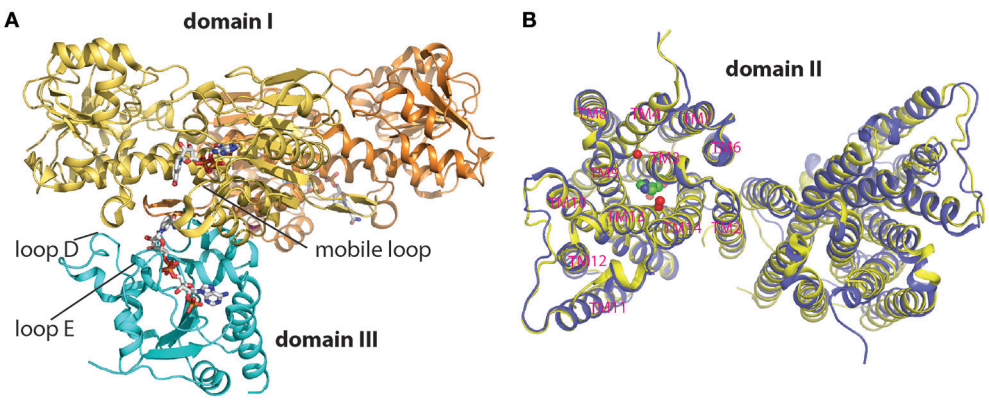

FIGURE 2 | Reaction catalysis and proton-translocating sites in TH. **(A)** Hydride transfer between the proximate NAD(H) and NADP(H) binding sites of domains I and III. Shown is a nucleotide-bound (sticks), trimeric (domain I)$_2$:(domain III) structure of TH from *T. thermophilus* (PDB: 4J16), with the NADP(H) binding site in domain III (cyan) facing up. Flexible loops involved in ligand binding are indicated. **(B)** Proton translocation in domain II. Domain II dimerization (from *T. thermophilus*) is mediated by TM2-TM2 interaction. Displacement of the second subunit is observed by the alignment of the two structures (PDB: 5UNI, blue; 4O93, yellow) solved under different pH conditions. Crystallographically solved water molecules (red balls) and the channel gating histidine residue (His42$^{\alpha 2}$ on TM3, green sphere) are shown inside the proton channel within one subunit of 5UNI. Structures shown represent a view from the cytoplasmic side.

are quite similar overall, although alignment shows a slight displacement of the second domain II monomer, suggesting a degree of conformational flexibility to the association; yet at this stage no evidence is found for a substantial conformational change related to channel opening or closure. The crystal structures also reveal a putative channel surrounded by six TM helices (TM 3, 4, 9, 10, 13, and 14). It should be noted that these channel-forming helices and the TM2 at the dimeric interface are highly conserved among species, suggesting a common proton translocation pathway and possibly a similar mode of dimerization despite considerable homolog variation in the organization of this domain II (e.g., the presence of extra TM1 and TM5 in human TH).

The pH 6.5 crystal structure solved at a resolution of 2.1 Å revealed water molecules inside the TM helix bundles, which, in combination with molecular dynamics (MD) simulations, allows a clearer interpretation of the proton translocation channel and its key functional residues (**Figure 2B**) (Padayatti et al., 2017). A cluster of polar residues including a central histidine ($His42^{\alpha2}$) form an extended H-bonded network together with two bound water molecules in the cytoplasmic half of the channel, and this connection likely provides a proton conduit to the cytoplasmic side. A central role for $His42^{\alpha2}$ in proton translocation by TH is consistent with extensive biochemical characterizations; the central histidine is conserved in other TH species although its position may shift (Olausson et al., 1995; Rydström et al., 1998; Bragg and Hou, 2001; Yamaguchi et al., 2002). MD simulation showed that a water conduit is formed only when $His42^{\alpha2}$ is protonated. Gating of the isolated channel appears to be controlled by $His42^{\alpha2}$ protonation and also a distinct hydrophobic barrier region spanning about 7.5 Å below $His42^{\alpha2}$ in the middle of the channel. The presence of this long stretch of hydrophobic region for proton gating is remarkable for TH, in contrast to the water penetration through thin hydrophobic layers known for some other proton channels (Pielak and Chou, 2011; Takeshita et al., 2014; Thomaston et al., 2017). During MD simulations, a transient water wire is formed connecting $His42^{\alpha2}$ and $Glu221^{\beta}$ through the hydrophobic barrier, and the presence of the water wire coincides with a conformational change of $Thr214^{\beta}$ side chain located slightly below $His42^{\alpha2}$. Mutation of $Thr214^{\beta}$ to Ala causes >90% loss of channel-coupled enzymatic activity, biochemically supporting the proposed role of $Thr214^{\beta}$ in proton translocation (Padayatti et al., 2017).

The domain II structure further shows formation of a salt bridge between $Asp202^{\beta}$ on the cytosolic end of TM13 and $Arg254^{\beta}$ at the start of the linker region connecting domain II and domain III. This linkage is positioned on the membrane surface adjacent to the entrance of the proton channel. The Asp-Arg salt bridge at equivalent positions in *E. coli* TH ($Asp213^{\beta}$ and $Arg265^{\beta}$) has been postulated and implicated as important for both proton translocation in domain II and NADP(H) binding in domain III (Althage et al., 2001; Bragg and Hou, 2001; Yamaguchi et al., 2002). Since in TH of various species the sequence of domain II always exists in conjunction with domain III (**Figure 1**), regulation of domain III movement may be directly linked to domain II and the proton channel activity, and vice versa.

HOLO-TH STRUCTURES

A holo-TH structure from *T. thermophilus* has recently been solved in detergent micelles, albeit only at 6.93 Å resolution (**Figure 1**) (Leung et al., 2015). This low resolution structure seemingly reflects substantial conformational flexibility of the complex protein and the significant challenge in identifying suitable crystallization conditions. The soluble domain I dimer and membrane-intercalated domain II components in the holo-TH are roughly aligned with individually obtained domain structures. A remarkable realization from this structure is the asymmetric orientation of two domain III subunits, one being flipped ∼180°C relative to the other. This distinct domain III arrangement in the dimeric TH brings one NADP(H) binding site close to the NAD(H) binding site of domain I, as shown in the heterotrimeric $(\text{domain I})_2$-domain III structures, while the other NADP(H) binding site faces down to approach the channel surface of domain II. The two orientations of domain III are supported by disulfide cross-linking of inserted cysteine pairs on separate domains (Leung et al., 2015). The flipped orientation of domain III also appears to coincide with that observed in the crystal packing of $(\text{domain I})_2$-domain III structures where a crystallographic symmetry mate of domain III is similarly facing down (Sundaresan et al., 2005; Bhakta et al., 2007). Consistent with crystal structures, cryogenic electron microscopy (EM) images (∼18 Å) of the holo-TH confirm an asymmetric organization of TH dimers in non-crystalline conditions (Leung et al., 2015). Cryo-EM structures also suggest that one subunit of domain III is more disordered than the other as evidenced by much weaker electron density. While a further high-resolution structure of holo-TH is warranted, based on current structural findings, the two copies of domain III have been proposed to play distinct functional roles in coupling to proton translocation in domain II and in hydride transfer from/to domain I (Jackson et al., 2015).

PERSPECTIVE AND CONCLUDING REMARKS

The mechanistic understanding of mitochondria TH has benefited from extensive structural and biochemical characterizations of isolated domains and homolog proteins, particularly those from lower organisms. The use of stably expressed and purified TH from *T. thermophilus* has resulted in the recent structural determinations of the membrane-intercalated domain II and holo-TH. For the latter, higher-resolution structural determinations of the large multidomain membrane protein complex remain a significant challenge due to its significant conformational flexibility/heterogeneity. The solved holo-TH structure in detergents is of low resolution and lacks information for the linker (14–19 amino acids present in all TH) that connects domain II and domain III, and which is supposedly important to mediate the two domain interactions and the rotation of domain III as well. Modeling of human TH structure based on homologs is challenging given the significant sequence disparity, especially

for domain II because of the presence of extra TM segments in the human enzyme (Metherell et al., 2016). The fusion of all three domains in a single polypeptide chain in human TH may impact its conformational landscape and energetics as well, although a common mechanism of the TH-catalyzed enzymatic reactions is expected for different species. At present, our understanding of the dynamic domain coupling and movements in TH is still very limited and mostly hypothetical. Structural insights into the mechanism of a dynamic TH will thus require the structural determinations of the protein complex in many conformational states. Recent technological breakthroughs in X-ray crystallography and cryo-EM have helped solve structures of many difficult-to-study systems. The use of novel lipid bilayer mimetics such as LCP (Caffrey, 2015) and nanodiscs (Denisov and Sligar, 2017) in the structural determinations of membrane proteins has gained popularity in addition to the traditional use of detergents. With the application and integration of these advanced techniques with new tools in TH studies, we anticipate that a comprehensive and detailed structural and mechanistic understanding can be achieved for this fundamentally important enzyme in many kingdoms of life.

AUTHOR CONTRIBUTIONS

All authors listed have made a substantial, direct and intellectual contribution to the work, and approved it for publication.

FUNDING

This work was supported by the National Institutes of Health (5R01GM103838).

REFERENCES

Albracht, S. P., Meijer, A. J., and Rydstrom, J. (2011). Mammalian NADH:ubiquinone oxidoreductase (Complex I) and nicotinamide nucleotide transhydrogenase (Nnt) together regulate the mitochondrial production of H(2)O(2)–implications for their role in disease, especially cancer. *J. Bioenerg. Biomembr.* 43, 541–564. doi: 10.1007/s10863-011-9381-4

Althage, M., Bizouarn, T., and Rydström, J. (2001). Identification of a region involved in the communication between the NADP(H) binding domain and the membrane domain in proton pumping *E-coli* transhydrogenase. *Biochemistry* 40, 9968–9976. doi: 10.1021/bi0103157

Bhakta, T., Whitehead, S. J., Snaith, J. S., Dafforn, T. R., Wilkie, J., Rajesh, S., et al. (2007). Structures of the dI2dIII1 complex of proton-translocating transhydrogenase with bound, inactive analogues of NADH and NADPH reveal active site geometries. *Biochemistry* 46, 3304–3318. doi: 10.1021/bi061843r

Bizouarn, T., van Boxel, G. I., Bhakta, T., and Jackson, J. B. (2005). Nucleotide binding affinities of the intact proton-translocating transhydrogenase from *Escherichia coli*. *Biochim. Biophys. Acta* 1708, 404–410. doi: 10.1016/j.bbabio.2005.04.004

Bragg, P. D., and Hou, C. (2001). Characterization of mutants of beta histidine91, beta aspartate213, and beta asparagine222, possible components of the energy transduction pathway of the proton-translocating pyridine nucleotide transhydrogenase of *Escherichia coli*. *Arch. Biochem. Biophys.* 388, 299–307. doi: 10.1006/abbi.2001.2298

Caffrey, M. (2015). A comprehensive review of the lipid cubic phase or in meso method for crystallizing membrane and soluble proteins and complexes. *Acta Crystallogr. F Struct. Biol. Commun.* 71(Pt 1), 3–18. doi: 10.1107/S2053230X14026843

Caffrey, M., and Cherezov, V. (2009). Crystallizing membrane proteins using lipidic mesophases. *Nat. Protoc.* 4, 706–731. doi: 10.1038/nprot.2009.31

Cotton, N. P., White, S. A., Peake, S. J., McSweeney, S., and Jackson, J. B. (2001). The crystal structure of an asymmetric complex of the two nucleotide binding components of proton-translocating transhydrogenase. *Structure* 9, 165–176. doi: 10.1016/S0969-2126(01)00571-8

Denisov, I. G., and Sligar, S. G. (2017). Nanodiscs in membrane biochemistry and biophysics. *Chem. Rev.* 117, 4669–4713. doi: 10.1021/acs.chemrev.6b00690

Diggle, C., Hutton, M., Jones, G. R., Thomas, C. M., and Jackson, J. B. (1995). Properties of the soluble polypeptide of the proton-translocating transhydrogenase from rhodospirillum-rubrum obtained by expression in *Escherichia-Coli*. *Eur. J. Biochem.* 228, 719–726. doi: 10.1111/j.1432-1033.1995.tb20315.x

Fjellström, O., Johansson, C., and Rydström, J. (1997). Structural and catalytic properties of the expressed and purified NAD(H)- and NADP(H)-binding domains of proton-pumping transhydrogenase from *Escherichia coli*. *Biochemistry* 36, 11331–11341. doi: 10.1021/bi970958f

Fujisawa, Y., Napoli, E., Wong, S., Song, G., Yamaguchi, R., Matsui, T., et al. (2015). Impact of a novel homozygous mutation in nicotinamide nucleotide transhydrogenase on mitochondrial DNA integrity in a case of familial glucocorticoid deficiency. *BBA Clin.* 3, 70–78. doi: 10.1016/j.bbacli.2014.12.003

Gameiro, P. A., Laviolette, L. A., Kelleher, J. K., Iliopoulos, O., and Stephanopoulos, G. (2013). Cofactor balance by nicotinamide nucleotide transhydrogenase (NNT) coordinates reductive carboxylation and glucose catabolism in the tricarboxylic acid (TCA) cycle. *J. Biol. Chem.* 288, 12967–12977. doi: 10.1074/jbc.M112.396796

Ghosh, D., Levault, K. R., and Brewer, G. J. (2014). Relative importance of redox buffers GSH and NAD(P)H in age-related neurodegeneration and Alzheimer disease-like mouse neurons. *Aging Cell* 13, 631–640. doi: 10.1111/acel.12216

Heiker, J. T., Kern, M., Kosacka, J., Flehmig, G., Stumvoll, M., Shang, E., et al. (2013). Nicotinamide nucleotide transhydrogenase mRNA expression is related to human obesity. *Obesity* 21, 529–534. doi: 10.1002/oby.20095

Ho, H. Y., Lin, Y. T., Lin, G., Wu, P. R., and Cheng, M. L. (2017). Nicotinamide nucleotide transhydrogenase (NNT) deficiency dysregulates mitochondrial retrograde signaling and impedes proliferation. *Redox Biol.* 12, 916–928. doi: 10.1016/j.redox.2017.04.035

Jackson, J. B. (2003). Proton translocation by transhydrogenase. *FEBS Lett.* 545:7. doi: 10.1016/S0014-5793(03)00224-2

Jackson, J. B. (2012). A review of the binding-change mechanism for proton-translocating transhydrogenase. *Biochim. Biophys. Acta* 1817, 1839–1846. doi: 10.1016/j.bbabio.2012.04.006

Jackson, J. B., Leung, J. H., Stout, C. D., Schurig-Briccio, L. A., and Gennis, R. B. (2015). Review and Hypothesis. New insights into the reaction mechanism of transhydrogenase: swivelling the dIII component may gate the proton channel. *FEBS Lett.* 589, 2027–2033. doi: 10.1016/j.febslet.2015.06.027

Johansson, T., Oswald, C., Pedersen, A., Tornroth, S., Okvist, M., Karlsson, B. G., et al. (2005). X-ray structure of domain I of the proton-pumping membrane protein transhydrogenase from *Escherichia coli*. *J. Mol. Biol.* 352, 299–312. doi: 10.1016/j.jmb.2005.07.022

Leskov, I., Neville, A., Shen, X., Pardue, S., Kevil, C. G., Granger, D. N., et al. (2017). Nicotinamide nucleotide transhydrogenase activity impacts mitochondrial redox balance and the development of hypertension in mice. *J. Am. Soc. Hypertens.* 11, 110–121. doi: 10.1016/j.jash.2016.12.002

Leung, J. H., Schurig-Briccio, L. A., Yamaguchi, M., Moeller, A., Speir, J. A., Gennis, R. B., et al. (2015). Division of labor in transhydrogenase by alternating proton translocation and hydride transfer. *Science* 347, 178–181. doi: 10.1126/science.1260451

Lopert, P., and Patel, M. (2014). Nicotinamide nucleotide transhydrogenase (Nnt) links the substrate requirement in brain mitochondria for hydrogen peroxide removal to the thioredoxin/peroxiredoxin (Trx/Prx) system. *J. Biol. Chem.* 289, 15611–15620. doi: 10.1074/jbc.M113.533653

Mather, O. C., Singh, A., van Boxel, G. I., White, S. A., and Jackson, J. B. (2004). Active-site conformational changes associated with hydride transfer

in proton-translocating transhydrogenase. *Biochemistry* 43, 10952–10964. doi: 10.1021/bi0497594

Meimaridou, E., Kowalczyk, J., Guasti, L., Hughes, C. R., Wagner, F., Frommolt, P., et al. (2012). Mutations in NNT encoding nicotinamide nucleotide transhydrogenase cause familial glucocorticoid deficiency. *Nat. Genet.* 44, 740–742. doi: 10.1038/ng.2299

Metherell, L. A., Guerra-Assunção, J. A., Sternberg, M. J., and David, A. (2016). Three-dimensional model of human nicotinamide nucleotide transhydrogenase (NNT) and sequence-structure analysis of its disease-causing variations. *Hum. Mutat.* 37, 1074–1084. doi: 10.1002/humu.23046

Nickel, A. G., von Hardenberg, A., Hohl, M., Loffler, J. R., Kohlhaas, M., Becker, J., et al. (2015). Reversal of mitochondrial transhydrogenase causes oxidative stress in heart failure. *Cell Metab.* 22, 472–484. doi: 10.1016/j.cmet.2015.07.008

Olausson, T., Fjellström, O., Meuller, J., and Rydström, J. (1995). Molecular biology of nicotinamide nucleotide transhydrogenase–a unique proton pump. *Biochim. Biophys. Acta* 1231, 1–19. doi: 10.1016/0005-2728(95)00058-Q

Padayatti, P. S., Leung, J. H., Mahinthichaichan, P., Tajkhorshid, E., Ishchenko, A., Cherezov, V., et al. (2017). Critical role of water molecules in proton translocation by the membrane-bound transhydrogenase. *Structure* 25, 1111–1119.e3. doi: 10.1016/j.str.2017.05.022

Peake, S. J., Venning, J. D., and Jackson, J. B. (1999). A catalytically active complex formed from the recombinant dI protein of *Rhodospirillum rubrum* transhydrogenase, and the recombinant dIII protein of the human enzyme. *Biochim. Biophys. Acta* 1411, 159–169. doi: 10.1016/S0005-2728(99)00013-4

Pedersen, A., Karlsson, G. B., and Rydström, J. (2008). Proton-translocating transhydrogenase: an update of unsolved and controversial issues. *J. Bioenerg. Biomembr.* 40, 463–473. doi: 10.1007/s10863-008-9170-x

Picard, M., McManus, M. J., Gray, J. D., Nasca, C., Moffat, C., Kopinski, P. K., et al. (2015). Mitochondrial functions modulate neuroendocrine, metabolic, inflammatory, and transcriptional responses to acute psychological stress. *Proc. Natl. Acad. Sci. U.S.A.* 112, E6614–E6623. doi: 10.1073/pnas.1515733112

Pielak, R. M., and Chou, J. J. (2011). Influenza M2 proton channels. *Biochim. Biophys. Acta* 1808, 522–529. doi: 10.1016/j.bbamem.2010.04.015

Prasad, G. S., Sridhar, V., Yamaguchi, M., Hatefi, Y., and Stout, C. D. (1999). Crystal structure of transhydrogenase domain III at 1.2 A resolution. *Nat. Struct. Biol.* 6, 1126–1131. doi: 10.1038/70067

Prasad, G. S., Wahlberg, M., Sridhar, V., Sundaresan, V., Yamaguchi, M., Hatefi, Y., et al. (2002). Crystal structures of transhydrogenase domain I with and without bound NADH. *Biochemistry* 41, 12745–12754. doi: 10.1021/bi020251f

Quirk, P. G., Jeeves, M., Cotton, N. P., Smith, J. K., and Jackson, B. J. (1999). Structural changes in the recombinant, NADP(H)-binding component of proton translocating transhydrogenase revealed by NMR spectroscopy. *FEBS Lett.* 446, 127–132. doi: 10.1016/S0014-5793(99)00198-2

Rossmann, M. G., Moras, D., and Olsen, K. W. (1974). Chemical and biological evolution of nucleotide-binding protein. *Nature* 250, 194–199. doi: 10.1038/250194a0

Roucher-Boulez, F., Mallet-Motak, D., Samara-Boustani, D., Jilani, H., Ladjouze, A., Souchon, P. F., et al. (2016). NNT mutations: a cause of primary adrenal insufficiency, oxidative stress and extra-adrenal defects. *Eur. J. Endocrinol.* 175, 73–84. doi: 10.1530/EJE-16-0056

Rydström, J. (2006a). Mitochondrial NADPH, transhydrogenase and disease. *Biochim. Biophys. Acta* 1757, 721–726. doi: 10.1016/j.bbabio.2006.03.010

Rydström, J. (2006b). Mitochondrial transhydrogenase - a key enzyme in insulin secretion and, potentially, diabetes. *Trends Biochem. Sci.* 31, 355–358. doi: 10.1016/j.tibs.2006.05.003

Rydström, J., Hu, X., Fjellstrom, O., Meuller, J., Zhang, J., Johansson, C., et al. (1998). Domains, specific residues and conformational states involved in hydride ion transfer and proton pumping by nicotinamide nucleotide transhydrogenase from *Escherichia coli*. *Biochim. Biophys. Acta* 1365, 10–16. doi: 10.1016/S0005-2728(98)00038-3

Santos, L. R. B., Muller, C., de Souza, A. H., Takahashi, H. K., Spégel, P., Sweet, I. R., et al. (2017). NNT reverse mode of operation mediates glucose control of mitochondrial NADPH and glutathione redox state in mouse pancreatic beta-cells. *Mol. Metab.* 6, 535–547. doi: 10.1016/j.molmet.2017.04.004

Sauer, U., Canonaco, F., Heri, S., Perrenoud, A., and Fischer, E. (2004). The soluble and membrane-bound transhydrogenases UdhA and PntAB have divergent functions in NADPH metabolism of *Escherichia coli*. *J. Biol. Chem.* 279, 6613–6619. doi: 10.1074/jbc.M311657200

Scott, R., Van Vliet, G., and Deladoëy, J. (2017). Association of adrenal insufficiency with insulin-dependent diabetes mellitus in a patient with inactivating mutations in nicotinamide nucleotide transhydrogenase: a phenocopy of the animal model. *Eur. J. Endocrinol.* 176, C1–C2. doi: 10.1530/EJE-16-0970

Sundaresan, V., Chartron, J., Yamaguchi, M., and Stout, C. D. (2005). Conformational diversity in NAD(H) and interacting transhydrogenase nicotinamide nucleotide binding domains. *J. Mol. Biol.* 346, 617–629. doi: 10.1016/j.jmb.2004.11.070

Sundaresan, V., Yamaguchi, M., Chartron, J., and Stout, C. D. (2003). Conformational change in the NADP(H) binding domain of transhydrogenase defines four states. *Biochemistry* 42, 12143–12153. doi: 10.1021/bi035006q

Takeshita, K., Sakata, S., Yamashita, E., Fujiwara, Y., Kawanabe, A., Kurokawa, T., et al. (2014). X-ray crystal structure of voltage-gated proton channel. *Nat. Struct. Mol. Biol.* 21, 352–357. doi: 10.1038/nsmb.2783

Thomaston, J. L., Woldeyes, R. A., Nakane, T., Yamashita, A., Tanaka, T., Koiwai, K., et al. (2017). XFEL structures of the influenza M2 proton channel: room temperature water networks and insights into proton conduction. *Proc. Natl. Acad. Sci. U.S.A.* doi: 10.1073/pnas.1705624114. [Epub ahead of print].

Venning, J. D., Bizouarn, T., Cotton, N. P. J., Quirk, P. G., and Jackson, J. B. (1998). Stopped-flow kinetics of hydride transfer between nucleotides by recombinant domains of proton-translocating transhydrogenase. *Eur. J. Biochem.* 257, 202–209. doi: 10.1046/j.1432-1327.1998.2570202.x

Venning, J. D., Rodrigues, D. J., Weston, C. J., Cotton, N. P., Quirk, P. G., Errington, N., et al. (2001). The heterotrimer of the membrane-peripheral components of transhydrogenase and the alternating-site mechanism of proton translocation. *J. Biol. Chem.* 276, 30678–30685. doi: 10.1074/jbc.M104429200

Weinberg-Shukron, A., Abu-Libdeh, A., Zhadeh, F., Carmel, L., Kogot-Levin, A., Kamal, L., et al. (2015). Combined mineralocorticoid and glucocorticoid deficiency is caused by a novel founder nicotinamide nucleotide transhydrogenase mutation that alters mitochondrial morphology and increases oxidative stress. *J. Med. Genet.* 52, 636–641. doi: 10.1136/jmedgenet-2015-103078

White, S. A., Peake, S. J., McSweeney, S., Leonard, G., Cotton, N. P., and Jackson, J. B. (2000). The high-resolution structure of the NADP(H)-binding component (dIII) of proton-translocating transhydrogenase from human heart mitochondria. *Structure* 8, 1–12. doi: 10.1016/S0969-2126(00)00075-7

Yamaguchi, M., Stout, C. D., and Hatefi, Y. (2002). The proton channel of the energy-transducing nicotinamide nucleotide transhydrogenase of *Escherichia coli*. *J. Biol. Chem.* 277, 33670–33675. doi: 10.1074/jbc.M204170200

Conflict of Interest Statement: The authors declare that the research was conducted in the absence of any commercial or financial relationships that could be construed as a potential conflict of interest.

frontiers in Physiology

PERSPECTIVE
published: 09 November 2017
doi: 10.3389/fphys.2017.00892

Combining Mass Spectrometry and X-Ray Crystallography for Analyzing Native-Like Membrane Protein Lipid Complexes

*Felipe A. Montenegro†, Jorge R. Cantero† and Nelson P. Barrera**

Laboratory of Nanophysiology and Structural Biology, Department of Physiology, Faculty of Biological Sciences, Pontificia Universidad Católica de Chile, Santiago, Chile

Membrane proteins represent a challenging family of macromolecules, particularly related to the methodology aimed at characterizing their three-dimensional structure. This is mostly due to their amphipathic nature as well as requirements of ligand bindings to stabilize or control their function. Recently, Mass Spectrometry (MS) has become an important tool to identify the overall stoichiometry of native-like membrane proteins complexed to ligand bindings as well as to provide insights into the transport mechanism across the membrane, with complementary information coming from X-ray crystallography. This perspective article emphasizes MS findings coupled with X-ray crystallography in several membrane protein lipid complexes, in particular transporters, ion channels and molecular machines, with an overview of techniques that allows a more thorough structural interpretation of the results, which can help us to unravel hidden mysteries on the membrane protein function.

Keywords: mass spectrometry, native mass spectrometry, membrane protein, gas phase, ligand binding, molecular dynamics

OPEN ACCESS

Edited by:
Mario Diaz,
Universidad de La Laguna, Spain

Reviewed by:
Jesus Perez-Gil,
Complutense University of Madrid, Spain
Stefano Piotto,
University of Salerno, Italy

****Correspondence:***
Nelson P. Barrera
nbarrera@bio.puc.cl

†These authors have contributed equally to this work.

Specialty section:
This article was submitted to Membrane Physiology and Membrane Biophysics, a section of the journal Frontiers in Physiology

Received: *03 August 2017*
Accepted: *24 October 2017*
Published: *09 November 2017*

Citation:
Montenegro FA, Cantero JR and Barrera NP (2017) Combining Mass Spectrometry and X-Ray Crystallography for Analyzing Native-Like Membrane Protein Lipid Complexes. Front. Physiol. 8:892. doi: 10.3389/fphys.2017.00892

INTRODUCTION

Membrane proteins (MPs) are not merely inserted in the lipid bilayer. Besides interacting with ligands (which includes lipids, nucleotides, ions, and drugs) to regulate their stability and function; they do not work as independent entities, instead, they interact with other proteins to become membrane complexes that require a defined lipid environment to carry out their cellular transduction pathways. Given their relevance to cellular physiology, MPs comprise around 60% of drug targets (Overington et al., 2006).

Stoichiometry of ligands in intact MPs is key to understand their role on the proper biological function; however structural methods such as X-ray crystallography (Moraes et al., 2014) and solid-state nuclear magnetic resonance (NMR) spectroscopy (Ding et al., 2013) encounter experimental difficulties because of protein solubility/heterogeneity and need high resolution to properly assign the nature of the small molecules. Additionally, X-ray crystallography provides location of small molecules bound to MPs but structural refinement for disordered ligands could produce ambiguity for the complete characterization of the binding site (Marsh and Páli, 2004). Furthermore, proteins are fast and dynamic molecules which could interfere with the necessary symmetry on protein crystals, delivering a snapshot in a particular condition that can be crystallized (Dill and MacCallum, 2012). Therefore, complementary structural methods can provide relevant insights

into the nature of ligands bound to transmembrane (TM) regions. Especially, Mass Spectrometry (MS) has been widely used for small molecule identification in protein samples. However, only recently it has been applied to get simultaneously structural information on MPs and protein-ligand stoichiometry. Strikingly within only a few years MS on native-like MPs has characterized several transporters, ion channels, and molecular machines which contain specific small molecular species tightly bound to the TM domains (Barrera and Robinson, 2011; Bechara and Robinson, 2015).

In this perspective, we address current experimental methods, as well as the contribution of computational approaches, to study MPs and lipid-binding events, with a focus on recent MS findings in the field.

BIOPHYSICAL METHODS TO ANALYZE MEMBRANE PROTEIN-LIPID BINDING

Apart from X-ray crystallography and NMR spectroscopy, there are other complementary methods that can characterize protein ligand interactions, such as dissociation binding constants (surface plasmon resonance, SPR), kinetics or thermodynamics of such interaction (isothermal titration calorimetry, ITC), and intra and intermolecular distances <10 nm (Forster resonance energy transfer, FRET). Nevertheless, their use on testing lipid species has been rather challenging due to the low solubility in physiological conditions, in particular once lipids are added exogenously after protein purification. Atomic force microscopy (AFM) can render a surface 3D image of MPs at physiological conditions, and even tracking their fast-conformational changes. Combined with Force Spectroscopy measurements, intramolecular or ligand-binding interactions can be quantified at single-molecule level (Shahin and Barrera, 2008; Suzuki et al., 2013). While many biophysical methods have been extensively reviewed (Vuignier et al., 2010; Fang, 2012; Pacholarz et al., 2012) and continuously developed for tackling the identification of ligand binding events in proteins, the vast majority of these reviews focus on drug discovery. Therefore, research focused on structural biology of cellular ligand-binding events in intact MPs has been just recently expanding.

An interesting example of an MP analyzed by a series of structural experimental techniques is the small multidrug resistance transporter EmrE (**Figure 1**). Traditional methods such as cryo-electron microscopy (cryo-EM) and X-ray crystallography have resolved the structure of the EmrE dimer topology (Chen et al., 2007; Korkhov and Tate, 2008). Further analyses of the intact dimer have shown stoichiometric lipid binding and posttranslational modifications (PTMs) by MS (Barrera et al., 2009) and identification of a specific residue involved in the substrate binding site of tetraphenylphosphonium by magic angle spinning-NMR (Ong et al., 2013). The interaction between annular lipids and EmrE has also been tested using Brewster angle microscopy (Nathoo et al., 2013), which showed longer unsaturated chains of cardiolipin (CL) forming the most stable monolayer in the presence of EmrE. Once a MP-ligand complex has been identified, especially for those lipids already co-purified from a cellular expression system, complementary results for their effect over soluble ligand binding can be provided by AFM, SPR, ITC, and FRET. Altogether, these experimental techniques could benefit from theoretical studies including Molecular Dynamics simulations (MDS) and steered MD (SMD) for the lipid-membrane protein interactions (Kalinin et al., 2012; Shoura et al., 2014). It is becoming clear that a better in-depth understanding of the binding process requires a combination of different structural techniques, involving unambiguous identification of the ligand, its atomic location and dynamic mechanisms of the binding event.

MASS SPECTROMETRY ON LIPID BINDING TO NATIVE-LIKE MEMBRANE PROTEINS

MS has evolved from an analytical chemistry method to a structural biology technique. It requires an ionized sample in vacuum, going through electromagnetic fields, and being identified by their mass/charge ratio. MS uses two main technologies for ionization: MALDI (matrix adsorbed laser desorption ionization) or ESI (electrospray ionization). Of those, ESI -which relies on electric-induced droplet formation and desolvation- has been the most employed in structural studies of biomolecules since it can be easily coupled to liquid chromatography (LC-MS) and facilitate the structural integrity of the protein in vacuum (Konermann et al., 2014).

Back in 2001, Cohen and Chait reviewed the use of MS during different stages of protein crystallization as a help tool for identification of proteins (via peptide mapping) or domain cores; the detection of PTMs and examining degradation/oxidation of proteins after crystallization over long periods of time (Cohen and Chait, 2001). In those days, MS used inert gas to trigger the fragmentation of selected ion peptides (process denominated tandem MS, or MS/MS).

Since the last decade, MS has been extensively used for intact membrane macromolecular complexes to determine their stoichiometry, subunit arrangement, binding events and PTMs (Barrera et al., 2009; Wang et al., 2010; Zhou et al., 2011; Laganowsky et al., 2014; Gault et al., 2016). For MPs, several approaches to mimic the membrane environment have been used. The first approach to study native-like MP complexes was achieved using detergents in high concentrations (Barrera et al., 2008). The inert gas previously used for fragmentation, is now used to destroy the micelle, thus releasing an MP complex for native MS analysis, a process diagramed in **Figure 2A**. Considering that micelles only mimic the hydrophobic section of the membrane, other approaches to mimic a cell membrane were used in the following years (amphipols, bicelles, nanodiscs) (Marty et al., 2016). As small molecule binding such as lipids are needed to carry out an efficient protein function, only few methods have been used to identify the type and stoichiometry of these bindings. Experimental procedures in the purification and crystallization stages can sometimes delipidate the protein and therefore only lipids strongly bound

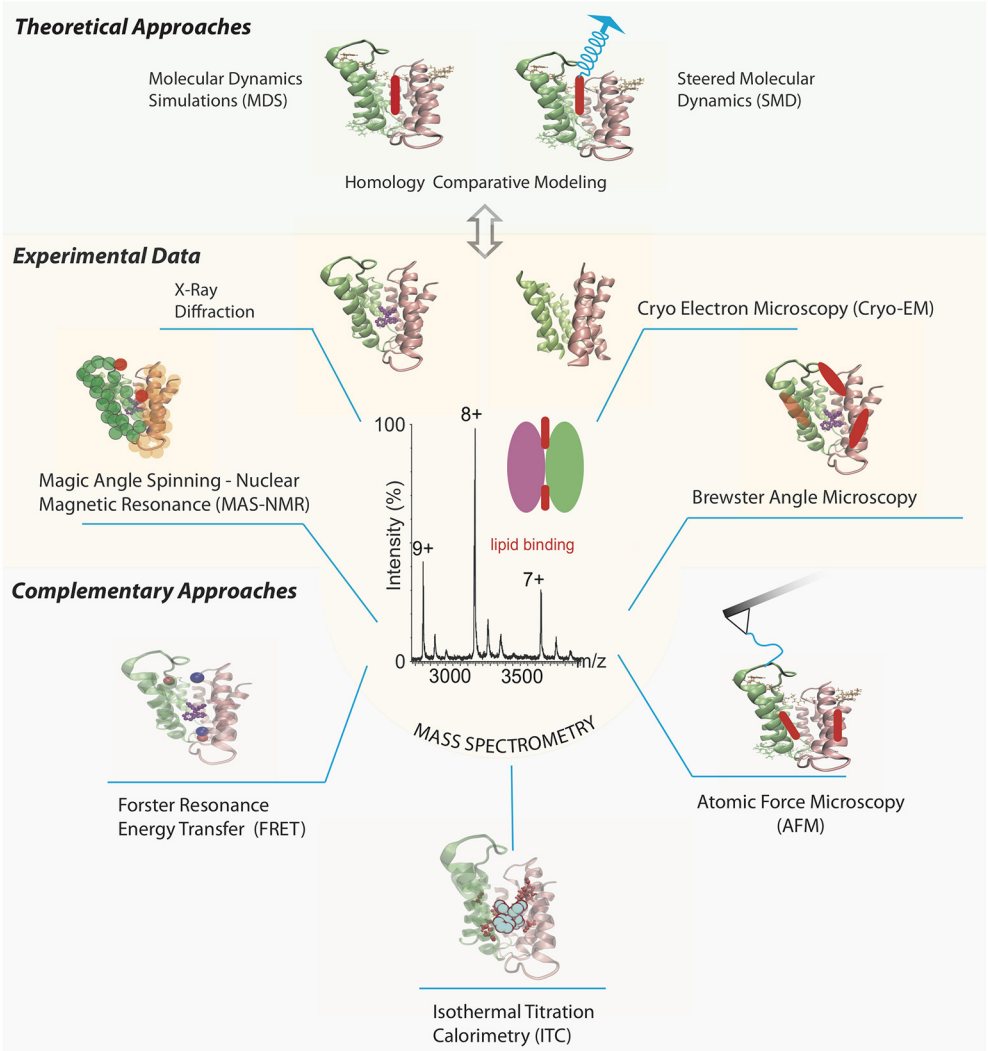

FIGURE 1 | Selection of different biophysical methods aimed to determine structural and functional information of multidrug transporter EmrE bound to lipids. Different panels represent features of the chosen method, and EmrE transporter is drawn using the X-ray crystallized protein PDB ID 3B5D (Chen et al., 2007) in all cases, except for the cryo-EM structure where the PDB ID 2I68 was chosen (Fleishman et al., 2006). Mass spectra of EmrE is simulated based on previous results (Barrera et al., 2009) highlighting its relevance between experimental and theoretical methods to tackle the study of MP-lipid complexes. AFM tip chemically functionalized with a residue in one EmrE monomer to get stability properties of the MP-lipid interaction via force spectroscopy. Labelling pair of residues or one residue and a ligand to analyze overall protein structure via FRET and MAS-NMR experiments. SPR and ITC measurements to analyze the role of additional soluble ligands on the MP-lipid complex kinetics and thermodynamical properties, respectively. Brewster angle microscopy to characterize the stability between the MP and lipid interaction. MD and SMD (from a particular target atom in the lipid) simulations to obtain all-atom characterization of the MP-lipid complex, based on the collected experimental data. Lipids are drawn as red and blue colored ovoids. Tetraphenylphosphonium structure is colored in purple.

to the TM domains survive to be identified by structural methods.

Fine-tuning of voltage and pressure settings of the mass spectrometer has allowed identification of lipids bound to the MPs, which were transferred from the cell membrane to the detergent micelle or nanodisc, thus preserving the MP-ligand interaction (Barrera et al., 2009; Barrera and Robinson, 2011; Zhou et al., 2011; Hopper et al., 2013; Laganowsky et al., 2013; Marcoux et al., 2013; Gault et al., 2016; **Figure 2A**). It is important to highlight though that the selection of the "membrane mimetic" strategy for the MP purification has practical issues in the MS analysis. While detergents cannot emulate lateral pressure profile or membrane curvature, that could reduce the MP stability, their removal from the complex requires lower collision energy. On the other hand, nanodiscs can maintain properties like membrane curvature or lateral pressure, but their removal requires much higher activation, preventing the identification of larger MP complexes (Hopper et al., 2013; Marty et al., 2016). So, there's a trade-off between simplifying the "membrane mimetic" environment to maintain

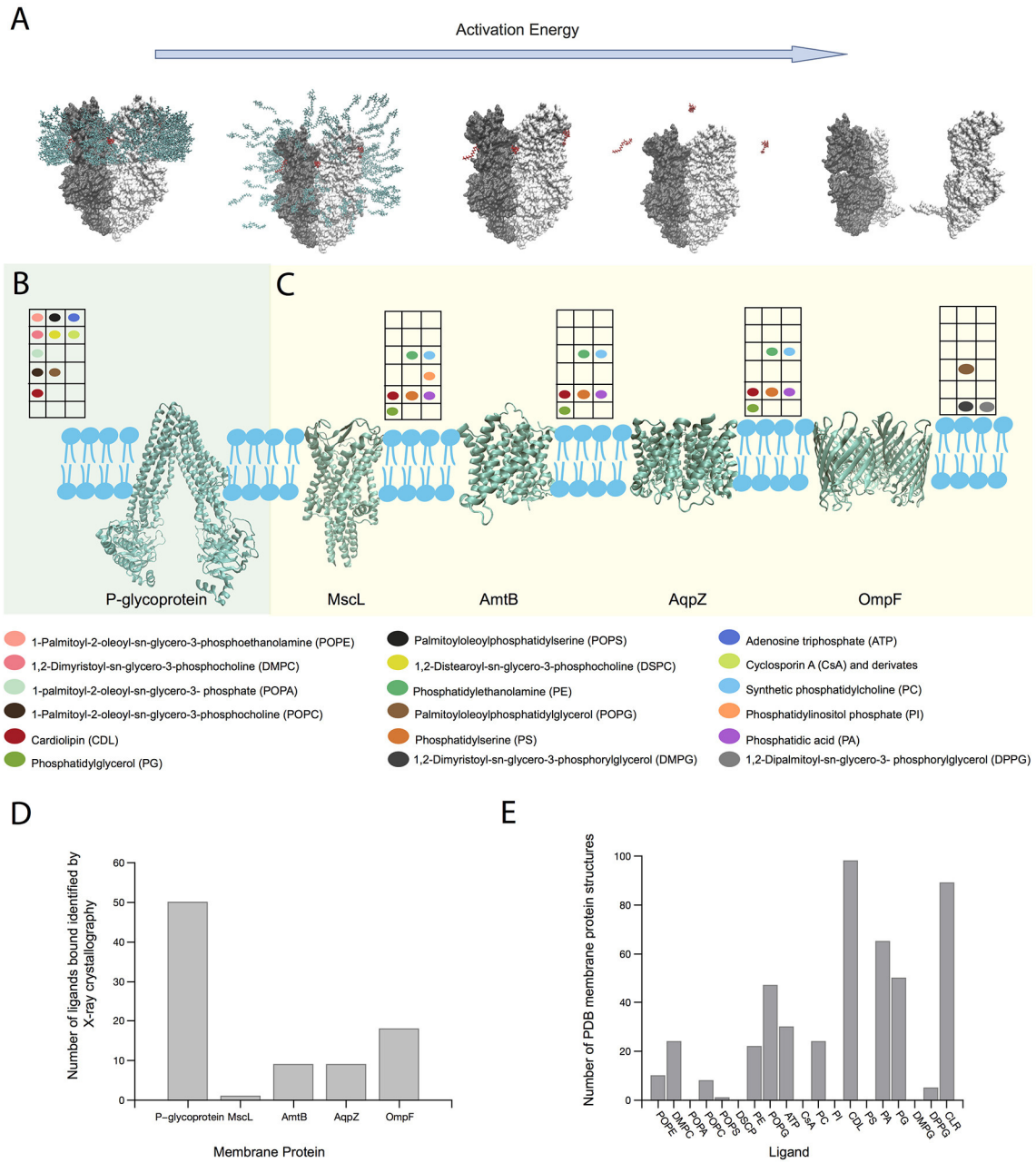

FIGURE 2 | Role of MS on MP-lipid binding structural characterization. **(A)** Scheme of the release of an intact MP-ligand complex (MexB) from a micelle after increasing energy activation in the gas phase. Ligands and detergent molecules are colored red and green, respectively. **(B)** P-glycoprotein and its ligand interactions determined by native MS (Marcoux et al., 2013). **(C)** Variety of lipid interactions with MPs MscL, AmtB, and AqpZ (Laganowsky et al., 2014) and OmpF (Gault et al., 2016) determined by native MS. Color-coded circles show the presence of particular ligands studied in each MP by MS. The position of each circle in the grid matches with its position in the colored legend describing the ligand name. **(D)** Number of ligands bound to those MPs shown in **(B,C)**, which have been identified by X-ray crystallography until August 2017. **(E)** Number of crystallized MPs bound to ligands shown in **(B,C)**, including cholesterol (CLR), until August 2017. Note that ion bindings were not considered in the selection. Protein structures were generated using PDB IDs 2V50 (MexB) (Sennhauser et al., 2009), 4Q9H (P-gp) (Szewczyk et al., 2015); 2OAR (MscL) (Steinbacher et al., 2007); 1U7G (AmtB) (Khademi et al., 2004); 2O9F (AqpZ) (Savage and Stroud, 2007) and 3POQ (OmpF) (Efremov and Sazanov, 2012).

native-like MP structure and the energy required to identify the MP.

The ionization process can be simulated through MD, assigning charge on basic residues (Friemann et al., 2009; Hall et al., 2012b) and calculating the solvent accessible surface area of the membrane complex (Morgner et al., 2012). Although it is clear that micelle protects the MP structure in vacuum (Barrera et al., 2008; Friemann et al., 2009; van der Spoel et al.,

2011; Reading et al., 2015), the molecular mechanism of the protein release remains poorly understood. Specifically, it would be relevant to understand how lipids can still be bound to the protein after micelle destruction in the gas phase (**Figure 2A**). By steering MD simulations, Rouse et al. have shown that a MP-micelle complex in solution can be transferred to the gas phase, observing conformational changes in the micelle structure (Rouse et al., 2013). Hall et al performed MD simulations of SAP soluble protein in vacuum at increasing temperatures, from 300 to 800°K, in order to represent increasing activation energy in Ion Mobility-Mass Spectrometry (IM-MS) experiments, which resulted in a good correlation between the experimental and theoretical values (Hall et al., 2012a). This could imply that increasing temperature to trigger micelle destruction in MD simulations can be comparable to inert gas collisions, which should increase the micelle internal energy, making it unstable and finally dismantle it, releasing the protein in a native-like state.

MASS SPECTROMETRY AS A COLLABORATIVE TOOL FOR CRYSTALLOGRAPHY

Considering lipid identification in native-like MPs, this high-resolution MS method shows important progresses leading to the understanding of structural features hidden on MPs. For example, on one hand, we can mention 3 MPs studied by MS prior to the knowledge of their atomic structure. MS has resolved 2 phosphatidylethanolamine (PE) molecules bound to the ATP binding cassette (ABC) transporter MacB dimer in 2009, probably located at the dimeric interface. In 2017, the MacB cryo-EM structure obtained at 3.3Å resolution did not show lipid binding perhaps due to the purification procedure and limited map local resolution (Fitzpatrick et al., 2017).

The resistance-nodulation division transporter MexB trimer was analyzed in 2009, where the presence of lipid clusters was identified using MS (Barrera et al., 2009). The same year a 3Å resolution crystal structure was available (Sennhauser et al., 2009), and an unidentified density was detected in the MexB pore domain, which was interpreted as maltose ring of a DDM detergent molecule, since no ligands were used in the crystallization process. Later, in 2013 a 2.7Å resolution crystal structure was published showing elongated electron densities in the central hole of the TM domain, which likely correspond to acyl chains of membrane phospholipids (Nakashima et al., 2013).

In 2015, the heterodimeric ABC exporter TmrAB was identified bound to negatively-charged phosphatidylglycerol (PG) and zwitterionic PE lipids, where PG showed a stronger affinity for the transporter. That same year, a cryo-EM structure of TmrAB was published with an 8Å resolution (Kim et al., 2015). A pocket in TmrB formed between two TM segments showed a density that the authors attributed to either detergent or lipid co-purified in the sample preparation steps. In 2017, a crystal structure with 2.7A resolution was available (Noll et al., 2017), which showed that pocket containing 5 arginine residues. MD simulations showed lipid interactions in the TmrB pocket, with the polar head interacting with the pocket while the aliphatic chains interacting with the hydrophobic part of the membrane, possibly showing a mechanism for lipid translocation, in accordance with the previous MS data.

In 2011, while studying the stochiometry of intact rotary adenosine triphosphatase (ATPase)/synthase from *Enterococcus hirae* via MS, 10 cardiolipins (CLs) were bound to the inside of the K10 ring in the enzyme. Interestingly these lipids were originally assigned to be 20 1,2-dipalmitoyl-phosphatidyl-glycerol molecules in the K10 ring crystal structure (Murata et al., 2005). In all of these examples detergent micelles were used as membrane mimicking strategies, demonstrating that MS can aid to identify small molecules bound, where high-resolution techniques, such as X-ray crystallography, can have difficulties to resolve them.

With the goal of studying the effect of ligands on MP stability, several recent MS studies have combined high resolution MS, and MD approaches. Marcoux et al. using MS on the ABC transporter P-glycoprotein (P-gp) (**Figure 2B**), commonly overexpressed in tumor cells, demonstrated that different phosphoglyceride lipids bind more energetically favorable than detergent, which could explain why intact MPs complexed to ligands can be actually detected in the gas phase, prior to protein unfolding. Concomitant binding of ATP and cyclosporine A (CsA) or CL and CsA, triggered greater populations of the smaller conformers which could arise from an unexpected outward-facing form (Marcoux et al., 2013). Laganowsky et al. studied the stability of three membrane transporters using MS. For mechanosensitive channel MscL, four intermediaries' stages were found, and by comparing the apo-state against the lipid bound state, lipid stabilization at each transition could be quantified. Seven different lipids were found and their contributions to MscL stability were similar, except for phosphatidylinositol phosphate (PI) with up to 4 molecules bound, which conferred large increase of stability with each molecule. For water efflux channel AqpZ, similar results were found, with each identified lipid contributing for protein stability with a linear cumulative effect, except for CL, which seems to augment the stability considerably. The ammonia transporter AmtB showed diverse lipid effects on protein stability. While anionic lipids, phosphatidic acid (PA) and phosphatidylserine (PS) did not contribute much to protein stability, CL and particularly phosphatidylglycerol (PG) contributed the most. In the case of PG, stabilization augmented linearly with each molecule bound (up to 4 detected) (**Figure 2C**). By using this method, lipid contribution to protein stability can be quantified and ranked, and lipids can be classified as crucial elements for protein function (Laganowsky et al., 2014). Finally, Gault et al. presented a MS method, aiming to identify multiple ligands bound to MPs. Considering small mass differences between lipids and drugs, the simultaneous identification of both of them was proven difficult. And yet, this high-resolution Orbitrap-based method allowed the identification not only for concomitant binding of drug and lipids, but also determined the acyl chain length that preferentially binds to the protein. For the outer membrane porin OmpF, using an equimolar mixture of DMPG, DPPG, and POPG, showed more preference toward the longer acyl chain POPG (**Figure 2C**; Gault et al., 2016).

Considering the same MPs shown in **Figures 2B,C** X-ray crystallography has been able to identify a much larger number of ligands bound. Among them, only ATP at P-glycoprotein was detected using both X-crystallography and MS methods (**Figure 2D**). Detergent or lipid molecules can be identified incomplete by X-ray crystallography, because the hydrophobic tail is free to interact with many atoms in the TM region, while the hydrophilic head tend to remain in specific places. However, differences from the expression system and purification experimental conditions cannot be dismissed. From crystal or cryo-EM structures, many densities were not appropriately defined because the bound ligand did not necessarily stay in the same conformation across the many protein crystals needed to obtain their atomic coordinates in the complex. Nevertheless, MS applications on native-like MP-ligand complexes allow testing the effect of multi ligands simultaneously, which is rather difficult to detect via crystal or cryo-EM structures. The ligands tested by MS were observed in 375 different Protein Data Bank (PDB) MP structures (**Figure 2E**), with the majority represented by CL and cholesterol, that are known to be non-bilayer forming lipids modulating the stability of MPs (van den Brink-van der Laan et al., 2004; Osman et al., 2011; Grouleff et al., 2015).

Altogether, by combining MS with X-ray crystallography, overall stoichiometry, location and stability data can be obtained for the simultaneous effect of several ligands in the protein.

FUTURE PERSPECTIVES

One essential question for expanding our understanding of the MS of lipid bound to native-like MP complexes is the precise location of the binding site. As ESI-MS can be combined with LC-MS/MS to identify unambiguously the nature and stoichiometry of the lipids bound, several parallel experimental approaches could be coupled to this methodology. Hydrogen/deuterium exchange mass spectrometry (HDX-MS) of MP-lipid complexes may be combined with docking simulations of the lipid into hypothetical binding sites (Hu et al., 2011) located at hydrophobic pockets or intersubunit interfaces. Those residues present in the binding sites would have a lower exchange compared to other equivalent TM residues located elsewhere. Novel simulation approaches in gas phase, combined with structural information such as shape and size via CCS data (Wang et al., 2010), are needed to characterize the dynamical properties of small molecules bound to native-like MPs. For example, Politis et al. developed a hybrid method combining native MS, IM-MS, and bottom-up approaches (HDX, labeling and cross-linking) with molecular modeling to elucidate the structural arrangement of protein assemblies. While it still uses structural information like low resolution atomic models or cryo-EM mapping as the basis for modeling, the refinement is made through the information obtained in the MS approaches (Politis et al., 2014).

Additionally, the application of nanodiscs can provide a more native lipid environment with a specified size or diameter to obtain functional proteins (Lyukmanova et al., 2012). This approach has been used with techniques like NMR (Susac et al., 2014), SPR (Glück et al., 2011), and MALDI (Marty et al., 2012), and has recently been used to study native-like MPs in gas phase (Hopper et al., 2013). Furthermore, Zhang et al. presented a method using stable isotope labeling by amino acids in cell culture (SILAC) and nanodiscs to identify potential interactions between a target protein and an entire proteome. In this study, 3 MP (SecYEG, $MalFGK_2$, and YidC) were screened against the *E. coli* proteome, isolated the interacting proteins by affinity pull-down and analyzed with tandem mass spectrometry, which allowed the recognition of several protein interactions captured from a whole cell extract (Zhang et al., 2012).

AUTHOR CONTRIBUTIONS

FM, JC, and NB contributed to the writing, data analysis and edition of the manuscript, as well as approved the final version to be published.

FUNDING

Conicyt Fondequip EQM150102, Conicyt Newton Picarte PCI-DPI20140080, Pontificia Universidad Catolica de Chile Puente VRI 2017.

REFERENCES

Barrera, N. P., and Robinson, C. V. (2011). Advances in the mass spectrometry of membrane proteins: from individual proteins to intact complexes. *Annu. Rev. Biochem.* 80, 247–271. doi: 10.1146/annurev-biochem-062309-093307

Barrera, N. P., Di Bartolo, N., Booth, P. J., and Robinson, C. V. (2008). Micelles protect membrane complexes from solution to vacuum. *Science* 321, 243–246. doi: 10.1126/science.1159292

Barrera, N. P., Isaacson, S. C., Zhou, M., Bavro, V. N., Welch, A., Schaedler, T. A., et al. (2009). Mass spectrometry of membrane transporters reveals subunit stoichiometry and interactions. *Nat. Methods* 6, 585–587. doi: 10.1038/nmeth.1347

Bechara, C., and Robinson, C. V. (2015). Different modes of lipid binding to membrane proteins probed by mass spectrometry. *J. Am. Chem. Soc.* 137, 5240–5247. doi: 10.1021/jacs.5b00420

Chen, Y. J., Pornillos, O., Lieu, S., Ma, C., Chen, A. P., and Chang, G. (2007). X-ray structure of EmrE supports dual topology model. *Proc. Natl. Acad. Sci. U.S.A.* 104, 18999–19004. doi: 10.1073/pnas.0709387104

Cohen, S. L., and Chait, B. T. (2001). Mass spectrometry as a tool for protein crystallography. *Annu. Rev. Biophys. Biomol. Struct.* 30, 67–85. doi: 10.1146/annurev.biophys.30.1.67

Dill, K. A., and MacCallum, J. L. (2012). The protein-folding problem, 50 years on. *Science* 338, 1042–1046. doi: 10.1126/science.1219021

Ding, X., Zhao, X., and Watts, A. (2013). G-protein-coupled receptor structure, ligand binding and activation as studied by solid-state NMR spectroscopy. *Biochem. J.* 450, 443–457. doi: 10.1042/BJ20121644

Efremov, R. G., and Sazanov, L. A. (2012). Structure of *Escherichia coli* OmpF porin from lipidic mesophase. *J. Struct. Biol.* 178, 311–318. doi: 10.1016/j.jsb.2012.03.005

Fang, Y. (2012). Ligand-receptor interaction platforms and their applications for drug discovery. *Expert Opin. Drug Discov.* 7, 969–988. doi: 10.1517/17460441.2012.715631

Fitzpatrick, A. W. P., Llabrés, S., Neuberger, A., Blaza, J. N., Bai, X. C., Okada, U., et al. (2017). Structure of the MacAB-TolC ABC-type tripartite multidrug efflux pump. *Nat. Microbiol.* 2:17070. doi: 10.1038/nmicrobiol.2017.70

Fleishman, S. J., Harrington, S. E., Enosh, A., Halperin, D., Tate, C. G., and Ben-Tal, N. (2006). Quasi-symmetry in the cryo-EM structure of EmrE provides the key to modeling its transmembrane domain. *J. Mol. Biol.* 364, 54–67. doi: 10.1016/j.jmb.2006.08.072

Friemann, R., Larsson, D. S., Wang, Y., and van der Spoel, D. (2009). Molecular dynamics simulations of a membrane protein-micelle complex in vacuo. *J. Am. Chem. Soc.* 131, 16606–16607. doi: 10.1021/ja902962y

Gault, J., Donlan, J. A., Liko, I., Hopper, J. T., Gupta, K., Housden, N. G., et al. (2016). High-resolution mass spectrometry of small molecules bound to membrane proteins. *Nat. Methods* 13, 333–336. doi: 10.1038/nmeth.3771

Glück, J. M., Koenig, B. W., and Willbold, D. (2011). Nanodiscs allow the use of integral membrane proteins as analytes in surface plasmon resonance studies. *Anal. Biochem.* 408, 46–52. doi: 10.1016/j.ab.2010.08.028

Grouleff, J., Irudayam, S. J., Skeby, K. K., and Schiøtt, B. (2015). The influence of cholesterol on membrane protein structure, function, and dynamics studied by molecular dynamics simulations. *Biochim. Biophys. Acta* 1848, 1783–1795. doi: 10.1016/j.bbamem.2015.03.029

Hall, Z., Politis, A., Bush, M. F., Smith, L. J., and Robinson, C. V. (2012a). Charge-state dependent compaction and dissociation of protein complexes: insights from ion mobility and molecular dynamics. *J. Am. Chem. Soc.* 134, 3429–3438. doi: 10.1021/ja2096859

Hall, Z., Politis, A., and Robinson, C. V. (2012b). Structural modeling of heteromeric protein complexes from disassembly pathways and ion mobility-mass spectrometry. *Structure* 20, 1596–1609. doi: 10.1016/j.str.2012.07.001

Hopper, J. T., Yu, Y. T., Li, D., Raymond, A., Bostock, M., Liko, I., et al. (2013). Detergent-free mass spectrometry of membrane protein complexes. *Nat. Methods* 10, 1206–1208. doi: 10.1038/nmeth.2691

Hu, W., Liu, J., Luo, Q., Han, Y., Wu, K., Lv, S., et al. (2011). Elucidation of the binding sites of sodium dodecyl sulfate to beta-lactoglobulin using hydrogen/deuterium exchange mass spectrometry combined with docking simulation. *Rapid Commun. Mass Spectrom.* 25, 1429–1436. doi: 10.1002/rcm.5012

Kalinin, S., Peulen, T., Sindbert, S., Rothwell, P. J., Berger, S., Restle, T., et al. (2012). A toolkit and benchmark study for FRET-restrained high-precision structural modeling. *Nat. Methods* 9, 1218–1225. doi: 10.1038/nmeth.2222

Khademi, S., O'Connell, J., Remis, J., Robles-Colmenares, Y., Miericke, L. J. W., and Stroud, R. M. (2004). Mechanism of ammonia transport by Amt/MEP/Rh: Structure of AmtB at 1.3.5 angstrom. *Science* 305, 1587–1594. doi: 10.1126/science.1101952

Kim, J., Wu, S., Tomasiak, T. M., Mergel, C., Winter, M. B., Stiller, S. B., et al. (2015). Subnanometre-resolution electron cryomicroscopy structure of a heterodimeric ABC exporter. *Nature* 517, 396–400. doi: 10.1038/nature13872

Konermann, L., Vahidi, S., and Sowole, M. A. (2014). Mass spectrometry methods for studying structure and dynamics of biological macromolecules. *Anal. Chem.* 86, 213–232. doi: 10.1021/ac4039306

Korkhov, V. M., and Tate, C. G. (2008). Electron crystallography reveals plasticity within the drug binding site of the small multidrug transporter EmrE. *J. Mol. Biol.* 377, 1094–1103. doi: 10.1016/j.jmb.2008.01.056

Laganowsky, A., Reading, E., Hopper, J. T., and Robinson, C. V. (2013). Mass spectrometry of intact membrane protein complexes. *Nat. Protoc.* 8, 639–651. doi: 10.1038/nprot.2013.024

Laganowsky, A., Reading, E., Allison, T. M., Ulmschneider, M. B., Degiacomi, M. T., Baldwin, A. J., et al. (2014). Membrane proteins bind lipids selectively to modulate their structure and function. *Nature* 510, 172–175. doi:10.1038/nature13419

Lyukmanova, E. N., Shenkarev, Z. O., Khabibullina, N. F., Kopeina, G. S., Shulepko, M. A., Paramonov, A. S., et al. (2012). Lipid-protein nanodiscs for cell-free production of integral membrane proteins in a soluble and folded state: comparison with detergent micelles, bicelles and liposomes. *Biochim. Biophys. Acta* 1818, 349–358. doi: 10.1016/j.bbamem.2011.10.020

Marcoux, J., Wang, S. C., Politis, A., Reading, E., Ma, J., Biggin, P. C., et al. (2013). Mass spectrometry reveals synergistic effects of nucleotides, lipids, and drugs binding to a multidrug resistance efflux pump. *Proc. Natl. Acad. Sci. U.S.A.* 110, 9704–9709. doi: 10.1073/pnas.1303888110

Marsh, D., and Páli, T. (2004). The protein-lipid interface: perspectives from magnetic resonance and crystal structures. *Biochim. Biophys. Acta* 1666, 118–141. doi: 10.1016/j.bbamem.2004.08.006

Marty, M. T., Das, A., and Sligar, S. G. (2012). Ultra-thin layer MALDI mass spectrometry of membrane proteins in nanodiscs. *Anal. Bioanal. Chem.* 402, 721–729. doi: 10.1007/s00216-011-5512-3

Marty, M. T., Hoi, K. K., and Robinson, C. V. (2016). Interfacing membrane mimetics with mass spectrometry. *Acc. Chem. Res.* 49, 2459–2467. doi: 10.1021/acs.accounts.6b00379

Moraes, I., Evans, G., Sanchez-Weatherby, J., Newstead, S., and Stewart, P. D. (2014). Membrane protein structure determination – the next generation. *Biochim Biophys Acta* 1838(1 Pt A), 78–87. doi: 10.1016/j.bbamem.2013.07.010

Morgner, N., Montenegro, F., Barrera, N. P., and Robinson, C. V. (2012). Mass spectrometry–from peripheral proteins to membrane motors. *J. Mol. Biol.* 423, 1–13. doi: 10.1016/j.jmb.2012.06.033

Murata, T., Yamato, I., Kakinuma, Y., Leslie, A. G., and Walker, J. E. (2005). Structure of the rotor of the V-Type Na^+-ATPase from *Enterococcus hirae*. *Science* 308, 654–659. doi: 10.1126/science.1110064

Nakashima, R., Sakurai, K., Yamasaki, S., Hayashi, K., Nagata, C., Hoshino, K., et al. (2013). Structural basis for the inhibition of bacterial multidrug exporters. *Nature* 500, 102–106. doi: 10.1038/nature12300

Nathoo, S., Litzenberger, J. K., Bay, D. C., Turner, R. J., and Prenner, E. J. (2013). Visualizing a multidrug resistance protein, EmrE, with major bacterial lipids using Brewster angle microscopy. *Chem. Phys. Lipids* 167–168, 33–42. doi: 10.1016/j.chemphyslip.2013.01.007

Noll, A., Thomas, C., Herbring, V., Zollmann, T., Barth, K., Mehdipour, A. R., et al. (2017). Crystal structure and mechanistic basis of a functional homolog of the antigen transporter TAP. *Proc. Natl. Acad. Sci. U.S.A.* 114, E438–E447. doi: 10.1073/pnas.1620009114

Ong, Y. S., Lakatos, A., Becker-Baldus, J., Pos, K. M., and Glaubitz, C. (2013). Detecting substrates bound to the secondary multidrug efflux pump EmrE by DNP-enhanced solid-state NMR. *J. Am. Chem. Soc.* 135, 15754–15762. doi: 10.1021/ja402605s

Osman, C., Voelker, D. R., and Langer, T. (2011). Making heads or tails of phospholipids in mitochondria. *J. Cell Biol.* 192, 7–16. doi: 10.1083/jcb.201006159

Overington, J. P., Al-Lazikani, B., and Hopkins, A. L. (2006). How many drug targets are there? *Nat. Rev. Drug Discov.* 5, 993–996. doi: 10.1038/nrd2199

Pacholarz, K. J., Garlish, R. A., Taylor, R. J., and Barran, P. E. (2012). Mass spectrometry based tools to investigate protein-ligand interactions for drug discovery. *Chem. Soc. Rev.* 41, 4335–4355. doi: 10.1039/c2cs35035a

Politis, A., Stengel, F., Hall, Z., Hernandez, H., Leitner, A., Walzthoeni, T., et al. (2014). A mass spectrometry-based hybrid method for structural modeling of protein complexes. *Nat. Methods* 11, 403–406. doi: 10.1038/nmeth.2841

Reading, E., Liko, I., Allison, T. M., Benesch, J. L., Laganowsky, A., and Robinson, C. V. (2015). The role of the detergent micelle in preserving the structure of membrane proteins in the gas phase. *Angew. Chem. Int. Ed Engl.* 54, 4577–4581. doi: 10.1002/anie.201411622

Rouse, S. L., Marcoux, J., Robinson, C. V., and Sansom, M. S. (2013). Dodecyl maltoside protects membrane proteins in vacuo. *Biophys. J.* 105, 648–656. doi: 10.1016/j.bpj.2013.06.025

Savage, D. F., and Stroud, R. M. (2007). Structural basis of aquaporin inhibition by mercury. *J. Mol. Biol.* 368, 607–617. doi: 10.1016/j.jmb.2007.02.070

Sennhauser, G., Bukowska, M. A., Briand, C., and Grutter, M. G. (2009). Crystal structure of the multidrug exporter MexB from *Pseudomonas aeruginosa*. *J. Mol. Biol.* 389, 134–145. doi: 10.1016/j.jmb.2009.04.001

Shahin, V., and Barrera, N. P. (2008). Providing unique insight into cell biology via atomic force microscopy. *Int. Rev. Cytol.* 265, 227–252. doi: 10.1016/S0074-7696(07)65006-2

Shoura, M. J., Ranatunga, R. J., Harris, S. A., Nielsen, S. O., and Levene, S. D. (2014). Contribution of fluorophore dynamics and solvation to resonant energy transfer in protein-DNA complexes: a molecular-dynamics study. *Biophys. J.* 107, 700–710. doi: 10.1016/j.bpj.2014.06.023

Steinbacher, S., Bass, R., Strop, P., and Rees, D. C. (2007). "Structures of the prokaryotic mechanosensitive channels MscL and MscS" in *Current Topics in*

Membranes: Mechanosensitive Ion Channels Part A, ed O. P. Hamill (Academic Press), 1–24. doi: 10.1016/S1063-5823(06)58001-9

Susac, L., Horst, R., and Wuthrich, K. (2014). Solution-NMR characterization of outer-membrane protein A from *E. coli* in lipid bilayer nanodiscs and detergent micelles. *Chembiochem* 15, 995–1000. doi: 10.1002/cbic.201300729

Suzuki, Y., Goetze, T. A., Stroebel, D., Balasuriya, D., Yoshimura, S. H., Henderson, R. M., et al. (2013). Visualization of structural changes accompanying activation of N-methyl-D-aspartate (NMDA) receptors using fast-scan atomic force microscopy imaging. *J. Biol. Chem.* 288, 778–784. doi: 10.1074/jbc.M112.422311

Szewczyk, P., Tao, H., McGrath, A. P., Villaluz, M., Rees, S. D., Lee, S. C., et al. (2015). Snapshots of ligand entry, malleable binding and induced helical movement in P-glycoprotein. *Acta Crystallogr. D Biol. Crystallogr.* 71(Pt 3), 732–741. doi: 10.1107/S1399004715000978

van den Brink-van der Laan, E., Killian, J. A., and de Kruijff, B. (2004). Nonbilayer lipids affect peripheral and integral membrane proteins via changes in the lateral pressure profile. *Biochim. Biophys. Acta* 1666, 275–288. doi: 10.1016/j.bbamem.2004.06.010

van der Spoel, D., Marklund, E. G., Larsson, D. S., and Caleman, C. (2011). Proteins, lipids, and water in the gas phase. *Macromol. Biosci.* 11, 50–59. doi: 10.1002/mabi.201000291

Vuignier, K., Schappler, J., Veuthey, J. L., Carrupt, P. A., and Martel, S. (2010). Drug-protein binding: a critical review of analytical tools. *Anal. Bioanal. Chem.* 398, 53–66. doi: 10.1007/s00216-010-3737-1

Wang, S. C., Politis, A., Di Bartolo, N., Bavro, V. N., Tucker, S. J., Booth, P. J., et al. (2010). Ion mobility mass spectrometry of two tetrameric membrane protein complexes reveals compact structures and differences in stability and packing. *J. Am. Chem. Soc.* 132, 15468–15470. doi: 10.1021/ja104312e

Zhang, X. X., Chan, C. S., Bao, H., Fang, Y., Foster, L. J., and Duong, F. (2012). Nanodiscs and SILAC-based mass spectrometry to identify a membrane protein interactome. *J. Proteome Res.* 11, 1454–1459. doi: 10.1021/pr200846y

Zhou, M., Morgner, N., Barrera, N. P., Politis, A., Isaacson, S. C., Matak-Vinkovic, D., et al. (2011). Mass spectrometry of intact V-type ATPases reveals bound lipids and the effects of nucleotide binding. *Science* 334, 380–385. doi: 10.1126/science.1210148

Conflict of Interest Statement: The authors declare that the research was conducted in the absence of any commercial or financial relationships that could be construed as a potential conflict of interest.

frontiers in Physiology

REVIEW
published: 01 November 2017
doi: 10.3389/fphys.2017.00887

An Update on Sec61 Channel Functions, Mechanisms, and Related Diseases

Sven Lang[1], Stefan Pfeffer[2], Po-Hsien Lee[3], Adolfo Cavalié[4], Volkhard Helms[3], Friedrich Förster[5] and Richard Zimmermann[1]*

[1] Competence Center for Molecular Medicine, Saarland University Medical School, Homburg, Germany, [2] Department of Molecular Structural Biology, Max-Planck Institute of Biochemistry, Martinsried, Germany, [3] Center for Bioinformatics, Saarland University, Saarbrücken, Germany, [4] Experimental and Clinical Pharmacology and Toxicology, Saarland University, Homburg, Germany, [5] Bijvoet Center for Biomolecular Research, Utrecht University, Utrecht, Netherlands

The membrane of the endoplasmic reticulum (ER) of nucleated human cells harbors the protein translocon, which facilitates membrane integration or translocation of almost every newly synthesized polypeptide targeted to organelles of the endo- and exocytotic pathway. The translocon comprises the polypeptide-conducting Sec61 channel and several additional proteins and complexes that are permanently or transiently associated with the heterotrimeric Sec61 complex. This ensemble of proteins facilitates ER targeting of precursor polypeptides, modification of precursor polypeptides in transit through the Sec61 complex, and Sec61 channel gating, i.e., dynamic regulation of the pore forming subunit to mediate precursor transport and calcium efflux. Recently, cryoelectron tomography of translocons in native ER membrane vesicles, derived from human cell lines or patient fibroblasts, and even intact cells has given unprecedented insights into the architecture and dynamics of the native translocon and the Sec61 channel. These structural data are discussed in light of different Sec61 channel activities including ribosome receptor function, membrane insertion, and translocation of newly synthesized polypeptides as well as the putative physiological roles of the Sec61 channel as a passive ER calcium leak channel. Furthermore, the structural insights into the Sec61 channel are incorporated into an overview and update on Sec61 channel-related diseases—the Sec61 channelopathies—and novel therapeutic concepts for their treatment.

Keywords: ATP import, BiP, calcium leakage, endoplasmic reticulum, protein biogenesis, Sec61 complex

OPEN ACCESS

Edited by:
Mario Diaz,
Universidad de La Laguna, Spain

Reviewed by:
Felipe Simon,
Universidad Andrés Bello, Chile
Michael Tamkun,
Colorado State University, United States

****Correspondence:***
Sven Lang
sven.lang@uni-saarland.de

Specialty section:
This article was submitted to Membrane Physiology and Membrane Biophysics, a section of the journal Frontiers in Physiology

Received: *03 July 2017*
Accepted: *19 October 2017*
Published: *01 November 2017*

Citation:
Lang S, Pfeffer S, Lee P-H, Cavalié A, Helms V, Förster F and Zimmermann R (2017) An Update on Sec61 Channel Functions, Mechanisms, and Related Diseases. Front. Physiol. 8:887. doi: 10.3389/fphys.2017.00887

INTRODUCTION

The endoplasmic reticulum (ER) represents the largest continuous tubular membrane network within nucleated mammalian cells (Friedman and Voeltz, 2011; **Figure 1**). Its striking dynamics were recently demonstrated via lattice light-sheet microscopy (Valm et al., 2017). While occupying up to a third of a cell's volume at any given time, the ER managed to "scan" and explore over 97% of a cell's volume within 15 min. Not surprisingly, this high mobility allows the ER to be the organelle with the highest contact rate to other compartments of the endomembrane system, such as lipid droplets or mitochondria and, therefore, the nexus of inter-organelle tethering. Together with the size of the ER comes both an array of different functions and morphological structures. The former include lipid and steroid synthesis, calcium storage, protein transport, maturation,

and proteostasis some of which are assumed to occur at distinct ER subdomains (Blobel and Dobberstein, 1975; Palade, 1975; Berridge, 2002; Brostrom and Brostrom, 2003; Clapham, 2007; Braakman and Bulleid, 2011). The latter include the nuclear envelope and the peripheral ER consisting of smooth tubular and rough sheet-like areas. Recently, advances in super-resolution imaging of live and fixed cells extended the concept of tubular and sheet-like peripheral ER domains by introducing ER matrices, densely packed ER tubular arrays, to the portfolio of ER structural domains. The combination of nanoscopic approaches revealed two features. One, the peripheral ER moves at high speeds broadly dependent on cellular energy sources. And two, many of the peripheral ER structures classically identified as sheets represent instead dense matrices of convoluted tubules (Nixon-Abell et al., 2016). In the context of the ER, rough and smooth refers to the presence or absence of membrane-associated ribosomes or polysomes on the cytosolic surface. The density of bound ribosomes is considered one driver for the formation of sheets. However, common to tubes, matrices and sheets is the lumenal distance of about 50 nm in mammalian cells most likely established by lumenal spacer proteins such as Climp-63 (Shibata et al., 2006, 2010; Schwarz and Blower, 2016). Furthermore, advances in ultrathin sectioning of electron microscopy preparations visualize ER sheets, especially juxtanuclear ones, being stacked in a parking garage like fashion with interconnecting helicoidal ramps to allow dense packing in a crowded environment of neuronal and secretory salivary gland cells (Terasaki et al., 2013; Nixon-Abell et al., 2016).

The heterotrimeric Sec61 complex in the ER membrane provides the dynamic polypeptide-conducting channel, which mediates membrane insertion of most membrane proteins of organelles involved in endo- and exocytosis and translocation of all precursors of polypeptides destined for these same organelles and most precursors of secretory proteins (Görlich et al., 1992) ("transport" in **Figure 2**). With respect to membrane proteins, the exceptions are tail-anchored (TA) membrane proteins (reviewed by Rabu et al., 2009; Borgese and Fasana, 2011), and with respect to secretory proteins, the mechanistically completely unrelated "unconventional secretion" is the alternative mechanism and described in detail elsewhere (Nickel and Rabouille, 2009). Precursors of soluble polypeptides and membrane proteins are targeted to the Sec61 complex via their amino-terminal signal peptides or transmembrane helices either during their synthesis (termed cotranslationally) or after completion of their synthesis (termed posttranslationally) (Blobel and Dobberstein, 1975; von Heijne, 1986). Predominantly, cotranslational targeting is supposed to involve the cytosolic signal recognition particle (SRP) plus its receptor on the ER surface, SRP receptor (SR) (**Table 1**); posttranslational targeting can involve one of several SRP-independent targeting machineries, which typically also comprise cytosolic and ER membrane resident components and may also interact with ribosomes. Thus, there is substrate overlap and redundancy in these targeting machineries that we are only beginning to appreciate. This is described in more detail below, under the subheading "Targeting of Precursor Polypeptides to the Sec61 Complex in the Human ER membrane."

After their targeting to the ER, precursor polypeptides with amino-terminal signal peptides or transmembrane helices associate with the Sec61 complex via their targeting peptides and trigger opening of the Sec61 channel or gating of the Sec61 channel to the open state. The latter is supported by binding of the ribosomes to the Sec61 complexes in cotranslational transport. Some precursor polypeptides require help from auxiliary components for Sec61 channel opening, such as the membrane protein complex "translocon-associated protein" (TRAP) complex or the ER lumenal Hsp70-type molecular chaperone BiP (Fons et al., 2003; Lang et al., 2012; Schäuble et al., 2012; Sommer et al., 2013). Thus, BiP and TRAP can be seen as allosteric effectors of the Sec61 channel. Subsequently, BiP and TRAP can bind to precursor polypeptides in transit through the Sec61 channel and support their partial or complete translocation by acting as molecular ratchets. This capacity was directly demonstrated for BiP by reconstitution of transport components, originally present in an ER-derived detergent extract, into proteoliposomes and their subsequent use in cell-free transport assays. Those experiments showed that inclusion of avidin into these proteoliposomes could substitute for BiP in complete and efficient translocation of precursor polypeptides, which carried biotin-modified amino acid residues, even in the case of SRP-dependent transport (Tyedmers et al., 2003). In the case of TRAP, this was suggested by cross-linking studies employing stalled precursor polypeptides and rough ER–derived membrane vesicles, i.e., rough microsomes (Conti et al., 2015). Details are given below, under the three subheadings "Structure and Dynamics of the Human Sec61 Complex during Membrane Insertion and Translocation of Polypeptides," "Structure and Dynamics of the Human Protein Translocon during Membrane Insertion and Translocation of Polypeptides" and "Assisted Opening of the Human Sec61 Channel for Insertion and Translocation of Polypeptides."

In many cases, membrane insertion and translocation of polypeptides in transit are accompanied by modifications, i.e., removal of signal peptides by signal peptidase, N-glycosylation by oligosaccharyltransferase (OST), or GPI anchor attachment by GPI transamidase. Simultaneously, folding and assembly of the newly imported polypeptides begins, which involves a network of molecular chaperones in the ER lumen (reviewed by Braakman and Bulleid, 2011) ("folding" in **Figure 2**). The central components of this chaperone network are BiP, an ATP- and Ca^{2+}-dependent Hsp70-type chaperone, plus its Hsp40-type co-chaperones (ERjs or ERdj) and nucleotide exchange factors (NEFs) (reviewed by Dudek et al., 2009; Otero et al., 2010; Melnyk et al., 2014; **Table 1**). Furthermore, folding can involve additional chaperones, such as the glycoprotein-specific calnexin and calreticulin, and folding catalysts, i.e., protein disulfide isomerases (PDIs) and peptidylprolyl-*cis/trans*-isomerases (PPIases). Eventually, native polypeptides are passed on from the ER along the secretory pathway by vesicular transport.

The term "quality control" was coined to describe the fact that only correctly folded and assembled proteins are delivered from the ER to their functional location in the cell or outside of the cell (Ellgaard and Helenius, 2003). Mis-folded polypeptides

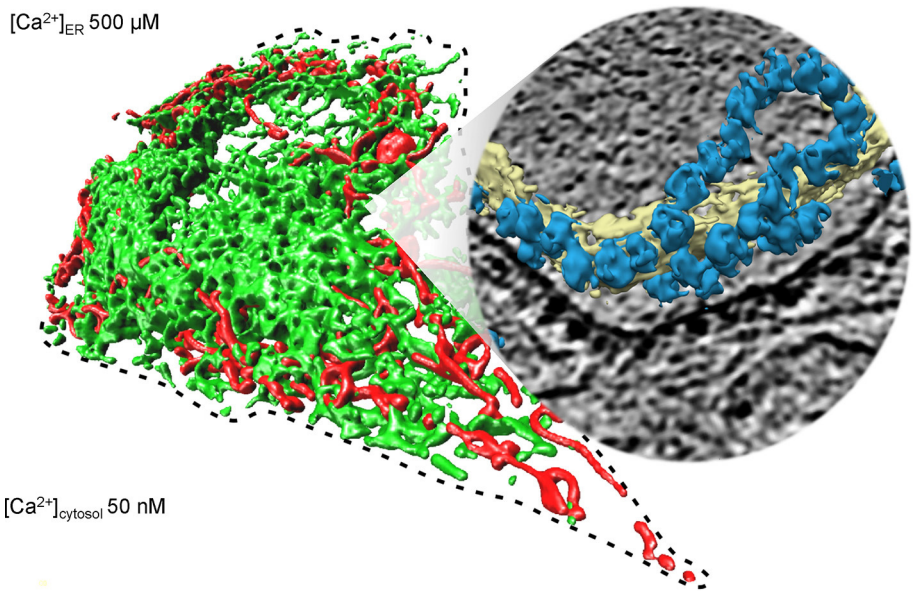

FIGURE 1 | Collage of 3D reconstructions of mammalian mitochondria and ER, respectively. The left part of the figure represents a 3D reconstruction after live cell fluorescence imaging, following import of a green fluorescent protein into the ER and of a red fluorescent protein into the mitochondria. The plasma membrane is indicated by a dashed line; the position of the round nucleus can be estimated in the upper part of the cell void of ER and mitochondria. Typical concentrations of free calcium are given for cytosol and ER of a resting cell. The right part represents a 3D reconstruction of cellular ER after CET, on top of a slice through the respective tomogram. ER membranes are shown in yellow; 80S ribosomes are shown in blue. The collage is based on Zimmermann (2016).

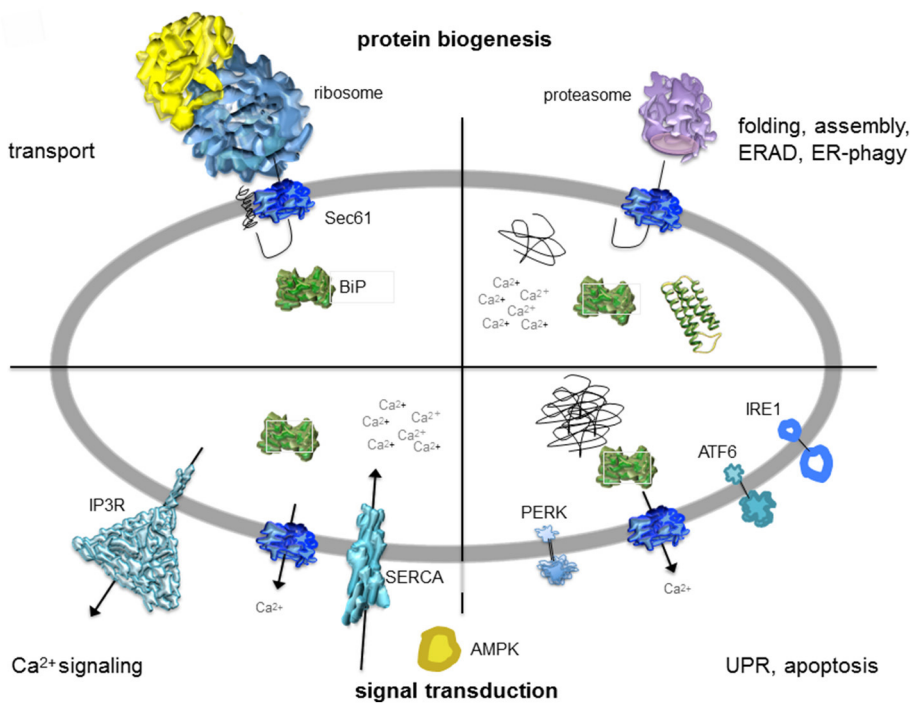

FIGURE 2 | Artist's depiction of cross-section through the mammalian ER with a focus on signal transduction and protein biogenesis. The non-annotated structures refer to a not yet-folded polypeptide, a natively folded protein, and an aggregate of non-native polypeptides, respectively. AMPK, AMP-activated protein kinase; IP3R, IP3-receptor; SERCA, sarcoplasmic/endoplasmic reticulum Ca^{2+} ATPase. The cartoon is based on Zimmermann (2016). See text for details.

TABLE 1 | Protein transport components and associated proteins in HeLa cells.

Component/ - Subunit	Abundance	Location	Linked diseases
Calmodulin	9,428	C	
Cytosolic Chaperones		C	
- Hsc70 (HSPA8)	3,559		
- Hdj2 (DNAJA1)			
- Bag1 (HAP, RAP46)			
#NAC		C	
- NACα	1,412		
- NACβ			
#SRP		C	
- SRP72	355		
- SRP68	197		
- SRP54	228		
- SRP19	33		
- SRP14	4,295		
- SRP9	3,436		
- 7SL RNA			
SRP receptor		ERM	
- SRα (docking protein)	249		
- SRβ	173		
- hSnd1	?		
Snd receptor			
- hSnd2 (TMEM208)	81	ERM	
- hSnd3	?		
#Bag6 complex		C	
- TRC35			
- Ubl4A			
- Bag6 (Bat3)			
SGTA		C	
TRC40 (Asna-1)		C	
TA receptor		ERM	
- CAML	5		Down syndrome, Congenital heart disease
- WRB (CHD5)	4		
#Sec62 (TLOC1)	26	ERM	Prostate cancer, Lung cancer
#Sec61 complex		ERM	
- Sec61α1	139		Diabetes, Common Variable Immune Deficiency (CVID), Tubulo-interstitial kidney disease (TKD)
- Sec61β	456		Polycystic Liver Disease (PLD)
- Sec61γ	400		Glioblastoma
Alternative Sec61 complex	?		
- Sec61α2	?		
- Sec61β			
- Sec61γ			

(Continued)

TABLE 1 | Continued

Component/ - Subunit	Abundance	Location	Linked diseases
Chaperone network			
- Sec63	168	ERM	Polycystic Liver Disease (PLD)
- #ERj1 (DNAJC1)	8	ERM	
- ERj3 (DNAJB11)	1,001	ERL	
- ERj4 (DNAJB9)	12	ERL	
- ERj5 (DNAJC10)	43	ERL	
- ERj6 (DNAJC3, $p58^{IPK}$)	237	ERL	Diabetes
- ERj7 (DNAJC25)	10	ERM	
- BiP (Grp78, HSPA5)	8,253	ERL	Hemolytic Uremic Syndrome (HUS)
- Grp170 (HYOU1)	923	ERL	
- Sil1 (BAP)	149	ERL	Marinesco-Sjögren-Syndrome (MSS)
$\#Calnexin_{palmitoylated}$	7,278	ERM	
#TRAM1	26	ERM	
TRAM2	40	ERM	
PAT-10			
#TRAP complex		ERM	
- TRAPα (SSR1)	568		
- TRAPβ (SSR2)			
- TRAPγ (SSR3)	1,701		Congenital Disorder of Glycosylation (CDG)
- TRAPδ (SSR4)	3,212		Congenital Disorder of Glycosylation (CDG)
#RAMP4 (SERP1)		ERM	
#Oligosaccharyltransferase		ERM	
- RibophorinI	1,956		
- RibophorinII	527		
- OST48	273		Congenital Disorder of Glycosylation (CDG)
- N33 (Tusc3)			Congenital Disorder of Glycosylation (CDG)
- IAP			
- Dad1	464		
- OST4			
- Stt3a*	430		Congenital Disorder of Glycosylation (CDG)
- Stt3b*	150		Congenital Disorder of Glycosylation (CDG)
- Kcp2			
Signal peptidase (SPC)		ERM	
- SPC12	2,733		
- SPC18*			
- SPC21*			
- SPC22/23	334		
- SPC25	94		

(Continued)

TABLE 1 | Continued

Component/ - Subunit	Abundance	Location	Linked diseases
GPI transamidase (GPI-T)		ERM	
- GPAA1	9		
- PIG-K	38		
- PIG-S	86		
- PIG-T	20		
- PIG-U	42		
Signal peptide peptidase		ERM	
#p34 (LRC59)	2,480	ERM	
#p180	10	ERM	
kinectin	263	ERM	

*Alternative names of components/subunits are given in parentheses. We note that oligosaccharyltransferase comes in four types, comprising Stt3a or Stt3b in combination with N33 or IAP. Abundance refers to HeLa cells and is given in nM (Hein et al., 2015); C, cytosolic; ERL, ER lumenal protein; ERM, ER membrane resident; *, catalytically active subunit; #, ribosome associated; ?, uncharacterized in mammalian cells.*

are subjected to ER-associated protein degradation (ERAD) or a specialized form of autophagy (ER-phagy) (**Figure 2**). ERAD can apparently involve BiP and the Sec61 complex for the export of certain mis-folded polypeptides from the ER to the cytosol for subsequent degradation by the proteasome (reviewed by Römisch, 2005). Thus, BiP and the Sec61 complex act at the crossroads of ER protein import and ERAD. In general, however, dedicated ERAD machineries that are specialized in mis-folded ER-lumenal polypeptides or membrane proteins are involved, which are described in detail elsewhere (reviewed by Bagola et al., 2011). Most recent cryo-EM data characterized Hrd1 as the protein-conducting channel for ER export of mis-folded polypeptides (Schoebel et al., 2017). ER-phagy can involve the interaction between either one of the ER membrane proteins FAM134 and Sec62 with cytosolic protein LC3 and delivers whole ER sections for degradation within lysosomes (Khaminets et al., 2015; Fumagalli et al., 2016). We note that Sec62 is also involved in ER protein import and therefore provides a link between protein transport and quality control (Lakkaraju et al., 2012; Lang et al., 2012).

Prolonged protein mis-folding triggers the unfolded protein response (UPR); when the rescue attempt by decreased protein synthesis and increased levels of ER chaperones and ERAD components is unproductive, programmed cell death (apoptosis) is initiated (reviewed by Ma and Hendershot, 2001; Zhang and Kaufman, 2004; **Figure 2**). Thus, UPR and activation of the "intrinsic" pathway to apoptosis represent ER resident signal transduction pathways, which initially work to protect cells from aggregation-prone polypeptides. Ultimately they secure survival of the multicellular organism by sacrificing cells with terminal protein aggregation problems. The major players in UPR are the ER membrane proteins ATF6, IRE1, PERK, and Sig-1R. These are similar to the membrane-integrated ERjs in being transmembrane proteins and comprising a lumenal domain that can interact with BiP. In brief, these signal transduction components are inactive when BiP is bound to the lumenal domain; when BiP becomes sequestered by unfolded polypeptides, however, it is released and the signal transduction components become activated. Interestingly, IRE1 also interacts with the Sec61 complex, which adds yet another layer of UPR regulation and provides a noteworthy interconnection between ER protein import and ER stress signaling (Sundaram et al., 2017). A more detailed picture about BiP and ERjs is given in the section below titled "BiP and Its Co-factors in the Human ER, a Prolog" as well as the paragraphs concerning the assisted opening and closing of the Sec61 complex and "Novel Concept for Physiologic Roles of the Human Sec61 Channel in Cellular Calcium Homeostasis and Energy Metabolism."

Induction of the intrinsic apoptosis pathway involves Ca^{2+} release from the ER, which may represent one potential physiological role of the passive ER Ca^{2+} leak that occurs at the level of the open Sec61 channel and is held at bay by BiP (Schäuble et al., 2012) ("Ca^{2+} signaling" in **Figure 2**). However, another potential role of the Sec61 complex acting in ER Ca^{2+} leakage may be related to regulation of ATP transport into the ER, which is essential for BiP activity. In any case, BiP and the Sec61 complex are also connected to intracellular Ca^{2+} signaling and cellular Ca^{2+} homeostasis. These issues are discussed below, in the sections on "Closing of the Human Sec61 Channel for Preservation of Cellular Calcium Homeostasis" and "Novel Concept for Physiologic Roles of the Human Sec61 Channel in Cellular Calcium Homeostasis and Energy Metabolism."

We note that quality control does not occur only after membrane insertion or translocation at the level of protein folding and assembly. Proteasomes can also eliminate precursor polypeptides that were not properly targeted, which involves cytosolic protein Bag6 (Wang et al., 2011; Leznicki and High, 2012), or became stuck at the cytosolic surface of the Sec61 complex or even in transit through the Sec61 channel. The elimination option has been termed "pre-emptive quality control" by R. Hegde and involves the cytosolic ubiquitin-ligase Listerin or the ER lumenal ERj6 (Kang et al., 2006; Rutkowski et al., 2007; von der Malsburg et al., 2015). The latter option was described by M. Schuldiner as resolving translocon "clogging" and depends on the ER membrane-resident protease ZMPSTE24 (Ast et al., 2016). Interestingly, Bag6 also acts in protein targeting to the ER, and ERj6 appears to be involved in Sec61 channel closing, adding more examples to the list of pathway interconnections.

BIP AND ITS CO-FACTORS IN THE HUMAN ER, A PROLOG

BiP was discovered and named as an immunoglobulin heavy chain binding protein for its role in immunoglobulin assembly. It is also known as glucose-regulated protein with a mass of 78 kDa (Grp78) because it is over-produced under ER stress conditions, such as glucose starvation (Haas and Wabl, 1983). BiP is the most abundant Hsp70-type molecular chaperone in the ER lumen, reaching concentrations in the millimolar range

even under non-stress conditions, and depends on ATP and Ca^{2+} for its activity (reviewed by Dudek et al., 2009; Otero et al., 2010; Melnyk et al., 2014). Another, but less abundant, member of the Hsp70 family in the ER is glucose-regulated protein with a mass of 170 kDa (Grp170). BiP and Grp170 can form a stable complex. Furthermore, various other components were found to form oligomeric complexes together with BiP, such as other chaperones, folding catalysts, and ER-resident proteins with functions in either protein transport, N-glycosylation, or cellular Ca^{2+} homeostasis (reviewed by Dudek et al., 2009).

Hsp70-type molecular chaperones, such as BiP, bind reversibly to substrate polypeptides via their substrate-binding domains (SBDs) (**Figure 3**). Typically, BiP substrates are hydrophobic oligopeptides within loosely- or un-folded polypeptides (Flynn et al., 1991; Blond-Elguindi et al., 1993). Binding of a substrate to the SBD inhibits unproductive interactions of the polypeptide and favors productive folding and assembly, which occur concomitantly with release from BiP. In addition, BiP can regulate the activities of folded polypeptides (e.g., Sec61α). This binding and release of substrates by BiP are facilitated by interaction of its SBD and its nucleotide-binding domain (NBD). NBD-conformation and BiP's ATPase cycle are modulated by different Hsp70 interaction partners (Dudek et al., 2009; Otero et al., 2010; Melnyk et al., 2014). The ATP-bound state of BiP has a low affinity for substrate polypeptides, and the ADP-bound state has a high substrate affinity. Hsp40-type co-chaperones of the ER lumen (ERjs or ERdjs or, more systematically, DNAJs) stimulate the ATPase activity of BiP and thereby favor substrate binding. NEFs of the ER lumen stimulate the exchange of ADP for ATP and thus induce substrate release.

As we have stated in more general terms before (Dudek et al., 2009), ERjs are characterized by J-domains that allow interaction with BiP via the bottom of its NBD. As of today, there are seven different ERjs present in the ER of a human cell (**Figure 3**), termed ERj1 through ERj7. They can be sub-classified as either ER membrane proteins or soluble ER lumenal proteins both with the characteristic lumenal J-domain. In more detail, ERjs can be classified according to the domains they have in common with the bacterial DnaJ protein (Cheetham and Caplan, 1998; Hennessy et al., 2005). "Type-I ERjs contain four domains: an amino-terminal J-domain, a glycine–phenylalanine (G/F)-rich domain, a Zn finger or cysteine repeat domain, and a carboxy-terminal SBD (ERj3). Type-II ERjs contain three domains: an amino-terminal J-domain, a G/F-rich domain, and a carboxy-terminal SBD (ERj4). Type III ERjs contain only the J-domain and, in general, have more specialized functions as compared to type I and II ERjs. Thus, ERj3 and ERj4 can bind substrate polypeptides and deliver them to BiP, i.e., facilitate polypeptide folding." However, the four thioredoxin domains within ERj5 and the tetratricopeptide repeat domain in ERj6 ($p58^{IPK}$) may also play a role in substrate binding. In addition, recent evidence provided further insight into the functional and regulatory role of three ERjs and how they balance Ca^{2+} flux across the ER membrane. While the pair of ERj3 and ERj6 minimizes the passive Ca^{2+} efflux across the Sec61 complex, ERj5 triggers the influx of Ca^{2+} via activation of the SERCA2 pump in a Ca^{2+} dependent manner (Schorr et al., 2015; Ushioda et al., 2016). Once Ca^{2+} levels in the ER are replenished, ERj5 is inactivated and forms oligomers. Interestingly, this circuit of Ca^{2+} flux across the ER membrane orchestrated by SERCA2 and

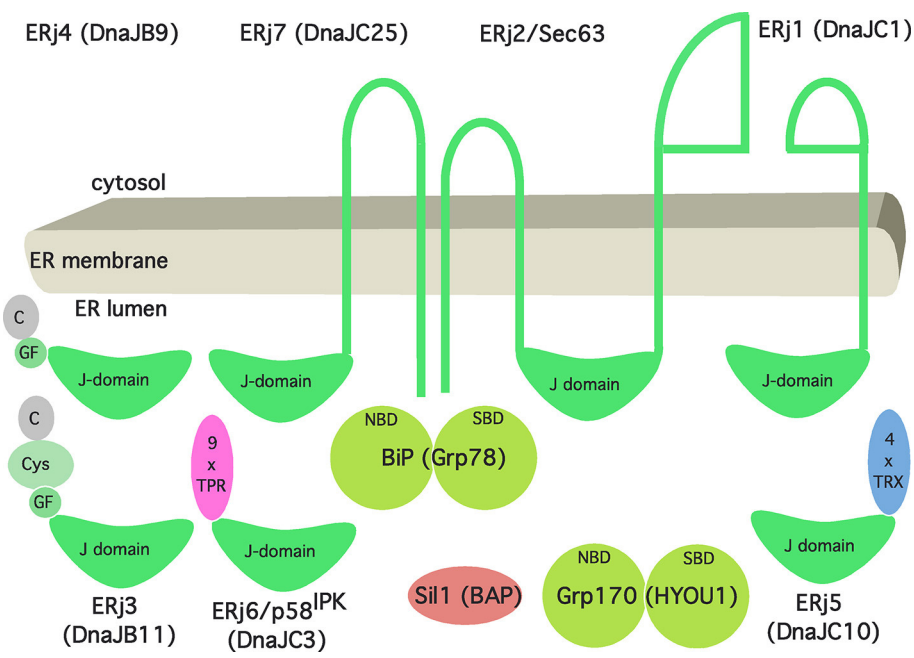

FIGURE 3 | Artist's view of the Hsp70/Hsp40 chaperone network of the human ER. See text for details. The following binding characteristics (K_D) were observed for BiP binding in the presence of ATP (in μM): ERj1, 0.12; Sec63, 5; ERj3, 3.5; ERj4, 6.07; ERj5, 0.45; ERj6, 0.59; ERj7, 1.1. The cartoon and affinities are based on Schorr et al. (2015).

the Sec61 complex is tightly connected to the master regulator of the UPR, BiP. On the one hand, direct binding of BiP to the lumenal loop 7 of the mammalian Sec61 complex prevents the leakage of Ca^{2+} (Schäuble et al., 2012). On the other hand, BiP, potentially in its function as classical chaperone, prevents oligomerization of ERj5 and, hence, inactivation of SERCA2 mediated Ca^{2+} influx (Ushioda et al., 2016). At a first glance, BiP seems to fine tune Ca^{2+} flux across the ER membrane. Yet, from a broader perspective, this circuitry sheds light on a potential connection between the Ca^{2+} balance of the ER and the UPR. Consequently, the passive Ca^{2+} efflux of the ER membrane might actually represent a signaling pathway reporting about protein homeostasis and folding capacity within the ER lumen.

Two NEFs are present in the ER lumen, Sil1 and Grp170 (**Figure 3**). Sil1 was predicted to be structurally related to cytosolic HspBP1, one of the NEFs of cytosolic Hsc70 in eukaryotes. Grp170 appears to be structurally related to Hsp110, an alternative NEF of cytosolic Hsc70 in eukaryotes. The structures of HspBP1 and Hsp110 suggested distinct interacting surfaces of their ER-lumenal equivalents with the top of BiP's NBD (reviewed by Bracher and Verghese, 2015).

TARGETING OF PRECURSOR POLYPEPTIDES TO THE SEC61 COMPLEX IN THE HUMAN ER MEMBRANE

A first concept for protein targeting to the ER was established by Blobel and Dobberstein (1975). In brief, an amino-terminal signal peptide in the nascent precursor polypeptide is recognized and bound by SRP in the cytosol and mediates a translational attenuation (Walter and Blobel, 1981; Halic et al., 2004, 2006; Voorhees and Hegde, 2015). The corresponding ribosome-nascent chain-SRP complex associates with the ER membrane via the heterodimeric SR, which is membrane anchored via the β-subunit (Meyer and Dobberstein, 1980; Gilmore et al., 1982; Miller et al., 1995). Interaction between SRP and SR drives the mutual hydrolysis of bound GTP and leads to release of the ribosome-nascent chain complex at the ER membrane in the vicinity of the Sec61 complex (**Supplementary Video 1**). Thus, in addition to its role in targeting precursor polypeptides to the ER, SRP is a molecular chaperone for nascent precursor polypeptides and an mRNA-targeting device. Interestingly, it also targets *XBP1* mRNA to the ER, where *XBP1* mRNA is cleaved by Sec61 complex associated Ire1, providing a link between ER protein import and the Ire1 branch of the UPR (Plumb et al., 2015; Kanda et al., 2016). A stalling element encoded in the 3′ region of the unspliced mRNA of XBP1 (XBP1u) leads to translational pausing after synthesis of a hydrophobic region and its emergence from the ribosomal tunnel exit (Yanagitani et al., 2011). The artifice, this mildly hydrophobic region paired with the translational arrest are allowing for unconventional SRP-mediated targeting to the Sec61 translocon, yet, avoiding efficient insertion into the ER membrane. Taking the interaction of Ire1α and the Sec61 complex into account targeting of XBP1u mRNA to the translocon allows efficient processing of XBP1u by Ire1α during ER stress conditions.

Besides SRP mediated targeting, bioinformatic analysis of the yeast secretome predicted up to 30% of all extracellular proteins being independent of SRP (Aviram and Schuldiner, 2014). Experimental identification of precursor proteins with the ability to facilitate ER targeting independent of SRP—such as GPI-anchored membrane proteins in yeast, TA membrane proteins in yeast and mammalian cells, and small presecretory proteins in the mammalian system—support the existence of alternative ER targeting machineries (Schlenstedt et al., 1990; Kutay et al., 1995; Ast et al., 2013). Accordingly, many studies determined the capacity of the ER handling a broad variety of structurally diverse precursor proteins (Stefanovic and Hegde, 2007; Schuldiner et al., 2008; Aviram et al., 2016). Their diversity is not restricted to differences in the amino acid sequence of matures domains, but equally evident in primary structure, length, hydrophobicity and location of the signal sequence itself (reviewed by von Heijne, 1985; Hegde and Bernstein, 2006). Although each of these signal sequence features has been addressed experimentally to demonstrate impact on the targeting process, the location of the targeting peptide within the precursor protein is what led to the identification of the first SRP-independent targeting route for TA membrane proteins.

TA proteins are classically defined as single spanning type 2 membrane proteins devoid of a cleavable signal sequence. Instead, TA proteins harbor a characteristic carboxy-terminally located transmembrane helix, the tail-anchor (Kutay et al., 1995; Rabu et al., 2009; Borgese and Fasana, 2011). Roughly 1% of the human genome encodes TA proteins, not all of which end up in membranes of the endo- or exocytotic pathways. TA proteins of the secretory pathway, such as the β- and γ-subunits of the Sec61 complex, Cytochrome b_5, and many components of vesicular transport, need to be targeted and inserted into the ER membrane. Equivalent to the underlying principle of the SRP-mediated targeting, TA proteins are chaperoned in a translocation-competent fashion through the cytosol and directed to the ER membrane via an ER membrane resident receptor complex. The minimal targeting machinery for TA proteins was termed the guided entry of tail-anchored proteins (GET)-complex in yeast and TA receptor complex (TRC) in the mammalian system (**Table 1**). In principle, the cytosolic ATPase Trc40 with its hydrophobic binding pocket binds the TA protein, and the heterodimeric receptor complex, comprising Wrb and Caml, is required for efficient ER targeting (Stefanovic and Hegde, 2007; Vilardi et al., 2011, 2014; Yamamoto and Sakisaka, 2012). At least in yeast, orthologs of the latter two proteins are also supposed to facilitate the actual TA membrane insertion (Wang et al., 2011). Furthermore, the mammalian TA-targeting machinery involves a ribosome-associating heterotrimeric Bag6 complex (comprising Bag6, Ubl4A, and Trc35) and SGTA, which appear to act upstream of Trc40 (Leznicki et al., 2010; Mariappan et al., 2010). Interestingly, Bag6 is also involved in degradation of TA proteins, i.e., at the crossroads of targeting and quality control (Wang et al., 2011; Leznicki and High, 2012).

Although about one dozen genes encoding for yeast TA proteins were characterized as essential, knockout strains of the yeast GET machinery were viable, suggesting the existence

of at least one alternative targeting route. Indeed, in 2016, a high-throughput screening approach in the lab of M. Schuldiner identified a hitherto uncharacterized targeting pathway in yeast, termed the SRP-independent (SND)-system (Aviram et al., 2016). This genetic screen used a fluorescent reporter substrate based on an obligate SRP-independent and only partially GET-dependent substrate protein. Hence, mislocalization of this reporter in any particular null mutant strain served as evidence of a targeting factor. Three novel components have been identified and characterized: Snd1, Snd2, and Snd3 (**Table 1**). Two hallmarks of the SND targeting pathway have been emphasized. First, similar to the SRP- and GET-targeting mechanisms, precursor substrates were targeted via the interplay of a cytosolic mediator (Snd1) and a heterodimeric receptor located at the ER membrane (Snd2, Snd3). We note that Snd1 had previously been described as a ribosome-interacting protein. Second, the SND machinery showed a preference for substrates with a central transmembrane domain. At the same time, the SND route could provide an alternative targeting pathway for substrates with a transmembrane helix at their extreme amino- or carboxy-terminus, i.e., typical SRP- or GET-dependent substrates. So far, no nucleotide requirement has been assigned to this targeting system. Sequence comparisons identified the previously characterized ER membrane protein TMEM208 as a putative human Snd2 orthologue, termed hSnd2 (Zhao et al., 2013; Aviram et al., 2016). According to experiments that combined siRNA-mediated gene silencing and protein transport into the ER of human cells in cell-free transport assays, hSnd2 appears to have the same function as its yeast counterpart (Haßdenteufel et al., 2017). So far, however, human orthologs of Snd1 and Snd3 have not been identified. Judging from the levels of SR, Wrb/Caml, and hSnd2 in HeLa cells, the impression is that the SND pathway may account for almost 30% of precursor targeting in this particular human cell (Hein et al., 2015; **Table 1**). Interestingly, TMEM208 was originally described as a player in ER-phagy, providing yet another link between ER protein import and protein quality control (Zhao et al., 2013).

In addition, fully synthesized precursors of small presecretory proteins in human cells were proposed to be targeted to the mammalian ER membrane in an SRP-independent fashion in several ways: (i) by their interaction with Trc40 and its putative interaction with the Trc40 receptor, (ii) by their interaction with the cytosolic protein calmodulin and its putative association with a calmodulin-binding IQ motif in the cytosolic amino-terminus of the Sec61α protein, and (iii) by direct interaction of their signal peptides with the ER membrane resident Sec62 (Shao and Hegde, 2011; Johnson et al., 2012, 2013; Lakkaraju et al., 2012). In the latter case, precursors may be chaperoned in the cytosol by Hsc70 and its Hsp40 type co-chaperones or by calmodulin, if or when the latter does not act in targeting via the IQ motif. In terms of interconnections between pathways, it is interesting to note that calmodulin was described to inhibit rather than stimulate targeting of TA proteins to the mammalian ER membrane (Haßdenteufel et al., 2011). Along the same lines, the Hsc70-interacting protein Bag1 can also deliver proteins to the proteasome, i.e., acts at the cross-roads of targeting and quality control (Alberti et al., 2003), and Sec62 can facilitate ER-phagy (Fumagalli et al., 2016).

Furthermore, the synthesis of many polypeptides is apparently initiated on ribosomes or large ribosomal subunits that are continuously attached to the ER membrane (Potter et al., 2001; Stephens et al., 2008). Therefore, direct mRNA targeting was suggested as an alternative ER-targeting mechanism, and the proteins p180 and kinectin were described as mRNA receptors in the ER membrane (**Table 1**). So far, there is no consensus about the possible specificity of this targeting reaction, and we are not aware of a single example of a precursor polypeptide in which mRNA targeting was a prerequisite for subsequent membrane insertion or translocation by the Sec61 complex. However, polypeptides that lack a signal peptide for ER targeting and whose synthesis was initiated on ER-bound ribosomes or large ribosomal subunits were found to be recognized by the nascent chain associated complex (NAC) (Wiedmann et al., 1994). Apparently, this interaction leads to release of the respective ribosomes from the membrane and completion of protein synthesis in the cytosol (Möeller et al., 1998; Gamerdinger et al., 2015). Thus, NAC-mediated targeting antagonism keeps the intrinsic affinity of ribosome-nascent chain complexes for the Sec61 complex in check and thereby prevents both extensive mistargeting of mitochondrial proteins to the ER and impairment of protein homeostasis in those organelles.

From a broader perspective, the emerging concept for ER protein targeting is that a molecular triage is occurring for ER-destined precursor polypeptides in the cytosol, determining the fates of nascent or fully synthesized but not-yet-folded polypeptides. It does so via a complex network of targeting signals in nascent chains and completed polypeptides and a whole variety of cytosolic factors that decode these signals. At first, these factors assist the precursors in staying in solution and remaining competent for ER targeting as well as subsequent insertion into or translocation across the ER membrane. If one of these tasks fails, the precursor is targeted to the proteasome. At later stages of protein biogenesis at the ER, this principle is repeated at the level of membrane insertion and translocation and eventually during folding and assembly.

STRUCTURE AND DYNAMICS OF THE HUMAN SEC61 COMPLEX DURING MEMBRANE INSERTION AND TRANSLOCATION OF POLYPEPTIDES

From a historical perspective the term "Sec" was allocated to proteins involved in protein "sec"retion and first introduced based on a yeast screen from the Schekman lab for mutants unable to efficiently secrete invertase and acid phosphatase (Novick et al., 1980; Spang, 2015). Although not among the initial 23 complementation groups, Sec61 was identified in a follow-up study also by the Schekman group (Deshaies and Schekman, 1987; Schekman, 2002). Subsequently, the structure of the hetero-trimeric Sec61 complex was first suggested by T. Rapoport and colleagues based on the X-ray crystallographic analysis of isolated archaean ortholog SecY complex (Van den Berg et al., 2004).

The high sequence conservation of the SecY and Sec61 subunits indicated that their architecture and dynamics are evolutionarily conserved, which was confirmed by a number of subsequent cryo-electron microscopy (EM)-studies on detergent-solubilized or reconstituted ribosome-bound SecY or Sec61 complexes (Gogala et al., 2014; Voorhees et al., 2014). The central channel-forming subunit (Sec61α) consists of 10 transmembrane helices and is arranged in two pseudo-symmetrical amino- and carboxy-terminal halves around a central constriction which is sealed by the "pore ring," a ring of bulky hydrophobic side chains, and a short "plug" helix (**Figures 4**, **5**). The Sec61β and Sec61γ subunits are present on the outskirts of the Sec61 complex and contain one TA each. Strikingly, two distinct conformations of the Sec61 channel could be distinguished, which differ in the relative positioning of the amino- and carboxy-terminal Sec61α halves. These conformations either allow or don't allow lateral access of signal peptides or transmembrane helices of polypeptides in transit from the central channel toward the phospholipid bilayer through a "lateral gate" formed by transmembrane helices 2 and 7 of Sec61α (**Figures 4**, **5**). This "lateral gate" enables insertion of nascent transmembrane helices or signal peptides emerging from the ribosome into the phospholipid bilayer. Without doubt, events at the "lateral gate" of the Sec61 complex are critical for understanding the process of protein translocation under physiological conditions, i.e., allowing transfer of a proteinaceous entity from one environment into a very different second one and simultaneously preserving the steep ER to cytosol Ca^{2+} gradient in the cell. Structural determination of programmed ribosome-Sec61 complexes implied a series of events upon arrival of a nascent precursor (Voorhees et al., 2014; Voorhees and Hegde, 2016). The idle or quiescent Sec61 complex unable to promote protein transfer is primed by binding of the ribosome to cytosolic loops 6 and 8 of Sec61α as well as the amino-terminus of Sec61γ, unveiling a hydrophobic patch in the cytosolic funnel of the engaged Sec61 complex (**Figures 5**, **6**). This patch, in vicinity to the lateral gate, serves as an interaction site for an incoming hydrophobic signal peptide that in turn displaces helix 2 of Sec61α in order to destabilize the "lateral gate" and open the aqueous channel in the Sec61 complex for protein translocation. The cryo-EM data also demonstrated that even in cotranslational translocation, some considerable stretch of a nascent precursor polypeptide can accumulate at the interface between the ribosome and the Sec61 complex without compromising translocation (Park et al., 2014; Conti et al., 2015). Thus, elongation does not necessarily provide a driving force in translocation.

Cryoelectron tomography (CET) of translocons in native ER membrane vesicles derived from human cell lines or primary fibroblasts and even intact cells has given unprecedented insights into the architecture and dynamics of the Sec61 channel in its physiological setting and of the native translocon (Pfeffer et al., 2014, 2015, 2017; Mahamid et al., 2016). The atomic model of the solubilized ribosome-bound Sec61 complex (Voorhees et al., 2014), opened laterally by a signal peptide, was easily docked into the CET density, defining the position and conformation of Sec61 subunits in the center of the native translocon (**Figure 4**). Furthermore, weak helical density opposing the "lateral gate" in the CET density map confirmed the position of signal peptides, as it had been observed after detergent solubilization of ribosome-nascent chain-bound Sec61 complexes. Sec61 was found with an open "lateral gate," possibly suggesting that Sec61 remains laterally open throughout protein translocation. At this point, the aqueous channel in the center of the complex is most likely occupied by the polypeptide chain in transit. However, computational sorting of subtomograms implied that the majority of ribosome–translocon complexes are idle and, therefore, not engaged in membrane protein insertion or protein translocation, although they were characterized by an open "lateral gate." A possible explanation for laterally open Sec61 bound to idle ribosomes may be that even after termination of protein synthesis, signal peptides or transmembrane helices remain bound to Sec61 and keep the "lateral gate" open. In line with this view, helical density coinciding with the position of signal peptides was observed opposite of the "lateral gate" also for idle ribosome–Sec61 complexes. In this case, the aqueous channel in the center of the complex should be closed by the "pore ring" and/or the "plug" helix.

STRUCTURE AND DYNAMICS OF THE HUMAN PROTEIN TRANSLOCON DURING MEMBRANE INSERTION AND TRANSLOCATION OF POLYPEPTIDES

As we have previously outlined (Zimmermann et al., 2011), "the first hints on participation of additional components in cotranslational protein transport came from the analysis of ribosome-associated ER membrane proteins present in detergent extracts of mammalian canine pancreatic microsomes. The term ribosome-associated membrane proteins (RAMPs) was coined for this class of membrane proteins after their solubilization in the presence of 400 mM potassium chloride (Görlich and Rapoport, 1993). By definition, the Sec61 complex is a RAMP, and so are RAMP4, TRAP and OST (**Table 1**). More recently, ERj1 and Sec62 were characterized as RAMPs, although their ribosome association is seen only under more physiological salt concentrations (up to 200 mM potassium chloride) and therefore may be more dynamic compared with the high-salt resistant RAMPs (Blau et al., 2005; Dudek et al., 2005; Benedix et al., 2010; Müller et al., 2010).

Additional information on the composition of the native protein transport machinery in the ER membrane came from fluorescence resonance energy transfer (FRET) experiments, which employed fluorescently labeled antibodies against transport components, permeabilized canine cells, and fluorescence microscopy." According to this more physiological experimental strategy, Sec61α1, Sec61β, Sec62, and ERj1 are RAMPs, i.e., they are associated with ribosomes in the intact ER (Snapp et al., 2004; Benedix et al., 2010; Müller et al., 2010). Furthermore, this approach demonstrated that SR, the TRAP complex, and translocating chain-associating membrane (TRAM) protein are permanently in close proximity to Sec61 complexes. Recent cross-linking data suggested that SR and Sec62 interact with Sec61α in a mutually exclusive manner

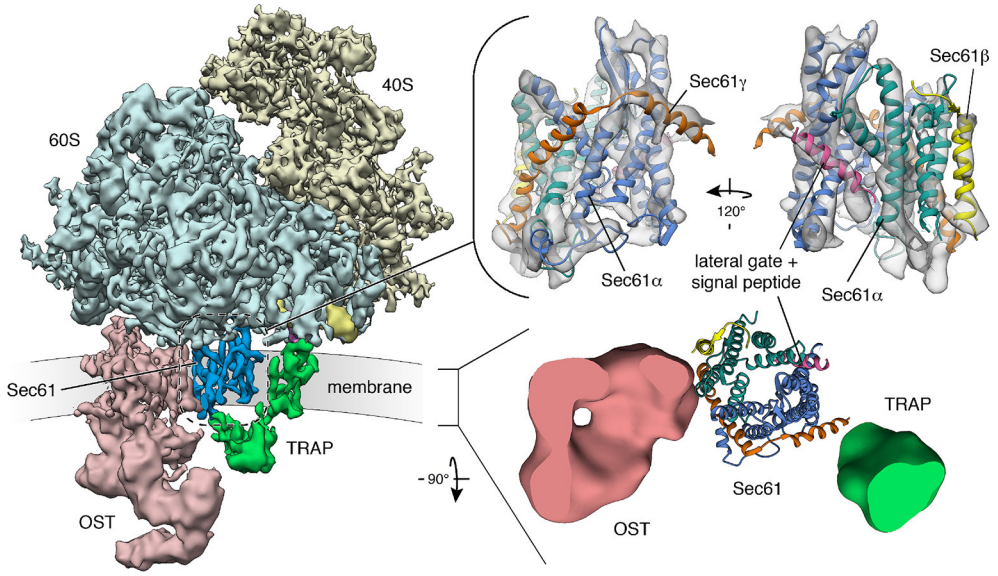

FIGURE 4 | Structure and architecture of the native mammalian translocon visualized using CET. (**Left**) Overall structure of the native ribosome-translocon complex (EMD 3069) with the ribosomal subunits (40S: yellow; 60S: light blue) and the translocon components Sec61 (dark blue), TRAP (green) and OST (red) depicted. Within the 60S subunit, eL38 (purple) and the short expansion segment (bright yellow), which are contacted by the cytosolic domain of TRAPγ, are highlighted. **Right, upper panel**: Isolated density for the Sec61 complex with an atomic model of the laterally opened Sec61 complex (PDB 3jc2) superposed. The Sec61α (N-terminal: green; C-terminal half: blue), Sec61β (yellow) and Sec61γ (orange) subunits are indicated. A signal peptide (magenta) is intercalated at the lateral gate. **Right, lower panel**: Transmembrane region of the translocon with down-filtered densities for membrane-embedded segments of TRAP (green) and OST (red) depicted. Sec61 is represented by an atomic model. The ER membrane resides in the paper plane.

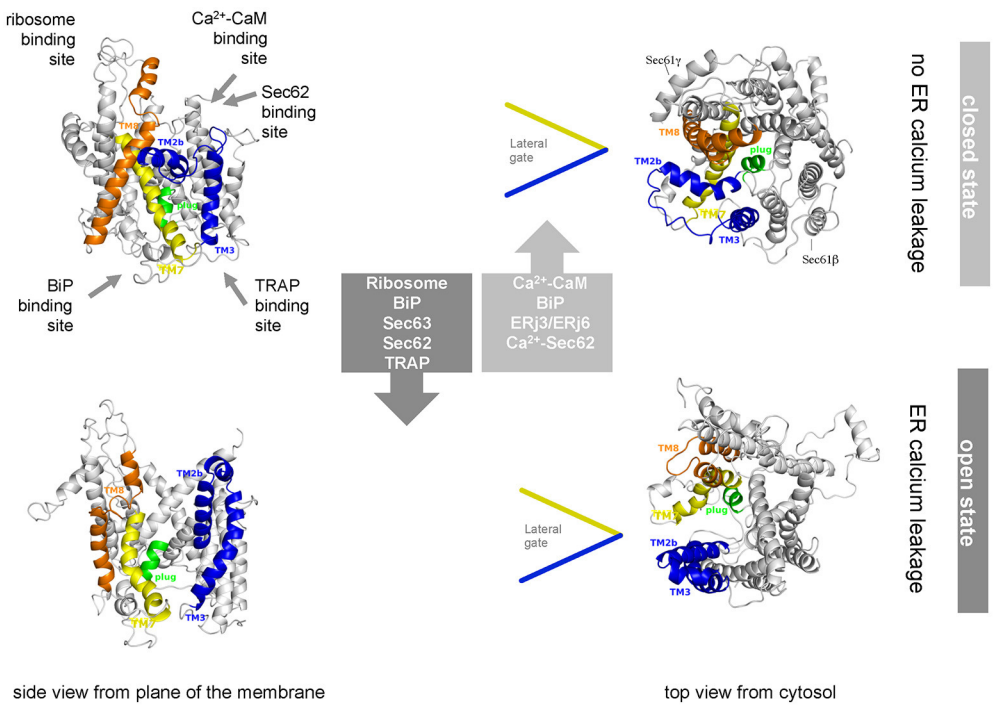

FIGURE 5 | Artist's view of the dynamic equilibrium and gating mechanisms of the human Sec61 complex. Allosteric effectors of the dynamic equilibrium of the Sec61 channel and their binding sites are indicated. The cartoon is based on Dudek et al. (2015). See text for details.

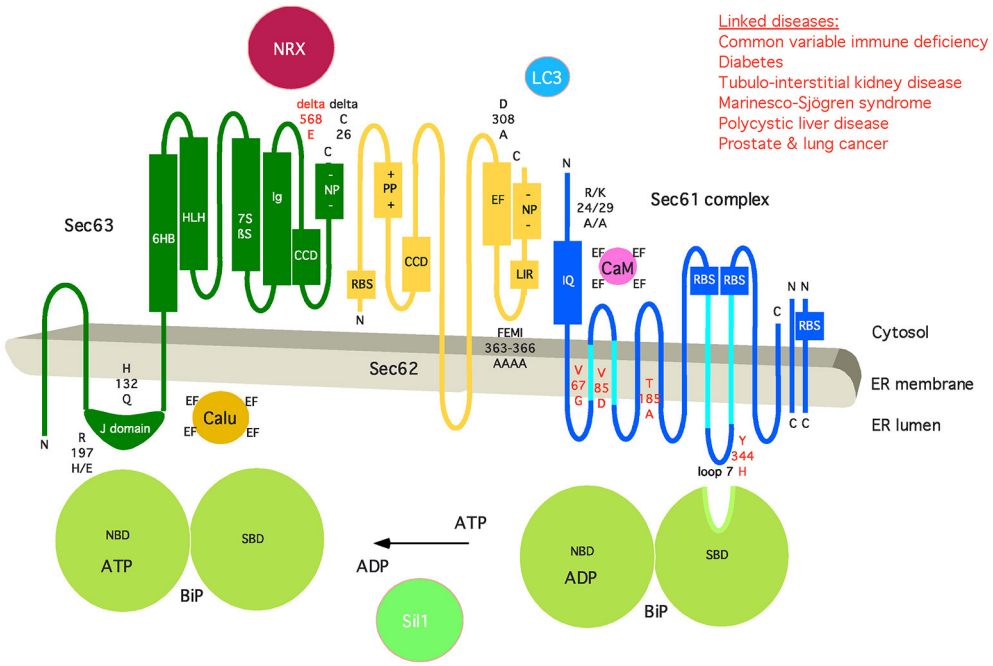

FIGURE 6 | Artist's depiction of the domain organization of Sec61 complex and its auxiliary components BiP, Sec62, and Sec63. Additional interaction partners of BiP (Sil1), Sec61 (Calmodulin, CaM), Sec62 (LC3), and Sec63 (Nucleoredoxin, NRX; Calumenin, Calu) are shown. Furthermore, relevant motifs (such as IQ and LIR) and domains are indicated, as well as point mutations that disturb the respective interaction or are linked to disease (in red). CCD, coiled-coil domain; EF, EF hand; NBD, nucleotide-binding domain; NP, negatively charged patch; PP, positively charged patch; RBS, ribosome-binding site; SBD, substrate-binding domain. The following binding characteristics were observed: BiP/Sec61α K_d 500 μM, ATP-dependent; BiP/Sec63 K_D 5 μM; CaM/Sec61α K_D 115 nM, Ca^{2+}-dependent, TFP-sensitive; Sec62/Sec61α Ca^{2+}-sensitive; Sec62/LC3 K_D 20 μM; Sec63/NRX H_2O_2-dependent; Sec63/Sec62 K_D 5 nM. C, carboxy-terminus; N, amino-terminus. See text for details.

and may use the same binding site at the cytosolic amino-terminus (Jadhav et al., 2015). Therefore, it was proposed that SR can switch the Sec61 channel from Sec62- to SRP-dependent translocation.

Other experiments addressing the dynamics of the human protein translocon showed that precursors of ERj3 and prion protein depend on BiP, Sec62, and Sec63 in their ER import in cell-free transport experiments (Lang et al., 2012; Schäuble et al., 2012). Additional cross-linking experiments with stalled, radiolabeled precursor polypeptides in transit through the translocon of canine pancreatic ER membranes demonstrated that Sec62 and Sec63 only transiently associate with the Sec61 complex in a substrate-specific manner (Conti et al., 2015). Both precursor polypeptides analyzed, ERj3 and prion protein, appeared to recruit Sec62 and Sec63 to the Sec61 complex rather late in their synthesis, i.e., at precursor polypeptide chain lengths of around 150 amino acid residues. And, their signal peptides become accessible to ER-lumenal signal peptidase at chain lengths of almost 200 amino acid residues. Interestingly, a similar situation, i.e., a dynamic recruitment of Sec62 and Sec63, could be forced even for preprolactin by introducing a tightly folded zinc finger domain in the presence of Zn^{2+}. As would be expected based on previous cross-linking studies with nascent preprolactin chains, preprolactin was first processed by signal peptidase at a chain length of 140 residues and found in complex with Sec61 complex, TRAP, TRAM, and OST at this stage of translocation. We conclude from these observations that in contrast to preprolactin, the two precursors of ERj3 and prion protein may contain "weak" or slowly-gating signal peptides. As a result, opening of the Sec61 channel occurred late in their synthesis, and extended sections of these two precursor polypeptides accumulated at the interface between the ribosome and the Sec61 complex triggering a rearrangement of the translocon composition to facilitate precursor translocation.

We note that a permanent association of ribosome-associated Sec61 complexes with TRAP and OST was confirmed in the recent three-dimensional (3D) reconstructions after CET of native translocons in ER membrane vesicles, derived from canine pancreas or various human cells and even intact cells (Pfeffer et al., 2014, 2015, 2016; Mahamid et al., 2016; **Figure 4**). Interestingly, all ribosome-associated Sec61 complexes were routinely found to be associated with TRAP, irrespective of the cellular origin of the native complexes. However, the occupancy of these Sec61/TRAP super-complexes by OST varied from one cell type to the next. While the OST occupancy was found to be around 70% in dog pancreas microsomes and microsomes isolated from several other cell types specialized in protein secretion, only 35% of translocon complexes contained OST in microsomes isolated from HeLa or HEK cells and in intact HeLa cells (Pfeffer et al., 2016). So far, our efforts to locate the position

of further ones of the abovementioned translocon components have not been successful. At present, only TRAM remains a candidate for permanent and stoichiometric presence in the translocon, because it does not comprise lumenal or cytosolic domains large enough for detection using CET. Therefore, it may represent the density that is consistently found opposite of the "lateral gate" in CET of native translocons (Pfeffer et al., 2012).

Mammalian TRAP is a heterotetrameric membrane protein complex, with three subunits (α, β, δ) predicted to comprise one transmembrane helix plus one lumenal domain each, while TRAPγ likely comprises a bundle of four transmembrane helices plus a cytosolic domain (Hartmann et al., 1993; Bañó-Polo et al., 2017; Pfeffer et al., 2017; **Figure 7**). This bundle of transmembrane helices appears to be flanking both Sec61γ and the carboxy-terminal half of Sec61α (**Figures 4**, **7**), and the cytosolic domain seems to interact with the ribosome via ribosomal protein eL38 and a short RNA expansion segment. The heterotrimeric ER-lumenal segment of TRAP reaches across the central Sec61 channel and binds to the crucial "hinge" region between the amino- and carboxy-terminal halves of Sec61α. Within the trimeric lumenal TRAP segment, the δ-subunit contacts OST (most likely ribophorin II), and the dimer formed by the lumenal domains of α- and β- subunits contacts ER lumenal loop 5 in the "hinge" region between the amino- and carboxy-terminal halves of Sec61α. In this position, the ER lumenal domain of TRAP may be able to act in a chaperone-like fashion on the conformational state of Sec61α or as a molecular ratchet on nascent precursor polypeptides in transit into the ER lumen or both, in analogy to BiP. We note that various algorithms predict a beta sandwich fold for the ER lumenal domains of TRAP's α- and β- subunits and that TRAPα was also characterized as Ca^{2+}-binding protein (Wada et al., 1991).

ASSISTED OPENING OF THE HUMAN SEC61 CHANNEL FOR MEMBRANE INSERTION AND TRANSLOCATION OF POLYPEPTIDES

The current view on opening of the Sec61 complex for protein translocation, i.e., channel gating from the closed to the open conformation, is that signal peptides of nascent presecretory polypeptides intercalate between the Sec61α transmembrane helices 2 and 7, displace helix 2, and open the "lateral gate" of the Sec61 complex formed by these two transmembrane helices (Van den Berg et al., 2004; Gumbart et al., 2009; Voorhees et al., 2014; **Figure 4**). Actually, it has been suggested that this intercalation rather than the originally proposed displacement of the "plug" helix represents the crucial reaction in the early phase of membrane insertion of translocation, i.e., the energetic barrier for Sec61 channel opening (**Figure 8**). Next, the nascent chain can be fully inserted into the Sec61 channel, either in "hairpin" (where the amino-terminus of the signal peptide stays in the cytosol) or "head-first" configuration (where the amino-terminus of the signal peptide reaches into the ER lumen), and initiate translocation (Devaraneni et al., 2011; Park et al., 2014; Vermeire et al., 2014). The "hairpin" insertion is considered to represent the more productive mode whereas a "head-first" insertion has to be followed by a reversal of orientation (termed "flip turn") to allow the sequence downstream of the signal peptide to enter the ER lumen. The latter may be considered a second energetically unfavorable reaction, typically requiring help from components, which can lower the energetic barrier for the "flip turn" (**Figure 8**). The idea is that some amino-terminal signal peptides or transmembrane helices may be "strong" or quickly-gating enough to trigger Sec61 channel opening quickly on their own, particularly after the ribosome has already primed the channel. However, precursor polypeptides with "weak" signal peptides appear to involve auxiliary components in Sec61 channel opening in order to facilitate insertion of precursor polypeptides into the Sec61 complex (**Table 1**). Alternatively, the auxiliary components may support the abovementioned "flip turn" in case of an original "head-first" insertion. Based on *in vitro* experiments the concept emerged that TRAP and BiP facilitate Sec61 channel opening in a substrate specific manner. In particular, precursor polypeptides with "weak" signal peptides or transmembrane helices are affected (Fons et al., 2003; Schäuble et al., 2012; **Figure 5**; **Supplementary Video 1**). Based on only a small set of model precursor polypeptides, the distinguishing factor that determines the requirement for BiP and its membrane bound co-chaperone Sec63 was suggested to be a short and rather apolar signal peptide, eventually to support it in displacing helix 2 of Sec61α on its own account. The TRAP complex was observed in *in vitro* transport studies to stimulate translocation of specific proteins, such as the prion protein. Recent studies in intact cells have suggested that TRAP might also affect the topology of transmembrane helices that do not promote a specific initial orientation of membrane protein precursors in the membrane (Sommer et al., 2013). As noted before (Haßdenteufel et al., 2014), several additional proteins in the mammalian ER membrane can be considered as auxiliary translocon components, most notably TRAM (Voigt et al., 1996; Hegde et al., 1998). In the case of TRAM, signal peptides of precursors with long amino-terminal as well as long hydrophobic core regions showed a low TRAM dependence in *in vitro* experiments. Interestingly, there is a second TRAM in mammalian cells, termed TRAM2, which can invert the topology of transmembrane helices that do not promote a specific initial orientation in the membrane (Chen et al., 2016).

We suggest that certain features of signal peptides may extend the "dwell" time or "sampling" of signal peptides on the cytosolic surface of the Sec61 channel and that BiP and TRAP can overcome this by facilitating Sec61 channel gating on the lumenal side (Zhang and Miller, 2012; Van Lehn et al., 2015). This raises the exciting possibility that BiP and TRAP have overlapping specificities, i.e., that there is also redundancy in this reaction, as discussed above for the targeting reaction. Another interesting and equally open question is what features make a signal peptide or transmembrane helix "weak" or "strong" for Sec61 channel opening and if it is really only these topogenic sequences that determine this "weakness" or "strength." Some features have already been mentioned above but were determined using only small sets of model proteins. However, our own unpublished work suggests that special features downstream of the signal peptides can also play a distinct role, which may be particularly

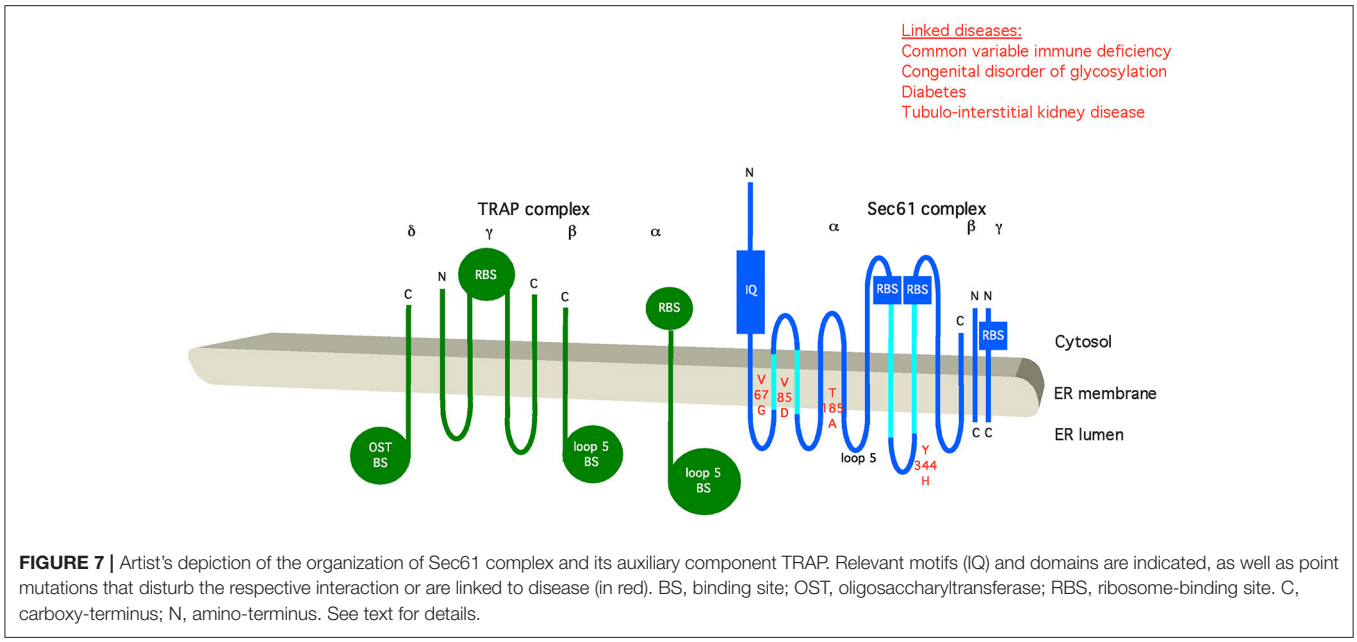

FIGURE 7 | Artist's depiction of the organization of Sec61 complex and its auxiliary component TRAP. Relevant motifs (IQ) and domains are indicated, as well as point mutations that disturb the respective interaction or are linked to disease (in red). BS, binding site; OST, oligosaccharyltransferase; RBS, ribosome-binding site. C, carboxy-terminus; N, amino-terminus. See text for details.

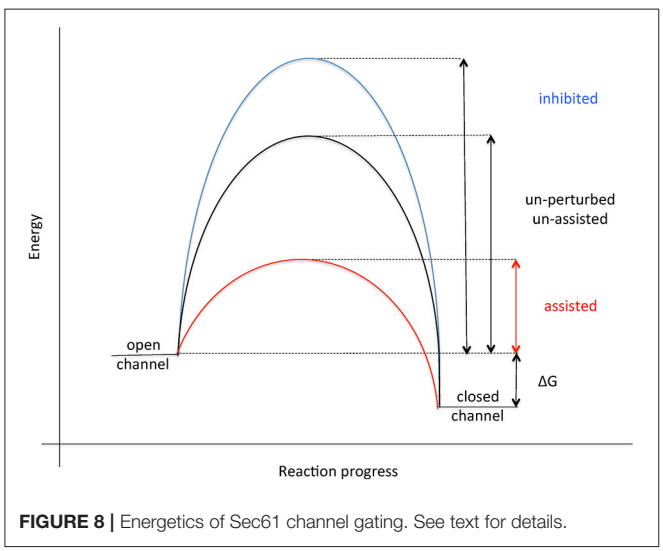

FIGURE 8 | Energetics of Sec61 channel gating. See text for details.

relevant in cotranslational translocation when a considerable stretch of a nascent precursor polypeptide accumulates at the interface between ribosome and Sec61 complex, i.e., prior to Sec61 channel opening (see above) and in posttranslational translocation (S. Haßdenteufel, personal communication). This is reminiscent of the effects of downstream sequences in the integration of transmembrane helices into the membrane (Junne and Spiess, 2017). Interestingly, yeast Sec62 and mammalian TRAP were found to affect the topology of transmembrane helices that do not promote a specific initial orientation of membrane protein precursors in the membrane (Reithinger et al., 2013; Sommer et al., 2013).

In the case of BiP, it has been suggested that the minihelix within loop 7 of Sec61α plays a role in gating of the Sec61 complex from closed to open and that BiP binding to this minihelix may be required for only some precursor polypeptides (**Figures 5**, **6**). "Thus, by providing binding energy, the ribosome and BiP may be able to 'pull' transmembrane helix 7 from opposite ends to facilitate channel opening (**Figure 8**; Schäuble et al., 2012). We find this hypothesis attractive because loop 7 connects transmembrane helices 7 and 8 and is thus close enough to the "lateral gate" to influence gate movements." Thus, BiP together with Sec63 protein represents an allosteric effector of the Sec61 complex for channel opening. This view was supported by the observations that the murine diabetes-linked mutation of tyrosine 344 to histidine within loop 7 destroys the BiP binding site and, when introduced into HeLa cells, prevents *in vitro* transport of BiP-dependent, i.e., slowly-gating precursor polypeptides.

As stated above, the dimer formed by the lumenal domains of the α- and β- subunits of TRAP contacts ER lumenal loop 5 in the "hinge" region between the amino- and carboxy-terminal halves of Sec61α (Pfeffer et al., 2017; **Figures 4**, **7**). Thereby, it may act as an alternative allosteric effector of Sec61 channel and thus may facilitate opening of the Sec61 channel to allow initiation of protein translocation and topogenesis of membrane proteins, in analogy to the action of BiP on loop 7. Therefore, the question arises of how TRAP may signal the presence of a signal peptide requiring help in Sec61 channel gating to the ER lumenal TRAP domains (see above).

CLOSING OF THE HUMAN SEC61 CHANNEL FOR PRESERVATION OF CELLULAR CALCIUM HOMEOSTASIS

As discussed before (Zimmermann, 2016), "the mammalian ER is also a central player in cellular calcium homeostasis

(**Figures 1**, **2**). It represents the major Ca^{2+} storage organelle in nucleated mammalian cells and allows controlled release of Ca^{2+} from the ER upon hormone stimulation of a resting cell, e.g., via IP3 receptor (Berridge, 2002; Clapham, 2007). Subsequently, Ca^{2+} is pumped back into the ER by sarcoplasmic/ER Ca^{2+} ATPase (SERCA) to re-establish the steep ER to cytosol Ca^{2+} gradient (Wuytack et al., 2002). This gradient is also constantly challenged by passive Ca^{2+} efflux from the ER, so SERCA has the additional task of counteracting this Ca^{2+} leakage. In addition, Ca^{2+} is taken up by mitochondria. In the course of the last 10 years, several proteins were linked to ER Ca^{2+} leakage, including the Sec61 channel (Lomax et al., 2002; Van Coppenolle et al., 2004; Erdmann et al., 2011). Other candidate proteins that were identified acting as putative Ca^{2+} permeable leak channel at the ER membrane are presenilin1 (Tu et al., 2006), Bcl2 (Chami et al., 2004), pannexin1 (Vanden Abeele et al., 2006), TRPC1 (Berbey et al., 2009), CALHM1 (Gallego-Sandín et al., 2011), and a truncated SERCA1 isoform (Chami et al., 2001, 2008). Some of those candidate proteins, however, were ruled out as passive Ca^{2+} leak channels allowing the efflux of Ca^{2+} from the ER observed in all nucleated cells. For example, presenilin was shown to have a stimulatory effect on IP3 receptors (Cheung et al., 2008, 2010), i.e., triggering a rather direct Ca^{2+} release from the ER. In addition, mature presenilin is predominantly located in the plasma and Golgi membrane (https://www.proteinatlas.org). Similarly, mature Bcl2, pannexin1, and TRPC1 are not present at the ER membrane to act as ubiquitous Ca^{2+} leak channel and their property as leak channel was addressed upon overexpression. Calcium homeostasis modulator 1 (CALHM1) increased Ca^{2+} efflux from the ER and reduced activity of SERCA (Gallego-Sandín et al., 2011), but the restricted and low expression of CALHM1 in tissues of the brain, kidney, bladder and immune cells render it an unlikely candidate as ubiquitous Ca^{2+} leak channel (https://www.proteinatlas.org). The proposed reverse Ca^{2+} flux through the SERCA pump of myocytes could represent yet another source of Ca^{2+} efflux from the ER (Shannon et al., 2000). Interestingly, a short splice variant of SERCA1 (S1T) found in different human tissues reduces ER Ca^{2+} loading via increased passive Ca^{2+} efflux from the ER and reduces activity of SERCA1 and SERCA2. S1T is induced during ER stress, homodimerizes and elevates ER Ca^{2+} depletion for induction of apoptosis, thus rendering S1T a specialized Ca^{2+} leak channel under stress conditions (Chami et al., 2001, 2008). However, the ubiquitously expressed, ER resident Sec61 complex with its pore forming subunit represents an ideal candidate as omnipresent passive Ca^{2+} leak channel. A genome-wide RNAi screen in Drosophila S2 cells identified Sec61α (but none of the aforementioned candidates) as component reducing Ca^{2+} release-activated Ca^{2+} channel activity (Zhang et al., 2006). Though, with such a highly abundant Ca^{2+} leak channel it is imperative to prevent excessive ER Ca^{2-}-efflux and disturbance of the Ca^{2+}-gradient across the ER membrane. Therefore, Sec61 channel gating has to be tightly controlled as described below (**Figure 5**).

Single-channel recordings from planar lipid bilayers characterized the Sec61 complex as a highly dynamic aqueous channel with a main calcium conductance of 165 ± 10 pS and a subconductance state of 733 ± 16 pS allowing a rough estimation about the opening diameter of the pore from 5 to 7 Å for the main conductance and 12–14 Å for the subconductance state. The Sec61 complex is transiently opened by signal peptides within precursor polypeptides and is permeable to Ca^{2+} at the end of protein translocation (Simon et al., 1989; Wirth et al., 2003; Erdmann et al., 2011; Lang et al., 2011). The same experimental strategy showed that the Sec61 channel closes either spontaneously or as induced by binding of BiP or Ca^{2+}-calmodulin (Erdmann et al., 2011; Schäuble et al., 2012). The fact that BiP is involved in closing the Sec61 channel was confirmed at the cellular level by combination of siRNA-mediated gene silencing or pharmacological manipulation and live cell Ca^{2+} imaging (Schäuble et al., 2012). In addition, cytosolic Ca^{2+}-calmodulin was shown under similar conditions to contribute to Sec61 channel closing via an unrelated mechanism once Ca^{2+} has started to leak from the ER (Erdmann et al., 2011). During the last 5 years, additional siRNA-mediated gene silencing and live cell Ca^{2+} imaging experiments characterized the pair of ERj 3 and 6 as co-chaperones of BiP as well as Ca^{2+}-Sec62 as a co-factor of calmodulin in Sec61 channel closure (Linxweiler et al., 2013; Schorr et al., 2015). Furthermore, the binding sites of BiP, Ca^{2+}-calmodulin, and Ca^{2+}-Sec62 were identified as the abovementioned di-tyrosine motif–containing mini-helix within ER lumenal loop 7 of the Sec61 α-subunit and an IQ motif in the cytosolic amino-terminus of the same subunit, respectively (**Figure 5**). Furthermore, the respective affinities of these interactions were determined by surface plasmon resonance spectroscopy and found to be physiologically relevant (**Figure 6**).

The following scenario for gating of the Sec61 channel has emerged from these studies (reviewed by Zimmermann et al., 2011; Dudek et al., 2015; Pfeffer et al., 2016; Zimmermann, 2016; **Figure 5**). As described above, binding of a precursor polypeptide to the closed Sec61 complex triggers channel opening, either on its own or facilitated by binding of the allosteric modulator of the Sec61 channel, BiP (Schäuble et al., 2012; **Figure 5**). Here, Sec63 acts as a BiP co-chaperone (Lang et al., 2012). After completion of protein translocation, i.e., in the absence of any bound precursor polypeptide, the channel closes on its own, or BiP facilitates efficient gating of the Sec61 channel to the closed state (Schäuble et al., 2012). At this stage, ERj3 and ERj6 are BiP co-chaperones, possibly acting in the form of a heterodimeric complex (Schorr et al., 2015). The idea is that binding of BiP to loop 7 of Sec61α provides energy for shifting the dynamic equilibrium of the Sec61 channel to the closed state. The idea that such a mechanism may indeed be at work came from single-channel recordings where Fab fragments directed against loop 7 could substitute for BiP in channel closing (Schorr et al., 2015). In case of inefficient channel closure in intact cells, Ca^{2+} starts to leak from the ER into the cytosol and binds calmodulin, and Ca^{2+}-calmodulin is recruited to the IQ motif in the Sec61 α-subunit (Erdmann et al., 2011; **Figures 5**, **6**). Once again, the involved binding energy may favor channel closure. Binding of Ca^{2+}-calmodulin is supported by Sec62, which may have bound Ca^{2+} because of a predicted EF hand within its cytosolic carboxy-terminal end (Linxweiler

et al., 2013). Next, the Sec61 channel is closed, and Ca^{2+} leakage subsides. SERCA pumps Ca^{2+} back into the ER, calmodulin and Sec62 return to the Ca^{2+}-free forms, and the next protein translocation cycle can be initiated. The crucial open question is if or when the Ca^{2+} permeability of the open Sec61 channel and its elaborate control mechanisms play a physiological role.

As previously outlined (Linxweiler et al., 2017), "an additional function beyond ER protein import and Ca^{2+} homeostasis was recently found for the Sec62 protein and represents yet another example of pathway overlaps (Fumagalli et al., 2016). Sec62 also plays a crucial role in the recovery of eukaryotic cells from conditions of ER stress. In the course of UPR, the level of several ER lumenal chaperones such as BiP is markedly increased (Ma and Hendershot, 2001; Zhang and Kaufman, 2004). If the cell can cope with ER stress conditions, the expanded ER as well as the high amount of ER lumenal chaperones have to be returned to a physiological level. Therefore, small vesicles derived from the ER membrane fuse with phagophores to build autophagosomes (ER-autophagy) (**Figure 6**). For this purpose, Sec62 bears a LIR motif at its carboxy-terminus that functions as a receptor for phagophore-bound LC3. Thus, Sec62 plays an important, Sec61- and Sec63-independent role during recovery from ER stress." A similar mechanism may be involved in ER-phagy when mis-folded polypeptides overwhelm the ERAD machinery and whole ER sections have to be sacrificed to protect the cell. We suggest that phosphorylation of the negative patch in the carboxy-terminus of Sec63 and/or Ca^{2+} binding to the EF hand in the carboxy-terminus of Sec62 may trigger dissociation of Sec62 from its interaction partners (Ampofo et al., 2013; Linxweiler et al., 2013).

NOVEL CONCEPT FOR PHYSIOLOGIC ROLES OF THE HUMAN SEC61 CHANNEL IN CELLULAR CALCIUM HOMEOSTASIS AND ENERGY METABOLISM

As stated above, the Ca^{2+} permeability of the open Sec61 channel may be involved in the intrinsic pathway to apoptosis, i.e., when cells have to be sacrificed to protect a multicellular organism from terminal protein aggregation problems. We suggest that under conditions of severe and prolonged protein mis-folding and aggregation even after UPR induction, BiP is terminally sequestered by mis-folded and aggregating polypeptides. As described, this sequestration will eventually lead to continuous Ca^{2+} leakage from the ER via open Sec61 channels (**Figure 2**). In the long run, the effect may contribute to increased cytosolic Ca^{2+} levels, which are typically involved in induction of apoptosis. We expect that such a scenario may be particularly relevant for secretory cells, such as the β cells of the pancreas or plasma cells of the immune system. Therefore, these two cell types are particularly sensitive to mutations in the *SEC61A1* gene (see below).

To fulfill its central role in protein biogenesis, the ER of all nucleated human cells contains the ATP dependent chaperone BiP in millimolar concentration and, thus, depends on a constant supply of ATP. So far, only for the plant *Arabidopsis thaliana* an ER-resident membrane ATP carrier has been described (Leroch et al., 2008). Thus, the question remains of how ATP gets into the human ER. Recent work has established a set of hallmarks for this nucleotide transport (Vishnu et al., 2013). There appears to be a regulatory circuit for maintenance of ATP supply of the human ER that involves ER-lumenal and cytosolic Ca^{2+}, the elusive ADP/ATP carrier, and cytosolic AMP–activated protein kinase (AMPK) (**Figure 2**). Decreasing ATP levels in the ER leads to decreasing ER Ca^{2+}- and increasing cytosolic Ca^{2+} levels, where the former activates the ER membrane–resident ADP/ATP carrier and the latter stimulates ADP phosphorylation in cytosol and mitochondria. Based on our observations on the Ca^{2+} permeability of the open Sec61 channel and its limitation by BiP, we propose that the above-described regulatory circuit for maintenance of ATP supply of the human ER also involves the Sec61 channel in the ER membrane and the ER lumenal BiP. According to this novel concept, decreased ATP levels in the ER should cause lower BiP activity, which in turn causes ER Ca^{2+} leakage via the Sec61 channel, in analogy to the situation where BiP is sequestered by mis-folded polypeptides. Next, decreasing ER lumenal Ca^{2+} activates the ER membrane–resident ADP/ATP carrier, and increasing cytosolic Ca^{2+} stimulates ADP phosphorylation in cytosol and mitochondria. Subsequently, ATP levels in the ER recover, BiP binds to the Sec61 channel and stops Ca^{2+} from leaking into the cytosol. This scenario may also serve as a framework for envisioning how breakdown of energy metabolism can cause apoptosis, e.g., when plasma cells are at the end of their lifespan. In this case, accumulation of mis-folded immunoglobulin polypeptide chains may further aggravate the situation (Kourtis and Tavernarakis, 2011).

SEC61-CHANNELOPATHIES AND THERAPEUTIC STRATEGIES

"In light of this elaborate system of Sec61 channel gating, it did not come as a surprise that various diseases were linked to components of the protein translocation machinery (Zimmermann, 2016)." The term Sec61-channelopathies was coined for the family of inherited or tumor-related diseases that either directly affect Sec61 subunits or are linked to components involved in Sec61 channel gating (Haßdenteufel et al., 2014; Linxweiler et al., 2017; **Table 1**; **Figures 5**, **9**). Mutations in the gene coding for the Sec61 α-subunit can cause diabetes in the mouse (Lloyd et al., 2010), and common variable immune deficiency (CVID) and tubulo-interstitial kidney disease with anemia in humans (Bolar et al., 2016; Schubert et al., 2017). Loss-of-function mutations in genes coding for Sec63 and ERj6, respectively, were linked to autosomal dominant polycystic liver disease and diabetes in both humans and mice (Davila et al., 2004; Ladiges et al., 2005; Fedeles et al., 2011; Synofzik et al., 2014). Furthermore, polycystic liver disease can be caused by heterozygous mutation of the *SEC61B* gene (Besse et al., 2017), and proteolytic inactivation of BiP by the bacterial subtilase cytotoxin SubAB causes the devastating hemolytic uremic syndrome (Paton et al., 2006).

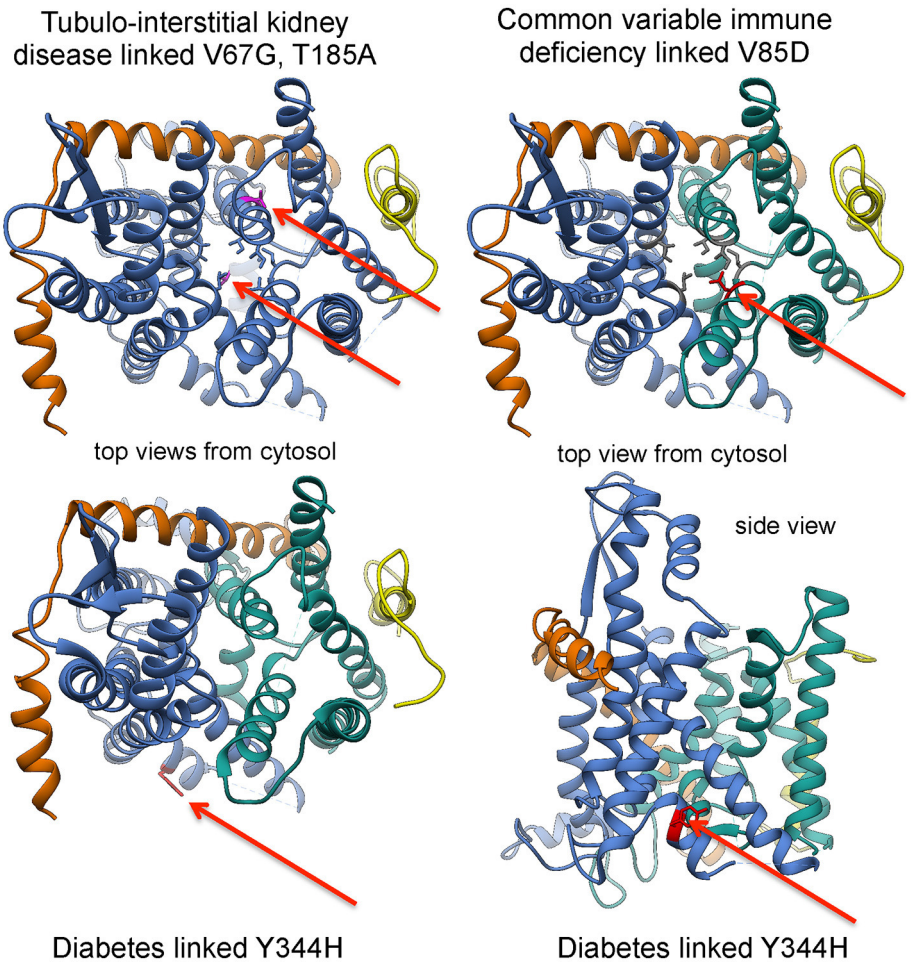

FIGURE 9 | Position of disease-linked mutations in 3D reconstructions of the Sec61 complex. See text for details.

Overproduction of components of the protein translocation machinery is associated with cancers of prostate, lung, head, and neck (Sec62) and with glioblastoma (Sec61γ) (Lu et al., 2009; Greiner et al., 2011; Linxweiler et al., 2012, 2013; Bochen et al., 2017). In addition, several diseases have been linked to subunits of OST (reviewed by Mohorko et al., 2011) and Sil1 (Senderek et al., 2005; Zhao et al., 2005; Roos et al., 2014), respectively, and appear to affect N-glycosylation of newly synthesized polypeptides and protein folding, respectively, rather than Sec61 channel gating (**Table 1**). As described before (Zimmermann, 2016), "the human diseases associated with mutations in OST and Sil1 are congenital disorders of glycosylation (CDG) Type I and the neurodegenerative Marinesco-Sjögren Syndrome, respectively. We note that CDG can also result from loss-of-function mutations in genes coding for different subunits of TRAP (Losfeld et al., 2014; Pfeffer et al., 2017; **Table 1**).

In the case of diabetes, loss of ERj6 function and homozygous *SEC61A1* mutation, respectively, were suggested to be caused by inefficient gating of Sec61 channels to the closed state with sustained ER Ca^{2+} leakage and, eventually, apoptosis of secretory cells, such as pancreatic ß cells (Schäuble et al., 2012; Schorr et al., 2015). The former is in agreement with ERj6 being involved in gating of the Sec61 channel to the closed state. The latter was explained by the observation that the diabetes-linked mutation of the *SEC61A1* tyrosine 344 to histidine affects the di-tyrosine motif-containing mini-helix of the Sec61 α-subunit, i.e., the BiP-binding site (Schäuble et al., 2012; **Figures 5**, **9**)." As a consequence, the mutated Sec61 channel cannot be efficiently gated by BiP and thus becomes permeable for Ca^{2+}. A similarly permeable Sec61 channel may exist in case of CVID, where a heterozygous mutation of the *SEC61A1* gene (resulting in the substitution of valine 85 by aspartate) introduces a polar amino acid side chain into the typically non-polar "pore ring" of the Sec61 channel (Schubert et al., 2017). This view was supported by the observation that the CVID-linked mutation, when introduced into HeLa cells, leads to permeable Sec61 channels, which may have a dominant-negative effect on the cells. Therefore, the lifespan of plasma cells may be shortened in the patients. Alternatively, the disease phenotype may be caused by

haploinsufficiency. The functional consequences are less clear in the case of tubulo-interstitial kidney disease, where two mutations in the *SEC61A1* gene have been reported (resulting in the substitution of valine 67 by glycine and of threonine 185 by valine), which are located in the "plug" domain and transmembrane helix 5, respectively (Bolar et al., 2016). In all diseases that are related to the ubiquitously expressed *SEC61A1* gene, the crucial question is why a particular mutation affects only a single cell type.

In the case of polycystic liver disease, reduction or loss of Sec63 function appears to cause a precursor polypeptide-specific defect in ER protein import, which results in the absence of certain plasma membrane proteins, such as polycystin 1, involved in planar cell polarity (Davila et al., 2004; Fedeles et al., 2011). This association is consistent with the idea that Sec63 is involved in gating of the Sec61 channel to the open state. In addition, the interaction of Sec63 with cytosolic nucleoredoxin may be relevant for the disease phenotype (Müller et al., 2011). Apparently, the loss-of-function mutation of the *SEC61B* allele also causes a precursor-specific ER protein import defect. Again, the open question is why only a certain cell type, in this case cholangiocytes, is affected by the partial or complete loss of function.

It appears that excessively efficient closing of the Sec61 channel can also lead to disease (Linxweiler et al., 2012, 2013). Amplification and/or over-expression of the *SEC62* gene (also termed *TLOC1*) were linked to various cancers and appear to be associated with poor prognosis. *SEC62* over-expression was found to result in elevated migratory potential and increased stress tolerance of the respective tumor cells, i.e., two "hallmarks" of cancer cells with a connection to cellular Ca^{2+} homeostasis. Furthermore, the *SEC62* gene has been characterized as a "tumor driver gene" (Hagerstrand et al., 2013). The two cancer hallmarks of *SEC62* over-expressing tumor cells can be overcome by siRNA-mediated gene silencing (Linxweiler et al., 2013). Based on our data on the role of Sec62 in Sec61 channel gating, we asked whether the effect of *SEC62* silencing on *SEC62* over-expressing tumor cells can be phenocopied by drugs. We reasoned that if Ca^{2+}-calmodulin secures efficient Sec61 channel closure in cooperation with Ca^{2+}-Sec62, calmodulin antagonists should mimick the effect of *SEC62* silencing on *SEC62* over-expressing tumor cells; indeed, this is what we found. One particular calmodulin antagonist of interest is trifluoperazine, since it has previously been in clinical use for depressive patients. Thus, we are currently addressing in murine tumor models if proliferation of *SEC62* over-expressing tumor cells can be inhibited by a combinatorial treatment that includes trifluoperazine and a SERCA inhibitor. We note that SERCA-targeting prodrugs are currently being evaluated in clinical trials (Mahalingam et al., 2016).

SEC61 CHANNEL INHIBITORS, AN EPILOG

In the course of the last 10 years, several small molecule inhibitors of the Sec61 channel have been discovered which, in analogy to mutations of the *SEC61A1* gene, affect ER protein import in a precursor-specific or non-selective manner. The first-described and precursor-selective class of such inhibitors were the cyclic heptadepsipeptides, i.e., CAM749 and cotransins (such as CT8) (Besemer et al., 2005; Garrison et al., 2005; MacKinnon et al., 2014). Subsequently, the structurally unrelated compounds apratoxin A and mycolactone were characterized as Sec61 effectors and shown to have selective (mycolactone) or non-selective (apratoxin A) effects on ER protein import by interaction with the channel (Liu et al., 2009; Hall et al., 2014; Baron et al., 2016; McKenna et al., 2016, 2017; Paatero et al., 2016). The model to explain a precursor-specific inhibitory effect suggests that certain signal peptides and transmembrane helices can either bypass or displace the drugs during their initial insertion into the Sec61 channel. Thus, both possibilities may, at least in some way, reiterate the above discussion of "weak" and "strong" signal peptides (see above): the bound small molecules may increase the energy barrier involved in opening of the Sec61 channel for protein translocation and precursors with "strong" signal peptides may overcome the barrier anyhow (**Figure 8**). Alternatively, selective inhibitors may occupy binding sites within the Sec61 channel, which are irrelevant for some signal peptides. Therefore, the exact mode of action of these compounds is an important open question. Furthermore, it will be interesting to address the questions of whether or not the selectivity of some of the small molecules correlates with the dependence of some precursors on certain auxiliary components in gating of the channel and if and how the inhibitory compounds affect cellular Ca^{2+} homeostasis.

Intriguingly, heptadepsipeptides are considered for the treatment of multiple myeloma, which is very much in line with the observation in CVID patients that physiological levels of functional Sec61 channels are essential for plasma cell viability. Mycolactone appears to be a good candidate to follow that same path.

CONCLUDING REMARKS

The mammalian Sec61 complex forms a dynamic and precursor gated channel, which can provide an aqueous path for polypeptides into the ER lumen and is regulated by various allosteric effectors. When the aqueous path is open, it can apparently also provide a channel for efflux of calcium ions from the ER lumen into the cytosol. We suggest that this feature is linked to the regulation of ATP import into the ER and the initiation of the intrinsic pathway to apoptosis, respectively. To us, the most pressing open questions concern (i) the structure of the native Sec61 complex in the ribosome-free state, (ii) the positioning of other transport and processing components within the native translocon, (iii) the rules of engagement of the allosteric effectors of the Sec61 channel plus their molecular mechanisms. The latter will undoubtedly also pave the way for a detailed understanding of the pathomechanisms which are involved in Sec61 channelopathies. Another burning question is the nature of the elusive ATP carrier(s) of the mammalian ER membrane.

AUTHOR CONTRIBUTIONS

SP and FF contributed 3D reconstructions after CET. PL and VH performed molecular modelings. SL and RZ wrote the first draft of the manuscript, which was contributed to by all authors.

ACKNOWLEDGMENTS

The authors are grateful to Drs Lars Kästner and Peter Lipp (Cell Biology, Saarland University, Homburg, Germany) for donating 3D reconstructions of cells after live cell fluorescence imaging, to Daniel Wiebelt and Maria Zimmermann for contributing artwork, and to the Deutsche Forschungsgemeinschaft (DFG) for continuous financial support.

SUPPLEMENTARY MATERIAL

The Supplementary Material for this article can be found online at: https://www.frontiersin.org/articles/10.3389/fphys.2017.00887/full#supplementary-material

Supplementary Video 1 | Artist's view of SRP/SR, BiP and Sec63 mediated transport of presecretory proteins via the Sec61 channel into the ammalian ER. J, J-domain of Sec63 recruits BiP to the Sec61 channel for channel opening and to incoming precursor polypeptides for ratcheting, respectively. Signal peptidase (SPase) cleaves the signal peptide from the incoming precursor polypeptide. See text for details.

REFERENCES

Alberti, S., Esser, C., and Höhfeld, J. (2003). BAG-1—a nucleotide exchange factor of Hsc70 with multiple cellular functions. *Cell Stress Chaperones* 8, 225–231.

Ampofo, E., Welker, S., Jung, M., Müller, L., Greiner, M., Zimmermann, R., et al. (2013). CK2 phosphorylation of human Sec63 regulates its interaction with Sec62. *Biochim. Biophys. Acta* 1830, 2938–2945. doi: 10.1016/j.bbagen.2012.12.020

Ast, T., Cohen, G., and Schuldiner, M. (2013). A network of cytosolic factors targets SRP-independent proteins to the endoplasmic reticulum. *Cell* 152, 1134–1145. doi: 10.1016/j.cell.2013.02.003

Ast, T., Michaelis, S., and Schuldiner, M. (2016). The protease Ste24 clears clogged translocons. *Cell* 164, 103–114. doi: 10.1016/j.cell.2015.11.053

Aviram, N., Ast, T., Costa, E. A., Arakel, E., Chuartzman, S. G., Jan, C. H., et al. (2016). The SND proteins constitute an alternative targeting route to the endoplasmic reticulum. *Nature* 540, 134–138. doi: 10.1038/nature20169

Aviram, N., and Schuldiner, M. (2014). Embracing the void-how much do we really know about targeting and translocation to the endoplasmic reticulum? *Curr. Opin. Cell Biol.* 29, 8–17. doi: 10.1016/j.ceb.2014.02.004

Bagola, K., Mehnert, M., Jarosch, E., and Sommer, T. (2011). Protein dislocation from the ER. *Biochim. Biophys. Acta* 1808, 925–936. doi: 10.1016/j.bbamem.2010.06.025

Bañó-Polo, M., Martínez-Garay, C. A., Grau, B., Martínez-Gil, L., and Mingarro, I. (2017). Membrane insertion and topology of the translocon-associated protein (TRAP) gamma subunit. *Biochim. Biophys. Acta* 1859, 903–909. doi: 10.1016/j.bbamem.2017.01.027

Baron, L., Onerva Paatero, A., Morel, J.-D., Impens, F., Guenin-Mace, L., Saint-Auret, S., et al. (2016). Mycolactone subverts immunity by selectively blocking the Sec61 translocon. *J. Exp. Med.* 213, 2885–2896. doi: 10.1084/jem.20160662

Benedix, J., Lajoie, P., Jaiswal, H., Burgard, C., Greiner, M., Zimmermann, R., et al. (2010). BiP modulates the affinity of its co-chaperone ERj1 to ribosomes. *J. Biol. Chem.* 285, 36427–36433. doi: 10.1074/jbc.M110.143263

Berbey, C., Weiss, N., Legrand, C., and Allard, B. (2009). Transient receptor potential canonical type 1 (TRPC1) operates as a sarcoplasmic reticulum calcium leak channel in skeletal muscle. *J. Biol. Chem.* 284, 36387–36394. doi: 10.1074/jbc.M109.073221

Berridge, M. J. (2002). The endoplasmic reticulum: a multifunctional signalling organelle. *Cell Calc.* 32, 235–249. doi: 10.1016/S0143416002001823

Besemer, J., Harant, H., Wang, S., Oberhauser, B., Marquardt, K., Foster, C. A., et al. (2005). Selective inhibition of cotranslational translocation of vascular cell adhesion molecule 1. *Nature* 436, 290–293. doi: 10.1038/nature03670

Besse, W., Choi, J., Punia, S., Fedeles, S. V., Choi, M., Gallagher, A.-R., et al. (2017). Isolated polycystic liver disease genes define effectors. Of poylcystin-1 function. *J. Clin. Invest.* 27, 1772–1785. doi: 10.1172/JCI90129

Blau, M., Mullapudi, S., Becker, T., Dudek, J., Zimmermann, R., Penczek, P. A., et al. (2005). ERj1p uses a universal ribosomal adaptor site to coordinate the 80S ribosome at the membrane. *Nat. Struct. Mol. Biol.* 12, 1015–1016. doi: 10.1038/nsmb998

Blobel, G., and Dobberstein, B. (1975). Transfer of proteins across membranes: I. Presence of proteolytically processed and unprocessed nascent immunoglobulin light chains on membrane-bound ribosomes of murine myeloma. *J. Cell Biol.* 67, 835–851.

Blond-Elguindi, S., Cwirla, S. E., Dower, W. J., Lipshutz, R. J., Sprang, S. R., Sambrook, J. F., et al. (1993). Affinity panning of a library of peptides displayed on bacteriophages reveals the binding specificity of BiP. *Cell* 75, 717–728. doi: 10.1016/0092-8674(93)90492-9

Bochen, F., Adisurya, H., Wemmert, S., Lerner, C., Greiner, M., Zimmermann, R., et al. (2017). Effect of 3q oncogenes *SEC62* and *SOX2* on lymphatic metastasis and clinical outcome of head and neck squamous cell carcinomas. *Oncotarget* 8, 4922–4934. doi: 10.18632/oncotarget.13986

Bolar, N. A., Golzio, C., Zivna, M., Hyot, G., van Hemelrijk, C., Schepers, D., et al. (2016). Heterozygous loss-of-function SEC61A mutations cause autosomal-dominant tubule-interstitial and glomerulocystic kidney disease with anemia. *Am. J. Hum. Gen.* 99, 174–187. doi: 10.1016/j.ajhg.2016.05.028

Borgese, N., and Fasana, E. (2011). Targeting pathways of C-tail-anchored proteins. *Biochim. Biophys. Acta* 1808, 937–946. doi: 10.1016/j.bbamem.2010.07.010

Braakman, I., and Bulleid, N. J. (2011). Protein folding and modification in the mammalian endoplasmic reticulum. *Ann. Rev. Biochem.* 80, 71–99. doi: 10.1146/annurev-biochem-062209-093836

Bracher, A., and Verghese, J. (2015). The nucleotide exchange factors of Hsp70 molecular chaperones. *Front. Mol. Biosci.* 2:10. doi: 10.3389/fmolb.2015.00010

Brostrom, M. A., and Brostrom, C. O. (2003). Calcium dynamics and endoplasmic reticular function in the regulation of protein synthesis: implications for cell growth and adaptability. *Cell Calcium* 34, 345–363. doi: 10.1016/S0143-4160(03)00127-1

Chami, M., Gozuacik, D., Lagorce, D., Brini, M., Falson, P., Peaucellier, G., et al. (2001). SERCA1 truncated proteins unable to pump calcium reduce the endoplasmic reticulum calcium concentration and induce apoptosis. *J. Cell Biol.* 153, 1301–1314. doi: 10.1083/jcb.153.6.1301

Chami, M., Oules, B., Szabadkai, G., Tacine, R., Rizzuto, R., and Paterlini-Bréchot, P. (2008). Role of SERCA1 truncated isoform in the proapoptotic calcium transfer from ER to mitochondria during ER stress. *Mol. Cell.* 32, 641–651. doi: 10.1016/j.molcel.2008.11.014

Chami, M., Prandini, A., Campanella, M., Pinton, P., Szabadkai, G., Reed, J. C., et al. (2004). Bcl-2 and Bax exert opposing effects on Ca^{2+} signaling, which do not depend on their putative pore-forming region. *J. Biol. Chem.* 279, 54581–54589. doi: 10.1074/jbc.M409663200

Cheetham, M. E., and Caplan, A. J. (1998). Structure, function and evolution of DnaJ: conservation and adaptation of chaperone function. *Cell Stress Chaperones* 3, 28–36. doi: 10.1379/1466-1268(1998)003<0028:SFAEOD>2.3.CO;2

Chen, Q., Denard, B., Lee, C.-E., Han, S., Ye, J. S., and Ye, J. (2016). Inverting the topology of a transmembrane protein by regulating the translocation of the first transmembrane helix. *Mol. Cell*, 63, 567–578. doi: 10.1016/j.molcel.2016.06.032

Cheung, K. H., Mei, L., Mak, D. O. D., Hayashi, I., Iwatsubo, T., Kang, D. E., et al. (2010). Gain-of-function enhancement of IP3-receptor modal gating

by familial Alzheimer's disease-linked presenilin mutants in human cells and mouse neurons. *Sci. Signal.* 3:ra22. doi: 10.1126/scisignal.2000818

Cheung, K.-H., Shineman, D., Müller, M., Cárdenas, C., Mei, L., Yang, J., et al. (2008). Mechanism of Ca^{2+} disruption in Alzheimer's disease by presenilin regulation of $InsP_3$-receptor channel gating. *Neuron* 58, 871–883. doi: 10.1016/j.neuron.2008.04.015

Clapham, D. E. (2007). Calcium Signaling. *Cell* 131, 1047–1058. doi: 10.1016/j.cell.2007.11.028

Conti, B. J., Devaraneni, P. K., Yang, Z., David, L. L., and Skach, W. R. (2015). Cotranslational stabilization of Sec62/63 within the ER Sec61 translocon is controlled by distinct substrate-driven translocation events. *Mol. Cell* 58, 269–283. doi: 10.1016/j.molcel.2015.02.018

Davila, S., Furu, L., Gharavi, A. G., Tian, X., Onoe, T., Qian, Q., et al. (2004). Mutations in SEC63 cause autosomal dominant polycystic liver disease. *Nat. Gen.* 36, 575–577. doi: 10.1038/ng1357

Deshaies, R. J., and Schekman, R. (1987). A yeast mutant defective at an early stage in import of secretory protein precursors into the endoplasmic reticulum. *J. Cell Biol.* 105, 633–645. doi: 10.1083/jcb.105.2.633

Devaraneni, P. K., Conti, B., Matsumara, Y., Yang, Z., Johnson, A. E., and Skach, W. R. (2011). Stepwise insertion and inversion of a type II signal anchor sequence in the ribosome-Sec61 translocon complex. *Cell* 146, 134–147. doi: 10.1016/j.cell.2011.06.004

Dudek, J., Benedix, J., Cappel, S., Greiner, M., Jalal, C., Müller, L., et al. (2009). Functions and pathologies of BiP and its interaction partners. *Cell. Mol. Life Sci.* 65, 1556–1569. doi: 10.1007/s00018-009-8745-y

Dudek, J., Greiner, M., Müller, A., Hendershot, L. M., Kopsch, K., Nastainczyk, W., et al. (2005). ERj1p plays a basic role in protein biogenesis at the endoplasmic reticulum. *Nat. Struct. Mol. Biol.* 12, 1008–1014. doi: 10.1038/nsmb1007

Dudek, J., Pfeffer, S., Lee, P.-H., Jung, M., Cavalié, A., Helms, V., et al. (2015). Protein transport into the human endoplasmic reticulum. *J. Mol. Biol.* 427, 1159–1175. doi: 10.1016/j.jmb.2014.06.011

Ellgaard, L., and Helenius, A. (2003). Quality control in the endoplasmic reticulum. *Nat. Rev. Mol. Cell Biol.* 4, 181–191. doi: 10.1038/nrm1052

Erdmann, F., Schäuble, N., Lang, S., Jung, M., Honigmann, A., Ahmad, M., et al. (2011). Interaction of calmodulin with Sec61α limits Ca^{2+} leakage from the endoplasmic reticulum. *EMBO J.* 30, 17–31. doi: 10.1038/emboj.2010.284

Fedeles, S. V., Tian, X., Gallagher, A.-R., Mitobe, M., Nishio, S., et al. (2011). A genetic interaction network of five genes for human polycystic kidney and liver disease defines polycystin-1 as the central determinant of cyst formation. *Nat. Gen.* 43, 639–647. doi: 10.1038/ng.860

Flynn, G. C., Pohl, J., Flocco, M. T., and Rothman, J. E. (1991). Peptide-binding specificity of the molecular chaperone BiP. *Nature* 353, 726–730. doi: 10.1038/353726a0

Fons, R. D., Bogert, B. A., and Hegde, R. S. (2003). Substrate-specific function of the translocon-associated protein complex during translocation across the ER membrane. *J. Cell Biol.* 160, 529–539. doi: 10.1083/jcb.200210095

Friedman, J. R., and Voeltz, G. K. (2011). The ER in 3D: a multifunctional dynamic membrane network. *Trends Cell Biol.* 21, 709–717. doi: 10.1016/j.tcb.2011.07.004

Fumagalli, F., Noack, J., Bergmann, T., Cebollero, E., Pisoni, G. B., Fasana, E., et al. (2016). Translocon component Sec62 acts in endoplasmic reticulum turnover during stress recovery. *Nat. Cell Biol.* 18, 1173–1184. doi: 10.1038/ncb3423

Gallego-Sandín, S., Alonso, M. T., and García-Sancho, J. (2011). Calcium homoeostasis modulator 1 (CALHM1) reduces the calcium content of the endoplasmic reticulum (ER) and triggers ER stress. *Biochem. J.* 437, 469–475. doi: 10.1042/BJ20110479

Gamerdinger, M., Hanebuth, M. A., Frickey, T., and Deuerling, E. (2015). The principle of antagonism ensures protein targeting specificity at the endoplasmic reticulum. *Science* 348, 201–207. doi: 10.1126/science.aaa5335

Garrison, J. L., Kunkel, E. J., Hegde, R. S., and Taunton, J. (2005). A substrate-specific inhibitor of protein translocation into the endoplasmic reticulum. *Nature* 436, 285–289. doi: 10.1038/nature03821

Gilmore, R., Blobel, G., and Walter, P. (1982). Protein translocation across the endoplasmic reticulum. I. Detection in the microsomal membrane of a receptor for the signal recognition particle. *J. Cell Biol.* 95, 463–469. doi: 10.1083/jcb.95.2.463

Gogala, M., Becker, T., Beatrix, B., Armache, J.-P., Barrio-Garcia, C., Berninghausen, O., et al. (2014). Structures of the Sec61 complex engaged in nascent peptide translocation or membrane insertion. *Nature* 506, 107–110. doi: 10.1038/nature12950

Görlich, D., and Rapoport, T. A. (1993). Protein translocation into proteoliposomes reconstituted from purified components of the endoplasmic reticulum membrane. *Cell* 75, 615–630. doi: 10.1016/0092-8674(93)90483-7

Görlich, D., Prehn, S., Hartmann, E., Kalies, K.-U., and Rapoport, T. A. (1992). A mammalian homolog of SEC61p and SECYp is associated with ribosomes and nascent polypeptides during translocation. *Cell* 71, 489–503. doi: 10.1016/0092-8674(92)90517-G

Greiner, M., Kreutzer, B., Lang, S., Jung, V., Cavalié, A., Unteregger, G., et al. (2011). Sec62 protein level is crucial for ER-stress tolerance of prostate cancer. *Prostate* 71, 1074–1083. doi: 10.1002/pros.21324

Gumbart, J., Trabuco, L. G., Schreiner, E., Villa, E., and Schulten, K. (2009). Regulation of the protein-conducting channel by a bound ribosome. *Structure* 17, 1453–1464. doi: 10.1016/j.str.2009.09.010

Haas, I. G., and Wabl, M. (1983). Immunoglobulin heavy chain binding protein. *Nature* 306, 387–389. doi: 10.1038/306387a0

Hagerstrand, D., Tong, A., Schumacher, S. E., Ilic, N., Shen, R. R., Cheung, H. W., et al. (2013). Systematic interrogation of 3q26 identifies TLOC1 and SKIL as cancer drivers. *Cancer Discov.* 3, 1045–1057. doi: 10.1158/2159-8290.CD-12-0592

Halic, M., Becker, T., Pool, M. R., Spahn, C. M. T., Grassucci, R. A., Frank, J., et al. (2004). Structure of the signal recognition particle interacting with the elongation-arrested ribosome. *Nature* 427, 808–814. doi: 10.1038/nature02342

Halic, M., Blau, M., Becker, T., Mielke, T., Pool, M. R., Wild, K., et al. (2006). Following the signal sequence from ribosomal tunnel exit to signal recognition particle. *Nature* 444, 507–511. doi: 10.1038/nature05326

Hall, B. S., Hill, K., McKenna, M., Ogbechi, J., High, S., Willis, A. E., et al. (2014). The pathogenic mechanism of the Mycobacterium ulcerans virulence factor, mycolactone, depends on blockade of protein translocation into the ER. *PLOS Pathog.* 10:e1004061. doi: 10.1371/journal.ppat.1004061

Hartmann, E., Görlich, D., Kostka, S., Otto, A., Kraft, R., Knespel, S., et al. (1993). A tetratmeric complex of membrane proteins in the endoplasmic reticulum. *Eur. J. Biochem.* 214, 375–381. doi: 10.1111/j.1432-1033.1993.tb17933.x

Haßdenteufel, S., Klein, M.-C., Melnyk, A., and Zimmermann, R. (2014). Protein transport into the human ER and related diseases: Sec61-channelopathies. *Biochem. Cell Biol.* 92, 499–509. doi: 10.1139/bcb-2014-0043

Haßdenteufel, S., Schäuble, N., Cassella, P., Leznicki, P., Müller, A., High, S., et al. (2011). Calcium-calmodulin inhibits tail-anchored protein insertion into the mammalian endoplasmic reticulum membrane. *FEBS Lett.* 585, 3485–3490. doi: 10.1016/j.febslet.2011.10.008

Haßdenteufel, S., Sicking, M., Schorr, S., Aviram, N., Fecher-Trost, C., Schuldiner, M., et al. (2017). hSnd2 protein represents an alternative targeting factor to the endoplasmic reticulum in human cells. *FEBS Lett.* 591, 3211–3224. doi: 10.1002/1873-3468.12831

Hegde, R. S., Voigt, S., Rapoport, T. A., and Lingappa, V. R. (1998). TRAM regulates the exposure of nascent secretory proteins to the cytosol during translocation into the endoplasmic reticulum. *Cell* 92, 621–631. doi: 10.1016/S0092-8674(00)81130-7

Hegde, R., and Bernstein, H. (2006). The surprising complexity of signal peptides. *Trends Biochem. Sci.* 31, 563–571. doi: 10.1016/j.tibs.2006.08.004

Hein, M. Y., Hubner, N. C., Poser, I., Cox, J., Nagaraj, N., Toyoda, Y., et al. (2015). A human interactome in three quantitative dimensions organized by stoichiometries and abundances. *Cell* 163, 712–723. doi: 10.1016/j.cell.2015.09.053

Hennessy, F., Nicoll, W. S., Zimmermann, R., Cheetham, M. E., and Blatch, G. L. (2005). Not all J domains are created equal: implications for the specificity of Hsp40-Hsp70 interactions. *Protein Sci.* 14, 1697–1709. doi: 10.1110/ps.051406805

Jadhav, B., McKenna, M., Johnson, N., High, S., Sinning, I., and Pool, M. (2015). Mammalian SRP receptor switches the Sec61 translocase from Sec62 to SRP-dependent translocation. *Nat. Commun.* 6:10133. doi: 10.1038/ncomms10133

Johnson, N., Haßdenteufel, S., Theis, M., Paton, A. W., Paton, J. C., Zimmermann, R., et al. (2013). The signal sequence influences posttranslational ER translocation at distinct stages. *PLoS ONE* 8:e75394. doi: 10.1371/journal.pone.0075394

Johnson, N., Vilardi, F., Lang, S., Leznicki, P., Zimmermann, R., and High, S. (2012). TRC-40 can deliver short secretory proteins to the Sec61 translocon. *J. Cell Sci.* 125, 3612–3620. doi: 10.1242/jcs.102608

Junne, T., and Spiess, M. (2017). Integration of transmembrane domains is regulated by their downstream sequences. *J. Cell Sci.* 130, 372–381. doi: 10.1242/jcs.194472

Kanda, S., Yanagitani, K., Yokota, Y., Esaki, Y., and Kohno, K. (2016). Autonomous translational pausing is required for Xbp1u Mrna recruitment to the ER via the SRP pathway. *Proc. Natl. Acad. Sci. U.S.A* 113, E5886–E5895. doi: 10.1073/pnas.1604435113

Kang, S. W., Rane, N. S., Kim, S. J., Garrison, J. L., Taunton, J., and Hegde, R. S. (2006). Substrate-specific translocational attenuation during ER stress defines a pre-emptive quality control pathway. *Cell* 127, 999–1013. doi: 10.1016/j.cell.2006.10.032

Khaminets, A., Heinrich, T., Mari, M., Grumati, P., Huebner, A. K., Akutsu, M., et al. (2015). Regulation of endoplasmic reticulum turnover by selective autophagy. *Nature* 522, 354–358. doi: 10.1038/nature14498

Kourtis, N., and Tavernarakis, N. (2011). Cellular stress response pathways and ageing: intircate molecular relationships. *EMBO J.* 30, 2520–2531. doi: 10.1038/emboj.2011.162

Kutay, U., Ahnert-Hilger, G., Hartmann, E., Wiedenmann, B., and Rapoport, T. A. (1995). Transport route for synaptobrevin via a novel pathway of insertion into the endoplasmic reticulum membrane. *EMBO J.* 14, 217–223.

Ladiges, W. C., Knoblaugh, S. E., Morton, J. F., Korth, M. J., Sopher, B. L., Baskin, C. R., et al. (2005). Pancreatic beta-cell failure and diabetes in mice with a deletion mutation of the endoplasmic reticulum molecular chaperone gene P58IPK. *Diabetes* 54, 1074–1081. doi: 10.2337/diabetes.54.4.1074

Lakkaraju, A. K., Thankappan, R., Mary, C., Garrison, J. L., Taunton, J., and Strub, K. (2012). Efficient secretion of small proteins in mammalian cells relies on Sec62-dependent posttranslational translocation. *Mol. Biol. Cell* 23, 2712–2722. doi: 10.1091/mbc.E12-03-0228

Lang, S., Benedix, J., Fedeles, S. V., Schorr, S., Schirra, C., Schäuble, N., et al. (2012). Different effects of Sec61α-, Sec62 and Sec63-depletion on transport of polypeptides into the endoplasmic reticulum of mammalian cells. *J. Cell Sci.* 125, 1958–1969. doi: 10.1242/jcs.096727

Lang, S., Erdmann, F., Jung, M., Wagner, R., Cavalié, A., and Zimmermann, R. (2011). Sec61 complexes form ubiquitous ER Ca^{2+} leak channels. *Channels* 5, 228–235. doi: 10.4161/chan.5.3.15314

Leroch, M., Neuhaus, H. E., Kirchberger, S., Zimmermann, S., Melzer, M., Gerhold, J., et al. (2008). Identification of a novel adenine nucleotide transporter in the endoplasmic reticulum of Arabidopsis. *Plant Cell* 20, 438–451. doi: 10.1105/tpc.107.057554

Leznicki, P., and High, S. (2012). SGTA antagonizes BAG6-mediated protein triage. *Proc. Natl. Acad. Sci. U.S.A.* 109, 19214–19219. doi: 10.1073/pnas.1209997109

Leznicki, P., Clancy, A., Schwappach, B., and High, S. (2010). Bat3 promotes the membrane integration of tail-anchored proteins. *J. Cell Sci.* 123, 2170–2178. doi: 10.1242/jcs.066738

Linxweiler, M., Linxweiler, J., Barth, M., Benedix, J., Jung, V., Kim, Y.-J., et al. (2012). Sec62 bridges the gap from 3q amplification to molecular cell biology in Non-Small Cell Lung Cancer. *Am. J. Pathol.* 180, 473–483. doi: 10.1016/j.ajpath.2011.10.039

Linxweiler, M., Schick, B., and Zimmermann, R. (2017). Lets talk about Secs: Sec61, Sec62, Sec63 in signal transduction, oncology and personalized medicine. *Signal Trans. Targ. Ther.* 2:e17002. doi: 10.1038/sigtrans.2017.2

Linxweiler, M., Schorr, S., Jung, M., Schäuble, N., Linxweiler, J., Langer, F., et al. (2013). Targeting cell migration and the ER stress response with calmodulin antagonists: a clinically tested small molecule phenocopy of SEC62 gene silencing in human tumor cells. *BMC Cancer* 13:574. doi: 10.1186/1471-2407-13-574

Liu, Y., Law, B. K., and Luesch, H. (2009). Apratoxin a reversibly inhibits the secretory pathway by preventing cotranslational translocation. *Mol. Pharm.* 76, 91–104. doi: 10.1124/mol.109.056085

Lloyd, D. J., Wheeler, M. C., and Gekakis, N. (2010). A point mutation inSec61α leads to diabetes and hepatosteatosis in mice. *Diabetes* 59, 460–470. doi: 10.2337/db08-1362

Lomax, R. B., Camello, C., Van Coppenolle, F., Petersen, O. H., and Tepikin, A. V. (2002). Basal and physiological Ca^{2+} leak from the endoplasmic reticulum of pancreatic acinar cells. Second messenger-activated channels and translocons. *J. Biol. Chem.* 277, 26479–26485 doi: 10.1074/jbc.M201845200

Losfeld, M. E., Ng, B. G., Kircher, M., Buckingham, K. J., Turner, E. H., Eroshkin, A., et al. (2014). A new congential disorder of glycosylation caused by a mutation in S.R4, the signal sequence receptor 4 protein of the TRAP complex. *Hum. Mol. Gen.* 23, 1602–1605. doi: 10.1093/hmg/ddt550

Lu, Z., Zhou, L., Killela, P., Rasheed, A. B., Di, C., Poe, W. E., et al. (2009). Glioblastoma proto-oncogene SEC61γ is required for tumor cell survival and response to endoplasmic reticulum stress. *Cancer Res.* 69, 9105–9111. doi: 10.1158/0008-5472.CAN-09-2775

Ma, Y., and Hendershot, L. M. (2001). The unfolding tale of the unfolded protein response. *Cell* 107, 827–830. doi: 10.1016/S0092-8674(01)00623-7

MacKinnon, A. L., Paavilainen, V. O., Sharma, A., Hegde, R. S., and Taunton, J. (2014). An allosteric Sec61 inhibitor traps nascent transmembrane helices at the lateral gate. *ELife* 3:e01483. doi: 10.7554/eLife.01483

Mahalingam, D., Wilding, G., Denmeade, S., Sarantopoulas, J., Cosgrove, J., Cetnar, J., et al. (2016). Mipsagargin, a novel thapsigargin-based PSMA-activated prodrug: results from a first-in-man phase I clinical trial in patients with refractory, advanced or metastatic solid tumors. *Br. J. Cancer* 114, 986–994. doi: 10.1038/bjc.2016.72

Mahamid, J., Pfeffer, S., Schaffer, M., Villa, E., Danev, R., Kuhn Cuellar, L., et al. (2016). Visualizing the molecular sociology at the HeLa cell nuclear periphery. *Science* 351, 969–972. doi: 10.1126/science.aad8857

Mariappan, M., Li, X., Stefanovic, S., Sharma, A., Mateja, A., Keenan, R. J., et al. (2010). A ribosome-associating factor chaperones tail-anchored membrane proteins. *Nature* 466, 1120–1124. doi: 10.1038/nature09296

McKenna, M., Simmonds, R. E., and High, S. (2016). Mechanistic insights into the inhibition of Sec61-dependent co- and post-translational translocation by mycolactone. *J. Cell Sci.* 129, 1404–1415. doi: 10.1242/jcs.182352

McKenna, M., Simmonds, R. E., and High, S. (2017). Mycolactone reveals the substrate-driven complexity of Sec61-dependent transmembrane protein biogenesis. *J. Cell Sci.* 130, 1307–1320. doi: 10.1242/jcs.198655

Melnyk, A., Rieger, H., and Zimmermann, R. (2014). Co-chaperones of the mammalian endoplasmic reticulum. *Subcell Biochem.* 78, 179–200. doi: 10.1007/978-3-319-11731-7_9

Meyer, D. I., and Dobberstein, B. (1980). A membrane component essential for vectorial translocation of nascent proteins across the endoplasmic reticulum: requirements for its extraction and reassociation with the membrane. *J. Cell Biol.* 8, 498–502. doi: 10.1083/jcb.87.2.498

Miller, J. D., Tajima, S., Lauffer, L., and Walter, P. (1995). The ß subunit of the signal recognition particle receptor is a transmembrane GTPase that anchors the α subunit, a peripheral membrane GTPase, to the endoplasmis reticulum membrane. *J. Cell Biol.* 128, 273–282. doi: 10.1083/jcb.128.3.273

Möeller, I., Jung, M., Beatrix, B., Levy, R., Kreibich, G., Zimmermann, R., et al. (1998). A general mechanism for regulation of access to the translocon: competition for a membrane attachment site on ribosomes. *Proc. Natl. Acad. Sci. U.S.A.* 95, 13425–13430. doi: 10.1073/pnas.95.23.13425

Mohorko, E., Glockshuber, R., and Aebi, M. (2011). OST: the central enzyme of N-linked protein glycosylation. *J. Inherit. Metab. Dis.* 34, 869–878. doi: 10.1007/s10545-011-9337-1

Müller, L., Diaz de Escauriaza, M., Lajoie, P., Theis, M., Jung, M., Müller, A., et al. (2010). Evolutionary gain of function of the ER membrane protein Sec62 from yeast to humans. *Mol. Biol. Cell* 21, 691–703. doi: 10.1091/mbc.E09-08-0730

Müller, L., Funato, Y., Miki, H., and Zimmermann, R. (2011). An interaction between human Sec63 with nucleoredoxin may provide the missing link between the SEC63 gene and polycystic liver disease. *FEBS Lett.* 585, 596–600. doi: 10.1016/j.febslet.2011.01.024

Nickel, W., and Rabouille, C. (2009). Mechanisms of regulated unconventional secretion. *Nat. Rev. Mol. Cell Biol.* 10, 148–155. doi: 10.1038/nrm2617

Nixon-Abell, J., Obara, C. J., Weigel, A. V., Li, D., Legant, W. R., Xu, C. S., et al. (2016). Increased spatiotemporal resolution reveals highly dynamic dense tubular matrices in the peripheral ER. *Science* 354, 433–445. doi: 10.1126/science.aaf3928

Novick, P., Field, C., and Schekman, R. (1980). Identification of 23 complementation groups required for post-translational events in the yeast secretory pathway. *Cell* 21, 205–215. doi: 10.1016/0092-8674(80)90128-2

Otero, J. H., Lizák, B., and Hendershot, L. M. (2010). Life and death of a BiP substrate. *Semin. Cell Dev. Biol.* 21, 472–478. doi: 10.1016/j.semcdb.2009.12.008

Paatero, A. O., Kellosalo, J., Dunyak, B. M., Almaliti, J., Gestwicki, J. E., and Gerwick, W. H., et al. (2016). Apratoxin kills cells by direct blockade of the Sec61 protein translocation channel. *Cell Chem. Biol.* 23, 561–566. doi: 10.1016/j.chembiol.2016.04.008

Palade, G. (1975). Intracellular aspects of the process of protein synthesis. *Science* 189, 347–358. doi: 10.1126/science.1096303

Park, E., Menetret, J. F., Gumbart, J. C., Ludtke, S. J., Li, W., Whynot, A., et al. (2014). Structure of the SecY channel during initiation of protein translocation. *Nature* 506, 102–106. doi: 10.1038/nature12720

Paton, A. W., Beddoe, T., Thorpe, C. M., Whisstock, J. C., Wilche, M. C., Rossjohn, J., et al. (2006). AB5 subtilase cytotoxin inactivates the endoplasmic reticulum chaperone BiP. *Nature* 443, 548–552. doi: 10.1038/nature05124

Pfeffer, S., Brandt, F., Hrabe, T., Lang, S., Eibauer, M., Zimmermann, R., et al. (2012). Structure and 3D arrangement of endoplasmic reticulum membrane-associated ribosomes. *Structure* 20, 1508–1518. doi: 10.1016/j.str.2012.06.010

Pfeffer, S., Burbaum, L., Unverdorben, P., Pech, M., Chen, Y., Zimmermann, R., et al. (2015). Structure of the native Sec61 protein-conducting channel. *Nature Commun.* 6:9403. doi: 10.1038/ncomms9403

Pfeffer, S., Dudek, J., Gogala, M., Schorr, S., Linxweiler, J., Lang, S., et al. (2014). Structure of the mammalian oligosaccharyl-transferase in the native ER protein translocon. *Nat. Commun.* 5:4072. doi: 10.1038/ncomms4072

Pfeffer, S., Dudek, J., Ng, B., Schaffa, M., Albert, S., Plitzko, J., et al. (2017). Dissecting the molecular organization of the translocon-associated protein complex. *Nat. Commun.* 8:14516. doi: 10.1038/ncomms14516

Pfeffer, S., Dudek, J., Zimmermann, R., and Förster, F. (2016). Organization of the native ribosome-translocon complex at the mammalian endoplasmic reticulum membrane. *BBA Gen. Sub.* 1860, 2122–2129. doi: 10.1016/j.bbagen.2016.06.024

Plumb, R., Zhang, Z.-R., Appathurai, S., and Mariappan, M. (2015). A functional link between the co-translational protein translocation pathway and the UPR. *eLife* 4:e07426. doi: 10.7554/eLife.07426

Potter, M. D., Seiser, R. M., and Nicchitta, C. V. (2001). Ribosome exchange revisited: a mechanism for translation-coupled ribosome detachment from the ER membrane. *Trends Cell Biol.* 11, 112–115. doi: 10.1016/S0962-8924(00)01905-X

Rabu, C., Schmid, V., Schwappach, B., and High, S. (2009). Biogenesis of tail-anchored proteins: the beginning for the end? *J. Cell Sci.* 122, 3605–3612. doi: 10.1242/jcs.041210

Reithinger, J. H., Kim, J. E. H., and Kim, H. (2013). Sec62 protein mediates membrane insertion and orientation of moderately hydrophobic signal anchor proteins in the endoplasmic reticulum (ER). *J. Biol. Chem.* 288, 18058–18067. doi: 10.1074/jbc.M113.473009

Römisch, K. (2005). Endoplasmic reticulum-associated degradation. *Annu. Rev. Cell Dev. Biol.* 21, 435–456. doi: 10.1146/annurev.cellbio.21.012704.133250

Roos, A., Buchlremer, S., Kollipara, L., Labisch, T., Gatz, C., Zitzelsberger, M., et al. (2014). Myopathy in Marinesco-Sjögren syndrome links endoplasmic reticulum chaperone dysfunction to nuclear envelope pathology. *Acta Neuropathol.* 127, 761–777. doi: 10.1007/s00401-013-1224-4

Rutkowski, D. T., Kang, S. W., Goodman, A. G., Garrison, J. L., Taunton, J., Katze, M. G., et al. (2007). The role of p58IPK in protecting the stressed endoplasmic reticulum. *Mol. Biol. Cell* 18, 3681–3691. doi: 10.1091/mbc.E07-03-0272

Schäuble, N., Lang, S., Jung, M., Cappel, S., Schorr, S., Ulucan, Ö., et al. (2012). BiP-mediated closing of the Sec61 channel limits Ca^{2+} leakage from the ER. *EMBO J.* 31, 3282–3296. doi: 10.1038/emboj.2012.189

Schekman, R. (2002). SEC mutants and the secretory apparatus. *Nat. Med.* 8, 1055–1058. doi: 10.1038/nm769

Schlenstedt, G., Gudmundsson, G. H., Boman, H. G., and Zimmermann, R. (1990). A large presecretory protein translocates both cotranslationally, using signal recognition particle and ribosome, and posttranslationally, without these ribonucleoparticles, when synthesized in the presence of mammalian microsomes. *J. Biol. Chem.* 265, 13960–13968.

Schoebel, S., Mi, W., Stein, A., Ovchinikov, S., Pavlovicz, R., DiMaio, R., et al. (2017). Cryo-EM structure of the protein-conducting ERAD channel Hrd1 in complex with Hrd3. *Nature* 548, 352–355. doi: 10.1038/nature23314

Schorr, S., Klein, M.-C., Gamayun, I., Melnyk, A., Jung, M., Schäuble, N., et al. (2015). Co-chaperone specificity in gating of the polypeptide conducting channel in the membrane of the human endoplamic reticulum. *J. Biol. Chem.* 290, 18621–11835. doi: 10.1074/jbc.M115.636639

Schubert, D., Klein, M.-C., Haßdenteufel, S., Caballero-Oteyza, A., Yang, L., Proietti, M., et al. (2017). Plasma cell deficiency in humans with heterozygous mutations in SEC61A1. *J. Allergy Clin. Immunol.* 6749, 31265–31274. doi: 10.1016/j.jaci.2017.06.042

Schuldiner, M., Metz, J., Schmid, V., Denic, V., Rakwalska, M., Schmitt, H. D., et al. (2008). The GET complex mediates insertion of tail-anchored proteins into the ER membrane. *Cell* 134, 634–645. doi: 10.1016/j.cell.2008.06.025

Schwarz, D. S., and Blower, M. D. (2016). The endoplasmic reticulum: structure, function and response to cellular signaling. *Cell. Mol. Life Sci.* 73, 79–94. doi: 10.1007/s00018-015-2052-6

Senderek, J., Krieger, M., Stendel, C., Bergmann, C., Moser, M., Breitbach-Faller, N., et al. (2005). Mutations in Sil1 cause Marinesco-Sjögren syndrome, a cerebellar ataxia with cataract and myopathy. *Nat. Gen.* 37, 1312–1314. doi: 10.1038/ng1678

Shannon, T. R., Ginsburg, K. S., and Bers, D. M. (2000). Reverse Mode of the Sarcoplasmic reticulum calcium pump and load-dependent cytosolic calcium decline in voltage-clamped cardiac ventricular myocytes. *Biophys. J.* 78, 322–333 doi: 10.1016/S0006-3495(00)76595-7

Shao, S., and Hegde, R. S. (2011). A calmodulin-dependent translocation pathway for small secretory proteins. *Cell* 147, 1576–1588. doi: 10.1016/j.cell.2011.11.048

Shibata, Y., Shemesh, T., Prinz, W. A., Palazzo, A. F., Kozlov, M. M., and Rapoport, T. A. (2010). Mechanisms determining the morphology of the peripheral ER. *Cell* 143, 774–788. doi: 10.1016/j.cell.2010.11.007

Shibata, Y., Voeltz, G. K., and Rapoport, T. A. (2006). Rough sheets and smooth tubules. *Cell* 126, 435–439. doi: 10.1016/j.cell.2006.07.019

Simon, S. M., Blobel, G., and Zimmerberg, J. (1989). Large aqueous channels in membrane vesicles derived from the rough endoplasmic reticulum of canine pancreas or the plasma membrane of *Escherichia coli*. *Proc. Natl. Acad. Sci. U.S.A.* 86, 6176–6180. doi: 10.1073/pnas.86.16.6176

Snapp, E. L., Reinhart, G. A., Bogert, B. A., Lippincott-Schwartz, J., and Hegde, R. S. (2004). The organization of engaged and quiescent translocons in the endoplasmic reticulum of mammalian cells. *J. Cell Biol.* 164, 997–1007. doi: 10.1083/jcb.200312079

Sommer, N., Junne, T., Spiess, M., and Hartmann, E. (2013). TRAP assists membrane protein topogenesis at the mammalian ER membrane. *Biochim. Biophys. Acta* 1833, 3104–3111. doi: 10.1016/j.bbamcr.2013.08.018

Spang, A. (2015). Anniversary of the discovery of sec mutants by Novick and Schekman. *Mol. Biol. Cell* 26, 1783–1785. doi: 10.1091/mbc.E14-11-1511

Stefanovic, S., and Hegde, R. S. (2007). Identification of a targeting factor for posttranslational membrane protein insertion into the ER. *Cell* 128, 1147–1159. doi: 10.1016/j.cell.2007.01.036

Stephens, S. B., Dodd, R. D., Lerner, R. S., Pyhtila, B. M., and Nicchita, C. V. (2008). Analysis of mRNA partitioning between the cytosol and endoplasmic reticulum compartments of mammalian cells. *Methods Mol. Biol.* 419, 197–214. doi: 10.1007/978-1-59745-033-1_14

Sundaram, A., Plumb, R., Appathurai, S., and Mariappan, M. (2017). The Sec61 translocon limits IRE1α signaling during the unfolded protein response. *eLife* 6:e27187. doi: 10.7554/eLife.27187

Synofzik, M., Haack, T. B., Kopaijtich, R., Gorza, M., Rapaport, D., Greiner, M., et al. (2014). Absence of BiP co-chaperone DNAJC3 causes diabetes mellitus and multisystemic neurodegeneration. *Am. J. Hum. Gen.* 95, 689–697. doi: 10.1016/j.ajhg.2014.10.013

Terasaki, M., Shemesh, T., Kasthuri, N., Klemm, R. W., Schalek, R., Hayworth, K. J., et al. (2013). Stacked endoplasmic reticulum sheets are connected by helicoidal membrane motifs. *Cell* 154, 285–296. doi: 10.1016/j.cell.2013.06.031

Tu, H., Nelson, O., Bezprozvanny, A., Wang, Z., Lee, S.-F., Hao, Y.-H., et al. (2006). Presenilins form ER Ca^{2+} leak channels, a function disrupted by familial Alzheimer's disease-linked mutations. *Cell* 126, 981–993. doi: 10.1016/j.cell.2006.06.059

Tyedmers, J., Lerner, M., Wiedmann, M., Volkmer, J., and Zimmermann, R. (2003). Polypeptide-binding proteins mediate completion of co-translational protein translocation into the mammalian endoplasmic reticulum. *EMBO Rep.* 4, 505–510. doi: 10.1038/sj.embor.embor826

Ushioda, R., Miyamoto, A., Inoue, M., Watanabe, S., Okumura, M., Maegawa, K., et al. (2016). Redox-assisted regulation of Ca^{2+} homeostasis in the endoplasmic reticulum by disulfide reductase Erdj5. *Proc. Natl. Acad. Sci. U.S.A.* 113, E6055–E6063. doi: 10.1073/pnas.1605818113

Valm, A. M., Cohen, S., Legant, W. R., Melunis, J., Hershberg, U., Wait, E., et al. (2017). Applying systems-level spectral imaging and analysis to reveal the organelle interactome. *Nature* 546, 162–167doi: 10.1038/nature22369

Van Coppenolle, F., Van den Abeele, F., Slomianny, C., Flourakis, M., Hesketh, J., Dewailly, E., et al. (2004). Ribosome-translocon complex mediates calcium leakage from endoplasmic reticulum stores. *J. Cell Sci.* 117, 4135–4142. doi: 10.1242/jcs.01274

Vanden Abeele, F., Bidaux, G., Gordienko, D., Beck, B., Panchin, Y. V., Baranova, A. V., et al. (2006). Functional implications of calcium permeability of the channel formed by pannexin 1. *J. Cell Biol.* 174, 535–546. doi: 10.1083/jcb.200601115

Van den Berg, B., Clemons, W. M., Collinson, I., Modis, Y., Hartmann, E., Harrison, S. C., et al. (2004). X-ray structure of a protein-conducting channel. *Nature* 427, 36–44. doi: 10.1038/nature02218

Van Lehn, R. C., Zhang, B., and Miller, I. I. I., T. F. (2015). Regulation of multispanning membrane protein topology via post-translational annealing. *ELife* 4:e08697. doi: 10.7554/eLife.08607

Vermeire, K., Bell, T. W., Van Puyenbroeck, V., Giraut, A., Noppen, S., Liekens, S., et al. (2014). Signal peptide-binding drug as a selective inhibitor of co-translational protein translocation. *PLoS Biol.* 12:e1002011. doi: 10.1371/journal.pbio.1002011

Vilardi, F., Lorenz, H., and Dobberstein, B. (2011). WRB is the recpetor for TRC40/Asna-1-mediated insertion of tail-anchored proteins into the ER membrane. *J. Cell Sci.* 124, 1301–1307. doi: 10.1242/jcs.084277

Vilardi, F., Stephan, M., Clancy, A., Janshoff, A., and Schwappach, B. (2014). WRB and caml are necessary and sufficient to mediate tail-anchored protein targeting to the ER membrane. *PLoS ONE* 9:e85033. doi: 10.1371/journal.pone.0085033

Vishnu, N., Khan, M. J., Karsten, F., Groschner, L. N., Waldeck-Weiermaier, M., Rost, R., et al. (2013). ATP increases within the lumen of the endoplasmic reticulum upon intracellular Ca^{2+} release. *Mol. Biol. Cell* 25, 368–379. doi: 10.1091/mbc.E13-07-0433

Voigt, S., Jungnickel, B., Hartmann, E., and Rapoport, T. A. (1996). Signal sequence-dependent function of the TRAM protein during early phases of protein transport across the endoplasmic reticulum membrane. *J. Cell Biol.* 134, 25–35. doi: 10.1083/jcb.134.1.25

von der Malsburg, K., Shao, S., and Hegde, R. S. (2015). The ribosome quality control pathway can access nascent polypeptides stalled at the Sec61 translocon. *Mol. Biol. Cell* 26, 2168–2180. doi: 10.1091/mbc.E15-01-0040

von Heijne, G. (1985). Signal sequences. *J. Mol. Biol.* 184, 99–105. doi: 10.1016/0022-2836(85)90046-4

von Heijne, G. (1986). Towards a comparative anatomy of N-terminal topogenic protein sequences. *J. Mol. Biol.* 189, 239–242. doi: 10.1016/0022-2836(86)90394-3

Voorhees, R. M., and Hegde, R. S. (2015). Structures of the scanning and engaged states of the mammalian SRP-ribosome complex. *Elife* 4:e07975. doi: 10.7554/eLife.07975

Voorhees, R. M., and Hegde, R. S. (2016). Structure of the Sec61 channel opened by a Signal Sequence. *Science* 351, 88–91. doi: 10.1126/science.aad4992

Voorhees, R. M., Fernández, I. S., Scheres, S. H. W., and Hegde, R. S. (2014). Structure of the mammalian ribosome-Sec61 complex to 3.4 Å resolution. *Cell* 157, 1632–1643. doi: 10.1016/j.cell.2014.05.024

Wada, I., Rindress, D., Cameron, P. H., Ou, W.-J., Doherty, I. I., Louvard, D., et al. (1991). SSRα and associated calnexin are major calcium binding proteins of the endoplasmic reticulum. *J. Biol. Chem.* 266, 19599–19610.

Walter, P., and Blobel, G. (1981). Translocation of proteins across the endoplasmic reticulum. II. Signal recognition protein, SRP, mediates the selective binding to microsomal membranes of *in-vitro*-assembled polysomes synthesizing secretory protein. *J. Cell Biol.* 91, 551–556. doi: 10.1083/jcb.91.2.551

Wang, Q., Liu, Y., Soetandyo, N., Baek, K., Hegde, R., and Ye, Y. (2011). A ubiquitin ligase-associated chaperone holdase maintains polypeptides in soluble states for proteasome degradation. *Mol. Cell* 42, 758–770. doi: 10.1016/j.molcel.2011.05.010

Wiedmann, B., Saki, H., Davis, T. A., and Wiedmann, M. (1994). A protein complex required for signal-sequence-specific sorting and translocation. *Nature* 370, 434–440. doi: 10.1038/370434a0

Wirth, A., Jung, M., Bies, C., Frien, M., Tyedmers, J., Zimmermann, R., et al. (2003). The Sec61p complex is a dynamic precursor activated channel. *Mol. Cell* 12, 261–268. doi: 10.1016/S1097-2765(03)00283-1

Wuytack, F., Raeymaekers, L., and Missiaen, L. (2002). Molecular physiology of the SERCA and SPCA pumps. *Cell Calc.* 32, 279–305. doi: 10.1016/S0143416002001847

Yamamoto, Y., and Sakisaka, T. (2012). Molecular machinery for insertion of tail-anchored membrane proteins into the endoplasmic reticulum membrane in mammalian cells. *Mol. Cell* 48, 387–397. doi: 10.1016/j.molcel.2012.08.028

Yanagitani, K., Kimata, Y., Kadokura, H., and Kohno, K. (2011). Translational pausing ensures membrane targeting and cytoplasmic splicing of *Xbp1u* Mrna. *Science* 331, 586–589. doi: 10.1126/science.1197142

Zhang, B., and Miller, T. F. III (2012). Long-timescale dynamics and regulation of Sec-facilitated protein translocation. *Cell Rep.* 2, 927–937. doi: 10.1016/j.celrep.2012.08.039

Zhang, K., and Kaufman, R. J. (2004). Signaling the unfolded protein response from the endoplasmic reticulum. *J. Biol. Chem.* 279, 25935–25938. doi: 10.1074/jbc.R400008200

Zhang, S. L., Yeromin, A. V., Zhang, X. H., Yu, Y., Safrina, O., Penna, A., et al. (2006). Genome-wide RNAi screen of Ca^{2+} influx identifies genes that regulate Ca^{2+} release-activated Ca^{2+} channel activity. *Proc. Natl. Acad. Sci. U.S.A.* 103, 9357–9362. doi: 10.1073/pnas.0603161103

Zhao, L., Longo-Guess, C., Harris, B. S., Lee, J.-W., and Ackerman, S. L. (2005). Protein accumulation and neurodegeneration in the woozy mutant mouse is caused by disruption of SIL1, a cochaperone of BiP. *Nat. Gen.* 37, 974–979. doi: 10.1038/ng1620

Zhao, Y., Hu, J., Miao, G., Qu, L., Wang, Z., Li, G., et al. (2013). Transmembrane protein 208: a Novel ER-localized protein that regulates autophagy and er stress. *PLoS ONE* 8:e64228. doi: 10.1371/journal.pone.0064228

Zimmermann, R. (2016). Components and mechanisms of import, modification, folding, and assembly of immunoglobulins in the endoplasmic reticulu. *J. Clin. Immunol.* 36(Suppl. 1), 5–11. doi: 10.1007/s10875-016-0250-0

Zimmermann, R., Eyrisch, S., Ahmad, M., and Helms, V. (2011). Protein translocation across the ER membrane. *Biochim. Biophys. Acta* 1808, 912–924. doi: 10.1016/j.bbamem.2010.06.015

Conflict of Interest Statement: The authors declare that the research was conducted in the absence of any commercial or financial relationships that could be construed as a potential conflict of interest.

frontiers in Physiology

REVIEW
published: 06 June 2017
doi: 10.3389/fphys.2017.00371

The Structure and Function of the Na,K-ATPase Isoforms in Health and Disease

*Michael V. Clausen, Florian Hilbers and Hanne Poulsen **

Department of Molecular Biology and Genetics, Aarhus University, Aarhus, Denmark

The sodium and potassium gradients across the plasma membrane are used by animal cells for numerous processes, and the range of demands requires that the responsible ion pump, the Na,K-ATPase, can be fine-tuned to the different cellular needs. Therefore, several isoforms are expressed of each of the three subunits that make a Na,K-ATPase, the alpha, beta and FXYD subunits. This review summarizes the various roles and expression patterns of the Na,K-ATPase subunit isoforms and maps the sequence variations to compare the differences structurally. Mutations in the Na,K-ATPase genes encoding alpha subunit isoforms have severe physiological consequences, causing very distinct, often neurological diseases. The differences in the pathophysiological effects of mutations further underline how the kinetic parameters, regulation and proteomic interactions of the Na,K-ATPase isoforms are optimized for the individual cellular needs.

Keywords: Na, K-ATPase, structure, expression, isoforms, subunits, disease

OPEN ACCESS

Edited by:
Mario Diaz,
University of La Laguna, Spain

Reviewed by:
Pablo Martín-Vasallo,
University of La Laguna, Spain
Tomas Obsil,
Charles University, Czechia
Lijun Catherine Liu,
University of Toledo, United States

***Correspondence:**
Hanne Poulsen
hp@mb.au.dk

Specialty section:
This article was submitted to Membrane Physiology and Membrane Biophysics, a section of the journal Frontiers in Physiology

Received: *01 February 2017*
Accepted: *18 May 2017*
Published: *06 June 2017*

Citation:
Clausen MV, Hilbers F and Poulsen H (2017) The Structure and Function of the Na,K-ATPase Isoforms in Health and Disease. Front. Physiol. 8:371. doi: 10.3389/fphys.2017.00371

INTRODUCTION

During the evolution of life, most living cells have maintained a similar ionic composition of their cytoplasms, including low calcium, low sodium, high potassium, and neutral pH (Mulkidjanian et al., 2012). When the extracellular ionic concentrations are significantly different, it requires perpetual ion pump activity to uphold the intracellular concentrations, which are important for numerous of the cell's enzymatic functions. Furthermore, much energy is stored in the ionic gradients across the plasma membrane, and the steep sodium and potassium gradients in animal cells are used to facilitate secondary transport of molecules (sugars, neurotransmitters, amino acids, metabolites) and other ions (H^+, Ca^{2+}, Cl^-). The ion gradients are also used for rapid signaling by opening of sodium or potassium selective channels in the plasma membrane in response to extracellular signals or the membrane potential.

Many organs use the sodium and potassium gradients for their specialized functions. In the kidneys, the Na,K-ATPase is highly expressed, an estimate says up to 50 million pumps per cell in the distal convoluted tubule (El Mernissi and Doucet, 1984), because the sodium gradient is utilized by the main kidney functions, to filter the blood of waste products, to reabsorb glucose and amino acids, to regulate electrolytes and to maintain pH. In sperm cells, the regulation of ions and membrane potential is crucial for motility and the acrosome reaction, and sperm cells express a unique Na,K-ATPase isoform, which is essential for male fertility (Jimenez et al., 2011a). Not least the brain has a massive demand for Na,K-ATPase activity, since neurons rely on the pump to reverse postsynaptic sodium flux, to reestablish the sodium and potassium gradients used to fire action potentials, and in astrocytes, the sodium gradient drives neurotransmitter reuptake. In gray matter, it is estimated that housekeeping like synthesis of proteins and other molecules use just a quarter of the energy, while the rest is consumed by Na,K-ATPases (Attwell and Laughlin, 2001).

CARDIOTONIC STEROIDS

The vital importance of the Na,K-ATPase for animals makes it a natural target for toxins produced by plants or animals that want to avoid being eaten. At least 12 different plant families and several species of the *Bufo* toads produce Na,K-ATPase inhibitors, the so-called cardiotonic steroids (Gao et al., 2011). Plant cells have no endogenous Na,K-ATPase, since they use a proton gradient to energize their membranes, so Na,K-ATPase inhibitors are not toxic to them.

Several insect species feed on plants with cardiotonic steroids and store the toxins to make themselves poisonous (Zhen et al., 2012). The poisonous insects and toads can, nonetheless, become prey to other animals, including reptiles, hedgehogs, and rodents. All animals that produce or ingest cardiotonic steroids tolerate the toxin because of specific mutations in their Na,K-ATPase encoding genes that make the pumps insensitive to the inhibitor (Ujvari et al., 2015), a classical example of an evolutionary arms race, where one species develops a weapon, and then its predator develops a defense against it.

Cardiotonic steroids like digitalis from the foxglove plant have been used to treat heart conditions for centuries. They are recommended for atrial fibrillation and reduce hospital admission for heart failure patients, but have not been shown to affect mortality rates (Ziff and Kotecha, 2016). The mechanism-of-action of digitalis is still a matter of debate. It has been believed that inhibition of the Na,K-ATPase in cardiomyocytes raises cytoplasmic sodium levels, thereby inhibiting the sodium-calcium exchanger and raising cytoplasmic calcium levels, which is imagined to have a direct effect on the heart's contractility, but there is also evidence to suggest that digitalis strengthens the parasympathetic nervous system by vagal activation and slows heart rate (Ziff and Kotecha, 2016).

At non-saturating levels (5–10 nM), cardiotonic steroids have been suggested to act as ligands and the Na,K-ATPase as a receptor that initiates intracellular signaling via e.g., the inositol 1,4,5-triphosphate receptor and the Src kinase to promote cellular proliferation. In the body, cardiotonic steroids may arise from medication, but low levels of endogenous cardiotonic steroids have also been measured (Aperia et al., 2016). It remains controversial what the physiological significance of Na,K-ATPase signaling may be, and transcriptome differences in response to cardiotonic steroids were only seen if the relative intracellular concentrations of sodium and potassium changed, i.e., if there was a direct effect on the ion pumping mechanism (Klimanova et al., 2017).

THE BASIC MECHANISM OF ION TRANSPORT

Cardiotonic steroids bind the Na,K-ATPase from the extracellular side in the suggested ion exchange pathway as revealed by the crystal structure of a high-affinity binding complex between the cardiotonic steroid digoxin and Na,K-ATPase purified from pig kidney (Laursen et al., 2015, **Figure 1**). The complex contains three protein subunits, namely the ten transmembrane (TM) helix alpha subunit and the single TM beta and FXYD subunits. The beta subunit has a large, glycosylated extracellular part, and for the smaller FXYD subunit, only the TM part is resolved in the structure. The alpha subunit has three cytoplasmic domains, the nucleotide binding (N), the phosphorylation (P) and the actuator (A) domains, which function as the kinase, the substrate and the phosphatase, respectively, in the catalytic cycle, when ATP is hydrolyzed (**Figure 2**). A conserved aspartate in the P-domain is phosphorylated and dephosphorylated during the cycle, and the movements of the cytoplasmic domains cause the connected TM helices to bind and release the pump's substrates in response. The Na,K-ATPase was the founding member of the P-type ATPase family (Skou, 1957) whose members share this basic mechanism to transport numerous different cations and even lipids. In addition to the ouabain-bound Na,K-ATPase, crystal structures of two major steps in the catalytic cycle have been solved, namely of the potassium (Morth et al., 2007; Shinoda et al., 2009) and sodium (Kanai et al., 2013; Nyblom et al., 2013) occluded forms (**Figure 2**).

The transport of ions against their concentration gradients requires that the transmembrane ion binding site acts like a space shuttle airlock with gates on either side of which at least one is always locked to avoid the energetically favored flow of ions in the opposite direction. When the Na,K-ATPase opens toward the cytoplasm, TM1 is believed to slide up (as in the related calcium pump SERCA, Winther et al., 2013) and allow three sodium ions to access the high-affinity binding sites in the middle of the membrane, where negative charges on aspartate and glutamate residues compensate for the charges of the positively charged ions (**Figure 2**). When bound, the inner gate closes to form an occluded pump, and the P-domain is phosphorylated by ATP. The pump is said to be in the E1 form when it has high affinity for sodium, and in the E2 form when it has high affinity for potassium. The transition from phosphorylated E1 (called E1P) to E2P is coupled to release of ADP, opening of the outer gate and release of the three sodium ions to the extracellular side. It is proposed that a proton from the cytoplasm promotes the sodium release and compensates for negative charge at the ion binding site unique for sodium, the so-called site III, when sodium is released (Poulsen et al., 2010). Potassium can then bind from the extracellular side, the outer gate closes to occlude the two potassium ions, and the aspartate in the P-domain is dephosphorylated. Binding of ATP, a transition back to the E1 form, and opening of the inner gate lead to cytoplasmic release of the proton in site III and of the potassium ions in sites I and II, and the pump is ready for another cycle (**Figure 2**).

ISOFORM EXPRESSION, FUNCTION AND PHYSIOLOGY

The first indication that there is more than one isoform of the Na,K-ATPase subunits came from titration with ouabain on mouse brain preparations, which showed a biphasic curve of ATPase activity (Marks and Seeds, 1978). It was later found that the biphasic curve, which is also found in rat, is due to

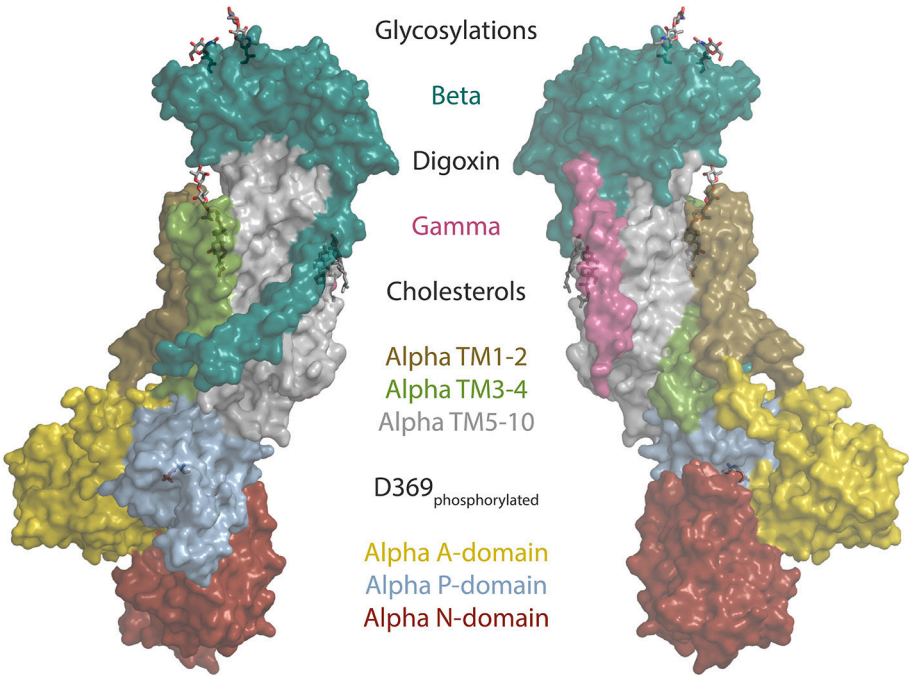

FIGURE 1 | The structure of the sodium pump. Surface representation of the digoxin bound alpha1 isoform structure from pig (Laursen et al., 2015) (PDB ID: 4RET). Sodium pump subunits and domains are shown in colors as indicated. The two beta glycosylations, digoxin, two cholesterols and the phosphorylated aspartate (D369) are shown as sticks.

a specific reduction in ouabain affinity (low mM) of alpha1 in rodents that makes it easily distinguished from the two high affinity isoforms found in brain, alpha2, and alpha3 (low μM affinities). The primary sequences of the alpha isoforms are well conserved: alpha1, 2, and 3 are about 87% identical to each other and about 78% identical to the sperm-specific alpha4 (Shamraj and Lingrel, 1994). Between species, the identity percentages of alpha1, 2, and 3 are in the high nineties and for alpha4 in the low eighties (Clausen et al., 2011). Mapping the isoform differences on homology models of each alpha (**Figure 3**) shows that the variation is generally found at the surface of the protein, while the ion binding interior of the membrane domain and the linkers to the cytoplasmic domains are highly conserved. The most diverse part of the protein is the surface of the N-domain, especially in alpha4. The basic function of the pump will depend most strongly on the interior parts where ions are transported in response to the ATP hydrolysis, while differences on the surface allow each isoform to have its own protein-protein interaction networks.

In addition to the four alpha isoforms, mammals express three beta and seven FXYD subunit isoforms. The combination of alpha1 and beta1 is expressed most widely (table), and any alpha can be expressed with any beta to yield a functional pump in *Xenopus* oocytes (Crambert et al., 2000; Hilbers et al., 2016), though *in vivo* the associations may be more selective (Tokhtaeva et al., 2012; Habeck et al., 2016).

The different isoforms have different kinetic properties and affinities. Depending on the assay used, the details can vary, but for example for the alphas, there is general consensus that alpha1 has relatively high apparent potassium affinity, and alpha3 relatively low sodium affinity (Blanco, 2005). The beta and FXYD subunits further affect the functional properties (Arystarkhova and Sweadner, 2016; Hilbers et al., 2016), so the different subunits allow cells to have Na,K-ATPase activity with optimized functional characteristics. In addition, the subunits differ in how they are trafficked to and localized in the membrane, which posttranslational modifications they are subject to, and importantly what cellular partners they interact with. Therefore, the distinct expression profiles of the Na,K-ATPase subunits enable fine-tuning in time and tissues of the pumping activity (Table).

Since the ionic gradients are of vital importance for any organ, disturbance of the Na,K-ATPase activity has been implicated in many pathophysiological conditions, including cancer (Durlacher et al., 2015), diabetes (Vague et al., 2004), and heart failure (Schwinger et al., 2003), and the pump has been suggested as a potential chemotherapy target (Alevizopoulos et al., 2014), though evidence is still lacking for its efficacy (Durlacher et al., 2015).

ALPHA1

The alpha1 subunit is essentially omnipresent at the tissue and cellular levels. One organ that relies heavily on sodium and potassium gradients is the heart, where the rhythmic action potentials and accompanying calcium fluxes determine the muscle contractions. All animal hearts examined express alpha1, while it varies between species if it is the only

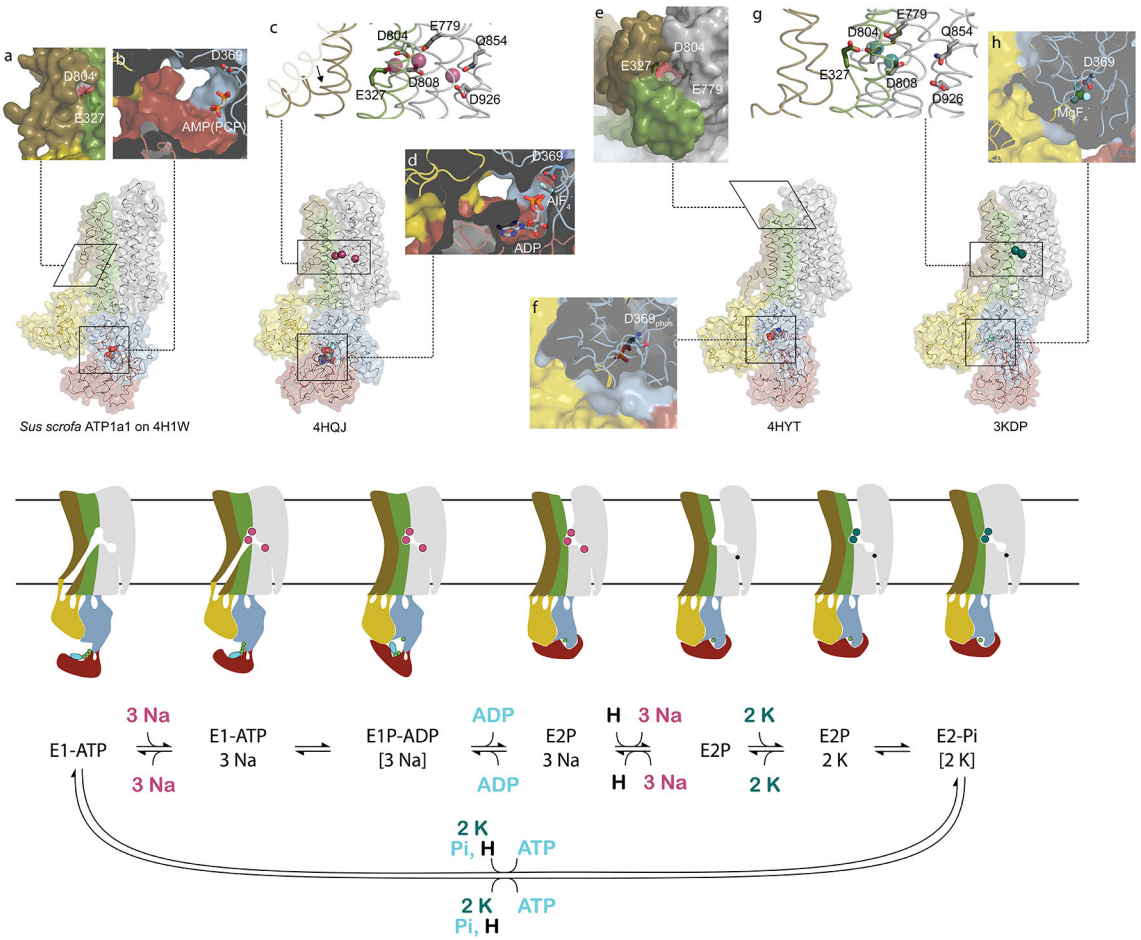

FIGURE 2 | Conformational changes during the sodium pump catalytic cycle. Three sodium pump structures and a homology model are positioned in accordance with the catalytic cycle shown below as both cartoon and reaction scheme. The eight inserts labeled with small letters highlight important structural details. The homology model of pig alpha1 on the SERCA E1-ATP state (Winther et al., 2013) (PDB ID: 4H1W) shows an inwardly opened conformation with access to the ion-binding sites, here visualized by D804 and E327 **(a)**. In the structure, only the beta and gamma phosphates of the non-hydrolysable ATP analog AMPPCP are resolved and demonstrate a non-primed positioning for reaction with D369 **(b)**. After binding of three sodium ions, TM1 rearranges to a position that blocks the cytoplasmic entrance pathway (arrow in **c**), and the cytoplasmic domains tighten around the nucleotide that reacts with D369 **(d)**. Following sodium occlusion ADP is released and an extracellular pathway allows the exit of the three sodium ions. In the externally opened conformation, here imitated by the ouabain bound structure 4HYT shown without the inhibitor, three ion-binding residues are directly visible from the outside **(e)**, and the intracellular domains are completely wrapped around the phosphorylated D369 **(f)**. Binding of two extracellular potassium ions **(g)** initiates closure of the extracellular gate and dephosphorylation of D369 **(h)**. The narrow pathway from the cytoplasm to the sodium specific binding site in the cartoon representation shows the proposed C-terminal proton path utilized for charge conservation. Color coding as in **Figure 1**.

isoform or if alpha2 and/or alpha3 can be detected (Sweadner et al., 1994; McDonough et al., 2002; Dostanic et al., 2004; Henriksen et al., 2013, Table). In human hearts, all three isoforms are expressed, and in failing human hearts the protein levels of alpha1 and alpha3 are reduced 30–40% in the left ventricle compared to non-failing hearts (Schwinger et al., 1999), and at the RNA level, the left and right ventricles of failing hearts show around 50% reduction in transcripts encoding alpha1 and alpha2 (Borlak and Thum, 2003). An increase in the intracellular sodium concentration due to lower levels of Na,K-ATPase will likely decrease calcium export by the Na^+/Ca^{2+}-exchanger, which may be the main extrusion pathway in cardiomyocytes. The downregulation of Na,K-ATPases is also a probable reason for higher sensitivity to cardiotonic steroids in failing hearts (Shamraj et al., 1993).

Several physiological processes depend on a very strict regulation of the subcellular localization of alpha1. Cavities and surfaces in the body are lined by sheets of polarized epithelial cells that have distinct membrane domains; an apical membrane that faces the lumen and a basolateral membrane that is oriented away from the lumen. Depending on the physiological role of an epithelial sheet, the cellular sorting machinery makes sure that alpha1 ends up in either the apical or the basolateral membrane.

When the intention is to minimize bodily loss of sodium through e.g., urine and sweat, alpha1 is sent to the basolateral

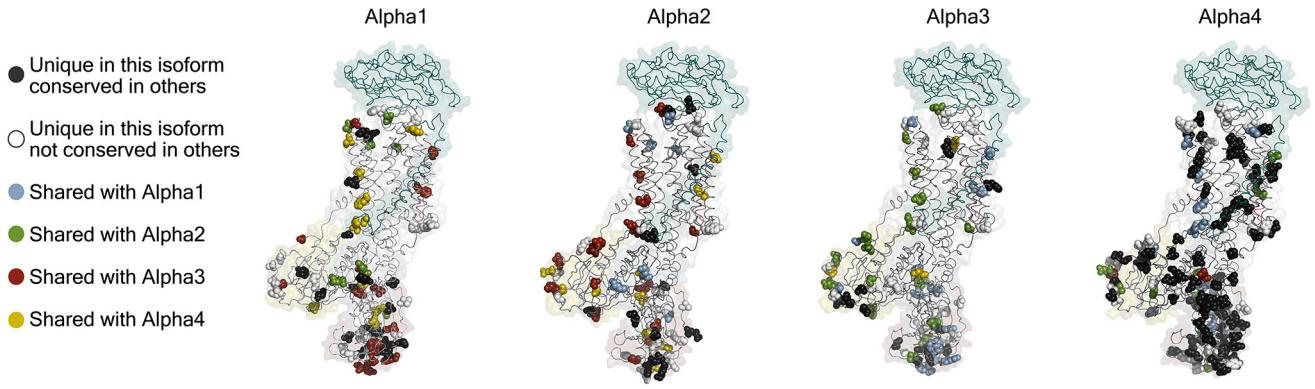

FIGURE 3 | Homology models of the four human alpha isoforms. Models were built from the potassium occluded 3KDP structure (Morth et al., 2007), and the isoform differences are highlighted as spheres. Conservative differences are not included which means that the following groups of amino acids were treated as identical (L, I, V), (E, D), (K, R), (Q, N), (S, T), (Y, F), and (M, C) while H, G, P, A, and W were ungrouped.

membrane of the epithelial cells as seen in the renal tubular system (Caplan et al., 1986) and in the secretory coils of sweat glands (Zhang et al., 2014), where sodium reuptake is driven by channels and secondary transporters.

To maintain a low level of potassium while indirectly supplying water to the cerebrospinal fluid of the central nervous system, the epithelial cells that line the choroid plexus sort alpha1 to the apical membrane (Gundersen et al., 1991; Brown et al., 2004). The same strategy of apical alpha1 sorting is utilized in the eye where retinal pigment epithelium supplies the fluid of the subretinal space with the high sodium concentration needed to maintain the dark current that keeps photoreceptor cells depolarized in the absence of light (Miller et al., 1978; Sparrow et al., 2010).

ALPHA2

The alpha2 isoform is predominantly expressed in muscle (heart and skeletal) and brain (in astrocytes and glia cells). It is noteworthy that while astrocytes co-cultured with neurons readily express alpha2, purified astrocytes grown without neurons only rarely express it (Peng et al., 1998). With a relatively high sensitivity to voltage (Crambert et al., 2000; Horisberger and Kharoubi-Hess, 2002; Larsen et al., 2014; Clausen et al., 2016) and in combination with beta2, a remarkably reduced affinity for potassium (K^+ $K_{0.5}$ 3 mM, other isoforms have $K_{0.5}$ ~ 1 mM, Crambert et al., 2000; Larsen et al., 2014), the alpha2beta2 complex in glia and astrocytes seems perfectly geared for clearance of potassium after intense neuronal activity, being maximally active when the potassium concentration is high, and the membrane potential depolarized.

In the heart, alpha2 preferentially assembles with beta2 and specifically localizes to the T-tubular membranes, while alpha1beta1 is more uniformly distributed in both T-tubular membranes and external sarcolemma membranes (Habeck et al., 2016). The alpha2 subunit localizes close to the Na^+/Ca^{2+}-exchanger in contractile tissue and may thereby indirectly serve to assist the regulation of calcium levels (Juhaszova and Blaustein, 1997). Similar to the suggested role in glia cells, the high voltage sensitivity and low potassium affinity of alpha2beta2 are proposed to ensure that additional Na,K-ATPase activity is available during the long-lasting cardiac action potential (Stanley et al., 2015; Habeck et al., 2016). In skeletal muscle, the alpha2 activity is rapidly controlled in response to changes in muscle use, suggesting that it may be adapted to reacting on dynamic changes in muscle activity (Kravtsova et al., 2016).

ALPHA3

Alpha3 is highly expressed in the brain with a main localization in neuronal projections (Bottger et al., 2011) and to some extend in dendritic spines (Kim et al., 2007; Blom et al., 2016). During intense neuronal activity, the concentration of sodium in dendrites and spines can increase dramatically, estimates as high as 100 mM have been proposed (Rose and Konnerth, 2001), and the required clearance of intracellular sodium is mainly attributed to alpha3 (Azarias et al., 2013), which has relatively low sodium affinity, 25–50 mM, compared to Na^+ $K_{0.5}$ of approximately 10 mM for other isoforms (Zahler et al., 1997; Blanco and Mercer, 1998; Crambert et al., 2000). The alpha3-containing pumps in neurons thus appear to be optimized for high intensity neuronal firing.

Interestingly, several studies of disease mechanisms have found that neurodegenerative effects may be caused by direct interactions with alpha3. In Alzheimer's disease, amyloid-beta can cause neurodegeneration, and the same is true for alpha-synuclein in Parkinson's disease. Amyloid-beta as well as alpha-synuclein assemblies were found to interact with alpha3, and mapping of the interaction domain located a specific extracellular loop in the pump as the target in both cases (Ohnishi et al., 2015; Shrivastava et al., 2015). Furthermore, misfolded SOD1 protein, which is associated with amyotrophic lateral sclerosis, can bind an intracellular domain of alpha3 and inhibit the pump function (Ruegsegger et al., 2016).

Alpha3 is also highly expressed in the human heart; interestingly with gender-specific differences: the relative expression of alpha3 to alpha1 is several-fold higher in men than in women as judged from RNA levels (Gaborit et al., 2010).

ALPHA4

Spermatozoa are exceedingly specialized cells unique in their dependence on being able to thrive and carry out complex tasks inside other organisms. Furthermore, they are subject to a more profound evolutionary pressure than other cells, because only a single spermatozoon from a batch of hundreds of millions has a chance of fertilizing an egg, and only mutations that make better spermatozoa count in this race. The competitive spermatozoa evolution is evident from the high number of unique sperm cell proteins, particularly membrane proteins (Dorus et al., 2010). One of the sperm specific proteins is the alpha4 isoform of the sodium pump (Hlivko et al., 2006; McDermott et al., 2012), and the strong evolutionary pressure on sperm proteins is very apparent for alpha4, which is the most divergent of the Na,K-ATPase alpha subunits, both when compared with the other three alpha isoforms (**Figure 3**), and when compared between different species (Clausen et al., 2011). While alpha4 is considered a sperm specific Na,K-ATPase, a smaller protein from human skeletal muscle cross react with an alpha4 antisera (Sugiura et al., 2005), and mRNA that hybridize with alpha4 probes are present in human and mouse skeletal muscle (Keryanov and Gardner, 2002).

Although sperm cells express alpha1 in addition to alpha4, male mice are completely sterile if they lack alpha4, and their spermatozoa are unable to fertilize eggs *in vitro* although their viability is unaffected (Jimenez et al., 2011a). Lack of alpha4 reduces sperm motility, depolarizes the membrane potential and increases intracellular sodium (Jimenez et al., 2011a), whereas overexpression of alpha4 increases their motility (Jimenez et al., 2011b; McDermott et al., 2015).

At the biophysical level, when compared with the other isoforms in a cell free system, alpha4 has low $K_{0.5}$ for ouabain and sodium, and regular for potassium (Blanco et al., 1999). When studied in a cellular system, alpha4 is less affected by changes in voltage, extracellular sodium and temperature than alpha1 (Clausen et al., 2016).

If greater evolutionary pressure has optimized alpha4 to increase the probability that spermatozoa reach and fertilize an egg in the female oviduct, there could be specific parameters that make this pump more suitable for the task than the other isoforms. Interestingly it has been demonstrated that as spermatozoa capacitate in the female genital tract, the catalytic activity of alpha4 is up-regulated due to an increased availability of pumps in the membrane (Jimenez et al., 2012), suggesting that alpha4 supports the hyperpolarization and decreased intracellular sodium concentration characteristic of capacitated spermatozoa. An alternative, and not necessarily conflicting, hypothesis is that since pumps in the membrane of spermatozoa experience dramatic changes in e.g., extracellular sodium levels and membrane potential as the cell passes from testis to oviduct, it could be advantageous with a pump that, like alpha4, responds less to environmental alterations (Clausen et al., 2016).

BETAS

The Na,K-ATPase beta subunit is part of the functional core of the pump and is required for its trafficking to the plasma membrane. The sequence identity of the three human isoforms are 39% (beta1 and 2), 36% (beta1 and 3), and 47% (beta2 and 3). It has a small (30 amino acid) N-terminal, intracellular domain, a TM helix, and a larger (∼240 amino acids) C-terminal, extracellular domain. Like the alpha isoforms, the different beta isoforms have distinct tissue and cell-type specific expression profiles (**Table 1**). The beta2 isoform was originally found in glia where it is involved in cell-cell contacts and hence it was initially called Adhesion Molecule On Glia (AMOG, Antonicek et al., 1987; Martin-Vasallo et al., 1989; Gloor et al., 1990).

There are three conserved disulfide bonds in the extracellular domain, which are important for forming a stable pump (Noguchi et al., 1994), and the domain has three, eight, and two glycosylation sites in beta1, 2, and 3, respectively. Removal of the glycosylations causes retention in the endoplasmatic reticulum of beta2, but not of beta1 or 3, suggesting that the glycosylations play individual roles in the different isoforms (Tokhtaeva et al., 2010).

Beta1 may further respond to oxidative stress by glutathionylation of a cysteine in the middle of its transmembrane helix, a cysteine not found in the other betas (Rasmussen et al., 2010). *In vitro* studies have shown that the E1 state of the enzyme favors the cysteine to be glutathionylated more than the E2 state (Garcia et al., 2015).

Functionally, beta2 has the strongest effects on the kinetic properties of the pump, reducing the apparent potassium affinity and raising the extracellular sodium affinity compared to beta1 and 3 (Larsen et al., 2014). This effect of beta on the pump was found to be due to the TM helix rather than the N- or C-terminal domains, and specifically to a difference between the three isoforms in the tilt angles of their TM helices (Hilbers et al., 2016).

The different beta isoforms and the variation in their post-translational modifications facilitate regulated Na,K-ATPase activity, adapted to different tissues and to environmental changes.

In mouse heart, the major beta isoform is beta1. Nonetheless, specific inactivation of its gene in cardiomyocytes results in a phenotype that appears healthy until approximately 10 months of age, and reduced contractility and enlarged hearts are only found after an additional 3–4 months (Barwe et al., 2009). Interestingly, heterozygous knock-out of alpha1 also results in reduced contractility, while heterozygous knock-out of alpha2 results in hyper contractility (James et al., 1999); the alpha2 phenotype may, however, be a secondary effect of alpha2 deficiency in the brain (Rindler et al., 2013). Beta2 knock-out mice succumb at day 17–18 after birth, possibly due to dysfunction of vitally important brain structures (Magyar et al., 1994). There are currently no confirmed human

TABLE 1 | Protein expression in tissues from the indicated mammals detected by western blots (WB) or immunostaining (IS) of Na,K-ATPase alpha1 (a1), alpha2 (a2), alpha3 (a3), alpha4(a4), beta1(b1), beta2(b2), beta3(b3), and FXYD(g). Cultured cells not included.

Organ/part	Tissue/structure	Cell/tubule type	Protein found	Protein probed for	Organism	Method	References
Brain	Microvessels		a1, a2, a3, b1, b2	a1, a2, a3, b1, b2	rat	WB	Zlokovic et al., 1993
Brain	Choroid plexus		a1, b1, b2	a1, a2, a3, b1, b2	rat	WB	Zlokovic et al., 1993
Brain	Several areas are extensively studied	Only neurons	a3	a3	mouse	IS	Bottger et al., 2011
Brain				a4	human	WB	Hlivko et al., 2006
Brain	Several areas are studied	Neurons and Astrocytes	b1, b2	b1, b2	rat	WB, IS	Lecuona et al., 1996
Brain	Cerebral cortex	Astroglia	a2	a2	rat	IS	Cholet et al., 2002
Brain	Axolemma, cerebrum, cerebellum, corpus callosum, optic nerve		a1, a2, a3	a1, a2, a3	rat	WB	Urayama et al., 1989
Brain	Microsomes		b3	b3	rat	WB	Arystarkhova and Sweadner, 1997
Colon	Mucosae, submucosae	Epithelial cells, mesenchymal cells	a1, a3, b1, b2	a1, a3, b1, b2	human	IS	Baker Bechmann et al., 2016
Colon	Myenteric plexus	Neurons	(a1), a3, b1, (b2)	a1, a3, b1, b2	human	IS	Baker Bechmann et al., 2016
Colon	Myenteric plexus	Glia cells	(a1), (a3), b1, b2	a1, a3, b1, b2	human	IS	Baker Bechmann et al., 2016
Colon	Muscularis propia	Smooth muscle cells	(a1), a3, b2	a1, a3, b1, b2	human	IS	Baker Bechmann et al., 2016
Erythrocytes			a1, a3, b1, b2, b3	a1, a2, a3, b1, b2, b3	human	WB	Hoffman et al., 2002
Eye	Pars plicata	Nonpigmented epithelium	a1, a2, a3	a1, a2, a3	bovine	IS	Ghosh et al., 1990
Eye	Pars plicata	Pigmented epithelium	a1	a1, a2, a3	bovine	IS	Ghosh et al., 1990
Eye	Pars plana	Nonpigmented epithelium	a1, a2	a1, a2, a3	bovine	IS	Ghosh et al., 1990
Eye	Pars plana	Pigmented epithelium	a1	a1, a2, a3	bovine	IS	Ghosh et al., 1990
Eye	Retina	Photoreceptors	a3, b2, b3	a1, a2, a3, b1, b2, b3	mouse	IS	Wetzel et al., 1999
Eye	Retina	Horizontal cells	a1, a3, b1	a1, a2, a3, b1, b2, b3	mouse	IS	Wetzel et al., 1999
Eye	Retina	Bipolar cells	a3, b2	a1, a2, a3, b1, b2, b3	mouse	IS	Wetzel et al., 1999
Eye	Retina	Ganglion cells	a1, a3, b1, b2	a1, a2, a3, b1, b2, b3	mouse	IS	Wetzel et al., 1999
Eye	Retina	Amacrine cells	a3, b1	a1, a2, a3, b1, b2, b3	mouse	IS	Wetzel et al., 1999
Eye	Retina	Müller cells	a1, a2, b2	a1, a2, a3, b1, b2, b3	mouse	IS	Wetzel et al., 1999
Eye	Retina	Pigmented epithelium	a1, b1	a1, a2, a3, b1, b2, b3	mouse	IS	Wetzel et al., 1999
Heart	Ventricular myocardium		a1, a2	a1, a2, a3	rat	WB	Sweadner et al., 1994
Heart	Ventricular myocardium		a1, a2, a3	a1, a2, a3	human	WB	Sweadner et al., 1994
Heart	Left ventricle, right ventricle, atrium, ventricular septum, papillary muscle, aorta		a1, a3	a1, a2, a3	macaque	WB	Sweadner et al., 1994
Heart		Cardiomyocytes	a1, a2, b1, b2, b3	a1, a2, b1, b2, b3	mouse/rat	WB, IS	Habeck et al., 2016

(Continued)

TABLE 1 | Continued

Organ/part	Tissue/structure	Cell/tubule type	Protein found	Protein probed for	Organism	Method	References
Heart	Microsomes		b3	b3	rat	WB	Arystarkhova and Sweadner, 1997
Inner ear	Cochlea	External sulcus cells, GER cells, Root cells, Interdental cells, Claudius cells, Reissner's membrane cells, Spiral ligament fibrocytes type IV	a1, b1	a1, a2, a3, b1, b2	rat	IS	Peters et al., 2001
Inner ear	Cochlea	Marginal cells	a1, b1, b2	a1, a2, a3, b1, b2	rat	IS	Peters et al., 2001
Inner ear	Cochlea	Suprastrial fibrocyes, Spiral ligament fibrocytes type II	a1, a2, b1	a1, a2, a3, b1, b2	rat	IS	Peters et al., 2001
Inner ear	Cochlea	Coclear neurons	a1, a3, b1	a1, a2, a3, b1, b2	rat	IS	Peters et al., 2001
Inner ear	Vestibulum	Supporting cells, transitional cells	a1, b1	a1, a2, a3, b1, b2	rat	IS	Peters et al., 2001
Inner ear	Vestibulum	Nonsensory cells, Dark cells	a1, b1, b2	a1, a2, a3, b1, b2	rat	IS	Peters et al., 2001
Inner ear	Vestibulum	Vestibular neurons	a1, a3, b1	a1, a2, a3, b1, b2	rat	IS	Peters et al., 2001
Inner ear	Endolymphatic sac/duct	Endolymphatic sac cells, endolymphatic duct cells	a1, b1	a1, a2, a3, b1, b2	rat	IS	Peters et al., 2001
Inner ear	Spiral ganglion, Organ of Corti	Type I spiral ganglion neurons	(a1), a3	a1, a2, a3	rat	IS	McLean et al., 2009
Inner ear	Spiral ganglion, Organ of Corti	Type II spiral ganglion neurons	(a1)	a1, a2, a3	rat	IS	McLean et al., 2009
Inner ear	Spiral ganglion, Organ of Corti	Phalangeal cells	a1	a1, a2, a3	rat	IS	McLean et al., 2009
Joints	Cartilage	Chondrocytes	a1, a3, b1, b2	a1, a2, a3, b1, b2	bovine	WB, IS	Mobasheri et al., 1997
Kidney	Renal medulla		a1, a3	a1, a2, a3	rat	WB	Urayama et al., 1989
Kidney	Nephron	Proximal convoluted tubule, proximal straight tubule, medullary thick ascending limb, distal convoluted tubule, connecting tubule	a1, b1, g	a1, b1, g	rat	IS	Wetzel and Sweadner, 2001
Kidney	Nephron	Cortical thick ascending limb, cortical collecting duct	a1, b1	a1, b1, g	rat	IS	Wetzel and Sweadner, 2001
Kidney	Nephron	Glomeruli, thin limbs of henle, medullary collecting duct		a1, b1, g	rat	IS	Wetzel and Sweadner, 2001
Kidney	Microsomes		b3	b3	rat	WB	Shyjan and Levenson, 1989
Kidney				a4	human	WB	Hlivko et al., 2006
Liver			a1	a1, a2, a3, b1	rat	WB	Shyjan and Levenson, 1989
Liver			b3	b3	rat	WB	Arystarkhova and Sweadner, 1997
Liver		Hepatocytes, ephitelial cells	a1, b1, b2	a1, a3, b1, b2	human	IS	Baker Bechmann et al., 2016
Liver		Endothelial cells		a1, a3, b1, b2	human	IS	Baker Bechmann et al., 2016
Lung			b3	b3	rat	WB	Arystarkhova and Sweadner, 1997
Lung			a1, a2	a1, a2, a3, b1	rat	WB	Shyjan and Levenson, 1989
Lung			b1	b1	rat	WB	Zhang et al., 1997

(Continued)

TABLE 1 | Continued

Organ/part	Tissue/structure	Cell/tubule type	Protein found	Protein probed for	Organism	Method	References
Placenta			a1, a2, a3	a1, a2, a3	human	WB	Esplin et al., 2003
Prostate		Epithelial cells	a1, b1, b2, b3	a1, a2, a3, b1, b2, b3, g	rat	IS	Mobasheri et al., 2003
Prostate		Smooth muscle, stroma	a1, a2, b1, b2	a1, a2, a3, b1, b2, b3, g	rat	IS	Mobasheri et al., 2003
Skeletal muscle	Extensor digitorum longus		a1, a2, b1, b2, b3	a1, a2, a3, b1, b2, b3	mouse	WB	He et al., 2001
Spleen	Microsomes		a1	a1, a2, a3, b	rat	WB	Shyjan and Levenson, 1989
Testis		Sperm	a1, a4	a1, a4	rat	IS	Blanco et al., 2000
Testis		Sperm	a4	a4	human	WB, IS	Hlivko et al., 2006
Testis		Sperm	a4	a4	bovine	WB, IS	Newton et al., 2009
Testis		Sperm	a1, a4	a1, a4	mouse	WB	Jimenez et al., 2011a
Testis	Microsomes		b3	b3	rat	WB	Arystarkhova and Sweadner, 1997
Uterus		Epithelial cells, smooth muscle cells	a1, a2, (a3), b1, b2, (b3), g	a1, a2, a3, b1, b2, b3, g	human	IS	Floyd et al., 2010

Shyjan and Levenson, 1989; Urayama et al., 1989; Ghosh et al., 1990; Zlokovic et al., 1993; Sweadner et al., 1994; Lecuona et al., 1996; Arystarkhova and Sweadner, 1997; Mobasheri et al., 1997, 2003; Zhang et al., 1997; Wetzel et al., 1999; Blanco et al., 2000; He et al., 2001; Peters et al., 2001; Wetzel and Sweadner, 2001; Cholet et al., 2002; Hoffman et al., 2002; Esplin et al., 2003; Hlivko et al., 2006; McLean et al., 2009; Newton et al., 2009; Floyd et al., 2010; Bottger et al., 2011; Jimenez et al., 2011a; Baker Bechmann et al., 2016; Habeck et al., 2016.

genetic diseases linked with mutations in any of the beta subunits.

FXYDs

The minimal functional unit of the Na,K-ATPase has an alpha and a beta subunit, but it can be further modified by a third subunit, the FXYD, named after a shared PFxYD motif in the N-terminal, extracellular part of the single TM protein. Mammals express seven FXYD proteins, most of which appear to lower the substrate affinities or Vmax of the pump, though they may also serve functions in addition to modulating Na,K-ATPase function (Geering, 2005).

FXYD1 is highly expressed in the heart, skeletal muscle and brain. Two serines in the intracellular part can be phosporylated by protein kinases A and C, and its alternative name, phospholemman, reflects that it was originally described as a highly phosphorylated (∼15–45%) heart protein (Palmer et al., 1991; Walaas et al., 1994; Cheung et al., 2010). Phosphorylation decreases the inhibitory effect of FXYD1 (Cheung et al., 2010; Mishra et al., 2015), and mouse knock-out of the subunit increases Na,K-ATPase activity in the heart (Jia et al., 2005; Bell et al., 2008).

FXYD2, or gamma, was the first FXYD found to be associated with the Na,K-ATPase (Forbush et al., 1978). It is highly expressed in the kidney, and like FXYD1, lowers pump activity, an inhibition that is also relieved if the protein is knocked out in mice (Jones et al., 2005; Arystarkhova, 2016). Mice lacking FXYD2 are viable, but have impaired reproduction, possibly because of a metabolic phenotype where glucose is highly tolerated (Arystarkhova et al., 2013). In the collecting duct of the kidney, FXYD4 is expressed, which, unlike most FXYDs, increases the pump's sodium affinity and thus enhances activity (Geering, 2005).

The roles of FXYD3 (Mat-8) and FXYD5 (dysadherin) are unclear, but they appear to be overexpressed in some cancer cells (Arimochi et al., 2007; Nam et al., 2007), and FXYD6 and 7 are expressed in the brain (Geering, 2005). There are currently no confirmed human genetic diseases linked with mutations in FXYD subunits.

DISEASE-CAUSING MUTATIONS IN Na,K-ATPASE ALPHA ISOFORMS

Alpha1 in Disease

Deleterious mutations in *ATP1A1* are unlikely to be compatible with life, but in a subset of aldosterone producing adenomas (APAs) in the adrenal gland, somatic mutations in *ATP1A1* can contribute to the altered hormone balance (Azizan et al., 2013; Beuschlein et al., 2013). Adrenal overproduction of aldosterone is the cause of hypertension in up to 10% of hypertensive patients, and if adrenal adenomas are identified and removed, the patients will typically be cured.

The normal signal pathway is that adrenal cells respond to the peptide hormone angiotensin II and to extracellular potassium by depolarization and opening of voltage-gated calcium channels, and the rise in cytoplasmic calcium levels stimulates expression of the aldosterone synthase. The dependence on extracellular stimuli can, however, be circumvented if the downstream signals are directly induced by mutations in the systems that normally

control membrane potential and calcium levels, including a potassium channel (*KCNJ5*, Choi et al., 2011), a calcium channel (*CACNA1D,* Azizan et al., 2013), and a calcium pump (*ATP2B3*, Beuschlein et al., 2013). Most recently, a link was found between APAs and mutations causing beta-catenin (*CTNNB1*) to excessively activate the Wnt-signaling pathway that normally controls adrenocortical development (Teo et al., 2015). Even in adrenal glands with hyperplasia but no adenoma, somatic mutations in *CACNA1D* (Scholl et al., 2015) and *ATP1A1* (Nishimoto et al., 2015) have been found.

The coupling of *ATP1A1* mutations to hypertension does not immediately make as much sense as for the potassium channel and calcium regulators. Why would a single non-functional copy of the gene have such marked effect on aldosterone production? One clue was that there is a prominent hotspot for mutation in TM1 next to the ion coordinating Glu327 in TM4, especially Leu104Arg is commonly found in APAs, and another reoccurring spot for alterations is in TM4 right next to Glu327 (**Figure 1**, Kopec et al., 2014). A third hotspot is in TM9, where deletions close to site III, the sodium-specific site, are found (**Figure 2**). Expression of the mutant forms of the pump cause depolarization (Beuschlein et al., 2013; Stindl et al., 2015), and expression studies in *Xenopus* oocytes show that the mutations all cause similar gain-of-function, namely that instead of being an ion pump, the mutations in *ATP1A1* make the Na,K-ATPases into ion channels that allow sodium or protons (depending on the specific mutation) to flow into the cell. Potassium is not (or for the TM9 deletions, only to a minor extend) transported, and physiological potassium levels have negligible effect (Azizan et al., 2013).

The effect of turning a pump into a channel is much more severe than simply inactivating the pump. The *ATP1A1* mutations clearly show this—only regions where mutations cause the pump to become a cation channel have been reported in APAs, while many of the disease-causing mutations in *ATP1A2* and *ATP1A3* seem to impair pump function (cf. below). Pharmacologically, the same is evident—pump inhibitors like cardiotonic steroids are toxic, but not nearly as toxic as a huge molecule produced in *Palythoa* corals, palytoxin, which binds the sodium pump and turns it into a channel by causing the inner and outer gates to open simultaneously. Palytoxin is the second deadliest non-peptide molecule known, since just a single molecule on a cell surface can dissipate the cell's ionic gradient (Rossini and Bigiani, 2011).

Alpha2 in Disease

Familial Hemiplegic Migraine (FHM) is an autosomally inherited form of migraine where the patients experience aura and weakness in one side of the body during attacks. FHM-causing mutations have been identified in three genes encoding a calcium channel (FHM1), a sodium channel (FHM3) and the alpha2 subunit (FHM2) (De Fusco et al., 2003). At least 80 mutations in *ATP1A2* have been described to cause FHM2 (**Figure 4**, reviewed in Bottger et al., 2012; Pelzer et al., 2016). In contrast to the *ATP1A1* mutations that all target recurrent hotspots, many of the mutations in *ATP1A2* have been reported just once, and they affect both the transmembrane and the cytoplasmic parts of the protein. Most of the mutations that have been characterized cause loss or reduction of function, either because the ATPase function of the pump is compromised or because ion binding and transport are affected, but many of the mutations also impair trafficking of the pump to the membrane (Morth et al., 2009; Spiller and Friedrich, 2014).

The Na,K-ATPase in astrocytes with alpha2 and the beta2 subunit has relatively low potassium affinity and is suggested to be particularly important when the extracellular potassium concentration is high (Larsen et al., 2014). In agreement with this suggestion, mouse models with FHM2 mutations knocked in show reduced clearance of potassium and glutamate (Bottger et al., 2016; Capuani et al., 2016). Elevated potassium and glutamate levels are known to augment cortical spreading depression, which is suggested to cause some of the symptoms experienced by patients having an attack of migraine with aura, and enhanced spreading depression was measured in the knock-in mice (Lauritzen et al., 2011). Cortical spreading depression is characterized by a wave of lack of neuronal activity that travels across the cerebral gray matter after a brief period of hyperexcitability. Normally, astrocytes protect against cortical spreading depression because they take up potassium and glutamate (Lauritzen et al., 2011), but when there is a high need for restoring of the ionic gradients and only one allele from which a fully functional alpha2 can be expressed, the astrocyte may not be able to fulfill that role to satisfaction: the Na,K-ATPase is both directly involved in potassium clearing and indirectly in glutamate clearing, because the glutamate transporter uses the energy from co-transport of three sodium ions and counter-transport of one potassium ion to transport one molecule of glutamate.

Alpha3 in Disease

Autosomal dominant mutations in *ATP1A3* were first shown to cause Rapid-onset Dystonia Parkinsonism (RDP, de Carvalho Aguiar et al., 2004), and later two other neurological syndromes, Alternating Hemiplegia of Childhood (AHC, Heinzen et al., 2012; Rosewich et al., 2012) and CAPOS (cerebellar ataxia, areflexia, pes cavus, optic atrophy, and sensorineural hearing loss, Demos et al., 2014). Although the three syndromes were originally identified as phenotypically distinct, it has become clear that many patients do not strictly fall into one category or the other, but may have symptoms that fall on a continuous spectrum as well as unique symptoms for individual mutations (Rosewich et al., 2014; Paciorkowski et al., 2015; Sweney et al., 2015; Kanemasa et al., 2016; Liu et al., 2016; Smedemark-Margulies et al., 2016; Sweadner et al., 2016).

RDP is characterized by a triggering, stressful event causing sudden (hours to days) onset of irreversible rostrocaudal gradient of dystonia with parkinsonism. The onset is typically caused by physical or emotional stress in early adulthood, and in addition to the motor effects, most patients have psychiatric symptoms (Brashear et al., 2012). The patients are unresponsive to L-DOPA, and there is no drug therapy available.

AHC patients are typically diagnosed before 18 months of age from recurring episodes of weakness or paralysis of one side of the body. The attacks can vary in length from

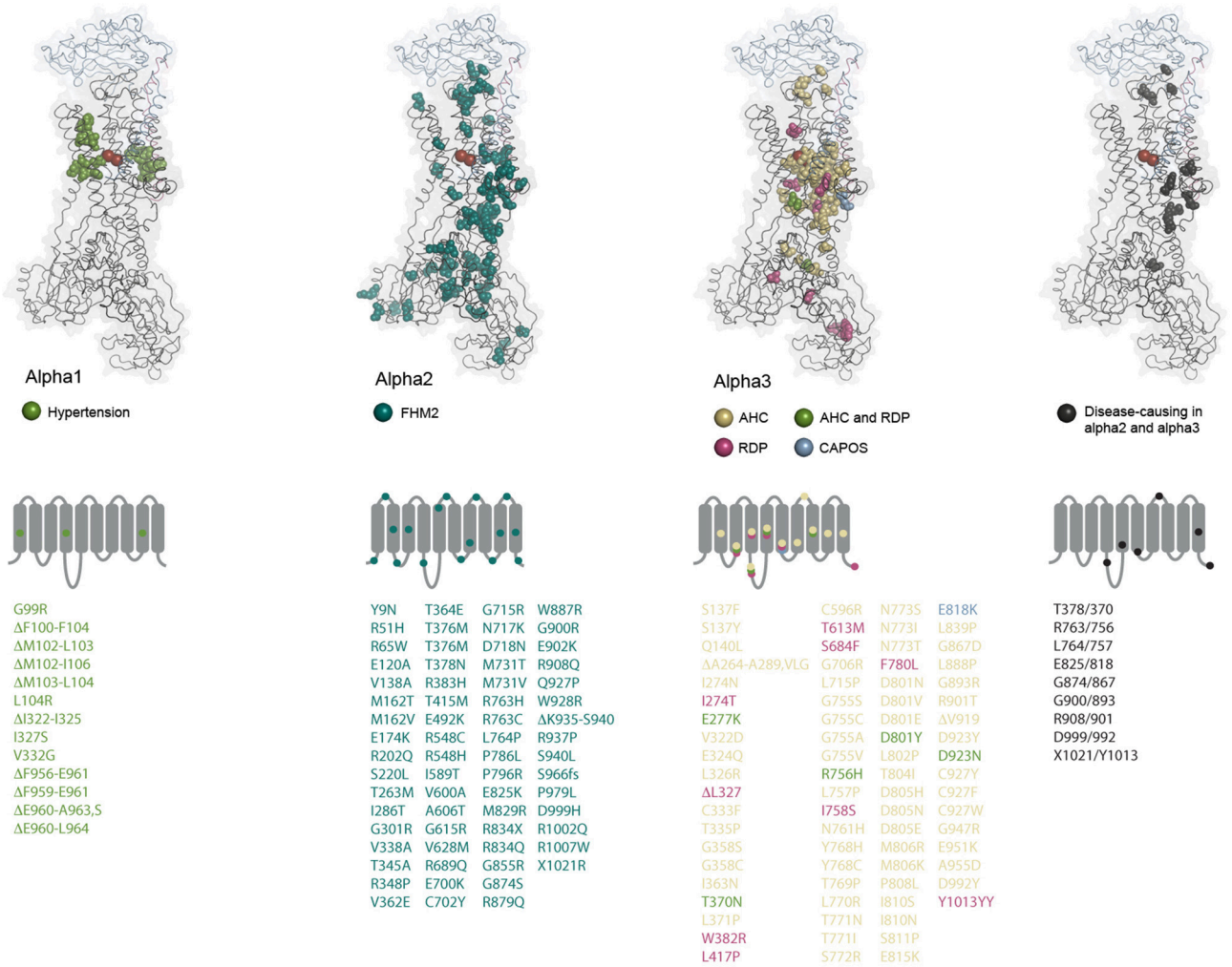

FIGURE 4 | Structural maps of the disease-causing mutations. The amino acids altered by disease-causing mutations in the three alpha subunit genes are shown as spheres and color-coded as indicated for each subunit. *ATP1A2* and *ATP1A3* mutations that affect similar positions in the two alphas are also indicated. The alpha1 amino acid alterations have not been reported in the other alphas. The residues are mapped on the potassium-occluded pig kidney structure 2ZXE (Shinoda et al., 2009) (alpha in black cartoon, beta in blue cartoon, gamma in purple cartoon, potassium ions as red spheres). In alpha1, all deleted residues are indicated. In alpha2 and 3, only cases with deletion of single residues are indicated. Under each subunit, it is schematically indicated which loops and TM helices are targeted by mutations. Multiple mutations affecting residues in a single segment are indicated by one mark if they cause the same disease. The mutations are listed underneath using the same color coding, fs: frameshift.

minutes to days and are typically combined with additional paroxysmal symptoms like dystonia, choreoathetosis, nystagmus and about half of the patients have epileptic seizures. During sleep, symptoms disappear (Heinzen et al., 2014). AHC is further associated with progressive deterioration of the patient's health between attacks, including developmental delay, retardation, hypotonia and compromised motor skills. For treatment, the calcium channel blocker flunarizine may reduce the length and severity of attacks in some patients, and benzodiazipines may have positive effect, possibly because they induce sleep. A ketonic diet has also been reported to stall disease progression (Roubergue et al., 2015).

CAPOS syndrome typically starts in childhood when fever triggers the disease, which is characterized by cerebellar ataxia, areflexia, and progressive loss of sight and hearing. Nystagmus and hypotonia are also common symptoms (Heimer et al., 2015).

For all of the three diseases, it is clear that the *ATP1A3* mutations have high penetrance, but also that the genetic background of an affected individual is important for its manifestations. Because of the severity of RDP and AHC, the mutations are typically *de novo*, while CAPOS is also inherited.

There are now close to 80 different disease-associated mutations reported in *ATP1A3* (**Figure 4**). At some positions, amino acid changes cause RDP as well as AHC, but most of the mutations are unique for one of the diseases, and there are genotype-phenotype correlations: all CAPOS patients sequenced have the same, single mutation, E818K, and all people identified with the mutation have CAPOS. For AHC and RDP, *ATP1A3*

mutations have been found in most but not all of the sequenced patients, so it remains to be determined if mutations in other genes can give similar symptoms. Strikingly, just two mutations, D801N and E815K, account for up to two thirds of the AHC patients, while the RDP-causing mutations seem to target the protein broadly with no obvious hotspots (**Figure 4**). Compared to the disease-causing mutations in *ATP1A1* and *ATP1A2*, RDP is in that respect more similar to FHM2 where many of the mutations may be associated with loss-of-function, while few hotspot positions give the phenotypes in AHC and CAPOS, as also seen for hypertension-causing *ATP1A1* mutations. It remains to be determined whether alpha3 gains any novel functions in AHC or CAPOS patients, but it has been suggested that the AHC-causing mutations may exert a dominant negative effect on the alpha3 expressed from the healthy allele by an unknown mechanism (Li et al., 2015).

Markedly, none of the mutations that change alpha1 from a pump to a channel have been described for the other genes, probably because that would be too severe an alteration. A few of the mutations in *ATP1A2* and *ATP1A3* target the same positions (**Figure 4**), but it is clear from the structural mapping that the *ATP1A3* mutations often target the ion binding sites, while that is not the case for *ATP1A2*, possibly suggesting that impaired ion binding in alpha2 would be incompatible with life or that they cause other symptoms than FHM.

CONCLUSION

The Na,K-ATPase was first described 60 years ago by Jens Christian Skou (Skou, 1957), but novel insight into the pump's atomic structure, cellular regulation and pathophysiological roles continues to emerge, and many aspects await future studies. The various subunit isoforms are optimized for the specific requirements and challenges that different cell types face for maintaining ionic homeostasis: the subunit variation allows for fine-tuning of the basic kinetic properties of the pump as elucidated in many studies, but much remains to be learned about how the variation determines interactions with other cellular partners and thereby regulates e.g., the activity, localization and stability of the pump. Furthermore, the amazingly improved possibilities for sequencing patient DNA will likely disclose novel links between mutations affecting alpha subunits and pathophysiological conditions: Adenomas other than the adrenal may gain advantage from somatic mutations affecting the alpha1 subunit, and mutations altering e.g., the ion binding residues in alpha2 may confer diseases other than FHM2. It is also still enigmatic why the different mutations in the alpha3 gene cause such varied diseases, and since alpha4 is essential for sperm function, mutations in its gene are highly likely to affect the male bearers' fertility. It further remains to be determined whether mutations in the beta or FXYD subunit genes are associated with diseases.

AUTHOR CONTRIBUTIONS

MC, FH, and HP discussed, wrote and edited the manuscript and made the tables and figures.

FUNDING

HP and FH were funded by the Lundbeck Foundation. MC was funded by AIAS, AU.

REFERENCES

Alevizopoulos, K., Calogeropoulou, T., Lang, F., and Stournaras, C. (2014). Na^+/K^+ ATPase inhibitors in cancer. *Curr. Drug Targets* 15, 988–1000. doi: 10.2174/1389450115666140908125025

Antonicek, H., Persohn, E., and Schachner, M. (1987). Biochemical and functional characterization of a novel neuron-glia adhesion molecule that is involved in neuronal migration. *J. Cell Biol.* 104, 1587–1595. doi: 10.1083/jcb.104.6.1587

Aperia, A., Akkuratov, E. E., Fontana, J. M., and Brismar, H. (2016). Na^+-K^+-ATPase, a new class of plasma membrane receptors. *Am. J. Physiol. Cell Physiol.* 310, C491–C495. doi: 10.1152/ajpcell.00359.2015

Arimochi, J., Ohashi-Kobayashi, A., and Maeda, M. (2007). Interaction of Mat-8 (FXYD-3) with Na^+/K^+-ATPase in colorectal cancer cells. *Biol. Pharm. Bull.* 30, 648–654. doi: 10.1248/bpb.30.648

Arystarkhova, E. (2016). Beneficial renal and pancreatic phenotypes in a mouse deficient in FXYD2 regulatory subunit of Na,K-ATPase. *Front. Physiol.* 7:88. doi: 10.3389/fphys.2016.00088

Arystarkhova, E., Liu, Y. B., Salazar, C., Stanojevic, V., Clifford, R. J., Kaplan, J. H., et al. (2013). Hyperplasia of pancreatic β cells and improved glucose tolerance in mice deficient in the FXYD2 subunit of Na,K-ATPase. *J. Biol. Chem.* 288, 7077–7085. doi: 10.1074/jbc.M112.401190

Arystarkhova, E., and Sweadner, K. J. (1997). Tissue-specific expression of the Na,K-ATPase β3 subunit. The presence of β3 in lung and liver addresses the problem of the missing subunit. *J. Biol. Chem.* 272, 22405–22408. doi: 10.1074/jbc.272.36.22405

Arystarkhova, E., and Sweadner, K. J. (2016). Functional studies of $Na(^+)$,$K(^+)$-ATPase using transfected cell cultures. *Methods Mol. Biol.* 1377, 321–332. doi: 10.1007/978-1-4939-3179-8_28

Attwell, D., and Laughlin, S. B. (2001). An energy budget for signaling in the grey matter of the brain. *J. Cereb. Blood Flow Metab.* 21, 1133–1145. doi: 10.1097/00004647-200110000-00001

Azarias, G., Kruusmagi, M., Connor, S., Akkuratov, E. E., Liu, X. L., Lyons, D., et al. (2013). A specific and essential role for Na,K-ATPase α3 in neurons co-expressing α1 and α3. *J. Biol. Chem.* 288, 2734–2743. doi: 10.1074/jbc.M112.425785

Azizan, E. A., Poulsen, H., Tuluc, P., Zhou, J., Clausen, M. V., Lieb, A., et al. (2013). Somatic mutations in ATP1A1 and CACNA1D underlie a common subtype of adrenal hypertension. *Nat. Genet.* 45, 1055–1060. doi: 10.1038/ng.2716

Baker Bechmann, M., Rotoli, D., Morales, M., Maeso Mdel, C., Garcia Mdel, P., Avila, J., et al. (2016). Na,K-ATPase isozymes in colorectal cancer and liver metastases. *Front. Physiol.* 7:9. doi: 10.3389/fphys.2016.00009

Barwe, S. P., Jordan, M. C., Skay, A., Inge, L., Rajasekaran, S. A., Wolle, D., et al. (2009). Dysfunction of ouabain-induced cardiac contractility in mice with heart-specific ablation of Na,K-ATPase β1-subunit. *J. Mol. Cell. Cardiol.* 47, 552–560. doi: 10.1016/j.yjmcc.2009.07.018

Bell, J. R., Kennington, E., Fuller, W., Dighe, K., Donoghue, P., Clark, J. E., et al. (2008). Characterization of the phospholemman knockout mouse heart: depressed left ventricular function with increased Na-K-ATPase activity. *Am. J. Physiol. Heart Circ. Physiol.* 294, H613–H621. doi: 10.1152/ajpheart.01332.2007

Beuschlein, F., Boulkroun, S., Osswald, A., Wieland, T., Nielsen, H. N., Lichtenauer, U. D., et al. (2013). Somatic mutations in ATP1A1 and ATP2B3 lead to aldosterone-producing adenomas and secondary hypertension. *Nat. Genet.* 45, 440–444, 444e1–2. doi: 10.1038/ng.2550

Blanco, G. (2005). Na,K-ATPase subunit heterogeneity as a mechanism for tissue-specific ion regulation. *Semin. Nephrol.* 25, 292–303. doi: 10.1016/j.semnephrol.2005.03.004

Blanco, G., Melton, R. J., Sanchez, G., and Mercer, R. W. (1999). Functional characterization of a testes-specific α-subunit isoform of the sodium/potassium adenosinetriphosphatase. *Biochemistry* 38, 13661–13669. doi: 10.1021/bi991207b

Blanco, G., and Mercer, R. W. (1998). Isozymes of the Na-K-ATPase: heterogeneity in structure, diversity in function. *Am. J. Physiol.* 275, F633–F650.

Blanco, G., Sanchez, G., Melton, R. J., Tourtellotte, W. G., and Mercer, R. W. (2000). The α4 isoform of the Na,K-ATPase is expressed in the germ cells of the testes. *J. Histochem. Cytochem.* 48, 1023–1032. doi: 10.1177/002215540004800801

Blom, H., Bernhem, K., and Brismar, H. (2016). Sodium pump organization in dendritic spines. *Neurophotonics* 3:041803. doi: 10.1117/1.NPh.3.4.041803

Borlak, J., and Thum, T. (2003). Hallmarks of ion channel gene expression in end-stage heart failure. *FASEB J.* 17, 1592–1608. doi: 10.1096/fj.02-0889com

Bottger, P., Doganli, C., and Lykke-Hartmann, K. (2012). Migraine- and dystonia-related disease-mutations of Na^+/K^+-ATPases: relevance of behavioral studies in mice to disease symptoms and neurological manifestations in humans. *Neurosci. Biobehav. Rev.* 36, 855–871. doi: 10.1016/j.neubiorev.2011.10.005

Bottger, P., Glerup, S., Gesslein, B., Illarionova, N. B., Isaksen, T. J., Heuck, A., et al. (2016). Glutamate-system defects behind psychiatric manifestations in a familial hemiplegic migraine type 2 disease-mutation mouse model. *EMBO Mol. Med.* 6:22047. doi: 10.1038/srep22047

Bottger, P., Tracz, Z., Heuck, A., Nissen, P., Romero-Ramos, M., and Lykke-Hartmann, K. (2011). Distribution of Na/K-ATPase α 3 isoform, a sodium-potassium P-type pump associated with rapid-onset of dystonia parkinsonism (RDP) in the adult mouse brain. *J. Comp. Neurol.* 519, 376–404. doi: 10.1002/cne.22524

Brashear, A., Cook, J. F., Hill, D. F., Amponsah, A., Snively, B. M., Light, L., et al. (2012). Psychiatric disorders in rapid-onset dystonia-parkinsonism. *Neurology* 79, 1168–1173. doi: 10.1212/WNL.0b013e3182698d6c

Brown, P. D., Davies, S. L., Speake, T., and Millar, I. D. (2004). Molecular mechanisms of cerebrospinal fluid production. *Neuroscience* 129, 957–970. doi: 10.1016/j.neuroscience.2004.07.003

Caplan, M. J., Anderson, H. C., Palade, G. E., and Jamieson, J. D. (1986). Intracellular sorting and polarized cell surface delivery of (Na^+,K^+)ATPase, an endogenous component of MDCK cell basolateral plasma membranes. *Cell* 46, 623–631. doi: 10.1016/0092-8674(86)90888-3

Capuani, C., Melone, M., Tottene, A., Bragina, L., Crivellaro, G., and Santello, M. (2016). Defective glutamate and K^+ clearance by cortical astrocytes in familial hemiplegic migraine type 2. 8, 967–986. doi: 10.15252/emmm.201505944

Cheung, J. Y., Zhang, X. Q., Song, J., Gao, E., Rabinowitz, J. E., Chan, T. O., et al. (2010). Phospholemman: a novel cardiac stress protein. *Clin. Transl. Sci.* 3, 189–196. doi: 10.1111/j.1752-8062.2010.00213.x

Choi, M., Scholl, U. I., Yue, P., Bjorklund, P., Zhao, B., Nelson-Williams, C., et al. (2011). K^+ channel mutations in adrenal aldosterone-producing adenomas and hereditary hypertension. *Science* 331, 768–772. doi: 10.1126/science.1198785

Cholet, N., Pellerin, L., Magistretti, P. J., and Hamel, E. (2002). Similar perisynaptic glial localization for the Na^+,K^+-ATPase α 2 subunit and the glutamate transporters GLAST and GLT-1 in the rat somatosensory cortex. *Cereb. Cortex* 12, 515–525. doi: 10.1093/cercor/12.5.515

Clausen, M. J., Nissen, P., and Poulsen, H. (2011). The pumps that fuel a sperm's journey. *Biochem. Soc. Trans.* 39, 741–745. doi: 10.1042/BST0390741

Clausen, M. V., Nissen, P., and Poulsen, H. (2016). The α4 isoform of the $Na(^+)$,$K(^+)$-ATPase is tuned for changing extracellular environments. *FEBS J.* 283, 282–293. doi: 10.1111/febs.13567

Crambert, G., Hasler, U., Beggah, A. T., Yu, C., Modyanov, N. N., Horisberger, J. D., et al. (2000). Transport and pharmacological properties of nine different human Na, K-ATPase isozymes. *J. Biol. Chem.* 275, 1976–1986. doi: 10.1074/jbc.275.3.1976

de Carvalho Aguiar, P., Sweadner, K. J., Penniston, J. T., Zaremba, J., Liu, L., Caton, M., et al. (2004). Mutations in the Na^+/K^+ -ATPase α3 gene ATP1A3 are associated with rapid-onset dystonia parkinsonism. *Neuron* 43, 169–175. doi: 10.1016/j.neuron.2004.06.028

De Fusco, M., Marconi, R., Silvestri, L., Atorino, L., Rampoldi, L., Morgante, L., et al. (2003). Haploinsufficiency of ATP1A2 encoding the Na^+/K^+ pump α2 subunit associated with familial hemiplegic migraine type 2. *Nat. Genet.* 33, 192–196. doi: 10.1038/ng1081

Demos, M. K., van Karnebeek, C. D., Ross, C. J., Adam, S., Shen, Y., Zhan, S. H., et al. (2014). A novel recurrent mutation in ATP1A3 causes CAPOS syndrome. *Orphanet J. Rare Dis.* 9:15. doi: 10.1186/1750-1172-9-15

Dorus, S., Wasbrough, E. R., Busby, J., Wilkin, E. C., and Karr, T. L. (2010). Sperm proteomics reveals intensified selection on mouse sperm membrane and acrosome genes. *Mol. Biol. Evol.* 27, 1235–1246. doi: 10.1093/molbev/msq007

Dostanic, I., Schultz Jel, J., Lorenz, J. N., and Lingrel, J. B. (2004). The α 1 isoform of Na,K-ATPase regulates cardiac contractility and functionally interacts and co-localizes with the Na/Ca exchanger in heart. *J. Biol. Chem.* 279, 54053–54061. doi: 10.1074/jbc.M410737200

Durlacher, C. T., Chow, K., Chen, X. W., He, Z. X., Zhang, X., Yang, T., et al. (2015). Targeting $Na(^+)/K(^+)$ -translocating adenosine triphosphatase in cancer treatment. *Clin. Exp. Pharmacol. Physiol.* 42, 427–443. doi: 10.1111/1440-1681.12385

El Mernissi, G., and Doucet, A. (1984). Quantitation of [3H]ouabain binding and turnover of Na-K-ATPase along the rabbit nephron. *Am. J. Physiol.* 247, F158–F167.

Esplin, M. S., Fausett, M. B., Faux, D. S., and Graves, S. W. (2003). Changes in the isoforms of the sodium pump in the placenta and myometrium of women in labor. *Am. J. Obstet. Gynecol.* 188, 759–764. doi: 10.1067/mob.2003.166

Floyd, R. V., Wray, S., Quenby, S., Martin-Vasallo, P., and Mobasheri, A. (2010). Expression and distribution of Na, K-ATPase isoforms in the human uterus. *Reprod. Sci.* 17, 366–376. doi: 10.1177/1933719109355196

Forbush, B. III., Kaplan, J. H., and Hoffman, J. F. (1978). Characterization of a new photoaffinity derivative of ouabain: labeling of the large polypeptide and of a proteolipid component of the Na, K-ATPase. *Biochemistry* 17, 3667–3676. doi: 10.1021/bi00610a037

Gaborit, N., Varro, A., Le Bouter, S., Szuts, V., Escande, D., Nattel, S., et al. (2010). Gender-related differences in ion-channel and transporter subunit expression in non-diseased human hearts. *J. Mol. Cell. Cardiol.* 49, 639–646. doi: 10.1016/j.yjmcc.2010.06.005

Gao, H., Popescu, R., Kopp, B., and Wang, Z. (2011). Bufadienolides and their antitumor activity. *Nat. Prod. Rep.* 28, 953–969. doi: 10.1039/c0np00032a

Garcia, A., Eljack, N. D., Sani, M. A., Separovic, F., Rasmussen, H. H., Kopec, W., et al. (2015). Membrane accessibility of glutathione. *Biochim. Biophys. Acta* 1848, 2430–2436. doi: 10.1016/j.bbamem.2015.07.016

Geering, K. (2005). Function of FXYD proteins, regulators of Na, K-ATPase. *J. Bioenerg. Biomembr.* 37, 387–392. doi: 10.1007/s10863-005-9476-x

Ghosh, S., Freitag, A. C., Martin-Vasallo, P., and Coca-Prados, M. (1990). Cellular distribution and differential gene expression of the three α subunit isoforms of the Na,K-ATPase in the ocular ciliary epithelium. *J. Biol. Chem.* 265, 2935–2940.

Gloor, S., Antonicek, H., Sweadner, K. J., Pagliusi, S., Frank, R., Moos, M., et al. (1990). The adhesion molecule on glia (AMOG) is a homologue of the β subunit of the Na,K-ATPase. *J. Cell Biol.* 110, 165–174. doi: 10.1083/jcb.110.1.165

Gundersen, D., Orlowski, J., and Rodriguez-Boulan, E. (1991). Apical polarity of Na,K-ATPase in retinal pigment epithelium is linked to a reversal of the ankyrin-fodrin submembrane cytoskeleton. *J. Cell Biol.* 112, 863–872. doi: 10.1083/jcb.112.5.863

Habeck, M., Tokhtaeva, E., Nadav, Y., Ben Zeev, E., Ferris, S. P., Kaufman, R. J., et al. (2016). Selective assembly of Na,K-ATPase α2β2 heterodimers in the heart: distinct functional properties and isoform-selective inhibitors. *J. Biol. Chem.* 291, 23159–23174. doi: 10.1074/jbc.M116.751735

He, S., Shelly, D. A., Moseley, A. E., James, P. F., James, J. H., Paul, R. J., et al. (2001). The α_1- and α_2-isoforms of Na-K-ATPase play different roles in skeletal muscle contractility. *Am. J. Physiol. Regul. Integr. Comp Physiol.* 281, R917–R925. Available online at: http://ajpregu.physiology.org/content/281/3/R917.long

Heimer, G., Sadaka, Y., Israelian, L., Feiglin, A., Ruggieri, A., Marshall, C. R., et al. (2015). CAOS-episodic cerebellar ataxia, areflexia, optic atrophy, and sensorineural hearing loss: a third allelic disorder of the ATP1A3 gene. *J. Child Neurol.* 30, 1749–1756. doi: 10.1177/0883073815579708

Heinzen, E. L., Arzimanoglou, A., Brashear, A., Clapcote, S. J., Gurrieri, F., Goldstein, D. B., et al. (2014). Distinct neurological disorders with ATP1A3 mutations. *Lancet Neurol.* 13, 503–514. doi: 10.1016/S1474-4422(14)70011-0

Heinzen, E. L., Swoboda, K. J., Hitomi, Y., Gurrieri, F., Nicole, S., de Vries, B., et al. (2012). *De novo* mutations in ATP1A3 cause alternating hemiplegia of childhood. *Nat. Genet.* 44, 1030–1034. doi: 10.1038/ng.2358

Henriksen, C., Kjaer-Sorensen, K., Einholm, A. P., Madsen, L. B., Momeni, J., Bendixen, C., et al. (2013). Molecular cloning and characterization of porcine $Na(^+)/K(^+)$-ATPase isoforms α1, α2, α3 and the ATP1A3 promoter. *PLoS ONE* 8:e79127. doi: 10.1371/journal.pone.0079127

Hilbers, F., Kopec, W., Isaksen, T. J., Holm, T. H., Lykke-Hartmann, K., Nissen, P., et al. (2016). Tuning of the Na,K-ATPase by the β subunit. *Sci. Rep.* 6:20442. doi: 10.1038/srep20442

Hlivko, J. T., Chakraborty, S., Hlivko, T. J., Sengupta, A., and James, P. F. (2006). The human Na,K-ATPase α 4 isoform is a ouabain-sensitive α isoform that is expressed in sperm. *Mol. Reprod. Dev.* 73, 101–115. doi: 10.1002/mrd.20383

Hoffman, J. F., Wickrema, A., Potapova, O., Milanick, M., and Yingst, D. R. (2002). Na pump isoforms in human erythroid progenitor cells and mature erythrocytes. *Proc. Natl. Acad. Sci. U.S.A.* 99, 14572–14577. doi: 10.1073/pnas.222539999

Horisberger, J. D., and Kharoubi-Hess, S. (2002). Functional differences between α subunit isoforms of the rat Na,K-ATPase expressed in *Xenopus oocytes*. *J. Physiol.* 539, 669–680. doi: 10.1113/jphysiol.2001.013201

James, P. F., Grupp, I. L., Grupp, G., Woo, A. L., Askew, G. R., Croyle, M. L., et al. (1999). Identification of a specific role for the Na,K-ATPase α 2 isoform as a regulator of calcium in the heart. *Mol. Cell* 3, 555–563. doi: 10.1016/S1097-2765(00)80349-4

Jia, L. G., Donnet, C., Bogaev, R. C., Blatt, R. J., McKinney, C. E., Day, K. H., et al. (2005). Hypertrophy, increased ejection fraction, and reduced Na-K-ATPase activity in phospholemman-deficient mice. *Am. J. Physiol. Heart Circ. Physiol.* 288, H1982–H1988. doi: 10.1152/ajpheart.00142.2004

Jimenez, T., McDermott, J. P., Sanchez, G., and Blanco, G. (2011a). Na,K-ATPase α4 isoform is essential for sperm fertility. *Proc. Natl. Acad. Sci. U.S.A.* 108, 644–649. doi: 10.1073/pnas.1016902108

Jimenez, T., Sanchez, G., and Blanco, G. (2012). Activity of the Na,K-ATPase α4 isoform is regulated during sperm capacitation to support sperm motility. *J. Androl.* 33, 1047–1057. doi: 10.2164/jandrol.111.015545

Jimenez, T., Sanchez, G., McDermott, J. P., Nguyen, A. N., Kumar, T. R., and Blanco, G. (2011b). Increased expression of the Na,K-ATPase α4 isoform enhances sperm motility in transgenic mice. *Biol. Reprod.* 84, 153–161. doi: 10.1095/biolreprod.110.087064

Jones, D. H., Li, T. Y., Arystarkhova, E., Barr, K. J., Wetzel, R. K., Peng, J., et al. (2005). Na,K-ATPase from mice lacking the γ subunit (FXYD2) exhibits altered Na^+ affinity and decreased thermal stability. *J. Biol. Chem.* 280, 19003–19011. doi: 10.1074/jbc.M500697200

Juhaszova, M., and Blaustein, M. P. (1997). Distinct distribution of different Na^+ pump α subunit isoforms in plasmalemma. Physiological implications. *Ann. N.Y. Acad. Sci.* 834, 524–536. doi: 10.1111/j.1749-6632.1997.tb52310.x

Kanai, R., Ogawa, H., Vilsen, B., Cornelius, F., and Toyoshima, C. (2013). Crystal structure of a Na^+-bound Na^+,K^+-ATPase preceding the E1P state. *Nature* 502, 201–206. doi: 10.1038/nature12578

Kanemasa H, Fukai R, Sakai Y, Torio M, Miyake N, Lee S (2016). *De novo* p.Arg756Cys mutation of ATP1A3 causes an atypical form of alternating hemiplegia of childhood with prolonged paralysis and choreoathetosis. *BMC Neurol.* 16, 174. doi: 10.1186/s12883-016-0680-6

Keryanov, S., and Gardner, K. L. (2002). Physical mapping and characterization of the human Na,K-ATPase isoform, ATP1A4. *Gene* 292, 151–166. doi: 10.1016/S0378-1119(02)00647-9

Kim, J. H., Sizov, I., Dobretsov, M., and von Gersdorff, H. (2007). Presynaptic $Ca2^+$ buffers control the strength of a fast post-tetanic hyperpolarization mediated by the α3 $Na(^+)/K(^+)$-ATPase. *Nat. Neurosci.* 10, 196–205. doi: 10.1038/nn1839

Klimanova, E. A., Tverskoi, A. M., Koltsova, S. V., Sidorenko, S. V., Lopina, O. D., Tremblay, J., et al. (2017). Time- and dose dependent actions of cardiotonic steroids on transcriptome and intracellular content of Na^+ and K^+: a comparative analysis. *Sci. Rep.* 7:45403. doi: 10.1038/srep45403

Kopec, W., Loubet, B., Poulsen, H., and Khandelia, H. (2014). Molecular mechanism of $Na(^+)$,$K(^+)$-ATPase malfunction in mutations characteristic of adrenal hypertension. *Biochemistry* 53, 746–754. doi: 10.1021/bi401425g

Kravtsova, V. V., Petrov, A. M., Matchkov, V. V., Bouzinova, E. V., Vasiliev, A. N., Benziane, B., et al. (2016). Distinct α2 Na,K-ATPase membrane pools are differently involved in early skeletal muscle remodeling during disuse. *J. Gen. Physiol.* 147, 175–188. doi: 10.1085/jgp.201511494

Larsen, B. R., Assentoft, M., Cotrina, M. L., Hua, S. Z., Nedergaard, M., Kaila, K., et al. (2014). Contributions of the $Na(^+)/K(^+)$-ATPase, NKCC1, and Kir4.1 to hippocampal $K(^+)$ clearance and volume responses. *Glia* 62, 608–622. doi: 10.1002/glia.22629

Lauritzen, M., Dreier, J. P., Fabricius, M., Hartings, J. A., Graf, R., and Strong, A. J. (2011). Clinical relevance of cortical spreading depression in neurological disorders: migraine, malignant stroke, subarachnoid and intracranial hemorrhage, and traumatic brain injury. *J. Cereb. Blood Flow Metab.* 31, 17–35. doi: 10.1038/jcbfm.2010.191

Laursen, M., Gregersen, J. L., Yatime, L., Nissen, P., and Fedosova, N. U. (2015). Structures and characterization of digoxin- and bufalin-bound Na^+,K^+-ATPase compared with the ouabain-bound complex. *Proc. Natl. Acad. Sci. U.S.A.* 112, 1755–1760. doi: 10.1073/pnas.1422997112

Lecuona, E., Luquin, S., Avila, J., Garcia-Segura, L. M., and Martin-Vasallo, P. (1996). Expression of the β 1 and β 2(AMOG) subunits of the Na,K-ATPase in neural tissues: cellular and developmental distribution patterns. *Brain Res. Bull.* 40, 167–174. doi: 10.1016/0361-9230(96)00042-1

Li, M., Jazayeri, D., Corry, B., McSweeney, K. M., Heinzen, E. L., Goldstein, D. B., et al. (2015). A functional correlate of severity in alternating hemiplegia of childhood. *Neurobiol. Dis.* 77, 88–93. doi: 10.1016/j.nbd.2015.02.002

Liu, Y., Lu, Y., and Zhang, X. (2016). A case of rapid-onset dystonia-parkinsonism accompanied by pyramidal tract impairment. *BMC Neurol.* 16, 218. doi: 10.1186/s12883-016-0743-8

Magyar, J. P., Bartsch, U., Wang, Z. Q., Howells, N., Aguzzi, A., Wagner, E. F., et al. (1994). Degeneration of neural cells in the central nervous system of mice deficient in the gene for the adhesion molecule on Glia, the β 2 subunit of murine Na,K-ATPase. *J. Cell Biol.* 127, 835–845. doi: 10.1083/jcb.127.3.835

Marks, M. J., and Seeds, N. W. (1978). A heterogeneous ouabain-ATPase interaction in mouse brain. *Life Sci.* 23, 2735–2744. doi: 10.1016/0024-3205(78)90654-9

Martin-Vasallo, P., Dackowski, W., Emanuel, J. R., and Levenson, R. (1989). Identification of a putative isoform of the Na,K-ATPase β subunit. Primary structure and tissue-specific expression. *J. Biol. Chem.* 264, 4613–4618.

McDermott, J. P., Sanchez, G., Chennathukuzhi, V., and Blanco, G. (2012). Green fluorescence protein driven by the Na,K-ATPase α4 isoform promoter is expressed only in male germ cells of mouse testis. *J. Assist. Reprod. Genet.* 29, 1313–1325. doi: 10.1007/s10815-012-9876-x

McDermott, J., Sanchez, G., Nangia, A. K., and Blanco, G. (2015). Role of human Na,K-ATPase α 4 in sperm function, derived from studies in transgenic mice. *Mol. Reprod. Dev.* 82, 167–181. doi: 10.1002/mrd.22454

McDonough, A. A., Velotta, J. B., Schwinger, R. H., Philipson, K. D., and Farley, R. A. (2002). The cardiac sodium pump: structure and function. *Basic Res. Cardiol.* 97(Suppl. 1), I19–I24. doi: 10.1007/s003950200024

McLean, W. J., Smith, K. A., Glowatzki, E., and Pyott, S. J. (2009). Distribution of the Na,K-ATPase α subunit in the rat spiral ganglion and organ of corti. *J. Assoc. Res. Otolaryngol.* 10, 37–49. doi: 10.1007/s10162-008-0152-9

Miller, S. S., Steinberg, R. H., and Oakley, B. II. (1978). The electrogenic sodium pump of the frog retinal pigment epithelium. *J. Membr. Biol.* 44, 259–279. doi: 10.1007/BF01944224

Mishra, N. K., Habeck, M., Kirchner, C., Haviv, H., Peleg, Y., Eisenstein, M., et al. (2015). Molecular mechanisms and kinetic effects of FXYD1 and phosphomimetic mutants on purified human Na,K-ATPase. *J. Biol. Chem.* 290, 28746–28759. doi: 10.1074/jbc.M115.687913

Mobasheri, A., Errington, R. J., Golding, S., Hall, A. C., and Urban, J. P. (1997). Characterization of the Na^+, $K(^+)$-ATPase in isolated bovine articular chondrocytes; molecular evidence for multiple α and β isoforms. *Cell Biol. Int.* 21, 201–212. doi: 10.1006/cbir.1997.0137

Mobasheri, A., Pestov, N. B., Papanicolaou, S., Kajee, R., Cozar-Castellano, I., Avila, J., et al. (2003). Expression and cellular localization of Na,K-ATPase isoforms in the rat ventral prostate. *BJU Int.* 92, 793–802. doi: 10.1046/j.1464-410X.2003.04460.x

Morth, J. P., Pedersen, B. P., Toustrup-Jensen, M. S., Sorensen, T. L., Petersen, J., Andersen, J. P., et al. (2007). Crystal structure of the sodium-potassium pump. *Nature* 450, 1043–1049. doi: 10.1038/nature06419

Morth, J. P., Poulsen, H., Toustrup-Jensen, M. S., Schack, V. R., Egebjerg, J., Andersen, J. P., et al. (2009). The structure of the Na^+,K^+-ATPase and mapping of isoform differences and disease-related mutations. *Philos. Trans. R. Soc. Lond. B Biol. Sci.* 364, 217–227. doi: 10.1098/rstb.2008.0201

Mulkidjanian, A. Y., Bychkov, A. Y., Dibrova, D. V., Galperin, M. Y., and Koonin, E. V. (2012). Origin of first cells at terrestrial, anoxic geothermal fields. *Proc. Natl. Acad. Sci. U.S.A.* 109, E821–E830. doi: 10.1073/pnas.1117774109

Nam, J. S., Hirohashi, S., and Wakefield, L. M. (2007). Dysadherin: a new player in cancer progression. *Cancer Lett.* 255, 161–169. doi: 10.1016/j.canlet.2007.02.018

Newton, L. D., Kastelic, J. P., Wong, B., van der Hoorn, and Thundathil, J. (2009). Elevated testicular temperature modulates expression patterns of sperm proteins in Holstein bulls. *Mol. Reprod. Dev.* 76, 109–118. doi: 10.1002/mrd.20934

Nishimoto, K., Tomlins, S. A., Kuick, R., Cani, A. K., Giordano, T. J., Hovelson, D. H., et al. (2015). Aldosterone-stimulating somatic gene mutations are common in normal adrenal glands. *Proc. Natl. Acad. Sci. U.S.A.* 112, E4591–E4599. doi: 10.1073/pnas.1505529112

Noguchi, S., Mutoh, Y., and Kawamura, M. (1994). The functional roles of disulfide bonds in the β-subunit of (Na,K)ATPase as studied by site-directed mutagenesis. *FEBS Lett.* 341, 233–238. doi: 10.1016/0014-5793(94)80463-X

Nyblom, M., Poulsen, H., Gourdon, P., Reinhard, L., Andersson, M., Lindahl, E., et al. (2013). Crystal structure of Na^+, $K(^+)$-ATPase in the $Na(^+)$-bound state. *Science* 342, 123–127. doi: 10.1126/science.1243352

Ohnishi, T., Yanazawa, M., Sasahara, T., Kitamura, Y., Hiroaki, H., Fukazawa, Y., et al. (2015). Na, K-ATPase α3 is a death target of Alzheimer patient amyloid-β assembly. *Proc. Natl. Acad. Sci. U.S.A.* 112, E4465–E4474. doi: 10.1073/pnas.1421182112

Paciorkowski, A. R., McDaniel, S. S., Jansen, L. A., Tully, H., Tuttle, E., Ghoneim, D. H., et al. (2015). Novel mutations in ATP1A3 associated with catastrophic early life epilepsy, episodic prolonged apnea, and postnatal microcephaly. *Epilepsia* 56, 422–430. doi: 10.1111/epi.12914

Palmer, C. J., Scott, B. T., and Jones, L. R. (1991). Purification and complete sequence determination of the major plasma membrane substrate for cAMP-dependent protein kinase and protein kinase C in myocardium. *J. Biol. Chem.* 266, 11126–11130.

Pelzer, N., Blom, D. E., Stam, A. H., Vijfhuizen, L. S., Hageman, A., van Vliet, J. A., et al. (2016). Recurrent coma and fever in familial hemiplegic migraine type 2. A prospective 15-year follow-up of a large family with a novel ATP1A2 mutation. *Cephalalgia*. doi: 10.1177/0333102416651284. [Epub ahead of print].

Peng, L., Arystarkhova, E., and Sweadner, K. J. (1998). Plasticity of Na,K-ATPase isoform expression in cultures of flat astrocytes: species differences in gene expression. *Glia* 24, 257–271.

Peters, T. A., Kuijpers, W., and Curfs, J. H. (2001). Occurrence of NaK-ATPase isoforms during rat inner ear development and functional implications. *Eur. Arch. Otorhinolaryngol.* 258, 67–73. doi: 10.1007/s004050000304

Poulsen, H., Khandelia, H., Morth, J. P., Bublitz, M., Mouritsen, O. G., Egebjerg, J., et al. (2010). Neurological disease mutations compromise a C-terminal ion pathway in the $Na(^+)/K(^+)$-ATPase. *Nature* 467, 99–102. doi: 10.1038/nature09309

Rasmussen, H. H., Hamilton, E. J., Liu, C. C., and Figtree, G. A. (2010). Reversible oxidative modification: implications for cardiovascular physiology and pathophysiology. *Trends Cardiovasc. Med.* 20, 85–90. doi: 10.1016/j.tcm.2010.06.002

Rindler, T. N., Lasko, V. M., Nieman, M. L., Okada, M., Lorenz, J. N., and Lingrel, J. B. (2013). Knockout of the Na,K-ATPase α2-isoform in cardiac myocytes delays pressure overload-induced cardiac dysfunction. *Am. J. Physiol. Heart Circ. Physiol.* 304, H1147–H1158. doi: 10.1152/ajpheart.00594.2012

Rose, C. R., and Konnerth, A. (2001). NMDA receptor-mediated Na^+ signals in spines and dendrites. *J. Neurosci.* 21, 4207–4214. Available online at: http://www.jneurosci.org/content/21/12/4207

Rosewich, H., Thiele, H., Ohlenbusch, A., Maschke, U., Altmuller, J., Frommolt, P., et al. (2012). Heterozygous de-novo mutations in ATP1A3 in patients with alternating hemiplegia of childhood: a whole-exome sequencing gene-identification study. *Lancet Neurol.* 11, 764–773. doi: 10.1016/S1474-4422(12)70182-5

Rosewich, H., Weise, D., Ohlenbusch, A., Gartner, J., and Brockmann, K. (2014). Phenotypic overlap of alternating hemiplegia of childhood and CAPOS syndrome. *Neurology* 83, 861–863. doi: 10.1212/WNL.0000000000000735

Rossini, G. P., and Bigiani, A. (2011). Palytoxin action on the $Na(^+)$,$K(^+)$-ATPase and the disruption of ion equilibria in biological systems. *Toxicon* 57, 429–439. doi: 10.1016/j.toxicon.2010.09.011

Roubergue, A., Philibert, B., Gautier, A., Kuster, A., Markowicz, K., et al. (2015). Excellent response to a ketogenic diet in a patient with alternating hemiplegia of childhood. *JIMD Rep.* 15, 7–12. doi: 10.1007/8904_2013_292

Ruegsegger, C., Maharjan, N., Goswami, A., Filezac de L'Etang, Weis, J., Troost, D., et al. (2016). Aberrant association of misfolded SOD1 with $Na(^+)/K(^+)$ATPase-α3 impairs its activity and contributes to motor neuron vulnerability in ALS. *Acta Neuropathol.* 131, 427–451. doi: 10.1007/s00401-015-1510-4.

Scholl, U. I., Healy, J. M., Thiel, A., Fonseca, A. L., Brown, T. C., Kunstman, J. W., et al. (2015). Novel somatic mutations in primary hyperaldosteronism are related to the clinical, radiological and pathological phenotype. *Clin. Endocrinol.* 83, 779–789. doi: 10.1111/cen.12873

Schwinger, R. H., Bundgaard, H., Muller-Ehmsen, J., and Kjeldsen, K. (2003). The Na, K-ATPase in the failing human heart. *Cardiovasc. Res.* 57, 913–920. doi: 10.1016/S0008-6363(02)00767-8

Schwinger, R. H., Wang, J., Frank, K., Muller-Ehmsen, J., Brixius, K., McDonough, A. A., et al. (1999). Reduced sodium pump α1, α3, and β1-isoform protein levels and Na^+,K^+-ATPase activity but unchanged Na^+-$Ca2^+$ exchanger protein levels in human heart failure. *Circulation* 99, 2105–2112. doi: 10.1161/01.CIR.99.16.2105

Shamraj, O. I., Grupp, I. L., Grupp, G., Melvin, D., Gradoux, N., Kremers, W., et al. (1993). Characterisation of Na/K-ATPase, its isoforms, and the inotropic response to ouabain in isolated failing human hearts. *Cardiovasc. Res.* 27, 2229–2237. doi: 10.1093/cvr/27.12.2229

Shamraj, O. I., and Lingrel, J. B. (1994). A putative fourth Na^+,$K(^+)$-ATPase α-subunit gene is expressed in testis. *Proc. Natl. Acad. Sci. U.S.A.* 91, 12952–12956. doi: 10.1073/pnas.91.26.12952

Shinoda, T., Ogawa, H., Cornelius, F., and Toyoshima, C. (2009). Crystal structure of the sodium-potassium pump at 2.4 A resolution. *Nature* 459, 446–450. doi: 10.1038/nature07939

Shrivastava, A. N., Redeker, V., Fritz, N., Pieri, L., Almeida, L. G., Spolidoro, M., et al. (2015). α-synuclein assemblies sequester neuronal α3-Na^+/K^+-ATPase and impair Na^+ gradient. *EMBO J.* 34, 2408–2423. doi: 10.15252/embj.201591397

Shyjan, A. W., and Levenson, R. (1989). Antisera specific for the α 1, α 2, α 3, and β subunits of the Na,K-ATPase: differential expression of α and β subunits in rat tissue membranes. *Biochemistry* 28, 4531–4535. doi: 10.1021/bi00437a002

Skou, J. C. (1957). The influence of some cations on an adenosine triphosphatase from peripheral nerves. *Biochim. Biophys. Acta* 23, 394–401. doi: 10.1016/0006-3002(57)90343-8

Smedemark-Margulies, N., Brownstein, C. A., Vargas, S., Tembulkar, S. K., Towne, M. C., Shi, J., et al. (2016). A novel *de novo* mutation in ATP1A3 and childhood-onset schizophrenia. *Cold Spring Harbor Mol. Case Stud.* 2:a001008. doi: 10.1101/mcs.a001008

Sparrow, J. R., Hicks, D., and Hamel, C. P. (2010). The retinal pigment epithelium in health and disease. *Curr. Mol. Med.* 10, 802–823. doi: 10.2174/156652410793937813

Spiller, S., and Friedrich, T. (2014). Functional analysis of human $Na(^+)/K(^+)$-ATPase familial or sporadic hemiplegic migraine mutations expressed in *Xenopus oocytes*. *World J. Biol. Chem.* 5, 240–253. doi: 10.4331/wjbc.v5.i2.240.

Stanley, C. M., Gagnon, D. G., Bernal, A., Meyer, D. J., Rosenthal, J. J., and Artigas, P. (2015). Importance of the voltage dependence of cardiac Na/K ATPase isozymes. *Biophys. J.* 109, 1852–1862. doi: 10.1016/j.bpj.2015.09.015

Stindl, J., Tauber, P., Sterner, C., Tegtmeier, I., Warth, R., and Bandulik, S. (2015). Pathogenesis of adrenal aldosterone-producing adenomas carrying mutations of the $Na(^+)/K(^+)$-ATPase. *Endocrinology* 156, 4582–4591. doi: 10.1210/en.2015-1466

Sugiura, M., Nakamura, M., Ikoma, Y., Yano, M., Ogawa, K., Matsumoto, H., et al. (2005). High serum carotenoids are inversely associated with serum γ-glutamyltransferase in alcohol drinkers within normal liver function. *J. Epidemiol.* 15, 180–186. doi: 10.2188/jea.15.180

Sweadner, K. J., Herrera, V. L., Amato, S., Moellmann, A., Gibbons, D. K., and Repke, K. R. (1994). Immunologic identification of Na^+,$K(^+)$-ATPase isoforms in myocardium. Isoform change in deoxycorticosterone acetate-salt hypertension. *Circ. Res.* 74, 669–678. doi: 10.1161/01.RES.74.4.669

Sweadner, K. J., Toro, C., Whitlow, C. T., Snively, B. M., Cook, J. F., Ozelius, L. J., et al. (2016). ATP1A3 mutation in adult rapid-onset ataxia. *PLoS ONE* 11:e0151429. doi: 10.1371/journal.pone.0151429

Sweney, M. T., Newcomb, T. M., and Swoboda, K. J. (2015). The expanding spectrum of neurological phenotypes in children with ATP1A3 mutations, alternating hemiplegia of childhood, rapid-onset dystonia-parkinsonism, CAPOS and beyond. *Pediatr. Neurol.* 52, 56–64. doi: 10.1016/j.pediatrneurol.2014.09.015

Teo, A. E., Garg, S., Shaikh, L. H., Zhou, J., Karet Frankl, F. E., Gurnell, M., et al. (2015). Pregnancy, primary aldosteronism, and adrenal CTNNB1 mutations. *N. Engl. J. Med.* 373, 1429–1436. doi: 10.1056/NEJMoa1504869

Tokhtaeva, E., Clifford, R. J., Kaplan, J. H., Sachs, G., and Vagin, O. (2012). Subunit isoform selectivity in assembly of Na,K-ATPase α-β heterodimers. *J. Biol. Chem.* 287, 26115–26125. doi: 10.1074/jbc.M112.370734

Tokhtaeva, E., Munson, K., Sachs, G., and Vagin, O. (2010). N-glycan-dependent quality control of the Na,K-ATPase β(2) subunit. *Biochemistry* 49, 3116–3128. doi: 10.1021/bi100115a

Ujvari, B., Casewell, N. R., Sunagar, K., Arbuckle, K., Wuster, W., Lo, N., et al. (2015). Widespread convergence in toxin resistance by predictable molecular evolution. *Proc. Natl. Acad. Sci. U.S.A.* 112, 11911–11916. doi: 10.1073/pnas.1511706112

Urayama, O., Shutt, H., and Sweadner, K. J. (1989). Identification of three isozyme proteins of the catalytic subunit of the Na,K-ATPase in rat brain. *J. Biol. Chem.* 264, 8271–8280.

Vague, P., Coste, T. C., Jannot, M. F., Raccah, D., and Tsimaratos, M. (2004). C-peptide, Na^+,$K(^+)$-ATPase, and diabetes. *Exp. Diabesity Res.* 5, 37–50. doi: 10.1080/15438600490424514

Walaas, S. I., Czernik, A. J., Olstad, O. K., Sletten, K., and Walaas, O. (1994). Protein kinase C and cyclic AMP-dependent protein kinase phosphorylate phospholemman, an insulin and adrenaline-regulated membrane phosphoprotein, at specific sites in the carboxy terminal domain. *Biochem. J.* 304(Pt 2), 635–640. doi: 10.1042/bj3040635

Wetzel, R. K., Arystarkhova, E., and Sweadner, K. J. (1999). Cellular and subcellular specification of Na,K-ATPase α and β isoforms in the postnatal development of mouse retina. *J. Neurosci.* 19, 9878–9889.

Wetzel, R. K., and Sweadner, K. J. (2001). Immunocytochemical localization of Na-K-ATPase α- and γ-subunits in rat kidney. *Am. J. Physiol. Ren. Physiol.* 281, F531–F545. Available online at: http://ajprenal.physiology.org/content/281/3/F531.long

Winther, A. M., Bublitz, M., Karlsen, J. L., Moller, J. V., Hansen, J. B., Nissen, P., et al. (2013). The sarcolipin-bound calcium pump stabilizes calcium sites exposed to the cytoplasm. *Nature* 495, 265–269. doi: 10.1038/nature11900

Zahler, R., Zhang, Z. T., Manor, M., and Boron, W. F. (1997). Sodium kinetics of Na,K-ATPase α isoforms in intact transfected HeLa cells. *J. Gen. Physiol.* 110, 201–213. doi: 10.1085/jgp.110.2.201

Zhang, M., Zeng, S., Zhang, L., Li, H., Chen, L., Zhang, X., et al. (2014). Localization of $Na(^+)$-$K(^+)$-ATPase α/β, $Na(^+)$-$K(^+)$-2Cl-cotransporter 1 and aquaporin-5 in human eccrine sweat glands. *Acta Histochem.* 116, 1374–1381. doi: 10.1016/j.acthis.2014.08.010

Zhang, X. L., Danto, S. I., Borok, Z., Eber, J. T., Martin-Vasallo, P., and Lubman, R. L. (1997). Identification of $Na(^+)$-$K(^+)$-ATPase β-subunit in alveolar epithelial cells. *Am. J. Physiol.* 272, L85–94.

Zhen, Y., Aardema, M. L., Medina, E. M., Schumer, M., and Andolfatto, P. (2012). Parallel molecular evolution in an herbivore community. *Science* 337, 1634–1637. doi: 10.1126/science.1226630

Ziff, O. J., and Kotecha, D. (2016). Digoxin: the good and the bad. *Trends Cardiovasc. Med.* 26, 585–595. doi: 10.1016/j.tcm.2016.03.011

Zlokovic, B. V., Mackic, J. B., Wang, L., McComb, J. G., and McDonough, A. (1993). Differential expression of Na,K-ATPase α and β subunit isoforms at the blood-brain barrier and the choroid plexus. *J. Biol. Chem.* 268, 8019–8025.

Conflict of Interest Statement: The authors declare that the research was conducted in the absence of any commercial or financial relationships that could be construed as a potential conflict of interest.

The reviewer PMV and handling Editor declared their shared affiliation, and the handling Editor states that the process nevertheless met the standards of a fair and objective review.

frontiers in Physiology

REVIEW
published: 09 February 2016
doi: 10.3389/fphys.2016.00030

Structural Features of Ion Transport and Allosteric Regulation in Sodium-Calcium Exchanger (NCX) Proteins

*Moshe Giladi, Inbal Tal and Daniel Khananshvili **

Department of Physiology and Pharmacology, Sackler Faculty of Medicine, Tel Aviv University, Tel Aviv, Israel

Na^+/Ca^{2+} exchanger (NCX) proteins extrude Ca^{2+} from the cell to maintain cellular homeostasis. Since NCX proteins contribute to numerous physiological and pathophysiological events, their pharmacological targeting has been desired for a long time. This intervention remains challenging owing to our poor understanding of the underlying structure-dynamic mechanisms. Recent structural studies have shed light on the structure-function relationships underlying the ion-transport and allosteric regulation of NCX. The crystal structure of an archaeal NCX (NCX_Mj) along with molecular dynamics simulations and ion flux analyses, have assigned the ion binding sites for $3Na^+$ and $1Ca^{2+}$, which are being transported in separate steps. In contrast with NCX_Mj, eukaryotic NCXs contain the regulatory Ca^{2+}-binding domains, CBD1 and CBD2, which affect the membrane embedded ion-transport domains over a distance of ~80 Å. The Ca^{2+}-dependent regulation is ortholog, isoform, and splice-variant dependent to meet physiological requirements, exhibiting either a positive, negative, or no response to regulatory Ca^{2+}. The crystal structures of the two-domain (CBD12) tandem have revealed a common mechanism involving a Ca^{2+}-driven tethering of CBDs in diverse NCX variants. However, dissociation kinetics of occluded Ca^{2+} (entrapped at the two-domain interface) depends on the alternative-splicing segment (at CBD2), thereby representing splicing-dependent dynamic coupling of CBDs. The HDX-MS, SAXS, NMR, FRET, equilibrium $^{45}Ca^{2+}$ binding and stopped-flow techniques provided insights into the dynamic mechanisms of CBDs. Ca^{2+} binding to CBD1 results in a population shift, where more constraint conformational states become highly populated without global conformational changes in the alignment of CBDs. This mechanism is common among NCXs. Recent HDX-MS studies have demonstrated that the apo CBD1 and CBD2 are stabilized by interacting with each other, while Ca^{2+} binding to CBD1 rigidifies local backbone segments of CBD2, but not of CBD1. The extent and strength of Ca^{2+}-dependent rigidification at CBD2 is splice-variant dependent, showing clear correlations with phenotypes of matching NCX variants. Therefore, diverse NCX variants share a common mechanism for the initial decoding of the regulatory signal upon Ca^{2+} binding at the interface of CBDs, whereas the allosteric message is shaped by CBD2, the dynamic features of which are dictated by the splicing segment.

Keywords: NCX, allosteric regulation, Ca^{2+} binding proteins, X-ray crystallography, HDX-MS, SAXS

OPEN ACCESS

Edited by:
Mario Diaz,
Universidad de La Laguna, Spain

Reviewed by:
John Cuppoletti,
University of Cincinnati, USA
Pablo Martín-Vasallo,
Universidad de La Laguna, Spain
Thomas Baukrowitz,
University of Kiel, Germany

****Correspondence:***
Daniel Khananshvili
dhanan@post.tau.ac.il

Specialty section:
This article was submitted to Membrane Physiology and Membrane Biophysics, a section of the journal Frontiers in Physiology

Received: *23 November 2015*
Accepted: *19 January 2016*
Published: *09 February 2016*

Citation:
Giladi M, Tal I and Khananshvili D (2016) Structural Features of Ion Transport and Allosteric Regulation in Sodium-Calcium Exchanger (NCX) Proteins. Front. Physiol. 7:30. doi: 10.3389/fphys.2016.00030

INTRODUCTION

Calcium (Ca^{2+}) is the most important and versatile secondary messenger in the cell; it carries vital information to virtually all processes important to cell life and function (e.g., it couples excitation to contraction, hormone secretion, gene transcription, and controls enzyme activity through protein phosphorylation-dephosphorylation involving numerous biochemical reactions). The evolutionary choice of Ca^{2+} as a universal and versatile intracellular messenger has been dictated by its coordination chemistry (Williams, 1999), although how these chemical properties of Ca^{2+} are realized in protein-calcium interactions and how this is translated to biological functions of diverse Ca^{2+}-binding proteins are currently not entirely clear (Gifford et al., 2007). Since Ca^{2+} promotes, maintains, and modifies the programmed function and demise of various cell types by governing numerous signal transduction pathways (Carafoli, 1987; Berridge et al., 2003), it is not surprising that an altered handing of Ca^{2+} homeostasis can precipitate disease-related conditions.

Maintenance of resting cytosolic Ca^{2+} levels (∼100 nM) is essential in every living cell, where the maintenance of resting cytosolic levels as well as the cell-specific dynamic oscillations of cytosolic Ca^{2+} requires tight regulation and integration of Ca^{2+} transport proteins. Notably, the Ca^{2+} transporting proteins are located in the plasma membrane and in the membranes of the organelles (the endo/sarcoplasmic reticulum, the mitochondria, and the nuclear envelope), thereby playing distinctive roles in the excitation-contraction coupling of cardiac (Bers, 2002) and skeletal (Melzer et al., 1995) muscle cells, the release of neurotransmitters (Neher and Sakaba, 2008), apoptosis (Orrenius et al., 2003), mitochondrial bioenergetics (Filadi and Pozzan, 2015), among others. These oscillations must occur in the right place and the right time to fulfill functional requirements in diverse cell types (e.g., excitable tissues) (Carafoli, 1987; Bers, 2002; Berridge et al., 2003; Brini et al., 2014).

The multifaceted effects of Ca^{2+} signaling pathways require dynamic regulation, coordination, and the integration of ion channels, pumps, and transporters involved in Ca^{2+} transport, buffering, and storage (Carafoli, 1987; Berridge et al., 2003). The PM (plasma membrane) Ca^{2+}-ATPase, and Na^+/Ca^{2+} exchanger (NCX) extrude Ca^{2+} from the cell, although their partial contributions to Ca^{2+} homeostasis differ among distinct cell types, depending on the functional specialization and regulatory specificity in a given cell type (Khananshvili, 2013, 2014; Brini et al., 2014). For example, in cardiomyocytes, NCX serves as a high-capacity (k_{cat} ∼ 2500 s^{-1}) and low-affinity (K_m ∼ 10–20 μM) system that allows rapid removal of Ca^{2+}; it can limit Ca^{2+} transients over a wide dynamic range (Carafoli, 1987; Bers, 2002; Khananshvili, 2013, 2014). NCX proteins mediate uphill Ca^{2+}-fluxes in exchange with downhill Na^+ transport, with a stoichiometry of $3Na^+$:$1Ca^{2+}$ (**Figure 1**), thus creating an electrogenic current (Reeves and Hale, 1984). NCX works mainly in the forward mode, i.e., it extrudes Ca^{2+} from the cell. However, under certain altered conditions (e.g., high intracellular Na^+, highly positive membrane potential) NCX may work in the reverse mode and induce Ca^{2+} influx (Blaustein and Lederer, 1999). Three mammalian NCX genes (*SLC8A1*, *SLC8A2*, and *SLC8A3*) and their splice variants are expressed in a tissue-specific manner (Philipson and Nicoll, 2000). By regulating cytosolic [Ca^{2+}], the protein products (NCX1, NCX2, and NCX3, respectively) modulate fundamental physiological events, such as muscle excitation-contraction coupling, neuronal long-term potentiation and learning, blood pressure regulation, immune responses, neurotransmitter and insulin secretion, and mitochondrial bioenergetics (Khananshvili, 2013, 2014; Filadi and Pozzan, 2015). Altered expression and regulation of NCXs actively contribute to distorted Ca^{2+}-homeostasis, resulting in molecular and cellular remodeling of distinct tissues, which is associated with pathophysiological states including heart failure, arrhythmia, cerebral ischemia, hypertension, diabetes, renal Ca^{2+} reabsorption, and muscle dystrophy, among others. Thus, NCX proteins represent a long-wanted target for selective pharmacological targeting (Khananshvili, 2014).

Structurally, eukaryotic NCX proteins are composed of 10 transmembrane (TM) helices and contain a large cytosolic regulatory loop (f-loop) between TM5 and TM6 (Ren and Philipson, 2013). The major difference between eukaryotic and prokaryotic NCX proteins is that prokaryotic NCXs lack the large f-loop, which includes two regulatory Ca^{2+}-binding domains, CBD1 and CBD2 (Hilge et al., 2006; Liao et al., 2012). In eukaryotes, these regulatory domains enable the dynamic adjustment of Ca^{2+}-extrusion rates from the cell in accordance with the dynamic oscillations of cytosolic Ca^{2+}, representing a regulatory feedback mechanism (Blaustein and Lederer, 1999; Philipson and Nicoll, 2000; Hilge et al., 2006). The dynamic regulation of NCX is especially diverse and complex, since it must remove large amounts of Ca^{2+} within a limited time window. Ca^{2+}-extrusion rates via NCX must change within milliseconds to match the dynamic oscillation in the cytosolic Ca^{2+}, i.e., during the action potential in cardiomyocytes (Berridge et al., 2003; Boyman et al., 2011). Ca^{2+} interaction with the regulatory CBDs (located 70–80 Å away from the transport sites) of cardiac NCX enhances the turnover rates of NCX up to 25-fold (Boyman et al., 2011), where Ca^{2+} extrusion rates dynamically change in response to dynamic changes in the membrane potential and the cytosolic Na^+ and Ca^{2+} concentrations during the action potential.

Over the last decade, diverse structural methods, including nuclear magnetic resonance (NMR), X-ray crystallography, small angle X-ray scattering (SAXS), fluorescence resonance energy transfer (FRET) and hydrogen-deuterium exchange mass spectrometry (HDX-MS) have been utilized to study the mechanisms underlying ion transport and the allosteric regulation of NCX. Despite the tremendous progress, some important questions remain open: Why are so many isoforms and splice variants required by different cell types and why does each cell type express a specific set of isoforms and splice variants? What are the exact mechanisms underlying the function and regulation of diverse isoforms and splice variants? What is the partial contribution of distinct splice variants to specific functions in a given cell type? During the last few years, huge progress has been made in better understanding the molecular

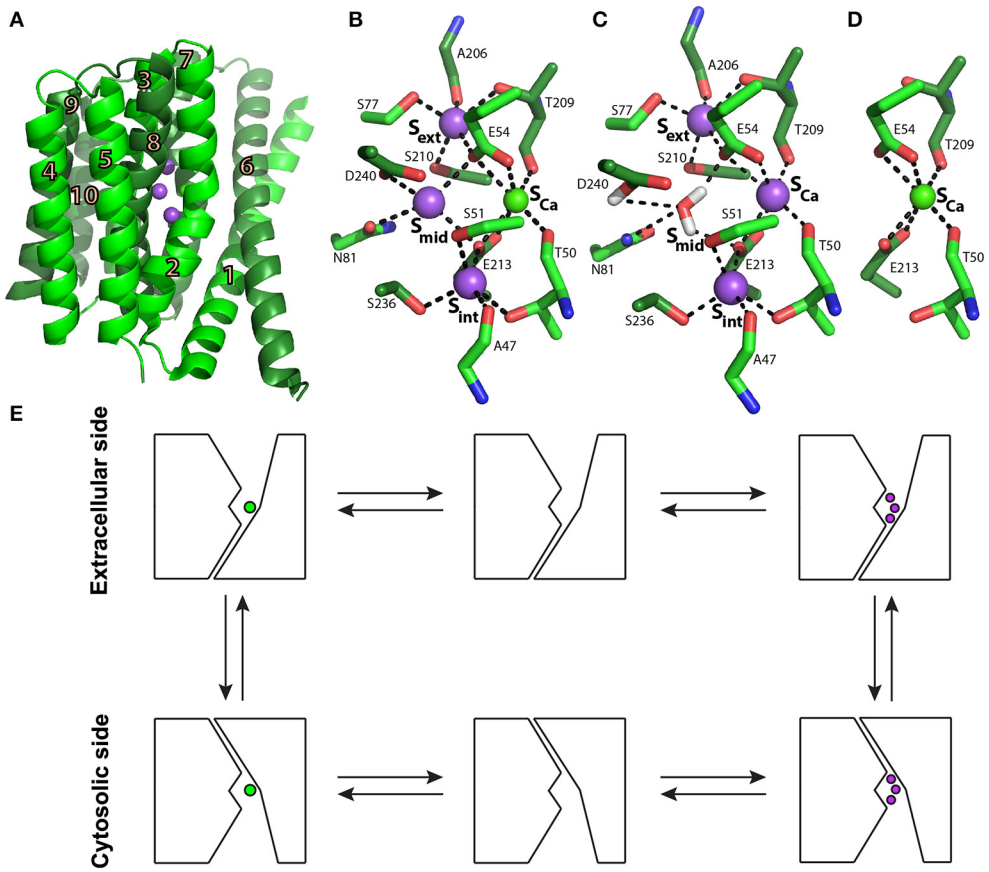

FIGURE 1 | NCX_Mj structure and transport mechanism. (A) Crystal structure of NCX_Mj (PDB 3V5U) in cartoon representation. Helices 1-5 (TM1-5) are light green and helices 6-10 (TM6-10) are dark green. Purple and green spheres represent the Na^+ and Ca^{2+} ions, respectively. **(B)** Ion coordination, as suggested by the crystal structure of NCX_Mj. **(C)** $3Na^+$ ion coordination, as suggested by molecular dynamics simulations and ion-flux assays. **(D)** Ca^{2+} binding site. **(E)** Schematic representation of the ion-exchange mechanism.

mechanisms underlying NCX regulation in tissue-specific isoforms and splice variants. This review will focus on insights into NCX ion transport and allosteric regulation mechanisms derived from structural biology techniques in recent years.

CRYSTAL STRUCTURE OF AN ARCHAEAL NCX AS A PROTOTYPE FOR THE NCX ION TRANSPORT MECHANISM

Biochemical studies utilizing transport assays in proteoliposomes (Khananshvili, 1990), followed by electrophysiological studies (Hilgemann et al., 1991; Niggli and Lederer, 1991), have concluded that NCX operates through a ping-pong mechanism in which one Ca^{2+} and three Na^+ ions are translocated sequentially in separate steps rather than simultaneously across the membrane. This mechanism implies the alternating access mechanism of the NCX ion binding sites in the inward (cytosolic) and outward (extracellular) conformations (**Figure 1E**). A major advancement in better understanding the transport mechanism and ion selectivity was provided by solving the crystal structure of NCX from the archaebacterium *Methanococcus jannaschii* (NCX_Mj) (Liao et al., 2012).

The structure depicts NCX_Mj in the outward-facing conformation, composed of 10 transmembrane helices (TM1-10) with a pseudo molecular dyad (**Figure 1A**). It appears that this membrane topology is the same in mammalian NCX proteins (Ren and Philipson, 2013). As mentioned above, in sharp contrast with eukaryotic NCX, the cytosolic loop between TM5 and TM6 is extremely short (only 12 residues) in NCX_Mj, meaning that this loop cannot serve as a prototype for the large cytosolic regulatory f-loop of eukaryotic NCX.

The ion-binding pocket of NCX_Mj contains four ion-binding sites: S_{ext}, S_{mid}, S_{int}, and S_{Ca}(**Figure 1B**). The binding sites are arranged in a diamond-shaped configuration, where 12 residues contribute to Na^+ and Ca^{2+} ligation (four in TM2 and TM7, and two in TM3 and TM8). Interestingly, 11 ion-coordinating residues (out of twelve) are highly conserved in organisms ranging from bacteria to humans, whereas in eukaryotic NCXs, D240 is consistently replaced by glutamine (Marinelli et al., 2014). Moreover, the ion exchange turnover rates increase nearly 10 times in the D240N mutant of NCX_Mj, thereby suggesting

that the aspartate to asparagine replacement in eukaryotic species may represent an evolutionary "improvement" in catalytic power in mammalian NCX orthologs (Marinelli et al., 2014). The proximity and ligand sharing by the ions implicate the progressive antagonistic effect of Na^+ binding on Ca^{2+} affinity and vice versa. In the outward conformation, the binding sites are exposed to high extracellular [Na^+] levels, which favors Na^+ binding and the release of Ca^{2+}. When exposed to low intracellular [Na^+] levels, Na^+ release is favored, thus restoring the high Ca^{2+} affinity, which upon binding further decreases Na^+ affinity (Liao et al., 2012).

According to the original interpretation of the crystallographic data, S_{ext}, S_{mid}, and S_{int} are occupied by $3Na^+$ ions, and S_{Ca} is occupied by one Ca^{2+} ion (**Figure 1B**) (Liao et al., 2012). However, the crystal structure of NCX_Mj revealed that this simultaneous occupation of all four sites by $3Na^+$ ions and one Ca^{2+} ion is thermodynamically forbidden (Marinelli et al., 2014). Recent molecular dynamics (MD) simulations and ion flux analyses revealed that $3Na^+$ ions occupy S_{ext}, S_{int}, and S_{Ca} (**Figure 1C**), whereas the Ca^{2+} ion occupies S_{Ca} (**Figure 1D**) (Marinelli et al., 2014). According to this interpretation, S_{mid} does not bind either the Na^+ or Ca^{2+} ions and one water molecule is bound to protonated D240.

Eight helices of NCX_Mj (TM2-5 and TM7-10) generate a tightly packed hub (which is perpendicularly inserted into the membrane), whereas two long/slanting helices (TM1 and TM6) are loosely packed in front of the rigid eight-helix core (**Figure 1A**) (Liao et al., 2012). The sliding of the gating bundle (TM1/TM6) toward the rigid eight-helix core was proposed as a major conformational change that occurs during alternating access. Recently, three crystal structures of Ca^{2+}/H^+ exchangers were determined and revealed striking similarities with NCX_Mj, suggesting that the sliding mechanisms could be a general feature of the gene families belonging to the Ca/CA superfamily (Nishizawa et al., 2013; Waight et al., 2013). However, it remains unclear how ion binding drives the sliding of the gating bundle (the TM1/TM6 cluster) to initiate alternating access. The resolution of this mechanism is essential for understanding how Ca^{2+} binding to the regulatory CBDs in eukaryotic NCX orthologs accelerates the ion transport cycle.

ALLOSTERIC REGULATION OF EUKARYOTIC NCX PROTEINS

Ionic Regulation of NCX

NCX is allosterically regulated by its substrates, Ca^{2+} and Na^+, and by H^+ (Hilgemann, 1990; Boyman et al., 2011). A rise in $[Na^+]_i$ results in a decrease in NCX current in a dose-response manner, a process termed I_1-inactivation or Na^+-dependent inactivation (Hilgemann, 1990; Hilgemann et al., 1992b). A decrease in pH results in decreased NCX activity within a physiological and pathophysiological pH range (6.9–7.5) (Boyman et al., 2011). Interestingly, the effects of H^+ and Na^+ are interlaced: in the absence of Na^+, pH has only a minor effect on NCX activity; under basic pH conditions, intracellular Na^+ does not induce inactivation (Blaustein and Lederer, 1999).

In contrast to Na^+ and H^+, a rise in $[Ca^{2+}]_i$ results in increased NCX current and counteracts the effect of $[Na^+]_i$(Hilgemann et al., 1992a). Moreover, regulatory cytoplasmic Ca^{2+} is obligatory for exchange activity (DiPolo, 1979). Removal of cytosolic Ca^{2+} results in slow inactivation of NCX, a process termed I_2-inactivation or Ca^{2+}-dependent inactivation (Hilgemann et al., 1992a). In patch-clamp recordings, a rise in NCX peak current represents $[Ca^{2+}]_i$-dependent activation of NCX, whereas the ratio between steady-state and peak currents represents the $[Ca^{2+}]_i$-induced relief of Na^+-dependent inactivation (**Figure 2A**) (Hilgemann et al., 1992a). The Ca^{2+} sensitivity of the two processes is different: An increase in peak current occurs at lower $[Ca^{2+}]$ levels ($\sim 0.2\,\mu M$) than the increase in the steady-state to peak-current ratio ($\sim 10\,\mu M$) (**Figure 2A**) (Hilgemann et al., 1992a; Ottolia et al., 2009).

Interestingly, treatment of the intracellular surface of NCX with α-chymotrypsin abolished the regulatory effects of Na^+, Ca^{2+}, and H^+ and resulted in constitutive NCX activation (Hilgemann, 1990; Matsuoka and Hilgemann, 1994). This finding demonstrates the existence of the ionic allosteric regulation of NCX through ions binding to one or more cytosolic regulatory domains that differ from those of the transport sites (Matsuoka et al., 1993).

Alternative Splicing and Regulatory Diversity of Mammalian NCX Proteins

In mammals, NCX1, NCX2, and NCX3 and their splice variants differ in their tissue-expression profiles—i.e., NCX1 is universally distributed, practically in every mammalian cell; NCX2 is expressed in the brain and spinal cord; and NCX3 is expressed in the brain and skeletal muscles (Philipson and Nicoll, 2000). At the post-transcriptional level, at least 17 NCX1 and 5 NCX3 splice variants are produced through alternative splicing of the primary nuclear *SLC8A1* and *SLC8A3* transcripts, whereas no splice variants have been identified for *SLC8A2* (Kofuji et al., 1994). Alternative splicing of NCX1 arises from combining six small exons (A, B, C, D, E, and F) located exclusively on CBD2, where all splice variants include a mutually exclusive exon, either A or B in order to maintain an open reading frame (Kofuji et al., 1994).

In general, excitable tissues contain exon A, whereas non-excitable tissues comprise NCX with exon B (Quednau et al., 1997). The cardiac (ACDEF), kidney (BD), and brain (AD) splice variants exhibit distinct properties for Ca^{2+}-dependent allosteric regulation of NCX activity, thereby suggesting that exon-dependent regulatory properties may have physiological relevance (Matsuoka et al., 1995; Dyck et al., 1999). For example, cytosolic Ca^{2+} elevation activates the brain, cardiac, and kidney splice variants, whereas Ca^{2+}-induced alleviation of Na^+-dependent inactivation is observed only in the cardiac and brain splice variants (containing exon A) (Matsuoka et al., 1995; Dyck et al., 1999). The lack of significant Na^+-transients in non-excitable tissues and their presence in excitable tissues explains the need for Ca^{2+}-dependent alleviation of Na^+-dependent inactivation only in excitable tissues. Although the cardiac (ACDEF) and brain (AD) variants exhibit similar regulatory

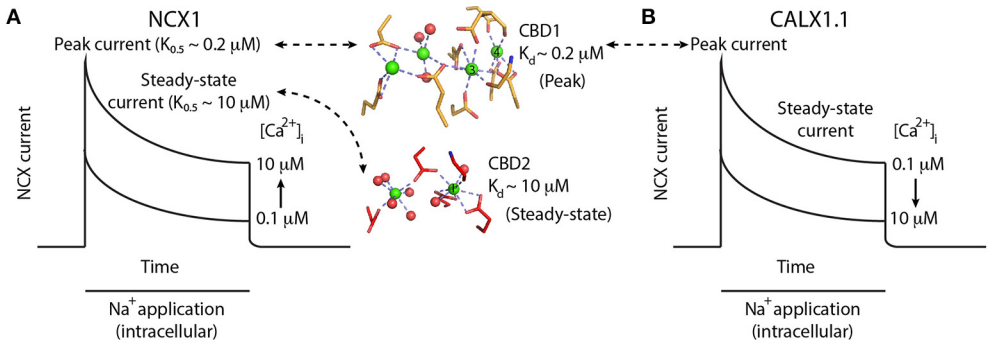

FIGURE 2 | Ca^{2+}-dependent regulation of NCX and CALX. (A) Schematic representation of NCX1 currents upon the application of intracellular Na^+ to initiate the exchange reaction in the presence of varying $[Ca^{2+}]_i$. Na^+ applications initially activates NCX1, followed by a slow decrease in exchange current representing Na^+-dependent inactivation. Higher $[Ca^{2+}]_i$ results in larger peak currents and reduced Na^+-dependent inactivation, as reflected by the higher steady-state current in the presence of 10 μM $[Ca^{2+}]_i$. Binding of Ca^{2+} ions (green spheres) to the Ca3-Ca4 sites of CBD1 (yellow sticks) results in peak-current activation, whereas the binding of one Ca^{2+} ion to the CaI site of CBD2 (red sticks) results in steady-state current activation. **(B)** Schematic representation of CALX1.1 currents upon the application of intracellular Na^+ to initiate the exchange reaction in the presence of varying amounts of $[Ca^{2+}]_i$. Na^+ application initially activates NCX, followed by a slow decrease in exchange current representing Na^+-dependent inactivation. Higher $[Ca^{2+}]_i$ results in smaller peak currents and increased Na^+-dependent inactivation, as reflected by the smaller steady-state current in the presence of 10 μM $[Ca^{2+}]_i$.

responses to Ca^{2+}, they differ in their response kinetics, with the kinetics of NCX1-ACDEF being ~ 10-fold slower compared with NCX1-AD (Matsuoka et al., 1995; Dyck et al., 1999). The kinetic differences are consistent with the slower Ca^{2+} transients involved in muscle contraction compared to the faster Ca^{2+} transients involved in neurotransmission (Berridge et al., 2003).

Anomalous Regulation of CALX

CALX1 is a *drosophila melanogaster* NCX ortholog, having a structure similar to that of mammalian NCXs (Schwarz and Benzer, 1997). However, electrophysiological characterization of the CALX1.1 splice variant revealed that despite having many properties common with NCX, it exhibits an opposite response to regulatory Ca^{2+} (Hryshko et al., 1996). That is, a rise in $[Ca^{2+}]_i$ (over the same range that activates NCX) inactivates CALX1.1 (**Figure 2B**). In the second variant, CALX1.2, Ca^{2+} has no regulatory effect on exchange activity (Omelchenko et al., 1998). CALX1 also undergoes alternative splicing only at CBD2, with its two variants differing only by five amino acids. The splicing region is at a position similar to that of the cassette exons in mammalian NCX1. The regulatory differences between CALX1 and NCX are especially interesting in light of the structural similarities between the regulatory CBDs among the different orthologs (see below).

STRUCTURAL AND FUNCTIONAL FEATURES OF THE REGULATORY CYTOSOLIC F-LOOP

All eukaryotic NCX orthologs (including CALX1 from *Drosophila melanogaster*, which exhibits an anomalous regulation) contain the large cytosolic f-loop between TM5 and TM6. At the N-terminus, adjacent to the membrane, is an amphipathic α-helical region (20 residues) termed XIP (eXchanger Inhibitory Peptide) because it inhibits NCX when applied exogenously (Li et al., 1991). This area has been implicated in regulation of intact NCX by Na^+ and phospholipids (Matsuoka et al., 1997). The XIP region is followed by a sequence predicted to be an α-helical Catenin-Like Domain (CLD) (Hilge et al., 2006), although this prediction has not been experimentally validated to date. Two consecutive CBDs are located downstream of the presumed CLD (Hilge et al., 2006), serving as sensors for regulatory Ca^{2+}. CBD1 and CBD2 (**Figures 3A–D**) are connected in a head-to-tail fashion through a very short linker (five residues) that forms a two-domain (CBD12) regulatory tandem (**Figure 4**) (Hilge et al., 2006; Giladi et al., 2012c). This arrangement appears to be a crucial factor for governing the structure-dynamic interactions between the two domains, which definitely has functional significance in terms of decoding and propagation of the allosteric signal upon Ca^{2+} binding to the primary allosteric sensor at CBD1 (Giladi et al., 2010, 2012c). Importantly, the alternatively spliced region of NCX is exclusively located in CBD2 (Hilge et al., 2006; Hilge, 2012).

Structures of Isolated CBD1 and CBD2

High-resolution X-ray and NMR structures of isolated CBD1 and CBD2 from NCX1 revealed that each domain exhibits an immunoglobulin-like β-sandwich structure with seven antiparallel β-strands (**Figures 3A,C**) (Hilge et al., 2006; Nicoll et al., 2006; Besserer et al., 2007). The domains are nearly identical structurally, with a root mean square deviation of 1.3 Å. The Ca^{2+} binding sites are located at the C-terminal region of the domains. CBD1 contains four Ca^{2+} binding sites (Ca1-Ca4); the brain splice variant (AD) of CBD2 contains two Ca^{2+} binding sites (CaI-CaII) (Nicoll et al., 2006; Besserer et al., 2007). In contrast, the kidney splice variant (BD) of CBD2 does not bind Ca^{2+} (Hilge et al., 2009). The differences in CBD2 Ca^{2+} binding capacity result from the fact that exons A and B encode strands E-F of CBD2, which form part of the ion-binding region. The

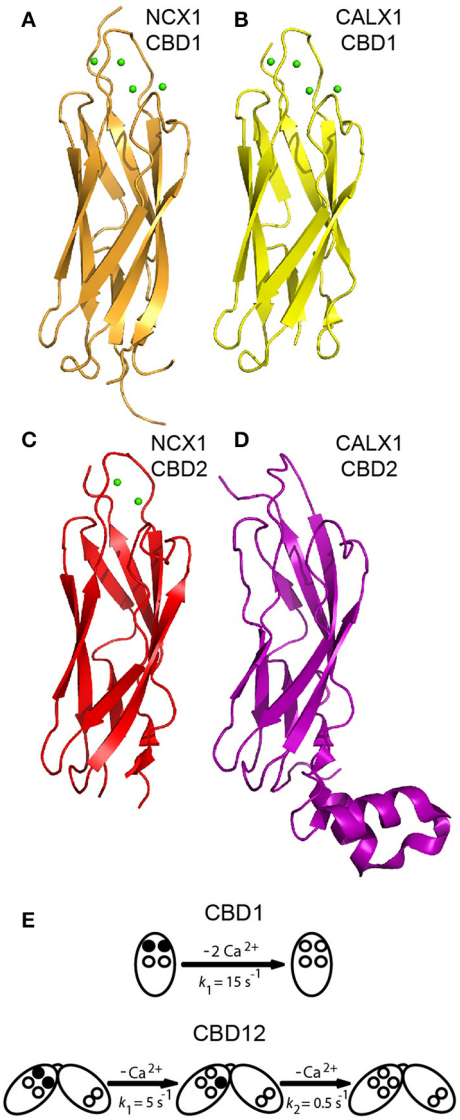

FIGURE 3 | Structures of isolated CBDs and dissociation kinetics. Crystal structures of CBD1 from NCX1 (PDB 2DPK) **(A)**, CBD1 from CALX1 (PDB 3EAD) **(B)**, CBD2 from NCX1-AD (PDB 2QVM) **(C)**, and CBD2 from CALX1.1 (PDB 3E9U) **(D)** in cartoon representation. **(E)** Dissociation kinetics of two Ca^{2+} ions from the Ca3-Ca4 sites of isolated CBD1 and CBD12. The Ca3-Ca4 sites occupied by Ca^{2+} ions are denoted by filled circles, whereas the open circles represent empty Ca^{2+} sites. The indicated k_{off} values represent typical values observed in stopped-flow experiments.

cassette exons (C, D, E, and F) are positioned at the N-terminal portion of CBD2's F-G loop, adjacent to the CBD1 binding sites (**Figure 4A**), and thus do not affect the CBD2 Ca^{2+} binding sites (Hilge et al., 2006, 2009; Giladi et al., 2012c). Ca^{2+} binding to CBD1 (which does not undergo alternative splicing), specifically to the Ca3-Ca4 sites, results in NCX activation (Ottolia et al., 2009). The alleviation of Na^+-dependent inactivation depends on Ca^{2+} binding to the CaI site of CBD2 (and thus variants containing B-exon cannot relieve Na^+-dependent inactivation, as mentioned above) (Besserer et al., 2007; Ottolia et al., 2009).

NMR and crystallographic analyses of the Ca^{2+}-bound and—free forms have shown that CBD2-AD retains its structural integrity in the absence of Ca^{2+} (Hilge et al., 2006; Besserer et al., 2007). In contrast, CBD1's binding sites become unstructured in the absence of Ca^{2+}, whereas the core of the domain retains its structure and dynamics (Hilge et al., 2006). This difference arises from the presence of K585 in CBD2, in a position homologous to E454 in CBD1. In the absence of Ca^{2+}, K585 forms salt bridges with negatively charged Ca^{2+} coordinating residues to stabilize CBD2's binding sites in the apo form (Besserer et al., 2007).

X-ray structures of isolated CBD1 and CBD2 from CALX (**Figures 3B,D**) revealed that they are highly similar to the NCX1 domains (Wu et al., 2009, 2010). CALX1-CBD1 binds four Ca^{2+} ions similarly to NCX1-CBD1, whereas CALX1-CBD2 does not bind Ca^{2+}. Most of the FG loop is unstructured in NCX-CBD2, except for a short α-helical region in the C-terminal portion of the FG loop (Hilge et al., 2006). In contrast, in CALX-CBD2 the FG loop is organized as two helices perpendicular to the β-sheets (Wu et al., 2009). Owing to the high structural similarity, the different regulatory responses of CALX1 and NCX1 to changes in $[Ca^{2+}]_i$ cannot be attributed to structural differences between the isolated CBDs.

Kinetic and Equilibrium Properties of Ca^{2+} Binding to Isolated CBDs

Isolated CBD1 and CBD2 exhibit distinct Ca^{2+} binding properties (Hilge et al., 2006; Boyman et al., 2009). The equilibrium binding constants (K_ds) were measured in our laboratory by $^{45}Ca^{2+}$ equilibrium binding assays and the rate constants of Ca^{2+} dissociation were measured using stopped-flow kinetics (Boyman et al., 2009). In both NCX1 and CALX1, CBD1 binds two Ca^{2+} ions with high affinity ($K_d \sim 0.2\,\mu M$) at its Ca3-Ca4 sites and two Ca^{2+} ions with lower affinity (>5–10 μM) at its Ca1-Ca2 sites. Monophasic dissociation of two Ca^{2+} ions from the Ca3-Ca4 sites is observed in both NCX1 and CALX1, with a rate constant of ~15 s^{-1} (**Figure 3E**) (Giladi et al., 2012a). Ca^{2+} dissociation from Ca1-Ca2 is too rapid to be measured using stopped-flow kinetics, since the rate constant is >300 s^{-1} (Boyman et al., 2009). NCX1-CBD2-AD binds two Ca^{2+} ions: one with moderate affinity ($K_d \sim 5\,\mu M$) at its CaI site and one with low affinity ($K_d > 20\,\mu M$) at its CaII site. Ca^{2+} dissociates from CaI with a rate constant of ~ 150 s^{-1}. As in CBD1, the dissociation rate constant from the low-affinity CaII site is too fast to be measured using stopped-flow kinetics (Boyman et al., 2009). As mentioned above, NCX1-CBD2-BD and both the CALX1-CBD2 splice variants do not bind Ca^{2+} (Giladi et al., 2012a). The K_d values measured for the Ca3-Ca4 sites of CBD1 match the $K_{0.5}$ value for the "peak-current" activation of NCX, and the K_d value of CaI matches the $K_{0.5}$ value for steady-state activation (and alleviation of Na^+-dependent inactivation) (Hilgemann et al., 1992a; Ottolia et al., 2009), thus supporting the role of each domain in allosteric NCX regulation. However, the Ca^{2+} dissociation rate constants from isolated CBD1 and CBD2 cannot represent the slow I_2 inactivation observed upon the removal of Ca^{2+} from the intracellular surface

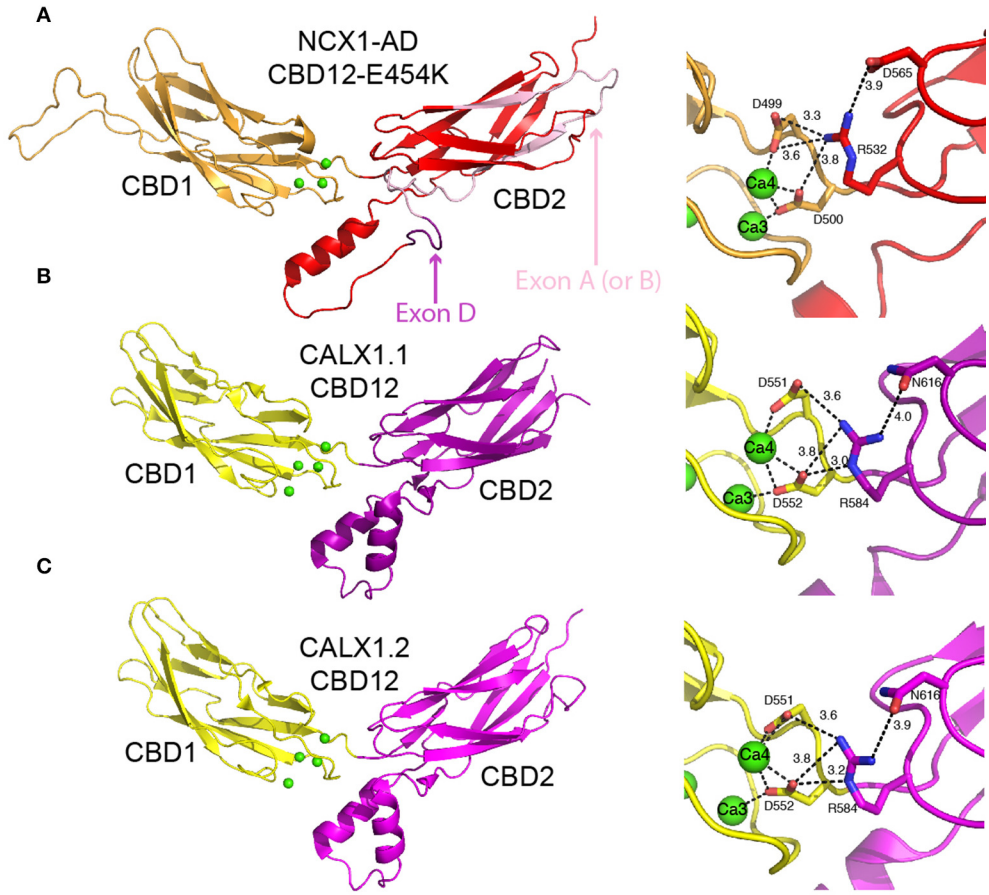

FIGURE 4 | Crystal structures of CBD12. Crystal structures of CBD12-E454K from NCX1-AD (PDB 3US9) **(A)**, CBD12 from CALX1.1 (PDB 3RB5) **(B)**, and CBD12 from CALX1.2 (PDB 3RB7) **(C)** in cartoon representation. Residues participating in the network of interdomain salt bridges are represented as sticks to the right of each structure, with the bond distances within the network indicated. In **(A)**, missing loops were constructed using MODELER. The region corresponding to the mutually exclusive exon is pink, whereas the cassette exon is purple, as indicated by the arrows.

of NCX1, occurring over several seconds (Hilgemann et al., 1992a).

CBDs Interact with H^+ and Mg^{2+}, But Not with Na^+

Eukaryotic NCX is extremely sensitive to cytosolic acidification (a pH decrease from 7.2 to 6.9 results in nearly 90% inactivation of NCX), thus demonstrating the physiological relevance of the NCX "proton block" under acidosis and ischemia conditions (Boyman et al., 2011). In general, H^+ may interact with the transport domains, although there is no evidence that within a physiological range of pHs the protons affect the ionization of the ion-binding transport sites. Recent studies in intact cardiomyocytes as well as on isolated preparations of CBD1, CBD2, and CBD12 proteins clearly demonstrated that Ca^{2+} and H^+ can compete with each other for binding to the functional CBD sites (Boyman et al., 2011). Notably, the close adjacency of the Ca^{2+} sites in the CBDs is consistent with the sharp dependence of Ca^{2+} binding on pH, thereby suggesting the cooperative nature of binding domain folding. Namely, the binding of the first Ca^{2+} ion may partially (or fully) deprotonate one or more coordinating residues, thereby enabling the next Ca^{2+} ion to bind to the remaining sites. A similar mechanism was proposed for the C_2 domain of phospholipase A2, in which two Ca^{2+} sites are separated by 4.1Å (Malmberg et al., 2004). The physiological significance of these findings is that acidic pH may shut down NCX in a very cooperative and effective way, and prevent NCX-mediated currents that impose a high risk for generating cardiac arrhythmias under ischemia/acidosis conditions.

In light of the fact that only three Ca^{2+} binding sites (Ca3, Ca4, and CaI) actually contribute to $[Ca^{2+}]$-dependent regulation of full-size NCX1 in the cellar system (Besserer et al., 2007; Ottolia et al., 2009), it is reasonable to ask what is the functional role of the remaining three low-affinity sites (K_d > 20 μM) (Boyman et al., 2009). Most probably, the low-affinity sites (Ca1, Ca2, and CaII) are Mg^{2+} rather than Ca^{2+} binding sites, which are constitutively occupied by Mg^{2+} under physiologically relevant ionic conditions (Boyman et al., 2009; Breukels et al., 2011; Giladi et al., 2013). Interestingly, the

occupation of the Ca1-Ca2 sites by Mg^{2+} decreases the affinity of the primary sensor (Ca3-Ca4 sites), whereas the occupation of the CaII site by Mg^{2+} increases the affinity of the CaI site (Boyman et al., 2009). The physiological significance of this could lie in keeping the primary and secondary Ca^{2+} sensors within a physiologically relevant range, thereby covering the effective concentration range of 0.2–10 μM Ca^{2+}.

Since Na^+-dependent regulation of NCX is abolished along with Ca^{2+}- and H^+- dependent regulation upon α-chymotrypsin treatment of NCX, one can hypothesize that Na^+, H^+, and Ca^{2+} compete over the same regulatory site. This possibility was examined by performing equilibrium Ca^{2+} binding and stopped-flow assays in buffers containing 100 mM choline chloride, 100 mM NaCl, or 100 mM KCl. No significant differences were observed in these experiments, excluding the possibility that Na^+ directly affects Ca^{2+} binding to CBDs (Boyman et al., 2009).

CBD Interactions in the Context of CBD12 Markedly Alter Ca^{2+} Sensing

As mentioned above, Ca^{2+} dissociation kinetics from either isolated CBD1 or CBD2 cannot account for the slow I_2-inactivation observed in intact NCX upon $[Ca^{2+}]_i$ removal. However, in the context of CBD12, the domains display markedly altered Ca^{2+} affinity and dissociation kinetics (Giladi et al., 2010). In NCX1-CBD12-AD, the CBD1 sites bind Ca^{2+} with ∼7–10 higher affinity compared with that observed in isolated CBD1 (Boyman et al., 2011; Giladi et al., 2012a). Strikingly, Ca^{2+} dissociates from the CBD1 Ca3-Ca4 sites in a bi-phasic (and not monophasic) fashion, with a fast component ($k_f \sim 5\ s^{-1}$) and a slow component ($k_s \sim 0.5\ s^{-1}$) (**Figure 3E**) (Giladi et al., 2010). The slow component, representing the occlusion of one Ca^{2+} ion, is a hallmark of domain interactions and closely matches the I_2-inactivation kinetics of NCX1-AD (Dyck et al., 1999). These interactions are dependent on the short interdomain linker, as either an elongation of the linker (by insertion of seven alanine residues) or the linker mutations abolish the domains' interactions (Giladi et al., 2010, 2012b). Similar observations were made for other NCX1-CBD12 splice variants (BD, ACDEF) and also for the CALX1-CBD12 splice variants (Hilge et al., 2009; Giladi et al., 2012a). However, alternative splicing of CBD2 modulates the domains' interactions, resulting in up to 10-fold differences in Ca^{2+} affinity and dissociation kinetics from CBD1 in the different CBD12 splice variants (Giladi et al., 2012a). These differences account for the differences in the I_2-inactivation kinetics observed in intact NCX. Thus, domain interactions are common among NCX orthologs and splice variants, but they are modulated in an ortholog and splice-variant dependent manner to meet physiological requirements.

STRUCTURAL BASIS FOR THE ALLOSTERIC REGULATION OF NCX PROTEINS

Crucial mechanistic questions that have emerged from the studies described above are as follows: (i) how does Ca^{2+} binding couple with regulatory conformational transitions to decode the allosteric signal, (ii) how is the regulatory signal diversified by alternative splicing, and (iii) how does the coupling of domains contribute to the transmission of regulatory information to ion transport domains. These questions were addressed using a variety of structural approaches, which are discussed below.

Crystal Structures of CBD12 Reveal the Ca^{2+}-Driven Structural Organization of a Highly Conserved Two-Domain Interphase

As an initial step to characterize the domains' interactions, the coupling of Ca^{2+} binding to conformational transitions underlying allosteric regulation, and the role played by alternative splicing, the crystal structures of CBD12-E454K (a mutant of NCX1-CBD12-AD), CALX1.1-CBD12, and CALX1.2-CBD12 were determined (**Figure 4**) (Wu et al., 2011; Giladi et al., 2012c). Intriguingly, the structures show striking overall similarity despite the different regulatory responses of the corresponding exchangers. The interface has a fairly small surface area (∼ 350 Å in CBD12-E454K), explaining the need for a short interdomain linker to allow the domains to interact (Giladi et al., 2012c). In NCX1, the most important feature of the interface is a network of salt bridges, centered at R532 from CBD2. R532 forms bifurcated salt bridges with D565 of CBD2, on the one hand, and with D499 and D500 at the Ca3-Ca4 sites of CBD1, on the other hand (**Figure 4A**). Importantly, D499 and D500 also coordinate Ca^{2+} at the Ca3-Ca4 sites. Thus, the interdomain salt bridges stabilize Ca^{2+} binding, resulting in Ca^{2+} occlusion at the interface. In return, Ca^{2+} binding to the Ca3-Ca4 sites stabilizes the interface, resulting in the coupling of Ca^{2+} binding to signal transmission through CBD2 to the membrane domains. This is supported by the fact that D499 and D500 are disordered in the apo form (Hilge et al., 2006), making Ca^{2+} binding essential for robust interdomain interactions. The structural role of Ca^{2+} is also suggested by the fact that the Ca3-Ca4 sites are completely buried in the interface. Finally, mutation of the central residue in the mentioned network, R532, abolishes Ca^{2+} occlusion and bi-phasic dissociation kinetics (Giladi et al., 2012c). Similar networks exist in CALX1.1 and CALX1.2, although an Asn residue is found in the position corresponding to D565 (**Figures 4B,C**).

Based on the crystal structures of the CALX1 splice variants, regulatory differences were attributed to the different hinge angles between the CBDs (118° and 110.5° for CALX1.1 and CALX1.2, respectively; Wu et al., 2011). However, this interpretation has been challenged by the crystal structure of CBD12-E454K, in which the hinge angle (117.4°) is nearly identical to that of CALX1.1 (Giladi et al., 2012c). These findings are especially interesting in the context of the regulatory differences in these variants, since NCX1 is activated by regulatory Ca^{2+}, whereas CALX1.1 is inhibited by allosteric interactions with Ca^{2+} (**Figure 2**). Notably, the alternatively spliced region is not directly involved in the interface of either of the examined CBD12 constructs (**Figure 4A**). Thus, the structural similarities between CBD12 from NCX and CALX imply that the different responses to regulatory Ca^{2+} cannot be attributed solely to the CBDs' orientation in the CBD12 tandem.

The sequence conservation of the two-domain interface and the structural similarities between the mentioned structures point to a general mechanism for regulating the NCX family (Giladi et al., 2012c). Importantly, the architecture of this interface differs from that of tandem Ca^{2+}-binding C_2 domains (e.g., of synaptotagmin and PKC) (Stahelin et al., 2005), implying a different mode of action. However, CBD12 shares a striking similarity with the cadherin extracellular domain, which bears multiple β-sandwich domains bridged by small interfaces, and which contains three Ca^{2+} sites. Cadherin undergoes Ca^{2+}-dependent rigidification (Häussinger et al., 2002), enabling cell-cell interactions. This supports the importance of stabilizing the domains' interactions by Ca^{2+} binding to the Ca3-Ca4 sites in the allosteric regulation of NCX. Nevertheless, the Ca^{2+} binding modes of cadherins and CBD12 are dissimilar. Namely, Ca^{2+} binding to the two-domain cadherin construct involves direct interactions with residues in the linker region, whereas the binding of Ca^{2+} to sites Ca3 and Ca4 in CBD1 involves ligation with residues 498–500 that directly precede the CBD12 linker.

SAXS Reveals a Ca^{2+}-Dependent Population Shift in CBD12

The crystallographic structures of CBD12 provided insight into the domains' interactions in the Ca^{2+}-bound state in atomic details. However, it is merely a snapshot, although in high resolution, of a dynamic protein. To assess the effect of ligand binding on CBD12, we utilized SAXS, which provides time- and space-averaged information regarding the protein conformation in solution, although in low resolution (10–20 Å) (Bernadó et al., 2007; Blanchet and Svergun, 2013). The data were analyzed using the ensemble optimization method (EOM), which fits the average theoretical scattering intensity from an ensemble of possible conformations (selected from a pool of random conformations) suitable to the experimental SAXS data (Bernadó et al., 2007).

Two splice variants of NCX1-CBD12 (AD, BD) were examined (Giladi et al., 2013). Whereas the global structural parameters (e.g., the maximal intramolecular distance, the radius of gyration) were largely similar in the apo- and the Ca^{2+}-bound forms, the EOM analysis revealed strikingly different conformational distributions (**Figures 5A,B**). That is, in the apo state CBD12 exhibits a wide range of conformations, whereas Ca^{2+} binding narrows the conformational distribution in line with a population-shift mechanism. According to these data, Ca^{2+} binding to the Ca3-Ca4 sites results in a population shift, where more constrained conformational states become highly populated at a dynamic equilibrium in the absence of global conformational transitions in CBD alignment (Giladi et al., 2013). This seems to be true for all the examined splice variants. In addition, the conformational distributions of CBD12 from CALX1.1 and CALX1.2 in the Ca^{2+}-bound state are nearly identical to those of the NCX1-CBD12 tandems examined (**Figure 5C**). These results are in line with Ca^{2+}-dependent domains' rigidification, and are in agreement with NMR studies of NCX1-CBD12-AD (Salinas et al., 2011). Notably, this is specifically a Ca^{2+}-switch rather than an electrostatic switch, since Mg^{2+} cannot impose a population shift (Giladi et al., 2013). Moreover, a population shift is also observed in the CBD12-E454K mutant, which has partial charge neutralization in the apo form (Giladi et al., 2013).

The crystallographic and SAXS data presented thus far suggested common Ca^{2+} dependent interactions between the domains. Although these data are highly important for understanding the allosteric signal propagation between the domains, it remains unclear how the allosteric signal is diversified and propagated in the different splice variants and orthologs. Two possibilities were raised: (i) additional structural elements in the regulatory f-loop and/or membrane domain are involved in decoding and specifying the regulatory effects or alternatively, (ii) the conformational dynamics differ between the NCX splice variants and CALX, despite the similar orientations observed in the crystal structures and the SAXS-EOM data obtained for diverse splice variants, because there are either positive, negative, or no responses to regulatory Ca^{2+}.

HDX-MS Reveals the Structure-Dynamic Basis of Diverse NCX Regulation

To test the possibility that dynamic interactions between the two domains underlie the differential responses to regulatory Ca^{2+}, CBD12 from NCX1-AD (positive response), CALX1.1 (negative response), and CALX1.2 (no response) were studied using the advanced approaches of HDX-MS (Giladi et al., 2015). In general, HDX-MS measures the exchange rates of peptide amide hydrogen with deuterium in the solvent. In folded proteins, the exchange rate varies, depending on the position of the amide hydrogen. The secondary structure, flexibility, and the dynamics of the protein conformation affect the deuterium uptake level. HDX was measured in the presence and absence of Ca^{2+} to study the structural outcomes of binding in the differentially regulated isoforms.

CBDs also Interact in the Absence of Ca^{2+}

To study the domains' interactions in the apo form, HDX-MS was used to study NCX1-CBD12-AD and its mutant, CBD12-F450G. F450 is a central residue in the hydrophobic core of the domains' interface (Giladi et al., 2012c) and the F450G mutation results in the domains' uncoupling, as reflected by the decreased Ca^{2+} affinity and the lack of Ca^{2+} occlusion (Giladi et al., 2015). The HDX-MS analysis revealed that in the uncoupled mutant, CBD1 is less stable in the apo form compared with WT NCX1-CBD12-AD. Thus, the domains' interactions in the apo form stabilize CBD1; however, this stabilization is interrupted by the uncoupling effect of F450. This may explain some of the Ca^{2+} binding properties of CBD12. The domains' interactions result in ∼50-fold slower dissociation kinetics of the occluded Ca^{2+} ion from CBD1, but the affinity is only ∼7-fold increased, implying ∼7-fold reduction in the association kinetics ($K_d = k_{off}/k_{on}$) (Giladi et al., 2010, 2012a; Boyman et al., 2011). As mentioned above, the isolated CBD1 binding sites are disordered in the absence of Ca^{2+} (Hilge et al., 2006; Wu et al., 2010). The stabilization of the apo form may reduce the Gibbs free energy (ΔG) for the disorder-to-order transition upon Ca^{2+} binding, thereby making the binding less favorable, due to the reduced values of k_{on}.

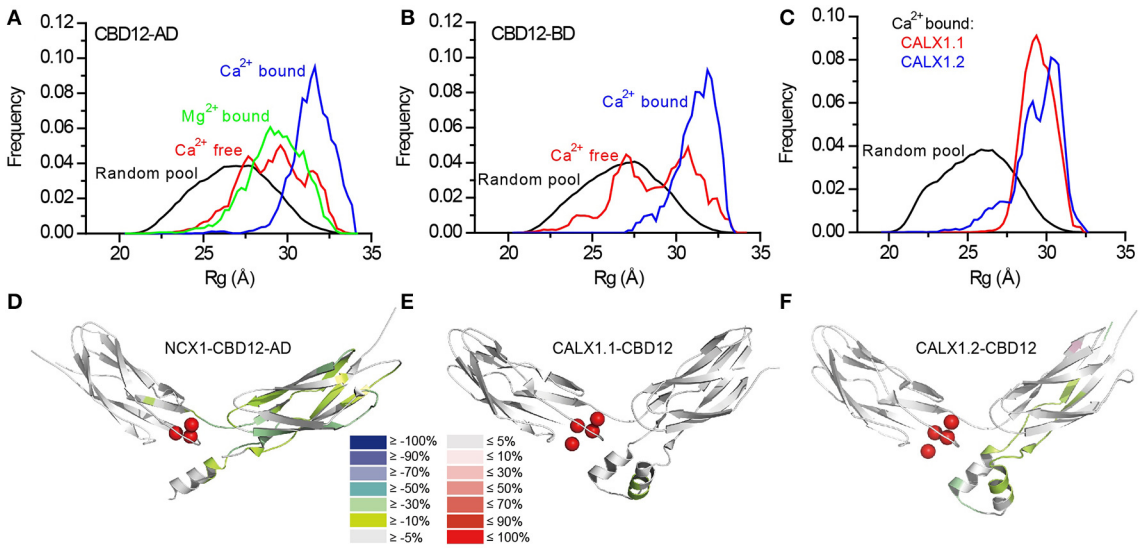

FIGURE 5 | SAXS-EOM analysis and HDX-MS of NCX orthologs and splice variants. Random R_g pools and selected EOM ensemble distributions for CBD12-AD **(A)**, CBD12-BD **(B)**, and Ca^{2+}-bound CALX1.1 and CALX1.2 CBD12 **(C)**. The difference between the HDX profiles of the apo and Ca^{2+}-bound forms of NCX1-CBD12-AD at 10.000 s exchange time **(D)**, CALX1.1-CBD12 at 100 s exchange time **(E)**, and CALX1.2-CBD12 at 100s exchange time **(F)** are overlaid onto the crystal structures of the different CBD12 proteins (PDB 3US9, 3RB5, and 3RB7, respectively). Ca^{2+} is indicated as red spheres. The color legend shows the differential HDX after Ca^{2+} binding.

Alternative Splicing Modifies the Domains' Coupling

Although the alternative splicing region of CBD2 is not directly involved in the interface, it clearly affects the domains' interactions as suggested by the equilibrium binding, kinetics, and HDX-MS assays (Giladi et al., 2012a, 2015). The helical region on CBD2, adjacent to the CBD1 binding sites, is similar for NCX1-CBD12-AD, and CALX1.2-CBD12, encompassing an additional turn as compared with CALX1.1-CBD12 (**Figures 5D–F**). The presence of this turn is thus dependent on the adjacent alternative splicing segment in the CALX1 splice variants. The additional helical turn exhibits reduced deuterium uptake upon Ca^{2+} binding in both NCX1-CBD12-AD (**Figure 5D**) and CALX1.2-CBD12 (**Figure 5F**) and the lack of this turn in CALX1.1-CBD12 may interfere with the stabilization of the interface by Ca^{2+} (**Figure 5E**). Thus, although not directly participating in the interface, the alternative-splicing segment can indirectly influence the domains' coupling, resulting in regulatory diversity.

Structural Dynamics Correlate with the Regulatory Response to Ca^{2+}

In all the constructs examined by HDX-MS, Ca^{2+} binding resulted in backbone rigidification of CBD2, as reflected by a decreased deuterium uptake (**Figures 5D–F**). The rigidification of CBD2 cannot be fully attributed to Ca^{2+} binding at CBD2, since the CALX splice variants bind Ca^{2+} only at CBD1 (Wu et al., 2009; Giladi et al., 2012a). Moreover, the uncoupling of the F450G mutation at CBD1 results in less Ca^{2+}-dependent rigidification of the main chain in CBD2. These results indicate that Ca^{2+} binding to CBD1 is sensed at CBD2. However, the extent and intensity of the Ca^{2+}-induced rigidification occur at varying degrees in distinct splice variants (**Figures 5D–F**). Most importantly, the Ca^{2+}-induced decrease in HDX at CBD2 upon Ca^{2+} binding correlates with regulatory specificity (negative, positive, or no response to Ca^{2+}) in a given splice variant. For CALX1.1-CBD12, in which a minimal response to Ca^{2+} occurs (**Figure 5E**), the exchanger remains inhibited. For NCX1-CBD12-AD, in which the maximal response to Ca^{2+} occurs (**Figure 5D**), the exchanger is activated; an intermediate phenotype (no response) is observed for CALX1.2-CBD12 (**Figure 5E**), which also exhibits intermediate HDX changes in response to Ca^{2+}. These data support the notion that the stabilization of CBD2 dynamics is involved in allosteric regulation in a splice variant-dependent manner. Further HDX-MS studies using NCX-CBD12 isoforms and splice variants will delineate the specific roles of individual exons in tissue-specific splice variants of NCX (Khananshvili, 2013, 2014).

IMPLICATIONS FOR NCX-SPECIFIC DRUG DESIGN

Since NCX participates in numerous physiological and pathophysiological processes (Blaustein and Lederer, 1999; Lytton, 2007; Khananshvili, 2013), developing specific drugs for NCX variants is highly desired. However, drugs that directly affect NCX are not currently clinically available. The major structural advancements described above may facilitate the development of appropriate drug candidates. The crystal structures of CBD12 can provide a framework for structure-based computational screening, in which small molecules are ranked on the basis of docking to protein structures (Kitchen

et al., 2004; Taboureau et al., 2012). This method allows the screening of enormous compound databases. Drugs targeting the CBDs, rather than the ion translocation sites, have the potential to efficiently target tissue-specific NCX variants since the alternative splicing region of NCX lies within CBD2 (Hilge et al., 2006). More specifically, drugs targeting the domains' interface, adjacent to the alternative splicing region, are of particular interest. These drugs can potentially enhance NCX activity via domain stabilization or inhibit NCX by disrupting the domains' interactions. The stabilizing or destabilizing effects of specific compounds can be further tested using the structural methods described above (SAXS-EOM, HDX-MS).

CONCLUSIONS

Recent structural and biophysical studies have shed light on the structural basis of ion transport and the allosteric regulation of NCX proteins. The structure of NCX_Mj (Liao et al., 2012), along with MD simulations and ion-flux analyses (Marinelli et al., 2014), verified the exchange mechanism and stoichiometry and provided important clues regarding the molecular basis of NCX ion selectivity (**Figure 1**). Structural and biochemical studies of the regulatory CBD12 tandem by a variety of techniques revealed some features that are common among all NCX orthologs and splice variants (Giladi et al., 2012c, 2013). These common features can be modulated in different NCX orthologs, isoforms, and splice variants to meet tissue-specific physiological demands (Giladi et al., 2012a, 2015). CBD1 and CBD2 interact in the context of CBD12 (**Figure 4**; Giladi et al., 2010), resulting in the increased affinity of the CBD1 binding sites and in Ca^{2+} occlusion (**Figure 3E**) (Boyman et al., 2011; Giladi et al., 2012a); the extent of these effects depends on the specific ortholog or splice variant examined (**Figures 5D–F**). Common and conserved interdomain interactions underlie this phenomenon, as demonstrated by X-ray crystallography and SAXS (**Figures 4**, **5A–C**; Giladi et al., 2012c, 2013). The binding of Ca^{2+} to the primary sensor (Ca3-Ca4 sites) in CBD1 rigidifies CBD12, whereas the domains' interactions in turn stabilize Ca^{2+} binding, resulting in Ca^{2+}-dependent regulation. This represents a common mechanism for decoding the initial information upon Ca^{2+} binding for all NCX isoform/splice variants. The CaI site on CBD2 exhibits structural variances, while being responsible for the Ca^{2+}-dependent alleviation of Na^{+}-dependent inactivation (Hilge et al., 2009). The structural basis for the diverse regulatory responses to Ca^{2+} binding in different orthologs and splice variants is related to the extent and strength of CBD2 rigidification upon Ca^{2+} binding to CBD1 (**Figures 5D–F**; Giladi et al., 2015). It is hoped that breakthroughs in understanding the structure-function relationships in NCX proteins will allow for the future pharmaceutical development of tissue-selective NCX-directed drugs.

AUTHOR CONTRIBUTIONS

All authors listed, have made substantial, direct and intellectual contribution to the work, and approved it for publication.

ACKNOWLEDGMENTS

This work was partially funded by the USA-Israel Binational Foundation Research Grant # 2009-334, and the Israel Science Foundation Grant #825/14. The support of the Fields Estate Foundation is highly appreciated.

REFERENCES

Bernadó, P., Mylonas, E., Petoukhov, M. V., Blackledge, M., and Svergun, D. I. (2007). Structural characterization of flexible proteins using small-angle X-ray scattering. *J. Am. Chem. Soc.* 129, 5656–5664. doi: 10.1021/ja069124n

Berridge, M. J., Bootman, M. D., and Roderick, H. L. (2003). Calcium signalling: dynamics, homeostasis and remodelling. *Nat. Rev. Mol. Cell Biol.* 4, 517–529. doi: 10.1038/nrm1155

Bers, D. M. (2002). Cardiac excitation-contraction coupling. *Nature* 415, 198–205. doi: 10.1038/415198a

Besserer, G. M., Ottolia, M., Nicoll, D. A., Chaptal, V., Cascio, D., Philipson, K. D., et al. (2007). The second Ca^{2+}-binding domain of the Na^{+} Ca^{2+} exchanger is essential for regulation: crystal structures and mutational analysis. *Proc. Natl. Acad. Sci. U.S.A.* 104, 18467–18472. doi: 10.1073/pnas.0707417104

Blanchet, C. E., and Svergun, D. I. (2013). Small-angle X-ray scattering on biological macromolecules and nanocomposites in solution. *Annu. Rev. Phys. Chem.* 64, 37–54. doi: 10.1146/annurev-physchem-040412-110132

Blaustein, M. P., and Lederer, W. J. (1999). Sodium/calcium exchange: its physiological implications. *Physiol. Rev.* 79, 763–854.

Boyman, L., Hagen, B. M., Giladi, M., Hiller, R., Lederer, W. J., and Khananshvili, D. (2011). Proton-sensing Ca^{2+} binding domains regulate the cardiac Na^{+}/Ca^{2+} exchanger. *J. Biol. Chem.* 286, 28811–28820. doi: 10.1074/jbc.M110.214106

Boyman, L., Mikhasenko, H., Hiller, R., and Khananshvili, D. (2009). Kinetic and equilibrium properties of regulatory calcium sensors of NCX1 protein. *J. Biol. Chem.* 284, 6185–6193. doi: 10.1074/jbc.M809012200

Breukels, V., Konijnenberg, A., Nabuurs, S. M., Touw, W. G., and Vuister, G. W. (2011). The second Ca^{2+}-binding domain of NCX1 binds Mg^{2+} with high affinity. *Biochemistry* 50, 8804–8812. doi: 10.1021/bi201134u

Brini, M., Calì, T., Ottolini, D., and Carafoli, E. (2014). The plasma membrane calcium pump in health and disease. *FEBS J.* 280, 5385–5397. doi: 10.1111/febs.12193

Carafoli, E. (1987). Intracellular calcium homeostasis. *Annu. Rev. Biochem.* 56, 395–433. doi: 10.1146/annurev.bi.56.070187.002143

DiPolo, R. (1979). Calcium influx in internally dialyzed squid giant axons. *J. Gen. Physiol.* 73, 91–113. doi: 10.1085/jgp.73.1.91

Dyck, C., Omelchenko, A., Elias, C. L., Quednau, B. D., Philipson, K. D., Hnatowich, M., et al. (1999). Ionic regulatory properties of brain and kidney splice variants of the NCX1 Na^{+}-Ca^{2+} exchanger. *J. Gen. Physiol.* 114, 701–711. doi: 10.1085/jgp.114.5.701

Filadi, R., and Pozzan, T. (2015). Generation and functions of second messengers microdomains. *Cell Calcium* 58, 405–414. doi: 10.1016/j.ceca.2015.03.007

Gifford, J. L., Walsh, M. P., and Vogel, H. J. (2007). Structures and metal-ion-binding properties of the Ca^{2+}-binding helix-loop-helix EF-hand motifs. *Biochem. J.* 405, 199–221. doi: 10.1042/BJ20070255

Giladi, M., Bohbot, H., Buki, T., Schulze, D. H., Hiller, R., and Khananshvili, D. (2012a). Dynamic features of allosteric Ca^{2+} sensor in tissue-specific NCX variants. *Cell Calcium* 51, 478–485. doi: 10.1016/j.ceca.2012.04.007

Giladi, M., Boyman, L., Mikhasenko, H., Hiller, R., and Khananshvili, D. (2010). Essential role of the CBD1-CBD2 linker in slow dissociation of Ca^{2+} from the regulatory two-domain tandem of NCX1. *J. Biol. Chem.* 285, 28117–28125. doi: 10.1074/jbc.M110.127001

Giladi, M., Friedberg, I., Fang, X., Hiller, R., Wang, Y. X., and Khananshvili, D. (2012b). G503 is obligatory for coupling of regulatory domains in NCX proteins. *Biochemistry* 51, 7313–7320. doi: 10.1021/bi300739z

Giladi, M., Hiller, R., Hirsch, J. A., and Khananshvili, D. (2013). Population shift underlies Ca^{2+}-induced regulatory transitions in the sodium-calcium exchanger (NCX). *J. Biol. Chem.* 288, 23141–23149. doi: 10.1074/jbc.M113.471698

Giladi, M., Lee, S. Y., Hiller, R., Chung, K. Y., and Khananshvili, D. (2015). Structure-dynamic determinants governing a mode of regulatory response and propagation of allosteric signal in splice variants of Na^+/Ca^{2+} exchange (NCX) proteins. *Biochem. J.* 465, 489–501. doi: 10.1042/BJ20141036

Giladi, M., Sasson, Y., Fang, X., Hiller, R., Buki, T., Wang, Y. X., et al. (2012c). A common Ca^{2+}-driven interdomain module governs eukaryotic NCX regulation. *PLoS ONE* 7:e39985. doi: 10.1371/journal.pone.0039985

Häussinger, D., Ahrens, T., Sass, H. J., Pertz, O., Engel, J., and Grzesiek, S. (2002). Calcium-dependent homoassociation of E-cadherin by NMR spectroscopy: changes in mobility, conformation and mapping of contact regions. *J. Mol. Biol.* 324, 823–839. doi: 10.1016/S0022-2836(02)01137-3

Hilge, M. (2012). Ca^{2+} regulation of ion transport in the Na^+/Ca^{2+} exchanger. *J. Biol. Chem.* 287, 31641–31649. doi: 10.1074/jbc.R112.353573

Hilge, M., Aelen, J., Foarce, A., Perrakis, A., and Vuister, G. W. (2009). Ca^{2+} regulation in the Na^+/Ca^{2+} exchanger features a dual electrostatic switch mechanism. *Proc. Natl. Acad. Sci. U.S.A.* 106, 14333–14338. doi: 10.1073/pnas.0902171106

Hilge, M., Aelen, J., and Vuister, G. W. (2006). Ca^{2+} regulation in the Na^+/Ca^{2+} exchanger involves two markedly different Ca^{2+} sensors. *Mol. Cell* 22, 15–25. doi: 10.1016/j.molcel.2006.03.008

Hilgemann, D. W. (1990). Regulation and deregulation of cardiac Na^+-Ca^{2+} exchange in giant excised sarcolemmal membrane patches. *Nature* 344, 242–245. doi: 10.1038/344242a0

Hilgemann, D. W., Collins, A., and Matsuoka, S. (1992a). Steady-state and dynamic properties of cardiac sodium-calcium exchange. Secondary modulation by cytoplasmic calcium and ATP. *J. Gen. Physiol.* 100, 933–961. doi: 10.1085/jgp.100.6.933

Hilgemann, D. W., Matsuoka, S., Nagel, G. A., and Collins, A. (1992b). Steady-state and dynamic properties of cardiac sodium-calcium exchange. Sodium-dependent inactivation. *J. Gen. Physiol.* 100, 905–932. doi: 10.1085/jgp.100.6.905

Hilgemann, D. W., Nicoll, D. A., and Philipson, K. D. (1991). Charge movement during Na^+ translocation by native and cloned cardiac Na^+/Ca^{2+} exchanger. *Nature* 352, 715–718. doi: 10.1038/352715a0

Hryshko, L. V., Matsuoka, S., Nicoll, D. A., Weiss, J. N., Schwarz, E. M., Benzer, S., et al. (1996). Anomalous regulation of the Drosophila Na^+-Ca^{2+} exchanger by Ca^{2+}. *J. Gen. Physiol.* 108, 67–74. doi: 10.1085/jgp.108.1.67

Khananshvili, D. (1990). Distinction between the two basic mechanisms of cation transport in the cardiac Na^+-Ca^{2+} exchange system. *Biochemistry* 29, 2437–2442. doi: 10.1021/bi00462a001

Khananshvili, D. (2013). The SLC8 gene family of sodium-calcium exchangers (NCX) - structure, function, and regulation in health and disease. *Mol. Aspects Med.* 34, 220–235. doi: 10.1016/j.mam.2012.07.003

Khananshvili, D. (2014). Sodium-calcium exchangers (NCX): molecular hallmarks underlying the tissue-specific and systemic functions. *Pflugers Arch.* 466, 43–60. doi: 10.1007/s00424-013-1405-y

Kitchen, D. B., Decornez, H., Furr, J. R., and Bajorath, J. (2004). Docking and scoring in virtual screening for drug discovery: methods and applications. *Nat. Rev. Drug Discov.* 3, 935–949. doi: 10.1038/nrd1549

Kofuji, P., Lederer, W. J., and Schulze, D. H. (1994). Mutually exclusive and cassette exons underlie alternatively spliced isoforms of the Na/Ca exchanger. *J. Biol. Chem.* 269, 5145–5149.

Li, Z., Nicoll, D. A., Collins, A., Hilgemann, D. W., Filoteo, A. G., Penniston, J. T., et al. (1991). Identification of a peptide inhibitor of the cardiac sarcolemmal Na^+-Ca^{2+} exchanger. *J. Biol. Chem.* 266, 1014–1020.

Liao, J., Li, H., Zeng, W., Sauer, D. B., Belmares, R., and Jiang, Y. (2012). Structural insight into the ion-exchange mechanism of the sodium/calcium exchanger. *Science* 335, 686–690. doi: 10.1126/science.1215759

Lytton, J. (2007). Na^+/Ca^{2+} exchangers: three mammalian gene families control Ca^{2+} transport. *Biochem. J.* 406, 365–382. doi: 10.1042/BJ20070619

Malmberg, N. J., Varma, S., Jakobsson, E., and Falke, J. J. (2004). Ca^{2+} activation of the cPLA2 C_2 domain: ordered binding of two Ca^{2+} ions with positive cooperativity. *Biochemistry* 43, 16320–16328. doi: 10.1021/bi0482405

Marinelli, F., Almagor, L., Hiller, R., Giladi, M., Khananshvili, D., and Faraldo-Gómez, J. D. (2014). Sodium recognition by the Na^+/Ca^{2+} exchanger in the outward-facing conformation. *Proc. Natl. Acad. Sci. U.S.A.* 111, E5354–E5362. doi: 10.1073/pnas.1415751111

Matsuoka, S., and Hilgemann, D. W. (1994). Inactivation of outward Na^+-Ca^{2+} exchange current in guinea-pig ventricular myocytes. *J. Physiol. (Lond).* 476, 443–458. doi: 10.1113/jphysiol.1994.sp020146

Matsuoka, S., Nicoll, D. A., He, Z., and Philipson, K. D. (1997). Regulation of cardiac Na^+-Ca^{2+} exchanger by the endogenous XIP region. *J. Gen. Physiol.* 109, 273–286. doi: 10.1085/jgp.109.2.273

Matsuoka, S., Nicoll, D. A., Hryshko, L. V., Levitsky, D. O., Weiss, J. N., and Philipson, K. D. (1995). Regulation of the cardiac Na^+-Ca^{2+} exchanger by Ca^{2+}. Mutational analysis of the Ca^{2+}-binding domain. *J. Gen. Physiol.* 105, 403–420. doi: 10.1085/jgp.105.3.403

Matsuoka, S., Nicoll, D. A., Reilly, R. F., Hilgemann, D. W., and Philipson, K. D. (1993). Initial localization of regulatory regions of the cardiac sarcolemmal Na^+-Ca^{2+} exchanger. *Proc. Natl. Acad. Sci. U.S.A.* 90, 3870–3874. doi: 10.1073/pnas.90.9.3870

Melzer, W., Herrmann-Frank, A., and Lüttgau, H. C. (1995). The role of Ca^{2+} ions in excitation-contraction coupling of skeletal muscle fibres. *Biochim. Biophys. Acta* 1241, 59–116. doi: 10.1016/0304-4157(94)00014-5

Neher, E., and Sakaba, T. (2008). Multiple roles of calcium ions in the regulation of neurotransmitter release. *Neuron* 59, 861–872. doi: 10.1016/j.neuron.2008.08.019

Nicoll, D. A., Sawaya, M. R., Kwon, S., Cascio, D., Philipson, K. D., and Abramson, J. (2006). The crystal structure of the primary Ca^{2+} sensor of the Na^+/Ca^{2+} exchanger reveals a novel Ca^{2+} binding motif. *J. Biol. Chem.* 281, 21577–21581. doi: 10.1074/jbc.C600117200

Niggli, E., and Lederer, W. J. (1991). Molecular operations of the sodium-calcium exchanger revealed by conformation currents. *Nature* 349, 621–624. doi: 10.1038/349621a0

Nishizawa, T., Kita, S., Maturana, A. D., Furuya, N., Hirata, K., Kasuya, G., et al. (2013). Structural basis for the counter-transport mechanism of a H^+/Ca^{2+} exchanger. *Science* 341, 168–172. doi: 10.1126/science.1239002

Omelchenko, A., Dyck, C., Hnatowich, M., Buchko, J., Nicoll, D. A., Philipson, K. D., et al. (1998). Functional differences in ionic regulation between alternatively spliced isoforms of the Na^+-Ca^{2+} exchanger from *Drosophila melanogaster*. *J. Gen. Physiol.* 111, 691–702. doi: 10.1085/jgp.111.5.691

Orrenius, S., Zhivotovsky, B., and Nicotera, P. (2003). Regulation of cell death: the calcium-apoptosis link. *Nat. Rev. Mol. Cell Biol.* 4, 552–565. doi: 10.1038/nrm1150

Ottolia, M., Nicoll, D. A., and Philipson, K. D. (2009). Roles of two Ca^{2+}-binding domains in regulation of the cardiac Na^+-Ca^{2+} exchanger. *J. Biol. Chem.* 284, 32735–32741. doi: 10.1074/jbc.M109.055434

Philipson, K. D., and Nicoll, D. A. (2000). Sodium-calcium exchange: a molecular perspective. *Annu. Rev. Physiol.* 62, 111–133. doi: 10.1146/annurev.physiol.62.1.111

Quednau, B. D., Nicoll, D. A., and Philipson, K. D. (1997). Tissue specificity and alternative splicing of the Na^+/Ca^{2+} exchanger isoforms NCX1, NCX2, and NCX3 in rat. *Am. J. Physiol.* 272, C1250–C1261.

Reeves, J. P., and Hale, C. C. (1984). The stoichiometry of the cardiac sodium-calcium exchange system. *J. Biol. Chem.* 259, 7733–7739.

Ren, X., and Philipson, K. D. (2013). The topology of the cardiac Na^+/Ca^{2+} exchanger, NCX1. *J. Mol. Cell. Cardiol.* 57, 68–71. doi: 10.1016/j.yjmcc.2013.01.010

Salinas, R. K., Bruschweiler-Li, L., Johnson, E., and Brüschweiler, R. (2011). Ca^{2+} binding alters the interdomain flexibility between the two cytoplasmic calcium-binding domains in the Na^+/Ca^{2+} exchanger. *J. Biol. Chem.* 286, 32123–32131. doi: 10.1074/jbc.M111.249268

Schwarz, E. M., and Benzer, S. (1997). Calx, a Na-Ca exchanger gene of *Drosophila melanogaster*. *Proc. Natl. Acad. Sci. U.S.A.* 94, 10249–10254. doi: 10.1073/pnas.94.19.10249

Stahelin, R. V., Wang, J., Blatner, N. R., Rafter, J. D., Murray, D., and Cho, W. (2005). The origin of C1A-C_2 interdomain interactions in protein kinase Calpha. *J. Biol. Chem.* 280, 36452–36463. doi: 10.1074/jbc.M506224200

Taboureau, O., Baell, J. B., Fernández-Recio, J., and Villoutreix, B. O. (2012). Established and emerging trends in computational drug discovery in the structural genomics era. *Chem. Biol.* 19, 29–41. doi: 10.1016/j.chembiol.2011.12.007

Waight, A. B., Pedersen, B. P., Schlessinger, A., Bonomi, M., Chau, B. H., Roe-Zurz, Z., et al. (2013). Structural basis for alternating access of a eukaryotic calcium/proton exchanger. *Nature* 499, 107–110. doi: 10.1038/nature12233

Williams, R. J. P. (1999). "Calcium: the developing role of its chemistry in biological evolution," in *Calcium as a Cellular Regulator*, eds E. Carafoli and C. Klee (New York, NY: Oxford University Press), 3–27.

Wu, M., Le, H. D., Wang, M., Yurkov, V., Omelchenko, A., Hnatowich, M., et al. (2010). Crystal structures of progressive Ca^{2+} binding states of the Ca^{2+} sensor Ca^{2+} binding domain 1 (CBD1) from the CALX Na^{+}/Ca^{2+} exchanger reveal incremental conformational transitions. *J. Biol. Chem.* 285, 2554–2561. doi: 10.1074/jbc.M109.059162

Wu, M., Tong, S., Gonzalez, J., Jayaraman, V., Spudich, J. L., and Zheng, L. (2011). Structural basis of the Ca^{2+} inhibitory mechanism of Drosophila Na^{+}/Ca^{2+} exchanger CALX and its modification by alternative splicing. *Structure* 19, 1509–1517. doi: 10.1016/j.str.2011.07.008

Wu, M., Wang, M., Nix, J., Hryshko, L. V., and Zheng, L. (2009). Crystal structure of CBD2 from the Drosophila Na^{+}/Ca^{2+} exchanger: diversity of Ca^{2+} regulation and its alternative splicing modification. *J. Mol. Biol.* 387, 104–112. doi: 10.1016/j.jmb.2009.01.045

Conflict of Interest Statement: The authors declare that the research was conducted in the absence of any commercial or financial relationships that could be construed as a potential conflict of interest.

frontiers in Physiology

MINI REVIEW
published: 18 December 2015
doi: 10.3389/fphys.2015.00386

Molecular Mechanism Underlying the Plant NRT1.1 Dual-Affinity Nitrate Transporter

Ji Sun[1*†] *and Ning Zheng*[1,2*]

[1] *Department of Pharmacology, University of Washington, Seattle, WA, USA,* [2] *Howard Hughes Medical Institute, University of Washington, Seattle, WA, USA*

Nitrate (NO_3^-) is one of the most important sources of mineral nitrogen, which also serves as a key signaling molecule for plant growth and development. To cope with nitrate fluctuation in soil that varies by up to four orders of magnitude, plants have evolved high- and low-affinity nitrate transporter systems, consisting of distinct families of transporters. Interestingly, the first cloned nitrate transporter in *Arabidopsis*, NRT1.1 functions as a dual-affinity transporter, which can change its affinity for nitrate in response to substrate availability. Phosphorylation of a threonine residue, Thr101, switches NRT1.1 from low- to high-affinity state. Recent structural studies have unveiled that the unmodified NRT1.1 transporter works as homodimers with Thr101 located in close proximity to the dimer interface. Modification on the Thr101 residue is shown to not only decouple the dimer configuration, but also increase structural flexibility, thereby, altering the substrate affinity of NRT1.1. The structure of NRT1.1 helps establish a novel paradigm in which protein oligomerzation and posttranslational modification can synergistically expand the functional capacity of the major facilitator superfamily (MFS) transporters.

Keywords: NRT1.1, dimer, dual-affinity, nitrate transporter, major facilitator superfamily, transceptor

OPEN ACCESS

Edited by:
Mario L. Diaz,
Universidad de La Laguna, Spain

Reviewed by:
Gabriel Krouk,
Centre National de la Recherche Scientifique, France
Eiji Nambara,
University of Toronto, Canada
Maria Isabel Bahamonde Santos,
Pompeu Fabra University, Spain

***Correspondence:**
Ji Sun
jsun@mail.rockefeller.edu;
Ning Zheng
nzheng@u.washington.edu

†Present Address:
Ji Sun,
Laboratory of Molecular Neurobiology and Biophysics, The Rockefeller University, New York, NY, USA

Specialty section:
This article was submitted to Membrane Physiology and Membrane Biophysics, a section of the journal Frontiers in Physiology

Received: *23 October 2015*
Accepted: *30 November 2015*
Published: *18 December 2015*

Citation:
Sun J and Zheng N (2015) Molecular Mechanism Underlying the Plant NRT1.1 Dual-Affinity Nitrate Transporter. Front. Physiol. 6:386. doi: 10.3389/fphys.2015.00386

INTRODUCTION

Nitrate (NO_3^-) is critical for plants, both as a primary nutrient and as an important signaling molecule (Crawford, 1995; Krouk et al., 2010a). Nitrogen (N) is a key constituent of nucleotides and amino acids, thus essential for life. In plants, about 2–5% of the dry biomass is made up of nitrogen, which is largely acquired by plant roots in the form of nitrate (Xu et al., 2012). Nitrate also functions as a critical signaling ion and regulates many aspects of plant growth and development (Castaings et al., 2011; Bouguyon et al., 2012), including nitrate-related gene expression (Wang et al., 2003), root architecture (Forde, 2014), seed dormancy (Alboresi et al., 2005), and flowering time (Castro Marín et al., 2011).

Active nitrate uptake through membrane transporters by plant roots represents the key first step of nitrogen acquisition (Dechorgnat et al., 2011). As sessile organisms, plants have evolved sophisticated nitrate transporter systems in response to the fluctuating nitrate environments (Wang et al., 2012). In *Arabidopsis thaliana*, one of the most well studied nitrate transporters is NRT1.1 (CHL1 or NPF6.3), which is a multifunctional protein with a crucial role in both nitrate acquisition and signaling. Firstly, NRT1.1 is a dual-affinity transporter, which can facilitate nitrate assimilation over a wide range of nitrate concentrations (Liu et al., 1999). Secondly, NRT1.1 has recently been shown to serve as a nitrate sensor, regulating the gene expression of other nitrate transporters such as NRT2.1 (Krouk et al., 2006; Ho et al., 2009). Last by not least, NRT1.1 also contributes

to the nitrate-regulated auxin translocation besides nitrate transport and sensing (Krouk et al., 2010b). In this review, we will mainly focus on the transporter functions of NRT1.1 and summarize recent structure-function studies, which have shed light on the molecular mechanism underlying its dual-affinity activity.

Nitrate Transporters in *Arabidopsis*

To cope with the fluctuation of nitrate level, plants have evolved two complementary nitrate transporter systems with distinct kinetics properties (Forde, 2000; Nacry et al., 2013; Krapp et al., 2014). The low-affinity transporter system (LATS), which consists members of the NRT1/PTR family (recently renamed as NPF family) (Steiner et al., 1995; Léran et al., 2014), drives nitrate uptake at millimolar concentration. This family shares sequence homology to SLC15/PTR/PepT/POT family of peptide transporter family in animal. In plants, the NRT1/PTR family has functionally diverged with individual members recognizing different substrates including peptides (Tsay et al., 2007), plant hormones (Krouk et al., 2010b), glucosinolates (Nour-Eldin et al., 2012), and nitrate (Tsay et al., 1993). The high-affinity transporter system (HATS), comprising the NRT2/NNP family, facilitates nitrate uptake with Michaelis constant (K_m) value in the micromolar range. Studies suggest that some NRT2 members require a second gene product for their functional activity. In the case of NRT2.1, NAR2 is needed to mediate its nitrate uptake (Kotur et al., 2012).

NRT1/PTR and NRT2/NNP together constitute a large NRT transporter family in plants, which are proton-coupled symporters and belong to the major facilitator superfamily (MFS) (Pao et al., 1998). Together there are 53 NRT1 genes and 7 NRT2 genes in *Arabidopsis* (Tsay et al., 2007). Besides ensuring the root capacity of nitrate uptake, NRT transporters are also involved in subsequent loading and unloading of nitrate to and from the xylem vessels, allowing its distribution to aerial organs or its remobilization from old leaves (Chiu et al., 2004; Lin et al., 2008; Fan et al., 2009; Wang and Tsay, 2011).

NRT1.1 is a Dual-Affinity Transporter

The *Arabidopsis* NRT1.1 (CHL1 or NPF6.3) protein is the founding member of the NRT1/PTR family. It was firstly cloned as a gene product that is responsible for chlorate sensitivity in *Arabidopsis* (Tsay et al., 1993). The NRT1.1 protein contains 12 membrane-spanning segments and confers proton-coupled nitrate transport activity.

Interestingly, NRT1.1 is essential for both high- and low-affinity nitrate absorptions in *Arabidopsis*. It presents a biphasic uptake curve in response to environmental nitrate availability, and thus functions as a dual-affinity transporter (Huang et al., 1996; Wang et al., 1998; Liu et al., 1999; Liu and Tsay, 2003). NRT1.1 shares sequence homology with members of the NRT1/PTR family that constitutes the LATS, and was initially shown to be a low-affinity nitrate transporter. Later, it was found that plants with *nrt1.1* mutation were also defective in high-affinity nitrate uptake, suggesting that NRT1.1 might be a dual-affinity transporter. Further experiments in plants and oocytes demonstrate that the uptake curve of NRT1.1 is biphasic with a Km of ∼50 μM for high-affinity phase of uptake and ∼4 mM for the low-affinity phase (Liu and Tsay, 2003).

The mode of action of the dual-affinity function of NRT1.1 is regulated through phosphorylation modification on a key threonine residue, Thr101 (Liu and Tsay, 2003). Thr101 is located at the intracellular side between the third and fourth transmembrane helix (TM) of NRT1.1. When phosphorylated by the CIPK23 kinase (Ho et al., 2009), NRT1.1 functions as a high-affinity nitrate transporter. When unphosphorylated, it works as a low-affinity transporter. Furthermore, mutations of Thr101 preventing or mimicking phosphorylation can effectively convert the dual-affinity transporter into a monophasic low-affinity or high-affinity transporter, respectively. This regulatory mechanism of NRT1.1 allows for the rapid adaption to changing nitrate levels.

Molecular Basis of the Dual-Affinity Function

How does Thr101 phosphorylation switch the transporter affinity of NRT1.1? Recently, two independent studies revealed the crystal structures of unmodified NRT1.1, shedding light on the molecular basis of the working mechanism of this transporter (Parker and Newstead, 2014; Sun et al., 2014). In both studies, NRT1.1 was crystallized with two molecules in each asymmetric unit (ASU), despite the different polypeptide boundaries, crystallization conditions, and space groups (**Figure 1A**). The two molecules in the ASU are almost identical to each other and adopt the canonical MFS fold, which is characterized by 12 transmembrane helices (TMs) with a central linker connecting the amino-terminal (TM1-TM6) and carboxyl-terminal (TM7-TM12) helix bundles (Law et al., 2008; Yan, 2013). The transporter is captured in the inward conformation with the substrate-binding site accessible from the cytosol side.

Both *in vitro* biochemical studies and cell-base fluorescence resonance energy transfer (FRET) assays suggest that the NRT1.1 dimer could be physiologically relevant (Sun et al., 2014). First of all, NRT1.1 dimer is observed in two different crystal forms. The two adjacent non-crystallographic related NRT1.1 molecules are in the same orientation with their amino-terminal halves facing and interacting with each other. This overall topology is perfectly compatible with its transporter function in the cell membrane (**Figure 1A**). Secondly, the dimer interface, burying a surface area of more than 2160 $Å^2$, has high shape-complementarity that is considered as an important determinant of helix packing specificity in membrane or micelles (Fleming et al., 1997; Mackenzie and Fleming, 2008; Chen et al., 2009). Thirdly, *in vitro* crosslinking experiments show that transient dimer of NRT1.1 could form in detergent solutions. Consistent with these *in vitro* observations, cell-based FRET assay also demonstrates that NRT1.1 oligomerizes in the membrane of *Xenopus* oocytes, where the dual-affinity function of NRT1.1 can be recapitulated.

More importantly, the oligomerization state of NRT1.1 could be affected by the phosphorylation modification on NRT1.1 (Sun et al., 2014). In the crystal structure, the key residue, Thr101 is buried in a hydrophobic pocket that is located right next to the dimer interface (**Figure 1A**). Phosphorylation of Thr101 was predicted to introduce electrostatic and conformational changes

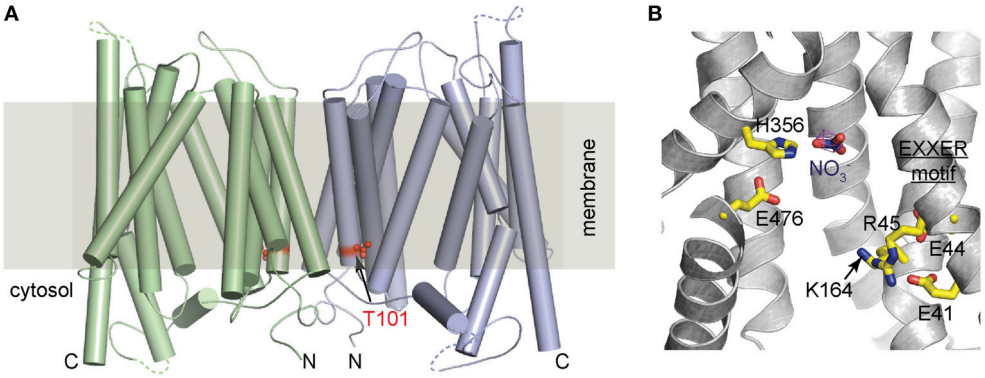

FIGURE 1 | Crystal structure of NRT1.1. (A) A cylinder representation of the NRT1.1 dimer with Thr101 shown as red spheres. The two monomers are colored in pale green and light blue. Within each monomer, the amino- and carboxyl-terminus are indicated by N and C. **(B)** Key residues involved in substrate binding and proton coupling. Nitrate and the side chain of the neighboring histidine, His356, EXXER motif, Glu476, and Lys164 are shown as sticks.

in its vicinity and disrupt the dimeric configuration of NRT1.1. This prediction was confirmed by oocyte-base FRET assays. Both wild-type NRT1.1 and the phosphorylation defective mutant NRT1.1-T101A generate robust and comparable FRET signals. In contrast, the phosphomimetic mutation, NRT1.1-T101D failed to show any significant signal, indicating a spatial separation of the two monomers. These data suggest a phosphorylation-dependent dimerization switching mechanism for the dual-affinity transporter: unmodified NRT1.1 forms structurally coupled dimers and works as a low-affinity transporter, whereas phosphorylated NRT1.1 undergoes dimer decoupling and adopts a high-affinity state.

Besides decoupling the dimer, phosphorylation on Thr101 also alters the transporter properties of each monomer (Parker and Newstead, 2014). NRT1.1-T101D has a lower melting temperature, indicating increased structure flexibility. Meanwhile, the transport rate of the phosphomimetic variant is also higher than wild-type protein by 2.8-folds in the liposome-base uptake assay. Therefore, enhanced structure flexibility of NRT1.1 through Thr101 phosphorylation leads to an increased transporter rate, which results in a lower K_m.

Taken together, phosphorylation on the Thr101 toggles NRT1.1 between the high- and low-affinity states by decoupling the dimer and increasing structure flexibility (Tsay, 2014; **Figure 2**). When nitrate is abundant, NRT1.1 is dephosphorylated. At this state, the transporter adopts a dimeric conformation, has lower structural flexibility, and functions as a low-affinity transporter. When the environmental nitrate concentration drops, NRT1.1 becomes phosphorylated on the Thr101 residue at the dimer interface, which decouples the NRT1.1 dimer. As a result, the phosphorylated transporter gains increased structural flexibility and uptake activity, and works as a high-affinity transporter.

Substrate Recognition and Proton Coupling in NRT1.1

A key question regarding to the working mechanism of a transporter is how substrate is recognized. High-resolution structures of bacterial nitrate transporter and nitrate/nitrite exchanger (NarU and NarK) from NNP family had been documented before the crystal structures of NRT1.1 were determined (Yan et al., 2013; Zheng et al., 2013). Nitrate in these two bacterial transporters is coordinated by two opposing conserved arginine residues through ionic interactions, which provides high-affinity contacts between the transporters and nitrate. Distinct from NarU and NarK, the overall substrate-binding pocket of NRT1.1 is mostly hydrophobic, with the exception of one histidine residue, His356 on TM7 (**Figure 1B**), which is shown to be critical in nitrate recognition. Despite the resolution limit, discernable electron density of nitrate is located in close vicinity to His356, mutation of which eliminated substrate uptake both at high and low nitrate concentrations. Notably, His356 is not conserved in transporters of the NRT1/PTR family, suggesting that other NRT1/PTR members may have different substrate recognition mechanism. The unique chargeable histidine residue at the substrate binding pocket provides a plausible explanation for the high-affinity activity acquired by NRT1.1. Sequence differences in the substrate binding sites may also explain why NRT/PTRs are able to recognize substrates as diverse as nitrate, peptides and plant hormones.

In addition to His356, an EXXER motif and a potential salt bridge between Lys164 and E476 (**Figure 1B**) are shown to be critical in proton coupling by uptake assays in liposomes and oocytes (Parker and Newstead, 2014; Sun et al., 2014). The importance of these residues is also validated by two independent assays, two-electrode voltage clamp (TEVC) and a novel fluorescent method, in which the activity of NRT1.1 was monitored through its tight correlation with FRET readout of fluorescent proteins linked to N- and C-terminus of the transporter (Ho and Frommer, 2014).

MFS oligomerization

Besides NRT1.1, numerous MFS transporters including TetL (Safferling et al., 2003), GalP (Zheng et al., 2010), GLUT1 (Graybill et al., 2006), hRFC (Hou and Matherly, 2009),

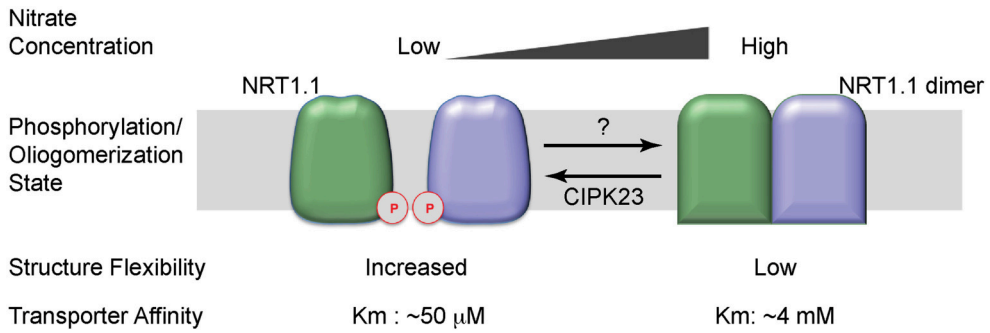

FIGURE 2 | Working model of the dual-affinity transporter, NRT1.1. When nitrate concentration is low, NRT1.1 is phosphorylated (P) at the amino-acid residue Thr101. The phosphorylation modification disrupts the dimer configuration and increases the structural flexibility of NRT1.1, leading to a high affinity for nitrate. When nitrate is abundant, Thr101 is dephosphorylated. NRT1.1 works as a coupled dimer, which has decreased structural flexibility, rendering the transporter in a low-affinity state. The two NRT1.1 molecules are colored in pale green and light blue. The phosphorylation modification is indicated by "P" in a red cycle.

MCT8 (Fischer et al., 2015), and LacS (Veenhoff et al., 2001) have been shown to exist as homo-oligomers. Functional importance of the MFS oligomerization has been indicated in several studies. For example, the lactose transporter LacS from *Streptococcus Thermophiles* functions as cooperative dimers with two substrate translocation pathways, and co-reconstitution of functional and defective transporters disrupts proton-coupled lactose uptake, suggesting a dominant-negative effect (Veenhoff et al., 2001). The human monocarboxylate transporter 8 (MCT8), mutation of which underlies the cause of a severe X-linked psychomotor retardation (known as the Allan-Herndon-Dudley syndrome), forms functional homodimers *in vivo*. Native occurring pathogenic mutations from patients that abolish the transporter function also largely affect the formation of homodimers, suggesting the potential significance of the transporter oligomerization (Fischer et al., 2015).

In the case of NRT1.1, phosphorylation-controlled dimerization provides a novel aspect on how dynamic transporter oligomerization involves in functional modulation. The dimerization state of NRT1.1 is fine-tuned by the posttranslational modification. Upon phosphorylation and dephosphorylation of the Thr101 residue, the transporter oligomerization state is regulated, which in turn further changes the structure flexibility of NRT1.1 and switches the transporter between high- and low-affinity modes. Thus, structure-function studies of NRT1.1 not only establishes a structural framework for understanding the dual-affinity activity, but also reveals how posttranslational modification and protein oligomerization can synergistically expand the functional capacity of an MFS transporter.

Perspective

In this review, we focused on the recent progress on the molecular basis of the dual-affinity activity of the key nitrate transporter, NRT1.1. Through structural and biochemical studies, the oligomerization state and the structural flexibility of the transporter are proposed to play a key role in the phosphorylation dependent transporter affinity switch. Yet many important questions remain to be answered to further our understanding on this important molecule. For example, what is the structure of the phosphorylated transporter like? Crystallographic analysis of the phosphorylated form will help us visualize the conformational difference between the high- and low-affinity states, and obtain a better picture of the working mechanism. Since the high-affinity property of NRT1.1 has been challenged (Glass and Kotur, 2013), it will be also valuable to systematically characterize the function of NRT1.1 at different oligomerization and phosphorylation states *in vitro*. By mutating and disrupting the dimer interface (Robertson et al., 2010), a phosphorylation-independent NRT1.1 monomer could be potentially obtained. Structural and functional analyses of such a mutant could help address the questions as to whether phosphorylation alters the properties of the transporter beyond controlling its oligomerization state and whether unphosphorylated NRT1.1 monomer is functional. Furthermore, how Thr101 becomes modified by the CIPK23 kinase if this residue is buried in a hydrophobic pocket at the dimer interface? It is proposed that the phosphorylation might occur when the transporter is at the occluded or outward conformation, yet this hypothesis awaits more evidence. Last but not least, do both protomer copies of the NRT1.1 dimer have to be phosphorylated before the affinity state of the transporter is changed? Designing a functional NRT1.1 concatemer with two individually manipulable copies of the transporter might help shed light on this and other questions.

Another interesting aspect of the NRT1.1 protein is its nitrate sensor function, which exemplifies the transceptor (transporter with sensor function) paradigm in *Arabidopsis* (Ho et al., 2009; Gojon et al., 2011). Transceptors have been found in many organisms from *E. coli* to mammals (Thevelein and Voordeckers, 2009), and almost all transceptors are important in nutrients transport and sensing (Donaton et al., 2003; Schwöppe et al., 2003; Hyde et al., 2007; Rebsamen et al., 2015; Wang et al., 2015). Recently, the mammalian amino acid transporter, SLC38A9 was identified as an amino acid sensor for lysosome-based activation of mTORC1, indicating the importance of transceptor in human disease (Abraham, 2015). A fundamental question

underlying the working mechanism of a transceptor is how substrate translocation and sensing is coupled? In the case of NRT1.1, its transceptor function also exhibits a biphasic manner switched by Thr101 phosphorylation, as the phosphorylation and non-phosphorylated forms of NRT1.1 have distinct signaling properties (Bouguyon et al., 2015). It will be interesting to know whether NRT1.1 dimerization is also involved in the sensor affinity switch. An equally important question is how nitrate signal is transduced through protein-protein interaction. In the crystal structure of NRT1.1, the well-ordered N-terminal loop at the dimer interface on the intracellular side presents a conserved docking interface that may have a putative role in nitrate signaling by recruiting downstream signal molecules such as kinases and phosphatases. Further genetic and biochemical studies will be needed to support this hypothesis.

Last but not least, NRT1.1 facilitates nitrate-regulated auxin transport. It has been reported that NRT1.1 could use both nitrate and auxin as its substrates, and enable soil nitrate availability to regulate the lateral root development (Krouk et al., 2010b). This reveals a surprising mechanism by which plants adjust their root architecture for soil exploitation, and raises another interesting question as to how NRT1.1 recognizes two structurally different substrates. Further studies will be required to fully uncover the role of NRT1.1 in nitrate transport and signaling, which enable plants to adapt to the fluctuated nitrate environment. Ultimately, these studies will potentially facilitate the development of new technologies for increasing crop yields as well as reducing nitrogen pollution in modern agriculture.

AUTHOR CONTRIBUTIONS

Both authors contributed to the drafting and revising the work.

FUNDING

This work is supported by the Howard Hughes Medical Institute and the National Science Foundation (NSF MCB-1157561).

REFERENCES

Abraham, R. T. (2015). Cell biology. Making sense of amino acid sensing. *Science* 347, 128–129. doi: 10.1126/science.aaa4570

Alboresi, A., Gestin, C., Leydecker, M. T., Bedu, M., Meyer, C., and Truong, H. N. (2005). Nitrate, a signal relieving seed dormancy in Arabidopsis. *Plant Cell Environ.* 28, 500–512. doi: 10.1111/j.1365-3040.2005.01292.x

Bouguyon, E., Brun, F., Meynard, D., Kubeš, M., Pervent, M., Leran, S., et al. (2015). Multiple mechanisms of nitrate sensing by Arabidopsis nitrate transceptor NRT1.1. *Nat. Plants* 1:15015. doi: 10.1038/nplants.2015.15

Bouguyon, E., Gojon, A., and Nacry, P. (2012). Nitrate sensing and signaling in plants. *Semin. Cell Dev. Biol.* 23, 648–654. doi: 10.1016/j.semcdb.2012.01.004

Castaings, L., Marchive, C., Meyer, C., and Krapp, A. (2011). Nitrogen signalling in Arabidopsis: how to obtain insights into a complex signalling network. *J. Exp. Bot.* 62, 1391–1397. doi: 10.1093/jxb/erq375

Castro Marín, I., Loef, I., Bartetzko, L., Searle, I., Coupland, G., Stitt, M., et al. (2011). Nitrate regulates floral induction in Arabidopsis, acting independently of light, gibberellin and autonomous pathways. *Planta* 233, 539–552. doi: 10.1007/s00425-010-1316-5

Chen, L., Merzlyakov, M., Cohen, T., Shai, Y., and Hristova, K. (2009). Energetics of ErbB1 transmembrane domain dimerization in lipid bilayers. *Biophys. J.* 96, 4622–4630. doi: 10.1016/j.bpj.2009.03.004

Chiu, C. C., Lin, C. S., Hsia, A. P., Su, R. C., Lin, H. L., and Tsay, Y. F. (2004). Mutation of a nitrate transporter, AtNRT1:4, results in a reduced petiole nitrate content and altered leaf development. *Plant Cell Physiol.* 45, 1139–1148. doi: 10.1093/pcp/pch143

Crawford, N. M. (1995). Nitrate: nutrient and signal for plant growth. *Plant Cell* 7, 859–868. doi: 10.1105/tpc.7.7.859

Dechorgnat, J., Nguyen, C. T., Armengaud, P., Jossier, M., Diatloff, E., Filleur, S., et al. (2011). From the soil to the seeds: the long journey of nitrate in plants. *J. Exp. Bot.* 62, 1349–1359. doi: 10.1093/jxb/erq409

Donaton, M. C., Holsbeeks, I., Lagatie, O., Van Zeebroeck, G., Crauwels, M., Winderickx, J., et al. (2003). The Gap1 general amino acid permease acts as an amino acid sensor for activation of protein kinase A targets in the yeast Saccharomyces cerevisiae. *Mol. Microbiol.* 50, 911–929. doi: 10.1046/j.1365-2958.2003.03732.x

Fan, S. C., Lin, C. S., Hsu, P. K., Lin, S. H., and Tsay, Y. F. (2009). The Arabidopsis nitrate transporter NRT1.7, expressed in phloem, is responsible for source-to-sink remobilization of nitrate. *Plant Cell* 21, 2750–2761. doi: 10.1105/tpc.109.067603

Fischer, J., Kleinau, G., Müller, A., Kühnen, P., Zwanziger, D., Kinne, A., et al. (2015). Modulation of monocarboxylate transporter 8 oligomerization by specific pathogenic mutations. *J. Mol. Endocrinol.* 54, 39–50. doi: 10.1530/JME-14-0272

Fleming, K. G., Ackerman, A. L., and Engelman, D. M. (1997). The effect of point mutations on the free energy of transmembrane alpha-helix dimerization. *J. Mol. Biol.* 272, 266–275. doi: 10.1006/jmbi.1997.1236

Forde, B. G. (2000). Nitrate transporters in plants: structure, function and regulation. *Biochim. Biophys. Acta* 1465, 219–235. doi: 10.1016/S0005-2736(00)00140-1

Forde, B. G. (2014). Nitrogen signalling pathways shaping root system architecture: an update. *Curr. Opin. Plant Biol.* 21, 30–36. doi: 10.1016/j.pbi.2014.06.004

Glass, A. D., and Kotur, Z. (2013). A re-evaluation of the role of Arabidopsis NRT1.1 in high-affinity nitrate transport. *Plant Physiol.* 163, 1103–1106. doi: 10.1104/pp.113.229161

Gojon, A., Krouk, G., Perrine-Walker, F., and Laugier, E. (2011). Nitrate transceptor(s) in plants. *J. Exp. Bot.* 62, 2299–2308. doi: 10.1093/jxb/erq419

Graybill, C., Van Hoek, A. N., Desai, D., Carruthers, A. M., and Carruthers, A. (2006). Ultrastructure of human erythrocyte GLUT1. *Biochemistry* 45, 8096–8107. doi: 10.1021/bi060398x

Ho, C. H., and Frommer, W. B. (2014). Fluorescent sensors for activity and regulation of the nitrate transceptor CHL1/NRT1.1 and oligopeptide transporters. *Elife* 3:e01917. doi: 10.7554/eLife.01917

Ho, C. H., Lin, S. H., Hu, H. C., and Tsay, Y. F. (2009). CHL1 functions as a nitrate sensor in plants. *Cell* 138, 1184–1194. doi: 10.1016/j.cell.2009.07.004

Hou, Z., and Matherly, L. H. (2009). Oligomeric structure of the human reduced folate carrier: identification of homo-oligomers and dominant-negative effects on carrier expression and function. *J. Biol. Chem.* 284, 3285–3293. doi: 10.1074/jbc.M807206200

Huang, N. C., Chiang, C. S., Crawford, N. M., and Tsay, Y. F. (1996). CHL1 encodes a component of the low-affinity nitrate uptake system in Arabidopsis and shows cell type-specific expression in roots. *Plant Cell* 8, 2183–2191. doi: 10.1105/tpc.8.12.2183

Hyde, R., Cwiklinski, E. L., Macaulay, K., Taylor, P. M., and Hundal, H. S. (2007). Distinct sensor pathways in the hierarchical control of SNAT2, a putative amino acid transceptor, by amino acid availability. *J. Biol. Chem.* 282, 19788–19798. doi: 10.1074/jbc.M611520200

Kotur, Z., Mackenzie, N., Ramesh, S., Tyerman, S. D., Kaiser, B. N., and Glass, A. D. (2012). Nitrate transport capacity of the *Arabidopsis thaliana* NRT2 family members and their interactions with AtNAR2.1. *New Phytol.* 194, 724–731. doi: 10.1111/j.1469-8137.2012.04094.x

Krapp, A., David, L. C., Chardin, C., Girin, T., Marmagne, A., Leprince, A. S., et al. (2014). Nitrate transport and signalling in Arabidopsis. *J. Exp. Bot.* 65, 789–798. doi: 10.1093/jxb/eru001

Krouk, G., Crawford, N. M., Coruzzi, G. M., and Tsay, Y. F. (2010a). Nitrate signaling: adaptation to fluctuating environments. *Curr. Opin. Plant Biol.* 13, 266–273. doi: 10.1016/j.pbi.2009.12.003

Krouk, G., Lacombe, B., Bielach, A., Perrine-Walker, F., Malinska, K., Mounier, E., et al. (2010b). Nitrate-regulated auxin transport by NRT1.1 defines a mechanism for nutrient sensing in plants. *Dev. Cell* 18, 927–937. doi: 10.1016/j.devcel.2010.05.008

Krouk, G., Tillard, P., and Gojon, A. (2006). Regulation of the high-affinity NO3- uptake system by NRT1.1-mediated NO3- demand signaling in Arabidopsis. *Plant Physiol.* 142, 1075–1086. doi: 10.1104/pp.106.087510

Law, C. J., Maloney, P. C., and Wang, D. N. (2008). Ins and outs of major facilitator superfamily antiporters. *Annu. Rev. Microbiol.* 62, 289–305. doi: 10.1146/annurev.micro.61.080706.093329

Léran, S., Varala, K., Boyer, J. C., Chiurazzi, M., Crawford, N., Daniel-Vedele, F., et al. (2014). A unified nomenclature of NITRATE TRANSPORTER 1/PEPTIDE TRANSPORTER family members in plants. *Trends Plant Sci.* 19, 5–9. doi: 10.1016/j.tplants.2013.08.008

Lin, S. H., Kuo, H. F., Canivenc, G., Lin, C. S., Lepetit, M., Hsu, P. K., et al. (2008). Mutation of the Arabidopsis NRT1.5 nitrate transporter causes defective root-to-shoot nitrate transport. *Plant Cell* 20, 2514–2528. doi: 10.1105/tpc.108.060244

Liu, K. H., Huang, C. Y., and Tsay, Y. F. (1999). CHL1 is a dual-affinity nitrate transporter of Arabidopsis involved in multiple phases of nitrate uptake. *Plant Cell* 11, 865–874. doi: 10.1105/tpc.11.5.865

Liu, K. H., and Tsay, Y. F. (2003). Switching between the two action modes of the dual-affinity nitrate transporter CHL1 by phosphorylation. *EMBO J.* 22, 1005–1013. doi: 10.1093/emboj/cdg118

Mackenzie, K. R., and Fleming, K. G. (2008). Association energetics of membrane spanning alpha-helices. *Curr. Opin. Struct. Biol.* 18, 412–419. doi: 10.1016/j.sbi.2008.04.007

Nacry, P., Bouguyon, E., and Gojon, A. (2013). Nitrogen acquisition by roots: physiological and developmental mechanisms ensuring plant adaptation to a fluctuating resource. *Plant Soil* 370, 29. doi: 10.1007/s11104-013-1645-9

Nour-Eldin, H. H., Andersen, T. G., Burow, M., Madsen, S. R., Jørgensen, M. E., Olsen, C. E., et al. (2012). NRT/PTR transporters are essential for translocation of glucosinolate defence compounds to seeds. *Nature* 488, 531–534. doi: 10.1038/nature11285

Pao, S. S., Paulsen, I. T., and Saier, M. H. Jr. (1998). Major facilitator superfamily. *Microbiol. Mol. Biol. Rev.* 62, 1–34.

Parker, J. L., and Newstead, S. (2014). Molecular basis of nitrate uptake by the plant nitrate transporter NRT1.1. *Nature* 507, 68–72. doi: 10.1038/nature13116

Rebsamen, M., Pochini, L., Stasyk, T., De Araújo, M. E., Galluccio, M., Kandasamy, R. K., et al. (2015). SLC38A9 is a component of the lysosomal amino acid sensing machinery that controls mTORC1. *Nature* 519, 477–481. doi: 10.1038/nature14107

Robertson, J. L., Kolmakova-Partensky, L., and Miller, C. (2010). Design, function and structure of a monomeric ClC transporter. *Nature* 468, 844–847. doi: 10.1038/nature09556

Safferling, M., Griffith, H., Jin, J., Sharp, J., De Jesus, M., Ng, C., et al. (2003). TetL tetracycline efflux protein from Bacillus subtilis is a dimer in the membrane and in detergent solution. *Biochemistry* 42, 13969–13976. doi: 10.1021/bi035173q

Schwöppe, C., Winkler, H. H., and Neuhaus, H. E. (2003). Connection of transport and sensing by UhpC, the sensor for external glucose-6-phosphate in Escherichia coli. *Eur. J. Biochem.* 270, 1450–1457. doi: 10.1046/j.1432-1033.2003.03507.x

Steiner, H. Y., Naider, F., and Becker, J. M. (1995). The PTR family: a new group of peptide transporters. *Mol. Microbiol.* 16, 825–834. doi: 10.1111/j.1365-2958.1995.tb02310.x

Sun, J., Bankston, J. R., Payandeh, J., Hinds, T. R., Zagotta, W. N., and Zheng, N. (2014). Crystal structure of the plant dual-affinity nitrate transporter NRT1.1. *Nature* 507, 73–77. doi: 10.1038/nature13074

Thevelein, J. M., and Voordeckers, K. (2009). Functioning and evolutionary significance of nutrient transceptors. *Mol. Biol. Evol.* 26, 2407–2414. doi: 10.1093/molbev/msp168

Tsay, Y. F. (2014). Plant science: how to switch affinity. *Nature* 507, 44–45. doi: 10.1038/nature13063

Tsay, Y. F., Chiu, C. C., Tsai, C. B., Ho, C. H., and Hsu, P. K. (2007). Nitrate transporters and peptide transporters. *FEBS Lett.* 581, 2290–2300. doi: 10.1016/j.febslet.2007.04.047

Tsay, Y. F., Schroeder, J. I., Feldmann, K. A., and Crawford, N. M. (1993). The herbicide sensitivity gene CHL1 of Arabidopsis encodes a nitrate-inducible nitrate transporter. *Cell* 72, 705–713. doi: 10.1016/0092-8674(93)90399-B

Veenhoff, L. M., Heuberger, E. H., and Poolman, B. (2001). The lactose transport protein is a cooperative dimer with two sugar translocation pathways. *EMBO J.* 20, 3056–3062. doi: 10.1093/emboj/20.12.3056

Wang, R., Liu, D., and Crawford, N. M. (1998). The Arabidopsis CHL1 protein plays a major role in high-affinity nitrate uptake. *Proc. Natl. Acad. Sci. U.S.A.* 95, 15134–15139. doi: 10.1073/pnas.95.25.15134

Wang, R., Okamoto, M., Xing, X., and Crawford, N. M. (2003). Microarray analysis of the nitrate response in Arabidopsis roots and shoots reveals over 1,000 rapidly responding genes and new linkages to glucose, trehalose-6-phosphate, iron, and sulfate metabolism. *Plant Physiol.* 132, 556–567. doi: 10.1104/pp.103.021253

Wang, S., Tsun, Z. Y., Wolfson, R. L., Shen, K., Wyant, G. A., Plovanich, M. E., et al. (2015). Metabolism. Lysosomal amino acid transporter SLC38A9 signals arginine sufficiency to mTORC1. *Science* 347, 188–194. doi: 10.1126/science.1257132

Wang, Y. Y., Hsu, P. K., and Tsay, Y. F. (2012). Uptake, allocation and signaling of nitrate. *Trends Plant Sci.* 17, 458–467. doi: 10.1016/j.tplants.2012.04.006

Wang, Y. Y., and Tsay, Y. F. (2011). Arabidopsis nitrate transporter NRT1.9 is important in phloem nitrate transport. *Plant Cell* 23, 1945–1957. doi: 10.1105/tpc.111.083618

Xu, G., Fan, X., and Miller, A. J. (2012). Plant nitrogen assimilation and use efficiency. *Annu. Rev. Plant Biol.* 63, 153–182. doi: 10.1146/annurev-arplant-042811-105532

Yan, H., Huang, W., Yan, C., Gong, X., Jiang, S., Zhao, Y., et al. (2013). Structure and mechanism of a nitrate transporter. *Cell Rep.* 3, 716–723. doi: 10.1016/j.celrep.2013.03.007

Yan, N. (2013). Structural advances for the major facilitator superfamily (MFS) transporters. *Trends Biochem. Sci.* 38, 151–159. doi: 10.1016/j.tibs.2013.01.003

Zheng, H., Taraska, J., Merz, A. J., and Gonen, T. (2010). The prototypical H+/galactose symporter GalP assembles into functional trimers. *J. Mol. Biol.* 396, 593–601. doi: 10.1016/j.jmb.2009.12.010

Zheng, H., Wisedchaisri, G., and Gonen, T. (2013). Crystal structure of a nitrate/nitrite exchanger. *Nature* 497, 647–651. doi: 10.1038/nature12139

Conflict of Interest Statement: The authors declare that the research was conducted in the absence of any commercial or financial relationships that could be construed as a potential conflict of interest.

Advantages of publishing in Frontiers

OPEN ACCESS
Articles are free to read for greatest visibility and readership

FAST PUBLICATION
Around 90 days from submission to decision

HIGH QUALITY PEER-REVIEW
Rigorous, collaborative, and constructive peer-review

TRANSPARENT PEER-REVIEW
Editors and reviewers acknowledged by name on published articles

Frontiers
Avenue du Tribunal-Fédéral 34
1005 Lausanne | Switzerland

Visit us: www.frontiersin.org
Contact us: info@frontiersin.org | +41 21 510 17 00

REPRODUCIBILITY OF RESEARCH
Support open data and methods to enhance research reproducibility

DIGITAL PUBLISHING
Articles designed for optimal readership across devices

FOLLOW US
@frontiersin

IMPACT METRICS
Advanced article metrics track visibility across digital media

EXTENSIVE PROMOTION
Marketing and promotion of impactful research

LOOP RESEARCH NETWORK
Our network increases your article's readership